Bubble Dynamics and Breakup in Straining Flows

Thesis by

In Seok Kang

in Partial Fulfillment of the Requirements

for the Degree of

Doctor of Philosophy

California Institute of Technology

Pasadena, California

1988

(Submitted January 11, 1988)

To my wife, Aesun

Acknowledgments

I would like to thank my research advisor, Professor L. Gary Leal, for the support and guidance he has provided throughout the course of this work. His encouragement and insight, and the freedom he granted me to pursue my research interests, are deeply appreciated.

Thanks are extended to my colleagues in the Leal research group for the many pleasant experiences and discussions we shared. Dave Dandy, a great master in computing, helped me a great deal to learn about the computing systems at Caltech as well as the CRAY X-MP at Boeing Computer Services. Ed Ascoli, a gifted mathematician, has provided me a lot of intellectual stimulus, and Howard Stone showed me the standard of a real scholar. I have to also mention Ricky Ng and Hway Kang with whom I prepared for the qualifying exam.

During my academic training at Caltech, I was taught by many professors who shared with me their knowledge and love for learning. I am grateful to all of them. Especially, I should recognize Professors Joel Franklin and John Brady. Their encouragement and interests in my future career plan are greatly appreciated.

Finally, I would like to express my sincere gratitude to all members of my family for their never-ending support and encouragement. Most of all, I wish to thank my wife, Aesun, and our three daughters Laura, Erin, and Christine. Without their love and sacrifice, my graduate education would never have come to a fruitful end.

Abstract

The dynamics and breakup of a bubble in axisymmetric flow fields has been investigated using numerical and analytical techniques. In particular, the transient bubble deformation, oscillation, and overshoot effects are considered in conjunction with the existence of steady-state solutions.

To explore the dynamics of a bubble with a high degree of deformation, a numerical technique suitable for solving axisymmetric, unsteady free boundary problems in fluid mechanics has been developed. The technique is based on a finite-difference solution of the equations of motion on a moving orthogonal curvilinear coordinate system, which is constructed numerically and adjusted to fit the boundary at any time. For example, the steady and unsteady deformations of a bubble in uniaxial and biaxial straining flows are examined for wide ranges of the Reynolds number and the Weber number. The computations reveal that a bubble in a uniaxial straining flow extends indefinitely if the Weber number is larger than a critical value ($W > W_c$). Furthermore, it is shown that a bubble may not achieve a stable steady state even at subcritical values of the Weber number if the initial state is sufficiently different from the steady state. Potential flow solutions for uniaxial straining flow show that an initially deformed bubble undergoes oscillatory motion if $W < W_c$, with a frequency of oscillation that decreases as the Weber number increases and equals zero at the critical Weber number.

In contrast to the uniaxial straining flow problem, a bubble at a finite Reynolds number in a biaxial straining flow has a stable steady state even though the deformation is extremely large. However, it is found that a bubble in a biaxial straining flow in the potential flow limit has exactly the same steady-state shape as in a uniaxial straining flow and a critical Weber number for breakup exists. Comparison of the results for the cases of high Reynolds numbers with the potential flow results suggests that the potential flow solution does not provide a uniformly valid approximation to the real flow at a high Reynolds number in

the biaxial straining flow.

As a complementary analytical study to the numerical analysis, the method of domain perturbations is used to investigate the problem of a nearly spherical bubble in an inviscid, axisymmetric straining flow. The steady-state solutions suggest the existence of a limit point at a critical value of the Weber number. Furthermore, the asymptotic analysis for oscillation has provided a formula of oscillation frequency for the principal mode such as $\omega^2 = \omega_0^2(1 - 0.31W)$, where ω_0 is the oscillation frequency of a bubble in a quiescent fluid.

To include the weak viscous effect on the oscillation, a general formula for viscous pressure correction for a spherical bubble in an arbitrary axisymmetric flow has been derived in terms of the vorticity distribution. This formula has been applied to obtain the drag coefficient $C_D = 48/R$ by directly integrating the normal stress over the surface for a spherical bubble in a uniform streaming flow at a high Reynolds number, which has so far been possible only via indirect macroscopic balances. The direct method also reveals that the drag coefficient up to $O(R^{-1})$ depends only on the $O(1)$ vorticity distribution right on the bubble surface, and is independent of the vorticity distribution inside the fluid.

Finally, a voidage bubble in a fluidized bed is considered in the low Reynolds number limit. The problem has been formulated as a generalized drop problem with one additional parameter. The analysis shows that the steady and unsteady deformations in the creeping flow limit are exactly the same as the conventional drop problem even though the flow fields are different. The effect of the additional parameter on deformation first appears when inertial effects are considered.

Table of Contents

Chapter I

Numerical solution of axisymmetric, unsteady, free-boundary problems at finite Reynolds number I. Finite-difference scheme and its application to the deformation of a bubble in a uniaxial straining flow

The text of Chapter I consists of an article which has appeared in the *Physics of Fluids* [**30** 1929 (1987)].

Numerical solution of axisymmetric, unsteady, free-boundary problems at finite Reynolds number
I. Finite-difference scheme and its application to the deformation of a bubble in a uniaxial straining flow

I.S. Kang and L.G. Leal

Department of Chemical Engineering
California Institute of Technology
Pasadena, California 91125

Abstract

A brief description is presented for a numerical technique suitable for solving axisymmetric, unsteady free-boundary problems in fluid mechanics. The technique is based on a finite-difference solution of the equations of motion on a moving orthogonal curvilinear coordinate system, which is constructed numerically and adjusted to fit the boundary shape at any time. The initial value problem is solved using a fully implicit first-order backward time-differencing scheme in order to insure numerical stability. As an example of application, we consider the unsteady deformation of a bubble in a uniaxial extensional flow for Reynolds numbers in the range of $0.1 \leq R \leq 100$. The computation shows that the bubble extends indefinitely if the Weber number is larger than a critical value ($W > W_c$). Furthermore, it is shown that a bubble may not achieve a stable steady state even at subcritical values of the Weber number if the initial shape is sufficiently different from the steady shape. Finally, we have also obtained potential-flow solutions as an approximation for $R \to \infty$. These show that an initially deformed bubble undergoes oscillatory motion if $W < W_c$, with a frequency of oscillation (based on the surface-tension time scale), which decreases as the Weber number increases and equals zero at the critical Weber number beyond which steady solutions could not be obtained in the earlier numerical work of Ryskin and Leal [J. Fluid Mech. 148, 37 (1984)].[15] This clearly indicates that the point of non-convergence of the steady-state numerical problem is, in fact, a limit point in the branch of steady-state solutions.

I. INTRODUCTION

We are concerned in this paper with the development of a method to solve unsteady free-boundary problems in fluid mechanics. Although the recent development of solution techniques for steady free-boundary problems was a very important advance, an unsteady approach is essential to understand certain types of fluid mechanics problems, for example, finite-amplitude drop (or bubble) oscillation, drop breakup, etc., and may also play an important role in understanding the limitations encountered by steady algorithms in obtaining solutions for some parameter values. For example, in the unresolved problem of a rising bubble in a quiescent fluid at asymptotically large Weber numbers, a transient approach might either lead to a stable steady solution on some new branch, or reveal the lack of steady solutions, or generate a time-periodic solution. In the present paper, we first discuss the general features of a new numerical algorithm for transient, free-boundary problems, and then apply it to the specific problem of unsteady deformation of a bubble in a viscous incompressible Newtonian fluid that is undergoing a uniaxial straining flow.

The existing literature on numerical methods for unsteady, free-boundary problems in fluid mechanics is quite limited. However, two quite distinct solution methods can be identified. One is the so-called boundary-integral technique, which has been applied to a wide range of problems in which an interface exhibits large departures from some initial shape.[1–4] Although extremely powerful when applicable, this method is currently restricted to the limiting cases of either zero Reynolds number, or inviscid irrotational flow and this reduces its general usefulness. The second and more general class of solution methods consists of numerical techniques that are suitable when the governing differential equations are nonlinear. In this class, there are three distinct methods.

The first is the so-called MAC (marker and cell) method. The MAC method employs an Eulerian mesh of computational cells and finite difference expressions to approximate the governing equations. Also used is a set of marker particles

that move with the fluid to track the position of the free surface. This method has been successfully applied to very largely deformed free surfaces but usually with surface tension neglected[5–7] (an exception is Foote[7]). However, an intrinsic difficulty is that the surface position does not generally coincide with the given mesh points. Thus, a special kind of interpolation technique must be used to apply the boundary conditions.

The second method, which has been used to obtain most of the existing solutions of unsteady, free-surface problems, is the finite-element method.[8–12] In this method the strategy for deforming the elements is the most critical factor in successful applications. Usually either a Lagrangian approach or a flow-independent scheme has been used depending on the problem. In a flow-independent scheme, the deformation of the elements is determined only by the boundary shape at each instant, so that the motion of the element nodes is independent of the velocity field of the fluid.

Finally, in the present paper, we consider a third alternative, based on a finite-difference approximation of the equations of motion applied on a boundary-fitted orthogonal curvilinear coordinate system. The finite-difference method that we have developed is a generalization of the steady algorithm reported earlier by Ryskin and Leal.[13] In this scheme, all boundary surfaces of the solution domain at any time coincide exactly with a coordinate line of a numerically generated orthogonal coordinate system. Since this *boundary-fitted* coordinate system is completely determined by the boundary shape only, we do not have to worry about unreasonable grid deformation during the calculation, a problem quite often encountered in application of the Lagrangian, finite-element method to unsteady, free-boundary problems. The orthogonal mapping technique has been previously applied successfully to steady axisymmetric free-boundary problems.[13–16] A simple but crude mapping technique, which is totally different from orthogonal mapping, has recently been reported by Christov and Volkov.[17] They introduced a boundary-fitted coordinate system

by normalizing the radial coordinate with the distance from the origin to the bubble surface for a given angle. However, the resulting grid is non-orthogonal, and it causes non-trivial difficulties when the deformation is sufficiently large. The primary objective of the present paper is the development of a transient algorithm to apply the orthogonal mapping technique to unsteady, free-boundary problems.

II. PROBLEM FORMULATION

In this section we outline the mathematical formulation of a typical unsteady, free-boundary problem in which the free boundary is a gas-liquid interface that is assumed to be completely characterized by a constant (i.e., spatially uniform) surface tension. We assume that the liquid in our system is incompressible and Newtonian, and that its density and viscosity are sufficiently large compared with those of the gas that the dynamic pressure and stress fields in the gas at the interface can be neglected compared with those on the liquid side.

We denote the time-dependent *boundary-fitted* orthogonal coordinate system as (ξ, η, ϕ). For the axisymmetric problems considered here, the azimuthal angle ϕ is measured about the axis of symmetry. Further, for axisymmetric problems, Ryskin and Leal[18] have shown that the boundary-fitted coordinates at any instant, t, can be connected with the common cylindrical coordinates (x, σ, ϕ) (with the axis of symmetry in this case being the x-axis) via a pair of mapping functions $x(\xi, \eta, t)$ and $\sigma(\xi, \eta, t)$, which satisfy the covariant Laplace equations

$$\frac{\partial}{\partial \xi}(f\frac{\partial x}{\partial \xi}) + \frac{\partial}{\partial \eta}(\frac{1}{f}\frac{\partial x}{\partial \eta}) = 0, \tag{1a}$$

$$\frac{\partial}{\partial \xi}(f\frac{\partial \sigma}{\partial \xi}) + \frac{\partial}{\partial \eta}(\frac{1}{f}\frac{\partial \sigma}{\partial \eta}) = 0. \tag{1b}$$

Here the function $f(\xi, \eta)$ is the so-called *distortion function* representing the ratio h_η/h_ξ of scale factors $(h_\eta \equiv (g_{\eta\eta})^{1/2}, h_\xi \equiv (g_{\xi\xi})^{1/2})$ for the boundary-fitted coordinate system. In the present application, we use the *strong constraint*

method of Ryskin and Leal[18] in which f is given explicitly as a function of ξ and η. Furthermore, the generation of mapping functions $x(\xi,\eta,t)$ and $\sigma(\xi,\eta,t)$ for any fixed t is done in exactly the same way as described by Ryskin and Leal.[13] In terms of the mapping functions $x(\xi,\eta,t)$ and $\sigma(\xi,\eta,t)$, the scale factors are given as

$$h_\xi = \{(\frac{\partial x}{\partial \xi})^2 + (\frac{\partial \sigma}{\partial \xi})^2\}^{1/2}, \tag{2a}$$

$$h_\eta = \{(\frac{\partial x}{\partial \eta})^2 + (\frac{\partial \sigma}{\partial \eta})^2\}^{1/2}. \tag{2b}$$

The main source of possible confusion in the use of boundary-fitted coordinates is in the calculation of time derivatives. The mapping is always defined in such a way that the time-dependent physical space domain is mapped onto the time-independent unit square in (ξ,η) (Fig. 1),

$$0 \leq \xi, \eta \leq 1.$$

However, since the shape of physical domain is time-dependent because of the deformation of the free-boundary, the location of any fixed point (ξ,η) is also time-dependent in the physical domain. As a consequence, care must be taken to properly transform from partial time derivatives at fixed points in space to partial time derivatives in the (ξ,η) system. Generally, the relationship between two time derivatives for an arbitrary dependent variable w is given by (see also Thompson *et al.*[19])

$$(\frac{\partial w}{\partial t})_{\mathbf{x}} = (\frac{\partial w}{\partial t})_{\underline{\xi}} - (\frac{\partial \mathbf{x}}{\partial t})_{\underline{\xi}} \cdot \nabla w. \tag{3}$$

In our orthogonal coordinate system,

$$(\frac{\partial w}{\partial t})_{x,\sigma} = (\frac{\partial w}{\partial t})_{\xi,\eta} + \frac{1}{h_\eta h_\xi}(\frac{\partial w}{\partial \xi}\frac{\partial \sigma}{\partial \eta} - \frac{\partial w}{\partial \eta}\frac{\partial \sigma}{\partial \xi})(\frac{\partial x}{\partial t})_{\xi,\eta} - \frac{1}{h_\eta h_\xi}(\frac{\partial w}{\partial \xi}\frac{\partial x}{\partial \eta} - \frac{\partial w}{\partial \eta}\frac{\partial x}{\partial \xi})(\frac{\partial \sigma}{\partial t})_{\xi,\eta}. \tag{4}$$

The fluid mechanics part of the problem, then, is to obtain solutions of the Navier-Stokes equations using a finite-difference approximation in the boundary-fitted (ξ,η)-coordinates. With axisymmetry assumed, the Navier-Stokes equations are most conveniently expressed in terms of the stream function ψ and

vorticity ω in the form

$$\frac{R}{2}\left[\left(\frac{\partial\omega}{\partial t}\right)_{x,\sigma}+\frac{1}{h_\eta h_\xi}\left\{\frac{\partial\psi}{\partial\xi}\frac{\partial}{\partial\eta}\left(\frac{\omega}{\sigma}\right)-\frac{\partial\psi}{\partial\eta}\frac{\partial}{\partial\xi}\left(\frac{\omega}{\sigma}\right)\right\}\right]=L^2(\omega\sigma), \tag{5}$$

$$L^2\psi+\omega=0, \tag{6}$$

where $(\partial\omega/\partial t)_{x,\sigma}$ is calculated according to the transformation shown in (4), and

$$L^2\equiv\frac{1}{h_\eta h_\xi}\left\{\frac{\partial}{\partial\xi}\left(\frac{f}{\sigma}\frac{\partial}{\partial\xi}\right)+\frac{\partial}{\partial\eta}\left(\frac{1}{f\sigma}\frac{\partial}{\partial\eta}\right)\right\}. \tag{7}$$

The symbol R denotes an appropriate Reynolds number for the specific problem of interest.

We assume, for convenience, that the coordinate mapping is defined with $\xi = 1$ corresponding to the interface (Fig. 1), and $\eta = 0$ and $\eta = 1$ to the symmetry axes. The boundary conditions at the symmetry axes are

$$\psi=0,\quad \omega=0 \qquad \text{at} \quad \eta=0,\ 1. \tag{8}$$

At the gas-liquid interface ($\xi = 1$) we require

$$\psi=\int_0^\eta(-u_\xi)\sigma h_\eta d\eta=\int_0^\eta\left(-\frac{1}{|\nabla F|}\frac{\partial F}{\partial t}\right)\sigma h_\eta d\eta, \tag{9}$$

corresponding to the kinematic condition. In (9) F is a function that describes the bubble shape as $F(\mathbf{x},t) = 0$, and u_ξ is the inward normal velocity. In addition, the vorticity at the bubble surface is given by

$$\omega=\frac{2}{h_\eta}\frac{\partial u_\xi}{\partial\eta}+2\kappa_{(\eta)}u_\eta, \tag{10}$$

corresponding to the condition of zero tangential stress (where $\kappa_{(\eta)}$ is the normal curvature of the interface in the η-direction and u_η is the tangential velocity). Finally, the normal stress contributions due to pressure and viscous forces, on the one hand, and the capillary force, on the other, are required to balance.

$$\tau_{\xi\xi}-\frac{4}{W}(\kappa_{(\eta)}+\kappa_{(\phi)})=0 \tag{11}$$

In (11) $\kappa_{(\phi)}$ is the normal curvature in the ϕ-direction, W is the (dimensionless) Weber number, and $\tau_{\xi\xi}$ is the total normal stress, which includes both static and dynamic pressure and viscous contributions. In terms of the (ξ,η)-coordinates, $\tau_{\xi\xi}$ can be calculated in the form

$$\tau_{\xi\xi} = -p + \frac{8}{R}e_{\xi\xi} = -p + \frac{8}{R}\left(\frac{1}{h_\xi}\frac{\partial u_\xi}{\partial \xi} + \frac{u_\eta}{h_\xi h_\eta}\frac{\partial h_\xi}{\partial \eta}\right).$$

To obtain the pressure at the interface, we use the equation of motion. For the problem of unsteady bubble deformation in a uniaxial straining flow, the pressure can be calculated from the equation of motion in the form

$$\nabla(u^2 + p) = -2\left(\frac{\partial \mathbf{u}}{\partial t}\right)_{x,\sigma} + 2(\mathbf{u} \wedge \underline{\omega}) - \frac{4}{R}(\nabla \wedge \underline{\omega}), \tag{12}$$

where $\underline{\omega} = (0, 0, -\omega)$. By taking the η-component of (12) and integrating with respect to η we get

$$\begin{aligned} p = &- (u_\xi^2 + u_\eta^2) + \int_0^\eta \Big[2u_\xi \omega h_\eta - \frac{4}{R}\left(\frac{1}{\sigma}\frac{h_\eta}{h_\xi}\right)\frac{\partial}{\partial \xi}(\sigma\omega) \\ &- 2\mathbf{e}_\eta(t) \cdot \left(\frac{\partial \mathbf{u}}{\partial t}\right)_{x,\sigma} h_\eta\Big] d\eta + C(t), \end{aligned} \tag{13}$$

where $\mathbf{e}_\eta(t)$ is the unit tangent vector at the bubble surface. The term $\mathbf{e}_\eta(t) \cdot (\partial \mathbf{u}/\partial t)_{x,\sigma}$ is calculated in the form

$$\mathbf{e}_\eta(t) \cdot \left(\frac{\partial \mathbf{u}}{\partial t}\right)_{x,\sigma} = \left(\frac{\partial u_\eta}{\partial t}\right)_{x,\sigma} + u_\xi\Big[e_{\eta\sigma}\left(\frac{\partial e_{\eta x}}{\partial t}\right)_{x,\sigma} - e_{\eta x}\left(\frac{\partial e_{\eta\sigma}}{\partial t}\right)_{x,\sigma}\Big], \tag{14}$$

where $e_{\eta x}$ and $e_{\eta\sigma}$ represent the x, and σ-directional components of $\mathbf{e}_\eta$, and all time derivatives are evaluated by the formula (4). The unknown time-dependent constant $C(t)$ is determined from the constraint of constant volume,

$$V = 2 \mid \pi \int_0^1 \left(\sigma^2 \frac{\partial x}{\partial \eta}\right)_{\xi=1} d\eta \mid = \text{constant}.$$

The normal curvatures $\kappa_{(\eta)}$ and $\kappa_{(\phi)}$ are calculated by

$$\kappa_{(\eta)} = \frac{1}{{h_\eta}^3}\left(\frac{\partial x}{\partial \eta}\frac{\partial^2 \sigma}{\partial \eta^2} - \frac{\partial^2 x}{\partial \eta^2}\frac{\partial \sigma}{\partial \eta}\right), \tag{15}$$

$$\kappa_{(\phi)} = -\frac{1}{\sigma h_\eta}\frac{\partial x}{\partial \eta}. \tag{16}$$

Since the boundary conditions at $\xi = 0$ (the far-field boundary in many cases) depend on the particular problem, they are not given here.

III. DISCRETIZATION AND BACKWARD TIME DIFFERENCING

In our numerical analysis, we want to solve the equations given in Sec. II in the time-independent square domain of (ξ, η). If we discretize the equations and boundary conditions onto an $N_\xi \times N_\eta$ grid system, then we can conceptually describe the resulting system of equations as a system of first-order ordinary differential equations in t with $(4 \times N_\xi \times N_\eta + 1)$ unknowns (the unknowns are the mapping functions x and σ, the stream function, and the vorticity values at all grid points and the unknown constant $C(t)$ in the pressure equation). Symbolically, we can write

$$\mathbf{M}(\mathbf{w}(t))\frac{d\mathbf{w}}{dt} = \mathbf{f}(\mathbf{w}(t)), \qquad \mathbf{f} : \mathbf{R}^{(4\times N_\xi \times N_\eta + 1)} \rightarrow \mathbf{R}^{(4\times N_\xi \times N_\eta + 1)} \tag{17}$$

with

$$\mathbf{w} = \mathbf{w}_0 \qquad \text{at} \quad t = 0,$$

where

$$\mathbf{w} = \left(x_{11}, \cdots, x_{N_\xi N_\eta}, \sigma_{11}, \cdots, \sigma_{N_\xi N_\eta}, \psi_{11}, \cdots, \psi_{N_\xi N_\eta}, \omega_{11}, \cdots, \omega_{N_\xi N_\eta}, C(t)\right),$$

and $\mathbf{M}(\mathbf{w}(t))$ is a non-invertible coefficient matrix.

A most important feature for any unsteady, numerical solution scheme is temporal stability since such techniques will frequently be used to study the time-dependent evolution of systems that are very near to critical or marginal stability points. To insure numerical stability in the present case, we adopt a fully implicit, backward time-differencing scheme for all governing equations and boundary conditions.

$$\mathbf{M}(\mathbf{w}^{n+1})\frac{\mathbf{w}^{n+1} - \mathbf{w}^n}{\Delta t} = \mathbf{f}(\mathbf{w}^{n+1}), \tag{18}$$

where $\mathbf{w}^n$ stands for the variable vector evaluated at the (n)-th time step. Although fully implicit time-differencing results in a huge system of highly coupled nonlinear algebraic equations for each time step, the absolute stability enables us to choose the step size arbitrarily as long as the discretization error is not significant.

The actual system of nonlinear algebraic equations in the present case is extremely complicated. In addition, the integrals in the boundary conditions (the kinematic condition, the normal stress condition, and the constant volume constraint) make the problem even more complicated. However, the governing equations can be expressed in a standard form after discretization and time stepping as

$$0 = f^2 \frac{\partial^2 w}{\partial \xi^2} + \frac{\partial^2 w}{\partial \eta^2} + q_1 \frac{\partial w}{\partial \xi} + q_2 \frac{\partial w}{\partial \eta} + q_3 w + q_4,$$

in which q's are coefficients that do not depend explicitly on w (the discretization is not shown explicitly here for simplicity). The q's for the example problem will be given explicitly in Sec. V. Although the boundary conditions are very complicated, the discretization of governing equations into the form above enables us to use the global iterative scheme, which is discussed below.

IV. SOLUTION ALGORITHM

The problem, from a numerical point of view, is to solve simultaneously the differential Eqs. (1),(4), and (5) for the mapping functions and the stream function/vorticity fields subject to conditions (8)-(11) at the interface $\xi = 1$ and $\eta = 0, 1$ as indicated above. Inherent in the mapping functions and boundary conditions is the shape of the interface as a function of time. Our transient algorithm is based on a fully implicit time-stepping procedure as described in the preceding section, and an iterative ADI method to solve the system of algebraic equations at each time step. A brief summary of our algorithm is as follows.

1. Choose some initial state (bubble shape and velocity field) for given values of the parameters R and W. Usually we take the steady or transient solution

for some different values of R or W as the initial state, and at $t = 0$ we suddenly change R or W to the desired values.

2. Starting from this initial state, solve simultaneously the discretized version of the governing equations (1), (4), and (5) subject to the boundary conditions (8)-(11) using the iterative ADI method, to determine the stream function/vorticity and coordinate mapping functions (and thus the interface shape) for $t = \Delta t$.
3. Predict the solution for $t = (n+1)\Delta t$, $(n \geq 1)$ using the two previous time step solutions (Predictor step : Here it should be noted that the predicted solution does not satisfy all equations and boundary conditions, and that this step does not change the final result for each time step at all).
4. Starting from the predicted initial guess for the solution at the (n+1)-st time step, iteratively solve the discretized version of the governing equations (1), (4), and (5), subject to the boundary conditions (8)-(11), for the (n+1)-st time step until all equations and boundary conditions are satisfied (Corrector step : Same as step 2).
5. Repeat steps 3 and 4 for the next time step.

Now let us look at the details of the predicor and corrector steps.

A. Prediction of the (n+1)-st time-step solution

In this step, we predict the (n+1)-st time-step solution from the (n)-th and (n-1)-st time-step solutions. Let $\tilde{\mathbf{w}}^n$ and $\mathbf{w}^n$ denote the predicted solution and the converged solution after the corrector step for the (n)-th time step $t = t^n$ (t^n stands for t at the (n)-th time step). In order to simplify this predictor step as much as possible, we use basically an explicit time-differencing. However, since the coefficient matrix $\mathbf{M}$ in (17) is singular (note that there is no time derivative in the mapping equations and the stream function equation), we cannot simply get an expression for $\tilde{\mathbf{w}}^{n+1}$ directly from the explicit time differencing formula. However, if the solution of (17) is regular everywhere at any time, then without

loss of any generality we can decompose $\mathbf{M}$ and $\mathbf{w}$ into singular and non-singular parts

$$\begin{pmatrix} \tilde{\mathbf{M}}_{11} & 0 \\ 0 & 0 \end{pmatrix} \begin{pmatrix} \dot{\mathbf{w}}_1 \\ \dot{\mathbf{w}}_2 \end{pmatrix} = \begin{pmatrix} \tilde{\mathbf{f}}_1(\mathbf{w}) \\ \tilde{\mathbf{f}}_2(\mathbf{w}) \end{pmatrix} \tag{19}$$

where $\tilde{\mathbf{M}}_{11}$ is a non-singular matrix and $\mathbf{w}_1$ and $\mathbf{w}_2$ are the variable vectors corresponding to non-singular and singular parts, respectively. Then, for the non-singular part we get

$$\tilde{\mathbf{M}}_{11}\dot{\mathbf{w}}_1 = \tilde{\mathbf{f}}_1(\mathbf{w}).$$

The explicit time differencing at $t = t^n$ gives

$$\tilde{\mathbf{M}}_{11}(\mathbf{w}^n)\frac{\tilde{\mathbf{w}}_1^{n+1} - \mathbf{w}_1^n}{(\Delta t)^n} = \tilde{\mathbf{f}}_1(\mathbf{w}^n), \tag{20}$$

and the implicit time differencing at $t = t^n$ gives

$$\tilde{\mathbf{M}}_{11}(\mathbf{w}^n)\frac{\mathbf{w}_1^n - \mathbf{w}_1^{n-1}}{(\Delta t)^{n-1}} = \tilde{\mathbf{f}}_1(\mathbf{w}^n), \tag{21}$$

where $(\Delta t)^n = t^{n+1} - t^n$. By eliminating $\tilde{\mathbf{M}}_{11}(\mathbf{w}^n)$ and $\tilde{\mathbf{f}}_1(\mathbf{w}^n)$ from (20) and (21), we get

$$\tilde{\mathbf{w}}_1^{n+1} - \mathbf{w}_1^n = \frac{(\Delta t)^n}{(\Delta t)^{n-1}}(\mathbf{w}_1^n - \mathbf{w}_1^{n-1}). \tag{22}$$

To obtain a predictor expression for $\mathbf{w}_2$, we consider $\tilde{\mathbf{f}}_2(\mathbf{w}) = \tilde{\mathbf{f}}_2(\mathbf{w}_1, \mathbf{w}_2) = 0$. By differentiating with respect to time, we have

$$\dot{\mathbf{w}}_2 = -\left[\frac{\partial \tilde{\mathbf{f}}_2}{\partial \mathbf{w}_2}\right]^{-1}\left[\frac{\partial \tilde{\mathbf{f}}_2}{\partial \mathbf{w}_1}\right]\dot{\mathbf{w}}_1. \tag{23}$$

Then, by a similar procedure to that shown above we obtain

$$\tilde{\mathbf{w}}_2^{n+1} - \mathbf{w}_2^n = \frac{(\Delta t)^n}{(\Delta t)^{n-1}}(\mathbf{w}_2^n - \mathbf{w}_2^{n-1}). \tag{24}$$

From (22) and (24), we have the expression for the prediction step,

$$\tilde{\mathbf{w}}^{n+1} - \mathbf{w}^n = \frac{(\Delta t)^n}{(\Delta t)^{n-1}}(\mathbf{w}^n - \mathbf{w}^{n-1}). \tag{25}$$

. Equation (25) is used to predict the (n+1)-st time-step values $\tilde{\mathbf{w}}^{n+1}$ from $\mathbf{w}^n$ and $\mathbf{w}^{n-1}$.

B. Iterative ADI method for the corrector step

The global iterative scheme used for this step is a slight modification of the steady ADI algorithm of Ryskin and Leal.[13] A brief summary of the scheme is as follows (see also the details in Ryskin and Leal[13]).

1. Start with the predicted values of ψ, ω and the mapping functions from the prediction step.
2. Obtain an approximation to the stream function and vorticity fields by carrying out some small number of iterations.
3. Check the normal stress condition, and if it is not satisfied, modify the interface shape so as to reduce the imbalance between the total stress $\tau_{\xi\xi}$ and the surface tension term $\frac{4}{We}(\kappa_{(\eta)} + \kappa_{(\phi)})$.
4. Compute a new orthogonal coordinate system by carrying out some small number of iterations on the mapping equations.
5. Calculate the outward normal velocity $(-u_\xi)$ of the interface from the kinematic condition and calculate the stream-function values at the interface grid points.
6. Return to step 2 and repeat until all equation and boundary conditions are satisfied to a pre-determined level of accuracy.

V. APPLICATION TO THE PROBLEM OF UNSTEADY BUBBLE DEFORMATION

The technique described above has been applied to the problem of unsteady bubble deformation in a uniaxial straining flow. Results from this solution will be discussed in the later part of this paper. Here we touch only upon the numerical aspects of implementing the above scheme.

The far-field boundary conditions for the uniaxial straining flow are

$$\psi \sim \frac{1}{2} x\sigma^2, \quad \omega \to 0 \quad \text{for} \quad \xi \to 0.$$

In this problem we assume symmetry with respect to the equatorial plane as well as axial symmetry, therefore only the $x \geq 0$, $\sigma \geq 0$ quadrant needs to be considered. The distortion function f was chosen as $f = \pi\xi/2$. In Fig. 2, one example of a coordinate system generated for this problem is shown for the region near the bubble; it should be noted, however, that the coordinate system actually extends to infinity (see below). For illustrative purpose we plot the coordinate system for the whole bubble, but in the real calculation we considered the $x \geq 0$, $\sigma \geq 0$ quadrant only.

In order to deal with the infinite domain, we use the two-step mapping technique of Ryskin and Leal[13]; first an orthogonal mapping is computed numerically, which maps the (ξ, η) unit square to an auxiliary finite domain in (x^*, σ^*)-coordinates (x^*, σ^* satisfy (1)); then a conformal inversion $x + i\sigma = (x^* - i\sigma^*)^{-1}$ is used to map the (x^*, σ^*) auxiliary domain to the infinite domain in the (x, σ) physical space. Since finite-difference equations are written only at interior points, all coefficients in the equations will be finite even though the (x, σ)-domain will be infinite. Since the stream function tends to ∞ as $\xi \to 0$, a new unknown stream function ψ^* was introduced, which is bounded (see Ryskin and Leal[13] for details).

$$\psi^* \equiv \psi - \frac{1}{2} x\sigma^2(1 - \xi^5)$$

With these newly introduced variables, the system of nonlinear equations for each time step (Eq.(18)) can be expressed in a standard form

$$0 = f^2 \frac{\partial^2 w}{\partial \xi^2} + \frac{\partial^2 w}{\partial \eta^2} + q_1 \frac{\partial w}{\partial \xi} + q_2 \frac{\partial w}{\partial \eta} + q_3 w + q_4, \tag{26}$$

in which the q's are coefficients that do not depend explicitly on w. The detailed expressions for the q's are given in Table I. The system of discretized equations

represented by (26) for the (ξ, η)-coordinate system has been solved with appropriate boundary conditions using the solution algorithm that was outlined previously.

The solutions reported in the next section were all obtained on a 40×40 grid in ξ and η, using a fully vectorized code on the CRAY X-MP/24 of Boeing Computer Services in Seattle. The computation times for several typical cases are shown in Table II. It should be noted that, however, there was considerable variation in the computation times depending upon ADI parameters, convergence criteria, the accuracy of the initial guess for steady-state solutions, and other factors. In our computation we have used the following three criteria to establish convergence.

1. The residual of the governing equations for each time step is given by Eq. (26). For the discrete solution of numerical analysis we can define the residual as ($\tilde{w}$ denotes the discrete solution)

$$R_i = f^2 \frac{\partial^2 \tilde{w}_i}{\partial \xi^2} + \frac{\partial^2 \tilde{w}_i}{\partial \eta^2} + q_1 \frac{\partial \tilde{w}_i}{\partial \xi} + q_2 \frac{\partial \tilde{w}_i}{\partial \eta} + q_3 \tilde{w}_i + q_4$$

$$\text{for} \quad i = 1, 2, \cdots, 6400 \quad (4 \times N \times N).$$

   The convergence criterion is

$$\max_{1 \le i \le 6400} | R_i | < 10^{-3}.$$

2. Volume conservation

$$\frac{| V - V_0 |}{V_0} < 10^{-3}$$

3. Normal stress condition

$$\max_{1 \le k \le 41} | \Pi(\eta_k) | = \max_{1 \le k \le 41} | W \tau_{\xi\xi} - 4(\kappa_{(\eta)} + \kappa_{(\phi)}) | < 10^{-2}$$

Since all other boundary conditions (the kinematic condition and the vanishing tangential stress condition) are included in the calculation of boundary values for ψ^* and ω, they are automatically satisfied if the maximum residual goes to zero.

VI. INTRODUCTION TO UNSTEADY BUBBLE DEFORMATION IN A UNIAXIAL STRAINING FLOW

In the following sections of this paper we consider the unsteady deformation of a bubble in a uniaxial straining flow at finite Reynolds number. Although many theoretical studies have been done on bubble motion in zero (or very small) Reynolds number flow,[1,20–25] very few investigations have been done for the finite-Reynolds-number regime. Recently, however, Ryskin and Leal[15] studied the *steady* bubble deformation problem in a uniaxial straining flow using the boundary-fitted orthogonal mapping technique for Reynolds numbers ranging from 0.1 to 100, as well as for potential flow, $R = \infty$. The potential flow problem was also studied by Miksis[26] using a boundary-integral method.

One interesting result in both of these previous investigations was that steady solutions could be obtained only for Weber numbers below a certain critical value, W_c, which depended on the Reynolds number. The critical values predicted by Miksis[26] and by Ryskin and Leal[15] for the potential flow problem using totally different numerical techniques were in very close agreement. Partly as a consequence of this, Ryskin and Leal suggested that steady axisymmetric solutions must not exist for larger values of W, i.e., that W_c represented a limit point for the branch of solutions that emanates from the zero flow limit. However, this speculation could not be verified using the ADI technique that they employed. Therefore, in this paper, we analyze the same problem using the full unsteady code that was described in the preceding sections of this paper.

In the first part of this study, we solve the initial value problem with given initial conditions for supercritical and subcritical Weber numbers. From this study we can verify the existence of a critical value of the Weber number for bubble breakup and we can also determine the effect of initial conditions on the critical value. In addition, we can also examine the bubble breakup mechanism in a straining flow at finite Reynolds number, which has not previously been studied.

In the second part, we study the oscillatory motion of a bubble in a potential flow for Weber numbers below the critical value. In a companion paper, Kang and Leal,[27] we have studied the small amplitude oscillatory motion of a nearly spherical bubble in an axisymmetric inviscid straining flow by means of a perturbation analysis for $W \ll 1$. We found that the frequency of oscillation decreases as the Weber number increases, for example, in the case of the principal mode ($n = 2$), $\omega^2 = \omega_0^2(1 - 0.31W)$ where ω_0 is the oscillation frequency of a bubble in a quiescent fluid. Furthermore, by extending the resulting formula for oscillation frequency to finite W, as well as a numerical analysis of bubble oscillations about a *spherical* base shape, we suggested that the oscillation frequency should go to zero at a certain value of the Weber number. Of course, the analysis of small amplitude oscillations is based upon small (or zero) W approximations of the steady-state shape, and one should expect that the true zero frequency point will be different from the value found by the perturbation analysis or, in the extreme, that the zero frequency point may not exist at all. In the present paper, we study the same problem by means of a full, unsteady numerical analysis to obtain accurate results for higher Weber numbers, and to find the zero frequency point.

VII. STATEMENT OF THE PROBLEM

We consider the unsteady deformation of an incompressible gas bubble of volume $\frac{4}{3}\pi a^3$ in an axisymmetric straining flow of a fluid with constant density ρ and constant viscosity μ. The density and viscosity of the gas inside the bubble are assumed to be negligible in comparison with those of the liquid. Furthermore, the surface of the bubble is assumed to be characterized completely by a uniform surface tension γ. Finally, we neglect all effects of gravity including the hydrostatic pressure variation in the fluid. If the x-axis of the cylindrical coordinate (x, σ, ϕ) is directed along the axis of symmetry, the (dimensional)

velocity field far from the bubble is given by

$$\mathbf{u} = \mathbf{E} \cdot \mathbf{r}, \quad \mathbf{E} = E \begin{pmatrix} 1 & 0 & 0 \\ 0 & -\frac{1}{2} & 0 \\ 0 & 0 & -\frac{1}{2} \end{pmatrix}, \quad E > 0,$$

where E is the principal strain rate. We use the equivalent radius a of the bubble as a characteristic length scale, the product Ea as a characteristic velocity scale, and E^{-1} as a characteristic time scale.

The numerical solution is computed in a time-dependent, boundary-fitted orthogonal coordinate system (ξ, η, ϕ) obtained by the technique described in Secs. II - V. All necessary equations and boundary conditions were also given in Sec. II. The results reported here were obtained on a 40×40 grid in the (ξ, η)-coordinate system and we used several time-step values ranging from 10^{-3} to 10^{-1} depending on the problem. The relevant dimensionless parameters are the Reynolds number $R \equiv 2\rho(Ea)a/\mu$ based on the equivalent diameter $2a$ of the bubble and the Weber number $W \equiv 2\rho(Ea)^2 a/\gamma$.

VIII. NUMERICAL RESULTS AND DISCUSSION

A. Unsteady deformation of the bubble for slightly supercritical Weber numbers

We have already noted that Ryskin and Leal[15] could not obtain steady solutions numerically beyond a *critical* Weber number, denoted below as W_c^{ss}, which depended on the Reynolds number. The critical values estimated by Ryskin and Leal were $0.9 < W_c^{ss} < 1.0$ for R=10, $2.1 < W_c^{ss} < 2.2$ for R=100, and $2.7 < W_c^{ss} < 2.8$ for $R = \infty$ (potential flow solution).

In this section, we consider the unsteady deformation of a bubble for Weber numbers that are slightly above the critical value for the $R = 10$, 100, and ∞ cases. We begin with the steady solution at slightly subcritical Weber numbers, specifically, $W = 0.9$ for $R = 10$, $W = 2.1$ for $R = 100$, and $W = 2.7$ for $R = \infty$. Then, at $t = 0$, we suddenly change the Weber number to slightly

supercritical values ($W = 1.0$ for $R = 10$, $W = 2.2$ for $R = 100$, and $W = 2.8$ for $R = \infty$) and follow the subsequent deformation of the bubble. The results are shown by the solid curves in Figs. 3, 4, and 5, which show the dimensionless half-length of the bubble $l_{1/2}$ (radius in the direction of x-axis) plotted as a function of dimensionless time. As we can see in Figs. 3, 4, and 5, if the Weber number is larger than the critical value, W_c^{ss}, the bubble will extend without limit eventually leading to bubble breakup. In Figs. 3, 4, and 5, the corresponding bubble shapes are also shown at points identified by letters A, B, C, D, etc. As we can see, the elongation rate increases rapidly after the waist appears ($\kappa_{(\eta)} < 0$), asymptotically approaching the rate of extension of a line element of the undisturbed flow ($dl_{1/2}/dt \rightarrow l_{1/2}$); It is noteworthy that the bubble deformation is primarily associated with an increase in length, rather than a rapid change in the magnitude of curvature at the waist, $\kappa_{(\eta)} < 0$, as might be expected if surface tension were a dominant factor.

The critical Weber numbers obtained above, by studying the time-dependent response to a small increment in W from a slightly sub-critical steady state, represent an upper bound on W for the existence of steady bubble shapes on the solution branch emanating from the spherical equilibrium state for zero Weber number. Specifically, a bubble may not attain a steady shape even at subcritical Weber numbers (i.e., $W < W_c^{ss}$) if the initial deformation is sufficiently far from the steady shape. In order to test the effect of initial deformation, we also reduced the Weber numbers to subcritical values after first achieving a finite deformation via the continuous stretching mode described in the preceding paragraph. When the Weber number was changed, the initial value of the velocity field was retained to simulate a real experiment. As we can see in Figs. 3-5, the bubble returns to the steady state only if the initial deformation does not exceed a certain critical magnitude. For example, in the $R = 10$ case, the two solution branches for $W = 0.9$ show very much different behavior, depending on the initial shape at the point where the Weber number is reduced.

When the Weber number is reduced with $l_{1/2} = 1.8$, the bubble returns to the steady shape obtained by Ryskin and Leal[15] via their steady code. When $l_{1/2}$ is increased only a little more to 2.0, however, a reduction of W to 0.9 only reduces the rate of bubble stretch, but does not stop it. On the other hand, when W is reduced to 0.8 from the same initial deformation, $l_{1/2} \sim 2$, the bubble returns to the steady-state shape for $W = 0.8$. Similar behavior is shown for $R = 100$ and $R = \infty$ in Figs. 4 and 5, with the added effect of overshoot in the shape for some cases as the bubble is driven back toward the appropriate steady state after reduction of W to a subcritical value.

B. Unsteady deformation of a bubble in start-up from rest

The results of the previous section show that a bubble will always extend without limit if the Weber number is larger than the critical value found by Ryskin and Leal[15] (i.e., $W > W_c^{ss}$). Furthermore, if a bubble is initially extended sufficiently beyond the steady-state shape, it will extend indefinitely even at some subcritical Weber numbers ($W < W_c^{ss}$). In this section we consider the unsteady deformation of a bubble starting from a spherical shape. This numerical experiment can be thought of as a step increase in W from zero to a new constant value at $t = 0$. In this case a bubble in a sub-critical flow (i.e., $W < W_c^{ss}$) might not attain a steady shape due, essentially, to an inertial *overshoot* of shape.

The results for $R = 10$, $R = 100$ and $R = \infty$ are shown in Fig. 6. For $R = 10$, the shape overshoot is negligible and the bubble monotonically approaches the steady state for all $W \leq W_c^{ss}$. On the other hand, for $R = 100$ and $R = \infty$, the bubble overshoots the steady-state shape at subcritical Weber numbers and may thus achieve a sufficient degree of elongation, i.e., a maximum value of $l_{1/2}$, that they cannot recover, and thus will extend indefinitely to breakup. For example, for $W = 2.1$ and $R = 100$, and for $W = 2.7$ and $R = \infty$, we see that the bubble undergoes a continuous stretching process, following the transient overshoot on start-up, even though a steady-state solution exists for

these values of W and R. In contrast, however, if W is decreased a little to values of 2.0 and 2.5, respectively, the degree of overshoot is not sufficient to reach the critical deformation for onset of continuous extension. In this case, for $R = 100$, $W = 2.0$, the bubble undergoes a damped oscillation to the steady state. For $R = \infty$, $W = 2.5$, the oscillation is undamped because of the absence of viscosity. Comparing the results of Fig. 6, with the earlier results of Figs. 3-5, it appears that the minimum value of $l_{1/2}$ required for continuous extension at a given W and R is the same, whether achieved via an inertial overshoot in start-up or by an initial stretching the bubble at some supercritical value of W.

The results in this and the previous section strongly suggest that steady state solutions are possible only for Weber numbers less than critical values that depend on the *initial* degree of deformation. The maximum critical value, W_c^{ss}, is the value obtained by Ryskin and Leal.[15] In the present study, we obtain the same upper bound by considering very small increments from a slightly subcritical initial steady state. If the bubble shape is sufficiently deformed at some initial instant, either as a consequence of stretching in a flow with $W > W_c^{ss}$, or as a consequence of initial overshoot of the shape in start-up from a sphere, the bubble will stretch at lower values of W. Of course, the initial shape cannot be simply characterized in terms of a single scalar parameter. However, if the initial deformation is not extremely large, we can attempt to correlate the initial half-length, $l_{1/2}$, with a critical Weber number, above which the bubble will not achieve a steady final shape. In Fig. 7, we plot this critical W as a function of $l_{1/2}$ at $t = 0$ for $R = 10$, 100 and ∞. From Fig. 7, we see that a bubble subjected to a flow that would be slightly subcritical if the bubble deformation were accomplished via a series of equilibrium steps will achieve a steady state shape only if the initial deformation is not too far from the steady shape when it is subjected to a step change in W at $t = 0$; in other words, the bubble shape in a subcritical flow is stable only in the neighborhood of steady state.

C. Sudden removal of external flow after very large deformation

In order to study the effect of a sudden removal of the external flow, we first generate a considerably elongated, though transient shape, by performing an unsteady analysis for $R = 10$ and $W = 1.5$ starting from the $R = 10$ and $W = 0.9$ steady solution as an initial condition. The half-length of the bubble and the corresponding bubble shapes are shown in Fig. 8. Since $W = 1.5$ is much larger than the critical value, the elongation is much faster than for the $W = 1.0$ case that was illustrated in Fig. 3, but the deformation characteristics (for example, the shape at the same value of $l_{1/2}$) are unchanged. Then after achieving a strongly deformed shape ($l_{1/2} = 2.63$, $w = 0.49$, $l_{1/2}/w = 5.4$: $l_{1/2}$ is the half-length along the axis and w is the half-width along the equatorial axis) at $t = 1.5$, we suddenly reduced the external flow rate by a factor of 100 (i.e., $E_{new} = E_{old}/100$). Thus, the new Reynolds number and Weber numbers are $R = 0.1$ and $W = 1.5 \times 10^{-4}$, respectively. Since the capillary number for this case is extremely small ($Ca = W/R = 1.5 \times 10^{-3}$), the changes in bubble shape after reduction of E are essentially due solely to surface tension driven motion. The most important factor for surface tension driven flows is the curvature of the bubble surface. In the specific case shown in Fig. 8, the total curvature at the end of the bubble ($\eta = 0$) is larger than that at the equator ($\eta = 1$), as shown in Fig. 9. Thus, upon removal of the external flow, the end points move in toward the equator, and as a consequence, the points near the equator move rapidly out. As the bubble changes shape, a circulatory flow is induced around the bubble as shown in Fig. 10. One more interesting fact is that an overshoot of the final steady shape is observed even at this very small Reynolds number. Since the initial deformation is very large and the surface tension driven motion is dominant, the contraction rate becomes so large that viscous damping is not sufficient to prevent overshoot of the shape.

In the specific case considered above, bubble breakup did not occur, because the initial deformation was not sufficient for the very small Weber number ($W =$

1.5×10^{-4}). Therefore, we performed the same calculations for larger Weber numbers ($W = 0.02$ and $W = 0.005$ for $R = 0.1$). The initial conditions were the same as the previous case, but from $t = 0$ we used different Weber numbers. The results are shown in Fig. 11. As we can see from Fig. 11, the $W = 0.02$ ($Ca = 0.2$) and the $W = 0.005$ ($Ca = 0.05$) cases exhibit totally different deformation behaviors. In the $W = 0.02$ case, the bubble is elongated continuously. On the other hand, for $W = 0.005$, the bubble will return to its steady-state shape. This result for $W = 0.02$ is consistent with the general perception that an elongated bubble or inviscid drop with a *waist* will extend indefinitely in an extensional flow at low Reynolds number (cf. Hinch[25]). However, the other cases considered in Fig. 11 show that this is not generally true. Specifically, the existence of a waist in an initially slender bubble does not lead to burst for very small Weber (or Capillary) numbers.

D. Oscillatory motion of a bubble in an inviscid straining flow

A bubble in a uniaxial straining flow exhibits quite interesting behavior as $R \to \infty$, because the bubble deformation is determined by the dynamic pressure distribution, which is governed by Bernoulli's theorem. For $R \to \infty$, Miksis[26] and Ryskin and Leal[15] obtained steady-state solutions using two different numerical techniques. However, to date unsteady transient solutions have not been obtained for this limiting case, except in the analytical work of Kang and Leal.[27]

Kang and Leal used a perturbation technique to study oscillatory motion of nearly spherical bubbles for small Weber numbers. They found, via a rigorous asymptotic solution for small Weber numbers, that the frequency of oscillation decreases (in terms of the surface tension based time scale) as the Weber number increases. This, in itself, is an interesting result because of the connection between the frequency of bubble shape oscillation and the bubble as a source of noise in hydro-acoustic flows. However, in addition, Kang and Leal suggested that the frequency of the lowest frequency mode should vanish at a critical We-

ber number of $O(1)$, and carried out an *ad hoc* perturbation analysis for finite W to demonstrate this fact, based upon a spherical base state rather than the actual bubble shape at each W, and small amplitude oscillations. The value of the Weber number at zero frequency, according to this *ad hoc* perturbation theory, is denoted henceforth as $W_{c,pert}$. For a Weber number exceeding $W_{c,pert}$, the bubble motion was found to be unstable. However, in an exact analysis, the zero frequency point of the lowest frequency mode should be the same as the limit point of the steady-state solution branch that includes the spherical shape as the zero Weber number solution. The reason is that the Jacobian matrix for the disturbance to steady state is singular at that point. In that sense, the zero frequency point obtained via the *ad hoc* perturbation analysis ($W_{c,pert}$) was interpreted as corresponding to the presence of a limit point for the existence of steady-state solutions rather than to a simple onset point of instability. The zero frequency point ($W_{c,pert}$) found in the perturbation analysis was 4.62, while the limit point predicted by Ryskin and Leal was $2.7 < W_c < 2.8$. It must be remembered, however, that the accuracy of the perturbation solution is limited in a rigorous sense to small Weber numbers where the base shape is nearly spherical. A more accurate analysis is required to show that the frequency of oscillation really goes to zero at a certain critical Weber number, and that the critical Weber number is exactly the same as the limit point for existence of steady-state solutions as predicted by Ryskin and Leal. In the present unsteady analysis, the frequency of oscillation is estimated as a function of the Weber number from finite amplitude changes of the bubble shape.

It should be noted, before discussing the results, that we use the natural surface tension based time scale in this case,

$$\tilde{t}_c = (\rho a^3/\gamma)^{1/2}.$$

The relationship between the two dimensionless times (t for $t_c = E^{-1}$ and $\tilde{t}$ for $\tilde{t}_c$) is easily shown to be

$$t = \sqrt{\frac{W}{2}}\,\tilde{t}.$$

The initial shapes in the numerical analysis were chosen in such a way to insure the dominance of the $P_2(\cos\theta)$ mode oscillation (for $W = 2.7$, we used the shape corresponding to point B in Fig. 5; for $W = 2.0$, 1.0, and 0.1, we used the steady state shape for $W = 2.7$). In order to illustrate typical numerical results, the half-length of the bubble along the symmetry axis $l_{1/2}$ is plotted as a function of time in Fig. 12 for $W = 1$. Several bubble shapes are also shown for the corresponding points indicated as $A \rightarrow G$. The effect of the time step size is also shown in Fig. 12. The dotted line and the solid line represent numerical solutions for the step sizes $\Delta t = 0.02$ and $\Delta t = 0.01$, respectively. It can be seen that there is considerable mode coupling for this finite amplitude oscillation.

In Fig. 13, the frequency of oscillation estimated from the numerical solution is compared with the approximate solutions of Kang and Leal.[27] The solid line represents the numerical results of the present work. The straight broken line is the rigorous first-order asymptotic solution for the small Weber number, as described earlier, while the curved broken line is the frequency change obtained under the *ad hoc* assumption that the steady-state shape is spherical for the whole Weber number range. As we can see in Fig. 13, all three results show excellent agreement for the small Weber number region. At larger Weber numbers, the exact numerical result and the *ad hoc* result for perturbation about the sphere diverge. Ironically, the straight-line estimate from the rigorous, $O(W)$, asymptotic theory provides a better estimate of the exact results in this regime than the *ad hoc* result, which was much more difficult to obtain. The most important results from Fig. 13, are that the oscillation frequency decreases as W increases and becomes zero at $W = W_c^{ss}$. In other words, the critical value of W obtained here for $\omega_2 = 0$ is exactly the same as the limit point of the steady solution branch predicted by Ryskin and Leal. By passing $W = W_c$, the oscillatory motion changes to indefinite deformation for $W > W_c$, which clearly indicates that a steady solution cannot be obtained numerically (see Fig. 5 and the discussion in Kang and Leal[27]).

IX. CONCLUSION

From the numerical study of unsteady bubble deformation in an axisymmetric straining flow we have reached the following conclusions;

1. Numerical analysis: The orthogonal mapping technique is very effective for investigation of transient free-boundary problems.

2. Fluid mechanics:

(1) The critical Weber number found from steady-state calculations has been confirmed as the point of onset of unsteady stretching, provided we start with a shape that is close to critical. In other words, the critical Weber number predicted by the breakdown of the steady algorithm corresponds to the limit point beyond which no steady solution exists on the solution branch emanating from the spherical equilibrium state for zero Weber number.

(2) We also found that the ability to attain a stable steady state at subcritical Weber numbers is strongly dependent on the initial shape. Generally, the critical Weber number decreases as the initial elongation from steady shape increases.

(3) We have shown, in one example, that a stretched bubble may return to equilibrium if the flow is removed too soon, instead of breaking up under the action of surface tension. The same behavior was found experimentally in an earlier study for drops in low Reynolds number stretching experiments (Stone *et al.*[28]).

(4) From the study of oscillatory motion of a bubble in an inviscid irrotational flow, we found that the oscillation frequency decreases as the Weber number increases, and becomes zero at a certain Weber number. We also found that the zero frequency point is exactly the same as the critical Weber number (the limit point) for the existence of steady solutions as found by the steady analyses of Miksis,[26] and Ryskin and Leal.[15] Therefore, once again the critical Weber number is confirmed to be the maximum Weber number under which a stable steady solution is possible, at least on this branch.

ACKNOWLEDGMENTS

All computations were carried out on CRAY X-MP/24 of Boeing Computer Services, and the authors wish to acknowledge the expert help and courtesy shown by Boeing employees. The authors also wish to thank Prof. R.A. Brown for his insightful comments on an earlier version of this paper.

This work was supported by grants from the Fluid Mechanics Program and the Office of Advanced Scientific Computing at the National Science Foundation.

REFERENCES

[1] G.K. Youngren and A. Acrivos, J. Fluid Mech. **76**, 433 (1976).

[2] J.M. Rallison and A. Acrivos, J. Fluid Mech. **89**, 191 (1978).

[3] A.S. Geller, S.H. Lee, and L.G. Leal, J. Fluid Mech. **169**, 27 (1986).

[4] J.-M. Vanden-Broeck and J.B. Keller, J. Fluid Mech. **101**, 673 (1980).

[5] F.H. Harlow and J.E. Welch, Phys. Fluids **8**, 2182 (1965).

[6] B.D. Nichols and C.W. Hirt, J. Comp. Phys. **8**, 434 (1971).

[7] G.B. Foote, J. Comp. Phys. **11**, 507 (1973).

[8] R. Bonnerot and P. Jamet, J. Comp. Phys. **25**, 163 (1977).

[9] C.S. Frederiksen and A.M. Watts, J. Comp. Phys. **39**, 282 (1981).

[10] D.R. Lynch, J. Comp. Phys. **47**, 387 (1982).

[11] P. Bach and O. Hassager, J Fluid Mech. **152**, 173 (1985).

[12] L.H. Ungar and R.A. Brown, J. Comp. Phys. submitted (1986).

[13] G. Ryskin and L.G. Leal, J. Fluid Mech. **148**, 1 (1984).

[14] G. Ryskin and L.G. Leal, J. Fluid Mech. **148**, 19 (1984).

[15] G. Ryskin and L.G. Leal, J. Fluid Mech. **148**, 37 (1984).

[16] D.S. Dandy and L.G. Leal, J. Fluid Mech., submitted (1986).

[17] C.I. Christov and P.K. Volkov, J. Fluid Mech. **158**, 341 (1985).

[18] G. Ryskin and L.G. Leal, J. Comp. Phys. **50**, 71 (1983).

[19] J.F. Thompson, Z.U.A. Warsi, and C.W. Masin, *Numerical Grid Generation* (North-Holland, Amsterdam, 1985).

[20] G.I. Taylor, Proc. R. Soc. Lond. **A 146**, 501 (1934).

[21] G.I. Taylor, in *Proc. 11th Intl Congr. Appl. Mech., (Munich, 1964)*, ed. by H. Görtler (Springer-Verlag, Berlin, 1966), p. 790.

[22] J.D. Buckmaster, J. Fluid Mech. **55**, 385 (1972).

[23] D. Barthes-Biesel and A. Acrivos, J. Fluid Mech. **61**, 1 (1973).

[24] A. Acrivos and T.S. Lo, J. Fluid Mech. **86**, 641 (1978).

[25] E.J. Hinch, J. Fluid Mech. **101**, 545 (1980).

[26] M.J. Miksis, Phys. Fluids **24**, 1229 (1981).

[27] I.S. Kang and L.G. Leal, J. Fluid Mech., submitted (1987).

[28] H.A. Stone, B.J. Bently, and L.G. Leal, J. Fluid Mech. **173,** 131 (1986).

TABLE I. Coefficients q's in Eq. (26).

w	q
x^*	$q_1 = f\dfrac{\partial f}{\partial \xi}$
σ^*	$q_2 = -\dfrac{1}{f}\dfrac{\partial f}{\partial \eta}$
	$q_3 = q_4 = 0$
ψ^*	$q_1 = f\dfrac{\partial f}{\partial \xi} - \dfrac{f^2}{\sigma}\dfrac{\partial \sigma}{\partial \xi}$
	$q_2 = -\dfrac{1}{f}\dfrac{\partial f}{\partial \eta} - \dfrac{1}{\sigma}\dfrac{\partial \sigma}{\partial \eta}$
	$q_3 = 0$
	$q_4 = -\dfrac{1}{2}(20f\sigma x\xi^3 + 15fx\xi^4\dfrac{\partial \sigma}{\partial \xi} + 5\sigma x\xi^4\dfrac{\partial f}{\partial \xi} + 10f\sigma\xi^4\dfrac{\partial x}{\partial \xi})(f\sigma) + h_\eta^2\sigma\omega$
ω	$q_1 = f\dfrac{\partial f}{\partial \xi} + \dfrac{f^2}{\sigma}\dfrac{\partial \sigma}{\partial \xi} - \dfrac{R}{2}fh_\eta u_\xi - \dfrac{R}{2}f(\dfrac{\partial \sigma}{\partial \eta})(\dfrac{\partial x}{\partial t})_{\xi,\eta} + \dfrac{R}{2}f(\dfrac{\partial x}{\partial \eta})(\dfrac{\partial \sigma}{\partial t})_{\xi,\eta}$
	$q_2 = \dfrac{1}{\sigma}\dfrac{\partial \sigma}{\partial \xi} - \dfrac{1}{f}\dfrac{\partial f}{\partial \eta} - \dfrac{R}{2}h_\eta u_\eta + \dfrac{R}{2}f(\dfrac{\partial \sigma}{\partial \xi})(\dfrac{\partial x}{\partial t})_{\xi,\eta} - \dfrac{R}{2}f(\dfrac{\partial x}{\partial \xi})(\dfrac{\partial \sigma}{\partial t})_{\xi,\eta}$
	$q_3 = \dfrac{R}{2}fh_\eta\dfrac{u_\xi}{\sigma}\dfrac{\partial \sigma}{\partial \xi} + \dfrac{R}{2}h_\eta\dfrac{u_\eta}{\sigma}\dfrac{\partial \sigma}{\partial \eta} - (\dfrac{f}{\sigma}\dfrac{\partial \sigma}{\partial \xi})^2 - (\dfrac{1}{\sigma}\dfrac{\partial \sigma}{\partial \eta})^2 - \dfrac{R}{2}\dfrac{fh_\eta h_\xi}{\Delta t}$
	$q_4 = \dfrac{R}{2}\dfrac{fh_\eta h_\xi}{\Delta t}\omega^{(n)}$

TABLE II. Computation time of typical cases on CRAY X-MP/24.

case	time step size	computation time(CPU sec/step)
$R = \infty$		
$W = 1.0^a$	0.01	0.5 - 0.7
(oscillatory motion)		
$R = 10$		
$W = 1.0$	0.1	2 - 3
(initial stage)		
$R = 10$		
$W = 1.0$	0.1	10 - 15
(after very large deformation)		

[a] Convergence criterion for the normal stress condition $| \Pi | < 10^{-1}$ was used for this case, and $| \Pi | < 10^{-2}$ was used for others.

FIGURE CAPTIONS

Fig. 1. Time-dependent boundary-fitted orthogonal curvilinear coordinate system.

Fig. 2. The boundary-fitted coordinate system for the problem of a unsteady bubble deformation in an uniaxial extensional flow.

Fig. 3. Unsteady bubble deformation near the critical Weber number (half-length and shapes for $R = 10$) (asymptotic curve is given by $dl_{1/2}/dt = l_{1/2}$ with an appropriate initial condition).

Fig. 4. Unsteady bubble deformation near the critical Weber number (half-length and shapes for $R = 100$) (asymptotic curve is given by $dl_{1/2}/dt = l_{1/2}$ with an appropriate initial condition).

Fig. 5. Unsteady bubble deformation near the critical Weber number (half-length and shapes for $R = \infty$) (asymptotic curve is given by $dl_{1/2}/dt = l_{1/2}$ with an appropriate initial condition).

Fig. 6. Unsteady deformation of a bubble in start-up from rest.

Fig. 7. The effect of initial condition (half-length) on the critical Weber number.

Fig. 8. Unsteady bubble deformation after a sudden removal of external flow after a very large deformation (half-length and shapes for $R = 10$, $W = 1.5$ case ——— ; $R = 0.1$, $W = 1.5 \times 10^{-4}$ case – – – – – ; E_0 is the strain rate of the original flow).

Fig. 9. The curvatures of bubble surface at the time of flow removal ($\eta = 0$ corresponds to the symmetric axis and $\eta = 1$ correponds to the equatorial plane).

Fig. 10. Unsteady flow field around a deforming bubble after a sudden removal of the external flow ($t = t'/E^{-1}$).

10a. Velocity field before and after overshoot.

10b. Magnified velocity field (factor of 3 compared with Fig. 10(a)) after overshoot.

Fig. 11. Unsteady deformation of a bubble at low Reynolds number, which is initially slender and has a long wave length.

Fig. 12. An example of oscillatory bubble motion in an inviscid straining flow, and the effect of time-step size on the artificial damping and the frequency change (half-length and shapes as a function of dimensionless time based on straining rate; .———— $\Delta t = 0.01$; - - - - - $\Delta t = 0.02$).

Fig. 13. Comparison of the present numerical solution, with the perturbation solution of Kang and Leal[27] (◊ numerical solution; – – – – perturbation solution; ω_2 is the oscillation frequency of the principal mode in terms of the surface tension time scale).

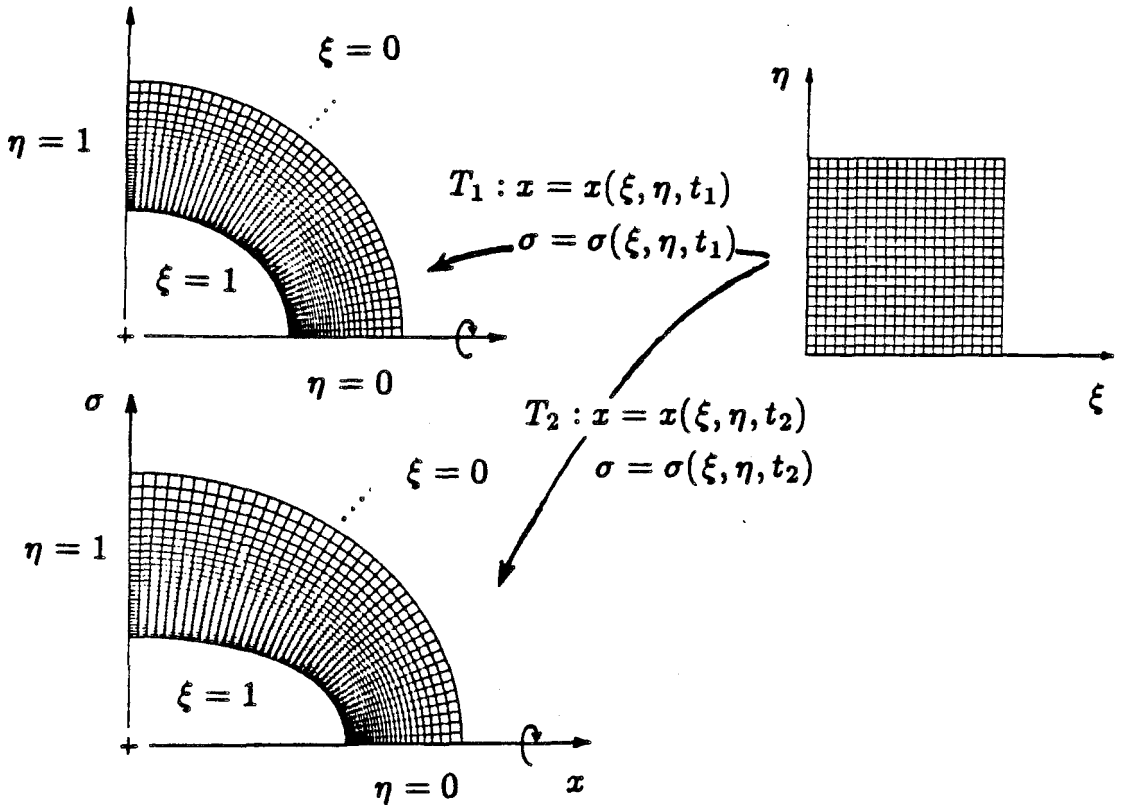
$\xi = 0$
$\eta = 1$
$\xi = 1$
$\eta = 0$
$T_1 : x = x(\xi, \eta, t_1)$
$\sigma = \sigma(\xi, \eta, t_1)$
η
ξ
$T_2 : x = x(\xi, \eta, t_2)$
$\sigma = \sigma(\xi, \eta, t_2)$
σ
$\xi = 0$
$\eta = 1$
$\xi = 1$
$\eta = 0$
x

Figure 1

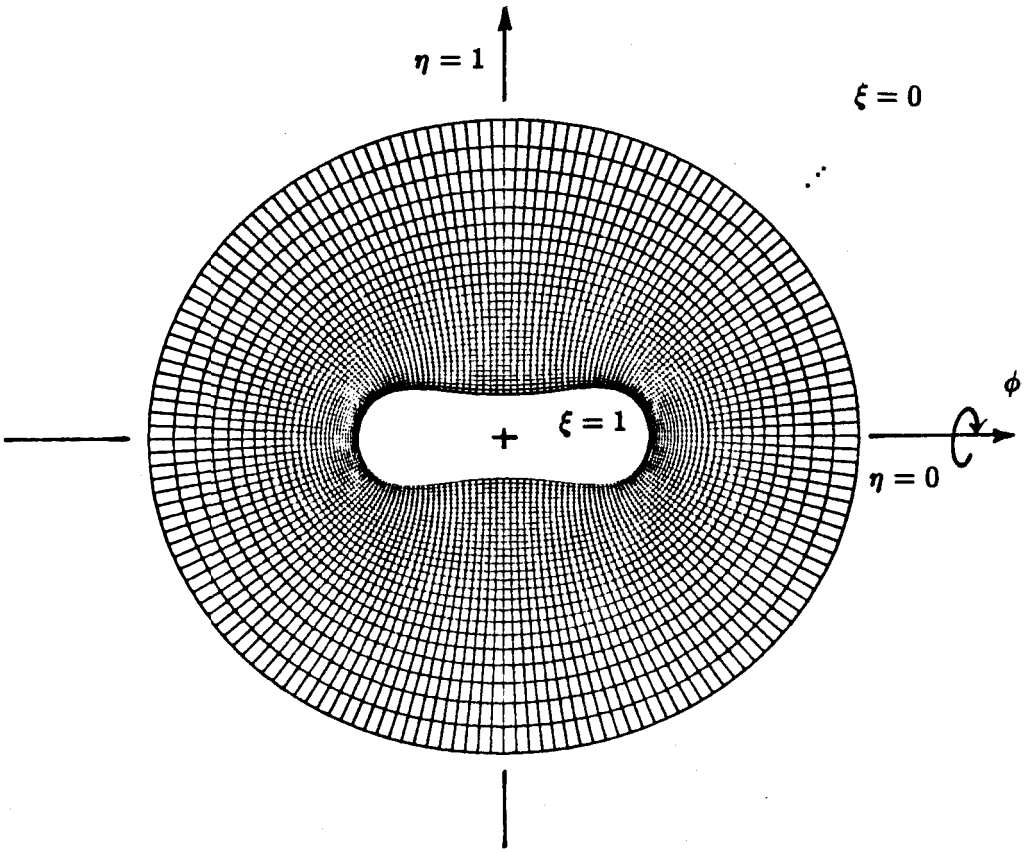

Figure 2

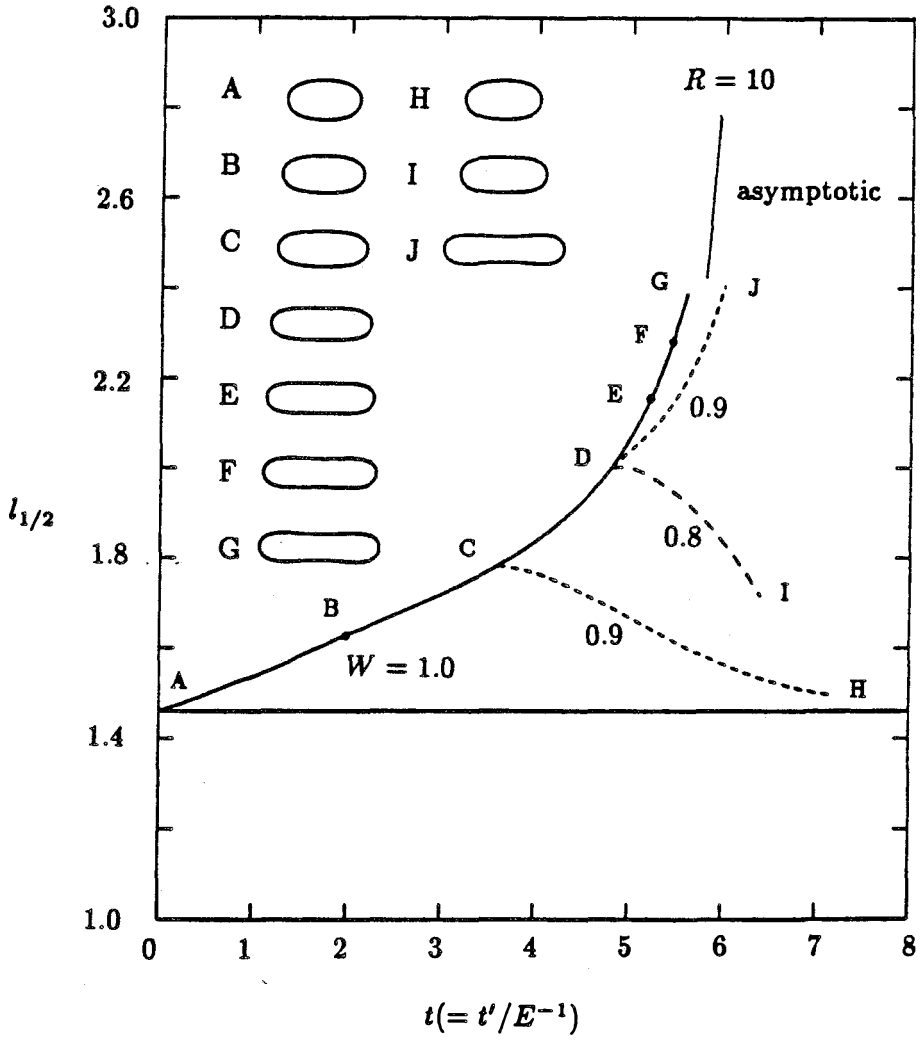
3.0
2.6
2.2
1.8
1.4
1.0
$l_{1/2}$
0
1
2
3
4
5
6
7
8
$t(= t'/E^{-1})$
A
B
C
D
E
F
G
H
I
J
$R = 10$
asymptotic
$W = 1.0$
0.9
0.8
0.9

Figure 3

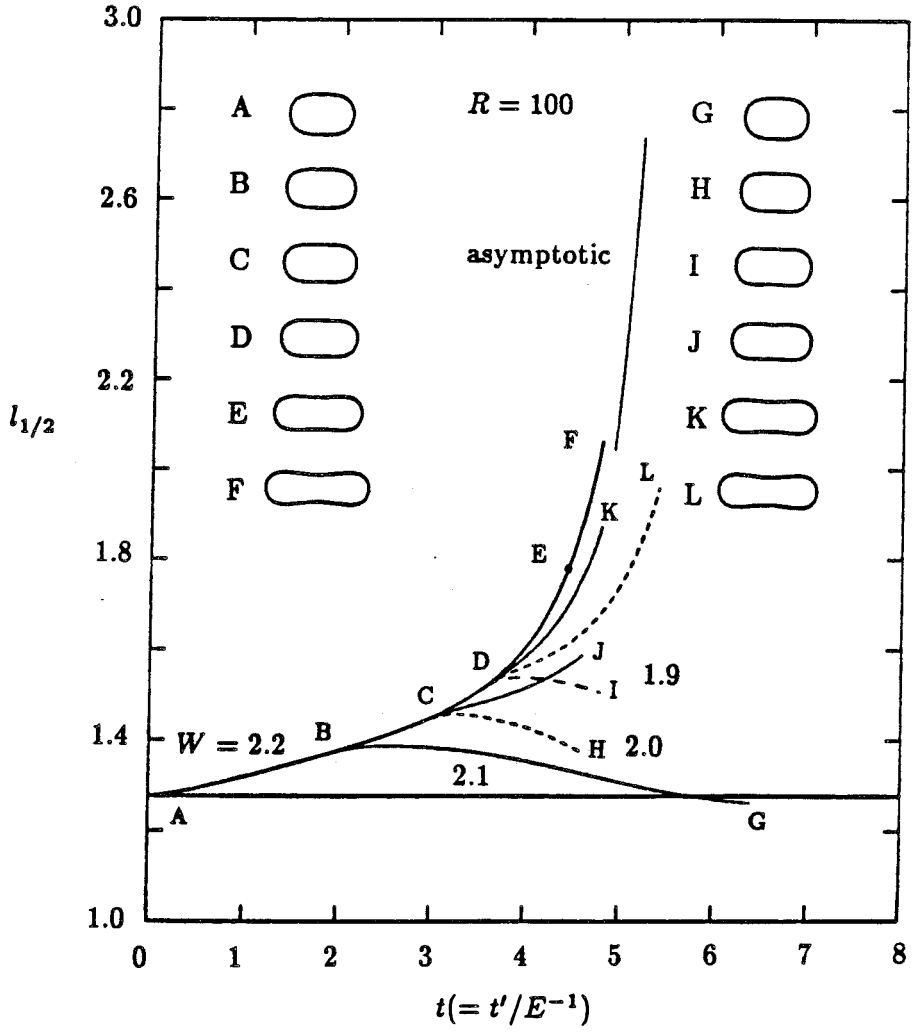
3.0
2.6
2.2
1.8
1.4
1.0
$l_{1/2}$
0
1
2
3
4
5
6
7
8
$t(= t'/E^{-1})$
A
B
C
D
E
F
G
H
I
J
K
L
$R = 100$
asymptotic
$W = 2.2$
2.1
2.0
1.9

Figure 4

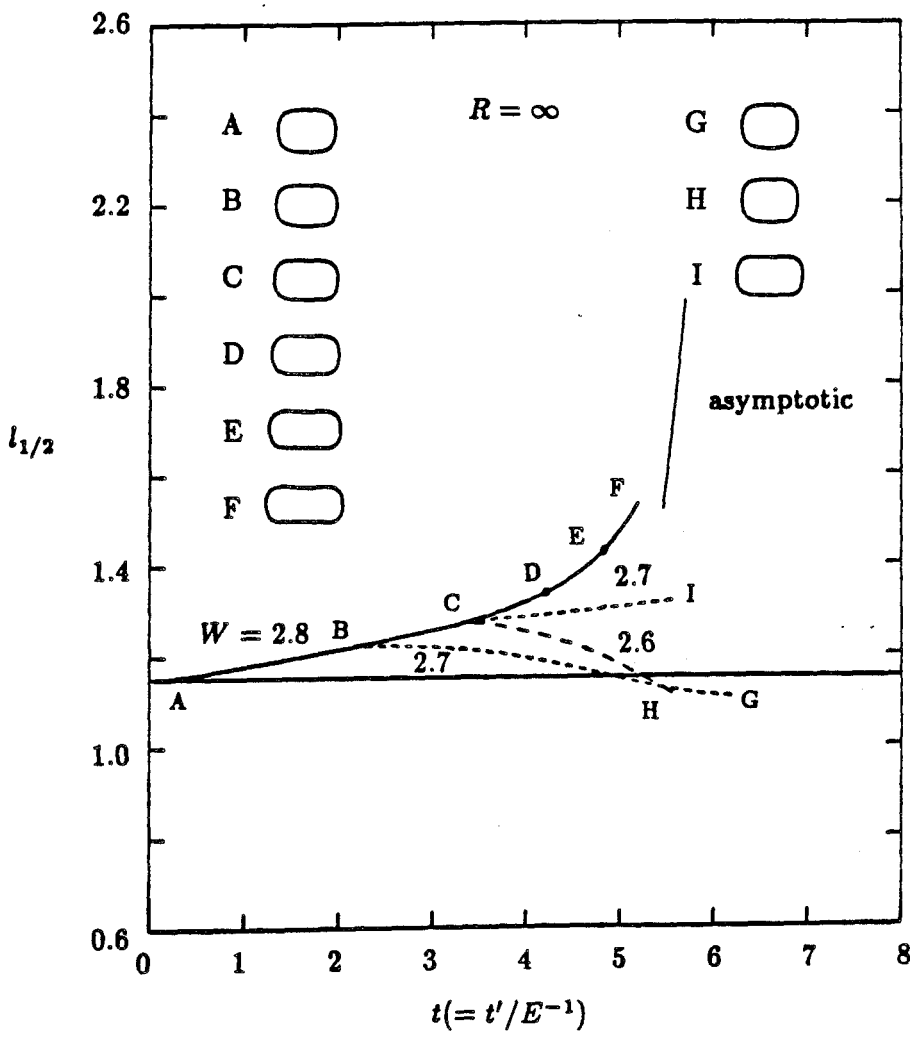
2.6
2.2
1.8
1.4
1.0
0.6
$l_{1/2}$
0
1
2
3
4
5
6
7
8
$t(= t'/E^{-1})$
$R = \infty$
A
B
C
D
E
F
G
H
I
asymptotic
$W = 2.8$
2.7
2.6
2.7

Figure 5

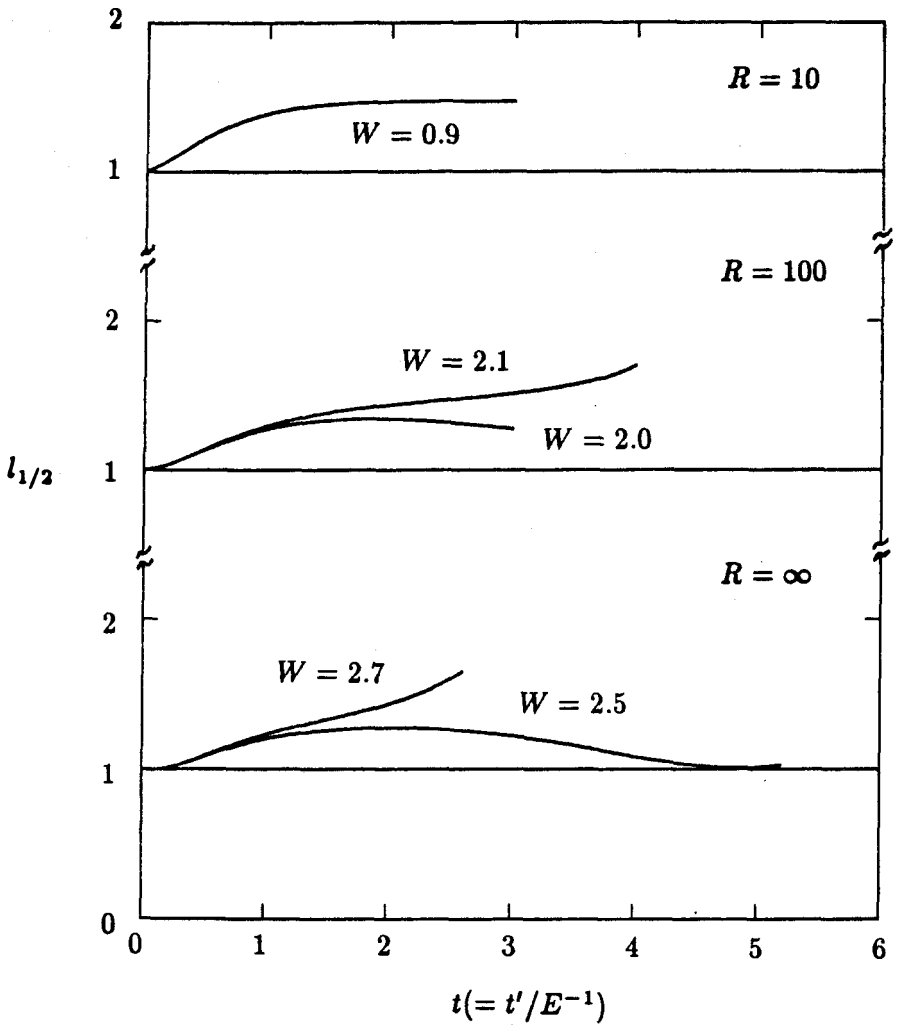

Figure 6

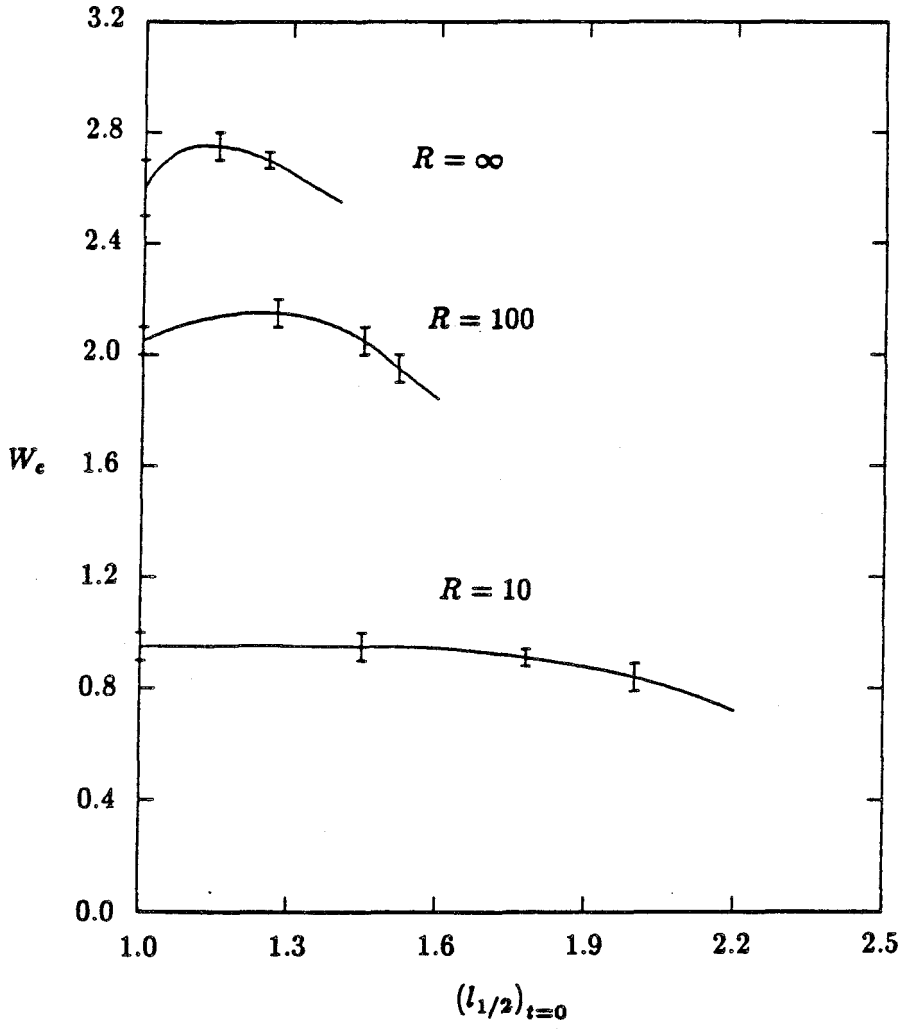
3.2
2.8
2.4
2.0
1.6
1.2
0.8
0.4
0.0
W_e
$R = \infty$
$R = 100$
$R = 10$
1.0
1.3
1.6
1.9
2.2
2.5
$(l_{1/2})_{t=0}$

Figure 7

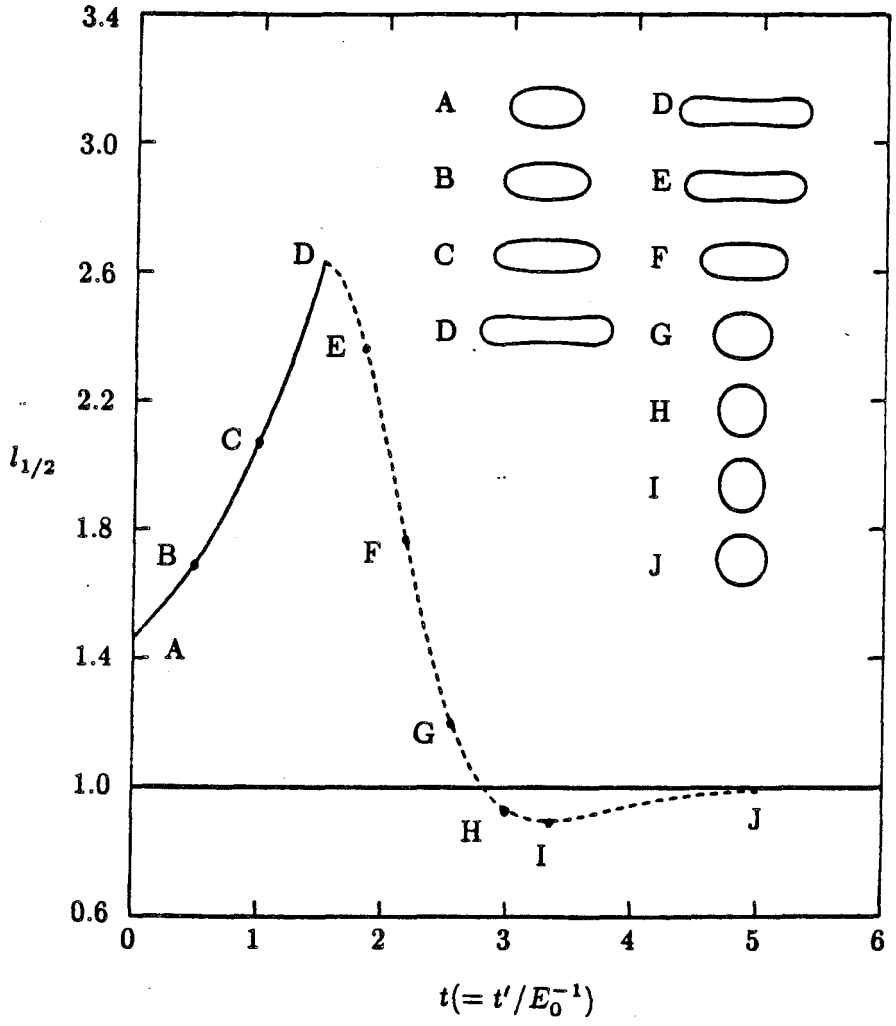

Figure 8

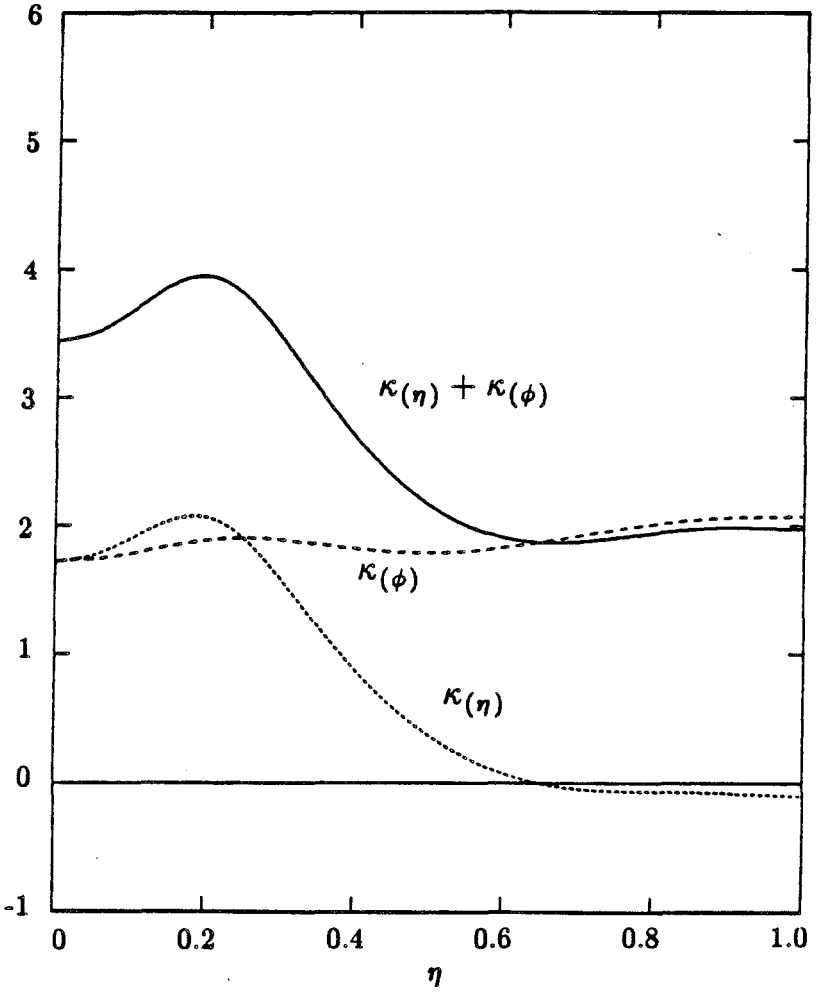

Figure 9

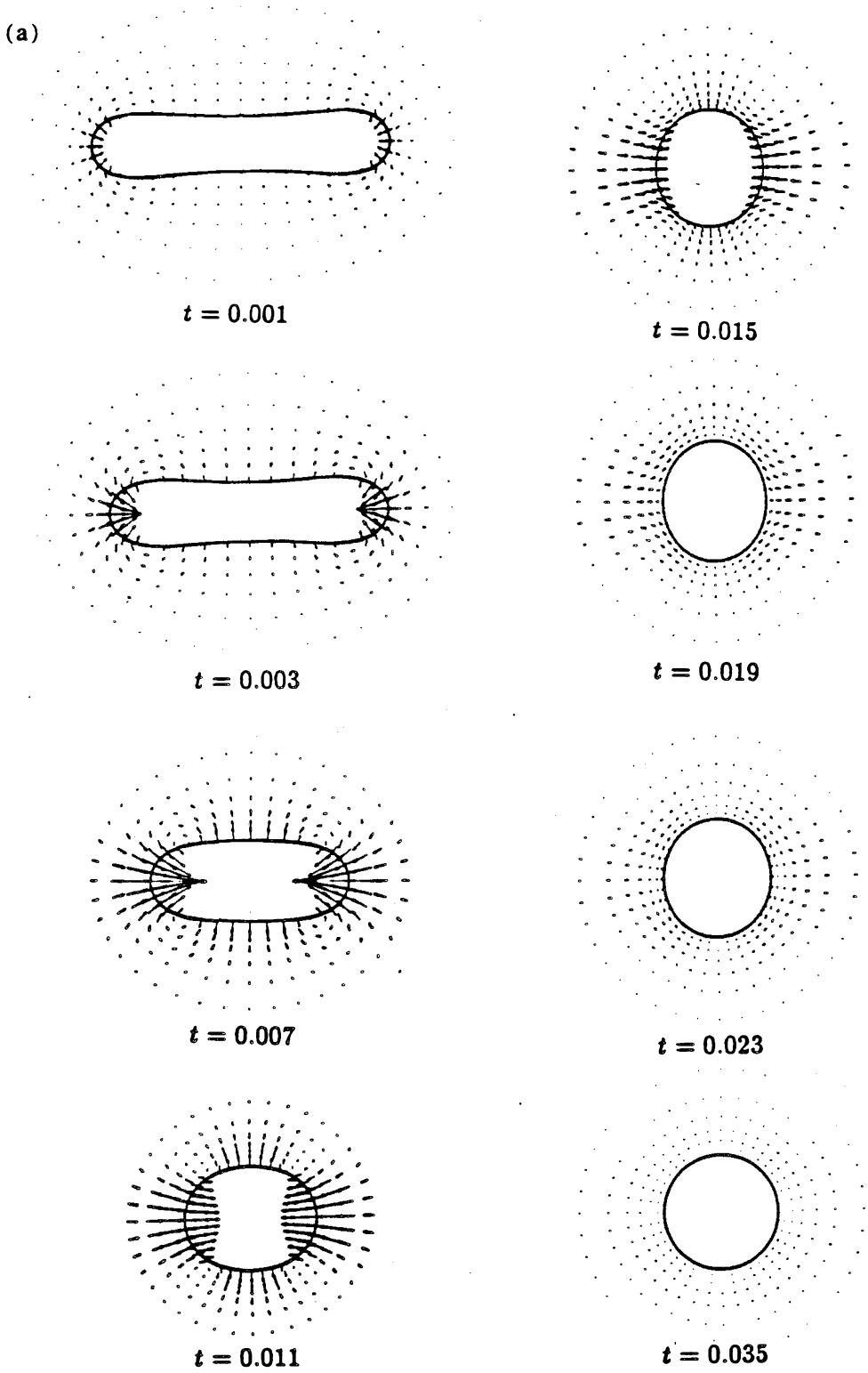

Figure 10a

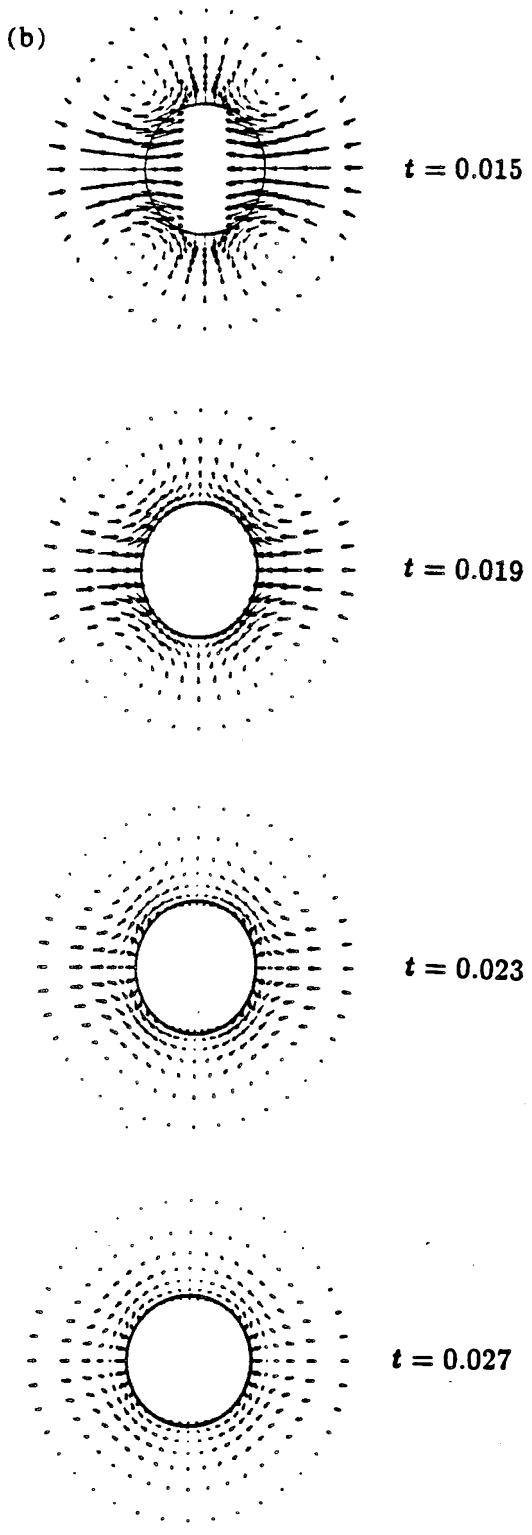

Figure 10b

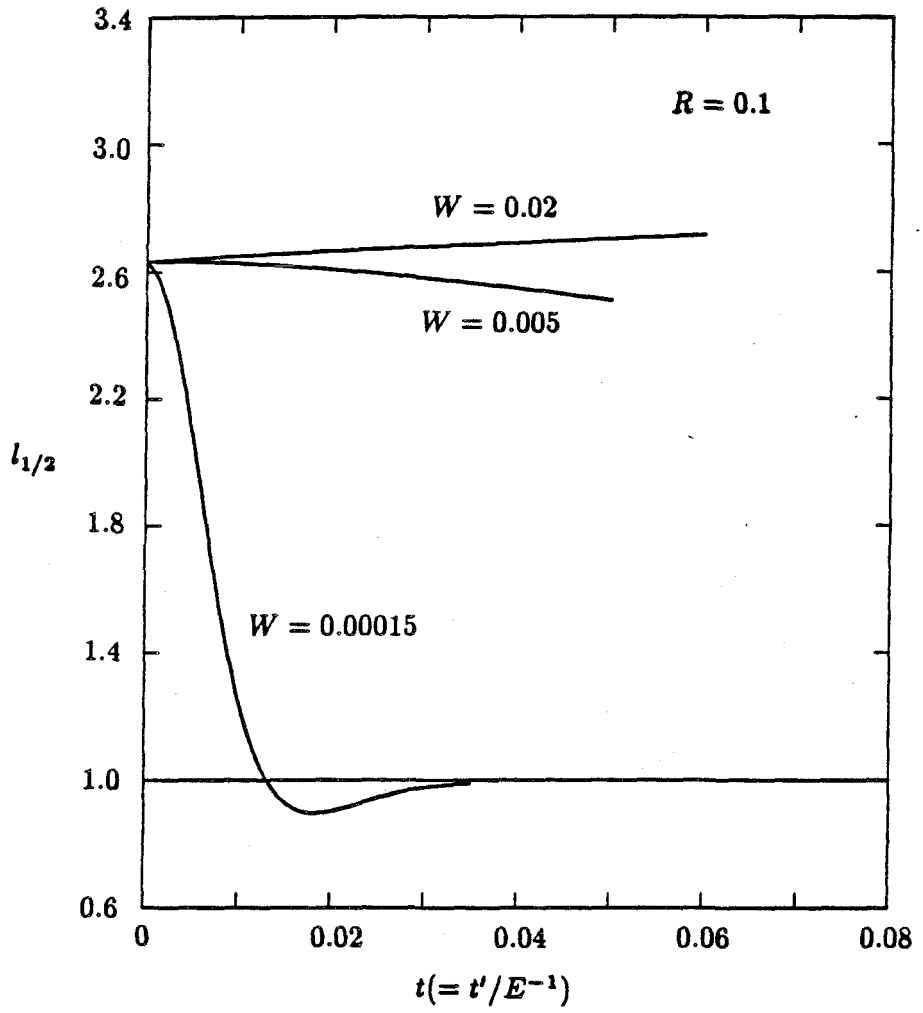
3.4
3.0
2.6
2.2
1.8
1.4
1.0
0.6
$l_{1/2}$
$R = 0.1$
$W = 0.02$
$W = 0.005$
$W = 0.00015$
0
0.02
0.04
0.06
0.08
$t(= t'/E^{-1})$

Figure 11

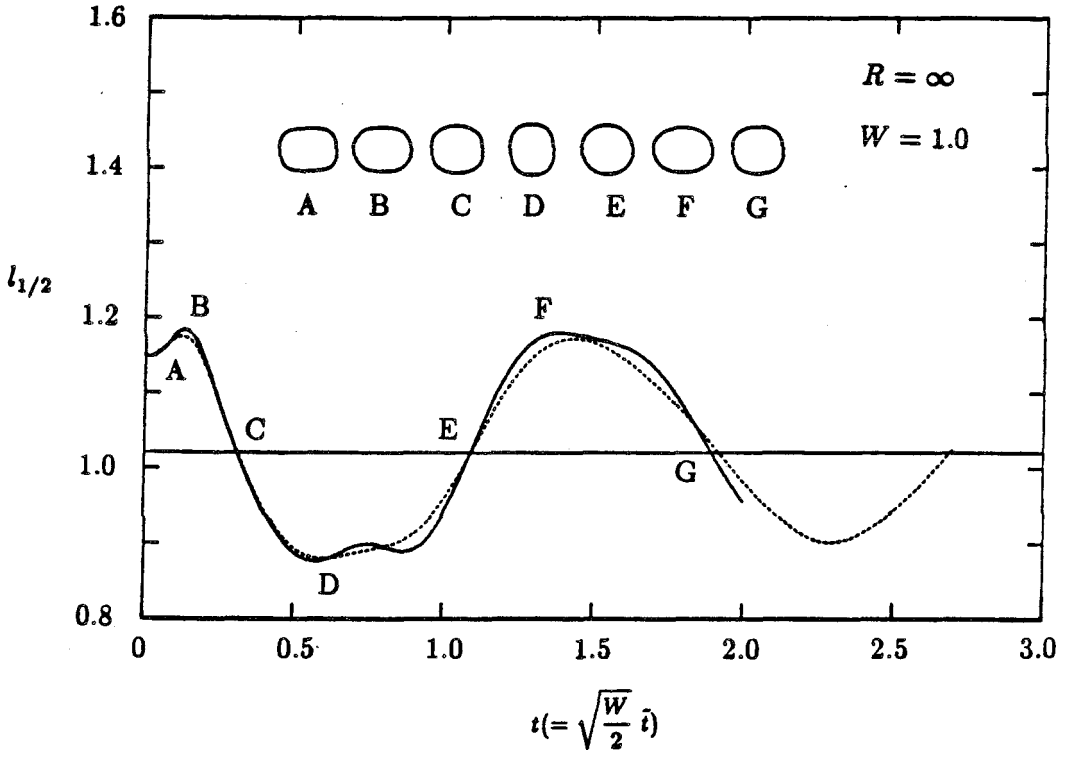
1.6
1.4
1.2
1.0
0.8
$l_{1/2}$
$R = \infty$
$W = 1.0$
A B C D E F G
A
B
C
D
E
F
G
0
0.5
1.0
1.5
2.0
2.5
3.0
$t(=\sqrt{\frac{W}{2}}\,\tilde{t})$

Figure 12

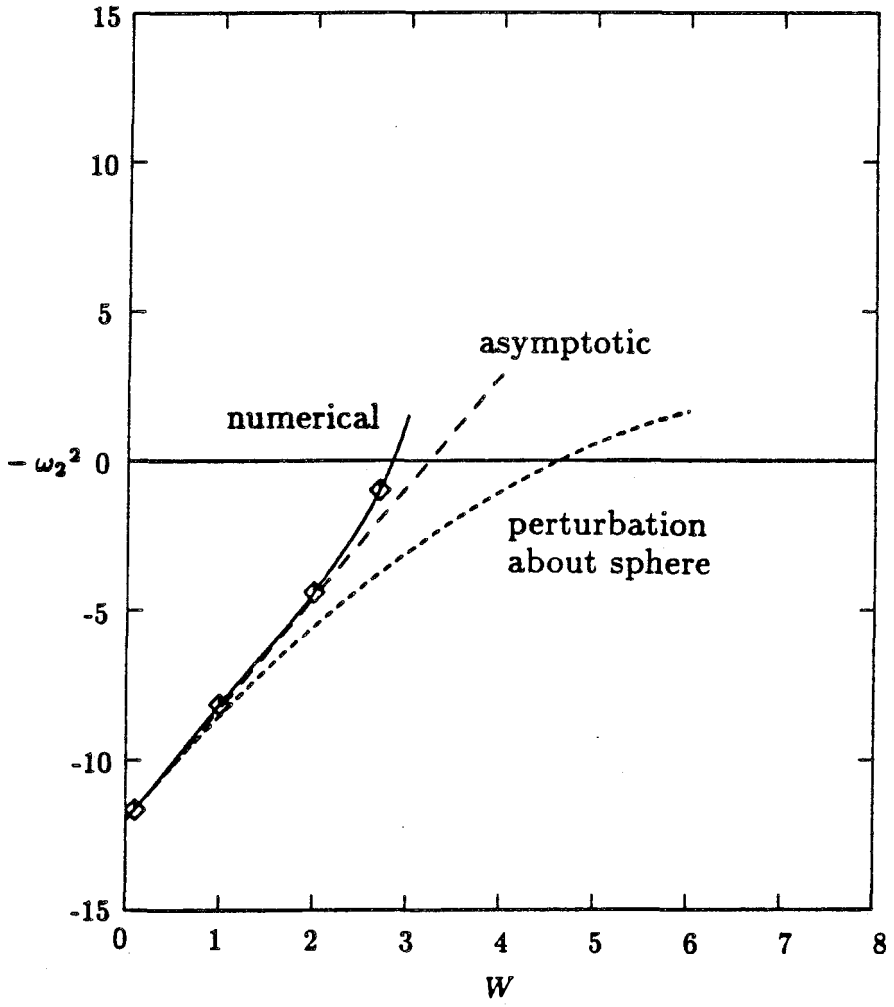
15
10
5
0
-5
-10
-15
$-\omega_2^2$
0
1
2
3
4
5
6
7
8
W
asymptotic
numerical
perturbation
about sphere

Figure 13

Chapter II

Numerical solution of axisymmetric, unsteady, free-boundary problems at finite Reynolds number
II. Deformation of a bubble in a biaxial straining flow

Numerical solution of axisymmetric, unsteady, free-boundary problems at finite Reynolds number
II. Deformation of a bubble in a biaxial straining flow

I.S. Kang and L.G. Leal

Department of Chemical Engineering
California Institute of Technology
Pasadena, California 91125

Abstract

The steady and unsteady deformation of a bubble in a biaxial straining flow is considered for Reynolds numbers in the range $0 \leq R \leq 200$. Numerical computations show that the bubble does not burst even at the stage of extremely high deformation. At the stage of early deformation, the elongation direction is changed from the equatorial direction to the axial direction at a marginal Reynolds number, R_m, which is between 100 and 200. The steady-state shape of a bubble in an inviscid, biaxial straining flow is identical to that in a uniaxial straining flow at the same Weber number, and the lowest mode for an oscillating bubble in an inviscid, biaxial straining flow has the same frequency as for a bubble in a uniaxial straining flow up to $O(W)$. Comparison of the results for the cases of high Reynolds numbers ($R = 100,\ 200$) with the potential flow results suggests that the potential-flow solution does not provide a uniformly valid (for all W) approximation to the real flow at high Weber numbers. The computations for unsteady deformations show that the steady-state shapes for all Weber numbers and Reynolds numbers considered in the present study are stable even to finite disturbances.

I. INTRODUCTION

The present paper is the second in a series (see Kang and Leal[1], hereafter denoted by I) in which we use numerical methods to study the unsteady deformation of a bubble in axisymmetric flow fields at finite Reynolds number. In I, we considered uniaxial straining flow. Here we consider the same problem for a *biaxial* straining flow. From a mathematical point of view, the problem of biaxial straining flow is identical to that of uniaxial straining flow except for a change in sign in the boundary condition at infinity. However, this simple change in the boundary condition can result in completely different solution behavior because of the nonlinear nature of the governing equations and boundary conditions.

The deformation of a bubble in a uniaxial straining flow has been studied extensively via numerical analyses[1–4] as well as by approximate analytic theories.[5–12] The most interesting result for a deforming bubble in a steady uniaxial straining flow is that steady solutions for bubble shape exist only for Weber numbers below a certain critical value W_c, which depends on the Reynolds number. The non-existence of steady-state solutions beyond a critical Weber number was first suggested by Miksis[3] and Ryskin and Leal[4] on the basis of the breakdown of their steady numerical solution algorithms. If true, the implication is that the critical Weber number should be approximately equal to the maximum Weber number at which a convergent steady-state solution could be obtained. These speculations were later confirmed by the present authors via an unsteady algorithm for the full transient problem. In particular, we found that the critical Weber number from the steady codes[3,4] is a point of onset of unsteady stretching, provided only that the initial shape is close to the steady shape at the same Weber number. In a companion paper to I,[11] we also studied the oscillation of a bubble in a uniaxial, inviscid straining flow using the domain perturbation technique, and showed that the frequency of the lowest oscillation mode decreases monotonically as the Weber number increases. On this basis,

we conjectured that a zero frequency point can exist for this mode at a certain Weber number, which must be identical to a limit point of the steady solution branch. The reason is that the governing equations for small oscillations are identical to the linearized equations for stability of the steady state, so that the existence of a zero frequency point (zero eigenvalue) implies a singularity in the Jacobian matrix for evolution of a disturbance about the steady state. The basic conjecture of a zero frequency point was confirmed by the numerical study of bubble oscillation in I. Furthermore, the zero frequency point turned out to be identical to the critical Weber number "predicted" by the breakdown of steady algorithms. Thus, the maximum Weber number under which steady-state solutions were found via the steady and transient algorithms was confirmed to be the limit point, at least on the solution branch that includes the rest state.

As discussed above, the behavior of a deforming bubble in a uniaxial straining flow is fairly well understood. However, in contrast to the uniaxial straining flow problem, relatively little is known about the behavior of a deforming bubble in a biaxial straining flow. We are made aware of only one analysis for this problem by Frankel and Acrivos[12] (Hinze,[13] and Lewis and Davidson[14] mentioned the biaxial flow problem, but did not give any analysis). Frankel and Acrivos calculated the bubble shape in the creeping flow limit to a moderate value of capillary number ($Ca \leq 0.2$) via a semi-analytical approach. In view of the simple change in the mathematical formulation compared with the uniaxial flow problem, it is rather surprising that so little has been done and so provides one primary motivation for the present study.

In this paper, we consider both steady-state shapes and unsteady deformation of a bubble in a biaxial straining flow at finite Reynolds numbers. As mentioned above, our primary concern is to compare behavior for uniaxial and biaxial straining flows in order to understand the effect of nonlinearities in the governing equations and boundary conditions.

II. STATEMENT OF THE PROBLEM

We consider the steady and unsteady deformation of an incompressible gas bubble of volume $\frac{4}{3}\pi a^3$ in a *biaxial* straining flow of a fluid with constant density ρ and constant viscosity μ (see Fig. 1). The density and viscosity of the gas inside the bubble are assumed to be negligible in comparison with those of liquid. Furthermore, the surface of the bubble is assumed to be characterized completely by a uniform surface tension γ. Finally, we neglect all effects of gravity including the hydrostatic pressure variation in the fluid. If the x-axis of a cylindrical coordinate system (x, σ, ϕ) is directed along the axis of symmetry, the (dimensional) velocity field far from the bubble is given by

$$\mathbf{u} = \mathbf{E} \cdot \mathbf{r}, \quad \mathbf{E} = E \begin{pmatrix} -1 & 0 & 0 \\ 0 & \frac{1}{2} & 0 \\ 0 & 0 & \frac{1}{2} \end{pmatrix}, \quad E > 0, \tag{1}$$

where E is the principal strain rate. We use the equivalent radius a of the bubble as a characteristic length scale, the product Ea as a characteristic velocity scale, and E^{-1} as a characteristic time scale.

The relevant dimensionless parameters in this problem are the Reynolds number $R \equiv 2\rho(Ea)a/\mu$ based on the equivalent diameter $2a$ of the bubble, and the Weber number $W \equiv 2\rho(Ea)^2 a/\gamma$.

From a mathematical point of view, the *biaxial* straining flow problem is exactly the same as the *uniaxial* straining flow problem except that the signs are changed in the boundary condition at infinity (Eq.1). However, as we shall see, this simple change in the boundary conditions turns out to result in completely different solution behavior due to the nonlinearities in the governing equations and the boundary condition at the bubble surface.

III. PRELIMINARY ANALYTICAL RESULTS

In this section, we present several analytical results that can be obtained without any detailed numerical analysis. These results will be essential in understanding and interpreting of the results of numerical computations, to be be given in later sections.

A. Steady-state shape and oscillation frequency of a bubble in potential flow

For potential flow problems, it can be shown that the steady-state shape of a bubble in a biaxial straining flow is identical to that of a bubble in a uniaxial straining flow. In itself, this assertion may not seem particularly noteworthy, and we shall see that its proof is trivial. However, it is well known,[3,4,11] that a bubble in a uniaxial straining flow is elongated in the axial direction (i.e., $f(0) > f(\frac{\pi}{2})$ when the surface is given by $r = 1 + f(\theta)$), and the identity of shape between uniaxial and biaxial flows implies that it should be elongated in the same direction in a biaxial flow. This result of our assertion does seem quite surprising at first because it implies the counter-intuitive result of bubble elongation against the flow direction. To prove that the steady-state shapes must be identical in uniaxial and biaxial potential flow, we need only to examine the dimensionless governing equations and boundary conditions for the steady-state potential flow. The governing equation is

$$\nabla^2 \phi = 0. \tag{2}$$

For the boundary conditions at the bubble surface ($r = 1 + f(\theta)$), we have the kinematic condition,

$$\nabla \phi \cdot \mathbf{n} = 0, \tag{3}$$

and the normal stress condition,

$$G + \nabla \phi \cdot \nabla \phi = \frac{4}{W} \nabla \cdot \mathbf{n}. \tag{4}$$

In (4), the unknown constant G must be determined from the condition of volume conservation. The far-field condition corresponding to the velocity field (1) is given by

$$\phi \to \pm \frac{1}{4}(3\cos^2\theta - 1)r^2 \quad \text{as} \quad r \to \infty, \tag{5}$$

where "+" and "−" refer to the uniaxial and the biaxial straining flows, respectively (hereafter the upper and lower signs of $\pm$ (or $\mp$) refer to the uniaxial and biaxial straining flows, respectively).

Now, it is a trivial matter to show that for any given W where a steady shape exists, exactly the same steady-state shapes must be obtained for both flow types. Let us assume that a steady-state shape exists, denoted as f_1, for the uniaxial flow problem. The assumption of the existence of the steady-state shape, f_1, implies the existence of a corresponding velocity potential, ϕ_1, so that the pair (f_1, ϕ_1) represent a solution of (2) - (5) for the given W (in fact, the velocity potential can be determined uniquely for a given shape from (2), (3), and (5), but the uniqueness is not necessary in this proof). Now, our assertion is that (f_1, $-\phi_1$) is a solution for the biaxial straining flow problem. Clearly, $\phi = -\phi_1$ satisfies the far field condition (5), and the governing equation (2) and boundary condition (3) are homogeneous and thus are invariant to a change in the sign of ϕ; i.e.,

$$\nabla^2(-\phi_1) = -\nabla^2\phi_1 = 0, \tag{6}$$

$$\nabla(-\phi_1)\cdot\mathbf{n} = -\nabla\phi_1\cdot\mathbf{n} = 0. \tag{7}$$

The left-hand side of the normal stress condition, on the other hand, does not change sign upon transformation from ϕ_1 to $-\phi_1$.

$$G + \nabla(-\phi_1)\cdot\nabla(-\phi_1) = G + \nabla\phi_1\cdot\nabla\phi_1 = \frac{4}{W}\nabla\cdot\mathbf{n}\,|_{r=1+f_1} \tag{8}$$

Thus, if f_1 is a solution for the shape for $\phi = \phi_1$, it is also a solution of (8) for $\phi = -\phi_1$. This proves our assertion. In physical terms, the change in the direction of the steady-state potential flow does not result in any shape change, because the deformation is due only to the distribution of dynamic pressure that has the form ($-u^2 + constant$) along a stream line.

Unlike the case of steady-state deformation, we were not able to derive any general relationship between unsteady deformations in uniaxial and biaxial flow, which is valid for the whole range of Weber numbers. However, we can show

that the oscillation frequency of the primary mode ($n = 2$) is identical in both types of flow field at small Weber numbers ($W << 1$). The oscillation of a bubble in a uniaxial straining flow was studied in detail by Kang and Leal.[11] The most important result in the paper is that the oscillation frequency of the primary mode ($n = 2$) decreases as Weber number increases; i.e.,

$$\omega_2^2 = \omega_{2,0}^2(1 - 0.31W) + o(W), \tag{9}$$

where $\omega_{2,0}$ is the frequency of the primary mode for an oscillating bubble in an otherwise quiescent fluid. Here we present only the minimum of analysis necessary to understand that (9) is true also for the biaxial straining flow problem. As in Kang and Leal,[11] we introduce characteristic velocity, length, and time scales that are appropriate to the oscillation problem

$$\tilde{\phi}_c = \left(\frac{\gamma a}{\rho}\right)^{\frac{1}{2}},$$

$$\tilde{t}_c = \left(\frac{\rho a^3}{\gamma}\right)^{\frac{1}{2}},$$

$$l_c = a.$$

Then the governing equation in dimensionless form is

$$\nabla^2\tilde{\phi} = 0, \tag{10}$$

while the kinematic condition takes the form

$$-\frac{1}{|\nabla F|}\frac{\partial F}{\partial \tilde{t}} = \nabla\tilde{\phi}\cdot\mathbf{n}, \tag{11}$$

and the normal stress condition becomes

$$G(\tilde{t}) + \frac{\partial\tilde{\phi}}{\partial\tilde{t}} + \frac{1}{2}\nabla\tilde{\phi}\cdot\nabla\tilde{\phi} = (\nabla\cdot\mathbf{n}). \tag{12}$$

In (11), F is a function that describes the bubble shape as $F(\mathbf{x}, t) = 0$. The far-field condition at infinity for the two types of flow is given by

$$\tilde{\phi}_\infty = \pm\sqrt{\frac{W}{2}}\frac{1}{2}(3\cos^2\theta - 1)\left(\frac{1}{2}r^2\right), \tag{13}$$

where "+" and "-" of "±" refer to the uniaxial and the biaxial straining flows, respectively.

The only parameter in this problem is "$\pm\sqrt{W}$" of (13), so let us define a general parameter, ξ, such that

$$\xi = +\sqrt{W} \quad \text{for uniaxial flow,}$$

$$\xi = -\sqrt{W} \quad \text{for biaxial flow.}$$

Then, the problem can be solved in terms of the general parameter, ξ, and the result (9) must have the form

$$\omega_2^2 = \omega_{2,0}^2(1 - 0.31\xi^2) + o(\xi^2).$$

Since the equation above is true for both types of flow and $\xi^2 = (\pm\sqrt{W})^2 = W$, the result (9) is true for both types of the flow field.

In this subsection we have discussed some invariants of potential flow solutions with respect to a change of sign in the boundary condition at infinity. The invariance of the steady-state shape in the potential flow limit implies an interesting result in the steady-state bubble deformation for a viscous fluid as the Reynolds number increases from zero to infinity, and this will be discussed in the following subsection.

B. Estimation of the marginal Reynolds number

A bubble in a biaxial straining flow, as shown in the previous subsection, has a steady-state shape in the potential flow approximation that is elongated in the axial direction. On the contrary, however, a bubble in the creeping flow limit will be deformed into an oblate shape.† Now, if we assume that the potential

† Since the pressure distribution is linear with respect to the velocity ($\nabla p = \nabla^2 \mathbf{u}$) and so is the viscous stress by definition, the normal stress is completely linear with respect to the velocity field. Furthermore, we know that a bubble in

flow solution is the limiting solution for the real flow in the limit $R \to \infty$, at least for a slightly deformed bubble (in general, the assumption is acceptable for a bubble that is smooth everywhere in the limit $R \to \infty$), then there must be an intermediate Reynolds number that gives exactly the same axial and equatorial elongation (i.e., $f(0) = f(\frac{\pi}{2})$). We call this the *marginal* Reynolds number. Estimation of the marginal Reynolds number is very interesting because the balance of the linear and nonlinear contributions at the marginal Reynolds number will result in an increasing deformation without elongation as the Weber number increases.

Let us begin by writing the normal stress condition in a form that is accurate to $O(R^{-1})$,

$$-2p_v + \nabla\phi_p \cdot \nabla\phi_p + \frac{8}{R}\frac{\partial^2\phi_p}{\partial n^2} = \frac{4}{W}\nabla \cdot \mathbf{n} \qquad \text{at} \quad r = 1 + f(\theta), \qquad (14)$$

where p_v denotes the dimensionless viscous pressure correction defined as $p_v = p_v'/(\rho U_c^2)$ and ϕ_p denotes the steady-state velocity potential. If we restrict ourselves to the case of small deformation at $W << 1$, the leading order shape change can be calculated by solving (14) with the L.H.S. evaluated with the solution for a spherical bubble.

Now, let us first consider the viscous pressure correction. Kang and Leal[11] derived a general formula for the viscous pressure correction under the assumption that the velocity perturbation around a spherical bubble due to viscosity approaches zero everywhere as $R \to \infty$; i.e.,

$$\| \mathbf{u}_v \| << \| \mathbf{u}_p \| \qquad \text{for} \quad R >> 1,$$

where $\mathbf{u}_p$ and $\mathbf{u}_v$ denote the potential flow velocity and the velocity perturbation due to viscosity, respectively. Since the vorticity is solenoidal ($\nabla \cdot \underline{\omega} = 0$), they

---

creeping flow is deformed into an prolate shape in the uniaxial extensional flow for arbitrary $E > 0$. It follows that a bubble in a biaxial extensional flow must be deformed into an oblate shape in the creeping flow limit.

expressed the vorticity in terms of toroidal (**T**) fields for an arbitrary axisymmetric problem,

$$\underline{\omega} = \mathbf{T} = \nabla \times \left(\sum_{n=0}^{\infty} T_n(r,t) P_n(\cos\theta) \mathbf{e}_r \right). \tag{15}$$

Then the leading order viscous pressure correction at the surface of a spherical bubble in an arbitrary axisymmetric flow (steady or unsteady) at a high Reynolds number is given by (see Kang and Leal[11] for a detailed derivation).

$$\begin{aligned} p_v(1,\theta,t) = \sum_{n=0}^{\infty} \Bigg[& n \int_1^{\infty} r^{-n-1} \sum_{k=-\infty}^{\infty} f_{n,k}(r) T_{n+k} dr \\ & + \int_1^{\infty} \sum_{l=-\infty}^{\infty} \left((r^{-n} g_{n,l}(r) - r^{-n-l} g_{n,l}(1)) T_{n+l} \right) dr \\ & + n \left(\frac{2}{R} \right) T_n(1,t) \Bigg] P_n(\cos\theta), \end{aligned} \tag{16}$$

where

$$\sum_{n=0}^{\infty} \Big(\sum_{k=-\infty}^{\infty} f_{n,k} T_{n+k} \Big) P_n = \sum_{n=0}^{\infty} \Big(\big(u_{pr} P_n - \int_0^{\theta} P_n \frac{\partial u_{pr}}{\partial \theta} d\theta \big) T_n \Big),$$

$$\sum_{n=0}^{\infty} \Big(\sum_{l=-\infty}^{\infty} g_{n,l} T_{n+l} \Big) P_n = \sum_{n=0}^{\infty} \Big(\frac{T_n}{r} u_{p\theta} \frac{dP_n}{d\theta} \Big).$$

Now, we want to estimate the first-order deformation with respect to W (for $W << 1$) using the following steady-state potential flow solutions around a spherical bubble for uniaxial and biaxial straining flows,

$$\phi_p = \pm P_2(\cos\theta) \big(\frac{1}{2} r^2 + \frac{1}{3} r^{-3} \big). \tag{17}$$

As we can see in (16), accurate evaluation of pressure correction on the surface of a spherical bubble requires the vorticity distribution in the region outside the bubble, which requires us to solve the vorticity equation. Here, however, we wish to estimate the marginal Reynolds number without solving the vorticity equation. For this purpose, we may assume, as a first approximation, that the

vorticity is confined to the boundary and is zero everywhere in the region outside the bubble. Then (16) reduces to

$$p_v(1) \simeq \sum_{n=0}^{\infty} n\left(\frac{2}{R}\right) T_n(1) P_n(\cos\theta). \tag{18}$$

Incorporating the condition of vanishing shear stress at the bubble surface into the definition of the vorticity and equating with (15) for $r = 1$, we have

$$\omega(1,\theta) = -\sum_{n=0}^{\infty} \frac{T_n(r)}{r} \frac{dP_n}{d\theta}|_{r=1} = 2\left(\frac{u_{p\theta}}{r} - \frac{1}{r}\frac{\partial u_{pr}}{\partial \theta}\right)|_{r=1} + o(1),$$

where u_{pr} and $u_{p\theta}$ are evaluated from the velocity potential ϕ_p in (17). By comparing the coefficient of $dP_n/d\theta$, we find

$$T_2 = \mp\frac{5}{3}, \qquad \text{if} \quad n = 2, \tag{19}$$

$$T_n = 0, \qquad \text{if} \quad n \neq 2.$$

Finally, by substituting (17), (18), and (19) into (14), we get

$$\nabla \cdot \mathbf{n} = 2 + \frac{W}{4}\left[-\frac{10}{7} P_4(\cos\theta) + \left(\frac{25}{42} \pm \frac{160}{3R}\right) P_2(\cos\theta)\right]. \tag{20}$$

To obtain the first-order deformation in W, let us assume that the bubble surface is described in the form

$$r = 1 + f = 1 + \frac{W}{4} g(\theta) = 1 + \frac{W}{4} \sum_{n=2}^{\infty} \beta_n P_n(\cos\theta). \tag{21}$$

Then, the curvature is given by

$$\nabla \cdot \mathbf{n} = 2 + \frac{W}{4} \sum_{n=2}^{\infty} (n-1)(n+2)\beta_n P_n(\cos\theta) + O(W^2). \tag{22}$$

By comparing (20) and (22), we get

$$g(\theta) = \left(\frac{25}{168} \pm \frac{40}{3R}\right) P_2(\cos\theta) - \frac{5}{63} P_4(\cos\theta).$$

Therefore, the deformation along the symmetry axis ($\theta = 0$) is

$$g(0) = \frac{5}{72} \pm \frac{40}{3R},$$

and the deformation along the equatorial plane ($\theta = \pi/2$) is

$$g(\frac{\pi}{2}) = -\frac{5}{48} \mp \frac{20}{3R}.$$

If we define $\Delta g = g(0) - g(\frac{\pi}{2})$, then

$$\Delta g \equiv g(0) - g(\frac{\pi}{2}) = \frac{25}{144} \pm \frac{20}{R}, \tag{23}$$

where "+" and "-" of $\pm$ indicate the uniaxial and the biaxial straining flows, respectively. The Δg's for both types of flow are plotted as functions of R in Fig. 2. From Fig. 2, we can see that a bubble in a uniaxial straining flow becomes less elongated as the Reynolds number increases, which is qualitatively consistent with the numerical solution of Ryskin and Leal.[4] However, in a biaxial straining flow the elongation direction changes at the marginal Reynolds number, R_m. The marginal Reynolds number is estimated as $R_m = 115.2$ by solving $\Delta g = 0$ for the Reynolds number.

C. Vorticity stretching and the vorticity distribution in the wake

The vorticity transport equation for an axisymmetric inviscid flow without swirl has the following simple form (Batchelor[15] 1967),

$$\frac{D(\omega/\sigma)}{Dt} = 0. \tag{24}$$

In fact, Eq. (24) is equivalent to Kelvin's circulation theorem. Eq. (24) suggests that vorticity can grow indefinitely in an inviscid, biaxial straining flow, because the fluid particle travels in the direction of increasing $\sigma \to \infty$ as $t \to \infty$. Now, the following question can be cast. Can the vorticity grow indefinitely in a biaxial straining flow if the Reynolds number is arbitrarily large but finite? This question can be answered by the following analysis for the wake region.

Let us begin by writing the vorticity transport equation in the cylindrical coordinate system that is illustrated in Fig. 1,

$$u_x\frac{\partial\omega}{\partial x}+u_\sigma\frac{\partial\omega}{\partial\sigma}-\frac{\omega u_\sigma}{\sigma}=\frac{2}{R}\left[\frac{\partial^2\omega}{\partial x^2}+\frac{1}{\sigma}\frac{\partial}{\partial\sigma}\left(\sigma\frac{\partial\omega}{\partial\sigma}\right)-\frac{\omega}{\sigma^2}\right]. \tag{25}$$

For $R >> 1$, the vorticity is assumed to be confined to a thin layer with the thickness of $O(\delta)$ near the equatorial plane (i.e., wake). Then, in the wake region, $x = O(\delta)$, $\sigma = O(1)$, $u_x = O(\delta)$, and $u_\sigma = O(1)$. Now, let us introduce the rescaled variables such that

$$\tilde{u}_x = u_x/\delta,$$

$$\tilde{x} = x/\delta.$$

Then Eq. (25) becomes

$$\tilde{u}_x\frac{\partial\omega}{\partial\tilde{x}}+u_\sigma\frac{\partial\omega}{\partial\sigma}-\frac{\omega u_\sigma}{\sigma}=\frac{2}{R}\left[\frac{1}{\delta^2}\frac{\partial^2\omega}{\partial\tilde{x}^2}+O(1)\right].$$

Therefore, the most appropriate choice for δ is

$$\delta=\frac{2}{\sqrt{R}}.$$

The introduction of a new variable of $\Omega \equiv \omega/\sigma$ further reduces the equation to the following simple form

$$\tilde{u}_x\frac{\partial\Omega}{\partial\tilde{x}}+u_\sigma\frac{\partial\Omega}{\partial\sigma}=\frac{1}{2}\frac{\partial^2\Omega}{\partial\tilde{x}^2}. \tag{26}$$

Eq. (26) is a parabolic partial differential equation, so we need an initial condition for the variable σ and two boundary conditions for the variable $\tilde{x}$. The initial condition can be given by the vorticity distribution ($\Omega = \Omega_o(\tilde{x})$) at a certain point $\sigma = \sigma_o$, that is outside the bubble. The boundary conditions in $\tilde{x}$ are quite obvious. At the equatorial plane outside the bubble ($\tilde{x} = 0$, $\sigma \geq \sigma_o$), the vorticity is cancelled to be zero because of the symmetry condition ($\Omega = 0$). The other condition is that the vorticity vanishes at the outer edge of wake region; i.e., $\Omega \to 0$ as $\tilde{x} \to \infty$.

To make the problem simpler, let us assume that $\sigma_o = O(1)$ but is sufficiently large so that the velocity field in the wake region can be approximated by the undisturbed biaxial straining flow. Here we must note that we have assumed implicitly that the vorticity in the wake region is small enough so that the velocity perturbation due to vorticity is negligible in the wake region. This assumption is valid if the vorticity in the wake is $O(1)$ at any σ. The validity of the assumption will be examined *a posteriori*. The undisturbed velocity field is given by

$$\tilde{u}_x = -\tilde{x}, \qquad u_\sigma = \frac{1}{2}\sigma.$$

Now, the governing equation and boundary conditions for the vorticity distribution in the wake are

$$\frac{\sigma}{2}\frac{\partial \Omega}{\partial \sigma} = \tilde{x}\frac{\partial \Omega}{\partial \tilde{x}} + \frac{1}{2}\frac{\partial^2 \Omega}{\partial \tilde{x}^2}, \tag{27}$$

with

$$\Omega = \Omega_o(\tilde{x}) \qquad \text{at} \quad \sigma = \sigma_o,$$

$$\Omega = 0 \qquad \text{at} \quad \tilde{x} = 0, \ (\sigma \geq \sigma_o),$$

$$\Omega \to 0 \qquad \text{as} \quad \tilde{x} \to \infty \ (\sigma \geq \sigma_o).$$

The solution of (27) can be easily obtained by separation of variables, and is given as

$$\Omega = \sum_{k=1}^{\infty} C_k e^{-\tilde{x}^2} H_{2k-1}(\tilde{x}) \sigma^{-4k}, \tag{28}$$

where $H_{2k-1}(\tilde{x})$ is the $(2k-1)$st Hermite polynomial and the coefficient C_k is given by

$$C_k = \frac{\sigma_o^{4k}}{2^{2k-2}\sqrt{\pi}(2k-1)!} \int_0^\infty \Omega_o(\tilde{x}) H_{2k-1}(\tilde{x}) d\tilde{x}.$$

Since $\Omega = \omega/\sigma$, the final expression for ω is

$$\omega = \sum_{k=1}^{\infty} C_k e^{-\tilde{x}^2} H_{2k-1}(\tilde{x}) \sigma^{1-4k}. \tag{29}$$

The primary and important conclusion we can draw from the result (29) is that although vorticity can grow locally for finite σ because of the *vortex*

stretching mechanism, it eventually vanishes because of *diffusion* as $\sigma \to \infty$. Physically, the equatorial plane plays the role of a vorticity sink, because $\omega = 0$ there because of the exact cancellation of vorticity of opposite signs. Therefore, the effectiveness of diffusion for removal of vorticity requires that a large gradient of vorticity be maintained near the equatorial plane. In the biaxial straining flow, such a large gradient is achieved by convection of vorticity with the x-directional velocity component, $\tilde{u}_x = -\tilde{x}$. This convection effect is sufficient to maintain a large gradient of vorticity close to the vorticity sink (note that the vorticity has a maximum at a certain finite position $\tilde{x}$ for all $\sigma_o < \sigma < \infty$). As a conclusion of this subsection, it should be noted that Eq. (29) gives a theoretical basis for use of the far-field boundary condition for vorticity, $\omega \to 0$ as $\sqrt{x^2 + \sigma^2} \to \infty$, for the numerical analysis in the following sections.

IV. PROBLEM FORMULATION FOR NUMERICAL ANALYSIS

In the previous section, we have discussed some preliminary analytical results that are essential in understanding the deformation of a bubble in a biaxial straining flow. Although the analytical results give us some key ideas about the bubble deformation, the analyses have been limited to the limit of small deformation (i.e., $W << 1$) except for the invariance of steady bubble shapes with respect to a change of flow direction in the potential flow limit. Therefore, we need a more comprehensive numerical study of bubble deformation for a better understanding of the problem. In the following sections, we will discuss steady and unsteady bubble deformation in a biaxial straining flow via numerical analyses for $0 \leq R \leq 200$, as well as for the potential flow limit.

In the numerical analysis that follows, we have used the numerical scheme for unsteady, free-boundary problems, which was developed in I except for modifications in the difference scheme for the vorticity transport equation, which will be discussed later. Therefore, in this section, we present only the minimum description necessary for the present work.

All of the computations are performed on a time-dependent (or time independent in the case of steady-state analysis) boundary-fitted orthogonal coordinate system (ξ, η) as described in I. Thus, the boundary coordinate at any instant, t, is connected with the common cylindrical coordinate (x, σ) (with the axis of symmetry being the x-axis) via a pair of mapping functions $x(\xi, \eta, t)$ and $\sigma(\xi, \eta, t)$, which satisfy the covariant Laplace equations

$$\frac{\partial}{\partial \xi}(f\frac{\partial x}{\partial \xi}) + \frac{\partial}{\partial \eta}(\frac{1}{f}\frac{\partial x}{\partial \eta}) = 0, \tag{30a}$$

$$\frac{\partial}{\partial \xi}(f\frac{\partial \sigma}{\partial \xi}) + \frac{\partial}{\partial \eta}(\frac{1}{f}\frac{\partial \sigma}{\partial \eta}) = 0. \tag{30b}$$

Here the function $f(\xi, \eta)$ is the so-called *distortion function* representing the ratio h_η/h_ξ of scale factors $(h_\eta \equiv (g_{\eta\eta})^{1/2}, h_\xi \equiv (g_{\xi\xi})^{1/2})$ for the boundary-fitted coordinate system.

The fluid mechanics part of the problem is to obtain solutions of the Navier-Stokes equations using a finite-difference approximation in the boundary-fitted (ξ, η)-coordinate domain. With axisymmetry assumed, the Navier-Stokes equations are most conveniently expressed in terms of the stream function ψ and vorticity ω in the form

$$\frac{R}{2}\left[\left(\frac{\partial \omega}{\partial t}\right)_{x,\sigma} + \frac{1}{h_\eta h_\xi}\left\{\frac{\partial \psi}{\partial \xi}\frac{\partial}{\partial \eta}\left(\frac{\omega}{\sigma}\right) - \frac{\partial \psi}{\partial \eta}\frac{\partial}{\partial \xi}\left(\frac{\omega}{\sigma}\right)\right\}\right] = L^2(\omega\sigma), \tag{31}$$

$$L^2\psi + \omega = 0, \tag{32}$$

where $(\partial\omega/\partial t)_{x,\sigma}$ is calculated according to the transformation

$$\left(\frac{\partial w}{\partial t}\right)_{x,\sigma} = \left(\frac{\partial w}{\partial t}\right)_{\xi,\eta} + \frac{1}{h_\eta h_\xi}\left(\frac{\partial w}{\partial \xi}\frac{\partial \sigma}{\partial \eta} - \frac{\partial w}{\partial \eta}\frac{\partial \sigma}{\partial \xi}\right)\left(\frac{\partial x}{\partial t}\right)_{\xi,\eta} - \frac{1}{h_\eta h_\xi}\left(\frac{\partial w}{\partial \xi}\frac{\partial x}{\partial \eta} - \frac{\partial w}{\partial \eta}\frac{\partial x}{\partial \xi}\right)\left(\frac{\partial \sigma}{\partial t}\right)_{\xi,\eta},$$

and

$$L^2 \equiv \frac{1}{h_\eta h_\xi}\left\{\frac{\partial}{\partial \xi}\left(\frac{f}{\sigma}\frac{\partial}{\partial \xi}\right) + \frac{\partial}{\partial \eta}\left(\frac{1}{f\sigma}\frac{\partial}{\partial \eta}\right)\right\}.$$

The stream function ψ in (31) and (32) is defined so as to satisfy

$$u_\xi = -\frac{1}{\sigma h_\eta}\frac{\partial \psi}{\partial \eta},$$

$$u_\eta = \frac{1}{\sigma h_\xi}\frac{\partial \psi}{\partial \xi}.$$

We assume, for convenience, that the coordinate mapping is defined with $\xi = 1$ corresponding to the interface (Fig. 3), and with $\eta = 0$ and $\eta = 1$ being the symmetry axes. The boundary conditions at the symmetry axes are

$$\psi = 0, \quad \omega = 0 \qquad \text{at} \quad \eta = 0,\ 1. \tag{33}$$

At the gas-liquid interface ($\xi = 1$) we require

$$\psi = \int_0^\eta (-u_\xi)\sigma h_\eta d\eta = \int_0^\eta (-\frac{1}{\mid \nabla F \mid}\frac{\partial F}{\partial t})\sigma h_\eta d\eta \tag{34}$$

corresponding to the kinematic condition. In (34), F is a function that describes the bubble shape as $F(\mathbf{x}, t) = 0$ and u_ξ is the inward normal velocity. In addition, the vorticity at the bubble surface is given by

$$\omega = \frac{2}{h_\eta}\frac{\partial u_\xi}{\partial \eta} + 2\kappa_{(\eta)}u_\eta, \tag{35}$$

corresponding to the condition of zero tangential stress (where $\kappa_{(\eta)}$ is the normal curvature of the interface in the η-direction and u_η is the tangential velocity). Finally, the normal stress contributions due to pressure and viscous forces, on the one hand, and the capillary force, on the other, are required to balance

$$\tau_{\xi\xi} - \frac{4}{W}(\kappa_{(\eta)} + \kappa_{(\phi)}) = 0. \tag{36}$$

In (36) $\kappa_{(\phi)}$ is the normal curvature in the ϕ-direction, W is the (dimensionless) Weber number, and $\tau_{\xi\xi}$ is the total normal stress, which includes both static and dynamic pressure and viscous contributions.

The far-field boundary condition for the biaxial straining flow is given as

$$\psi \sim -\frac{1}{2}x\sigma^2, \quad \omega \to 0 \qquad \text{as} \quad \xi \to 0\ (\sqrt{x^2 + \sigma^2} \to \infty). \tag{37}$$

Since the stream function tends to $-\infty$ as $\xi \to 0$, a new unknown stream function ψ^* is introduced, which is bounded (see I and Ryskin and Leal[16])

$$\psi^* \equiv \psi + \frac{1}{2}x\sigma^2(1-\xi^5),$$

where $-\frac{1}{2}x\sigma^2(1-\xi^5)$ is subtracted instead of $-\frac{1}{2}x\sigma^2$ in order to have a simple boundary condition at the bubble surface ($\xi = 1$) and to have $\psi^* \equiv 0$ for the limiting case of potential flow around a sphere.

V. NUMERICAL SCHEME

The problem, from a numerical point of view, is to solve simultaneously the governing differential equations (30)-(32) subject to boundary conditions (33)-(37) as indicated above. In the present analysis, the transient algorithm described in I has been used with only a modification in the difference scheme for the vorticity equation as described below (note that the transient algorithm given in I with the time step $\Delta t = \infty$ degenerates to the steady-state algorithm of Ryskin and Leal[16]).

In I and in the paper by Ryskin and Leal, a non-conservative difference scheme was used for the vorticity equation. However, we have found that this non-conservative difference scheme results in an unconditionally unstable numerical scheme for high Reynolds numbers in the present biaxial straining flow problem. Therefore, in the present work, we have utilized a conservative difference scheme for the vorticity transport equation. This modified scheme is stable for both uniaxial and biaxial straining flows. Since conservation does not necessarily imply accuracy (although the experiences of many researchers indicate that a conservative method does usually give more accurate results, there are a number of counter examples: see Roache,[17] p.32), both methods have been used with equal preference in numerical analysis. However, in the present biaxial flow problem, the numerical algorithm with a non-conservative scheme is unconditionally unstable for $R >> 1$ because of the vorticity stretching term in

the vorticity transport equation. An analysis of this instability is presented in the following subsection.

A. Non-conservative difference scheme for the vorticity equation

Although we are concerned with unsteady as well as steady numerical solutions, we restrict our discussion in this and the following subsections to the steady-state algorithm for convenience. Since a successful algorithm should work for all situations, a discussion of the steady-state algorithm is enough to show instabilities (a discussion of the stabilitity for the unsteady algorithm will be essentially the same, with only minor modifications).

Let us start with the steady-state vorticity transport equation

$$\mathbf{u} \cdot \nabla \underline{\omega} - \underline{\omega} \cdot \nabla \mathbf{u} = \frac{2}{R} \nabla^2 \underline{\omega}. \tag{38}$$

For axisymmetric problems, we have $\underline{\omega} = (0, 0, \omega)$, and $\mathbf{u} = (u_\xi, u_\eta, 0)$ in the (ξ, η, ϕ) coordinate system. Thus, the equation for ω can be expressed in the following form

$$0 = f^2 \frac{\partial^2 \omega}{\partial \xi^2} + \frac{\partial^2 \omega}{\partial \eta^2} + q_1 \frac{\partial \omega}{\partial \xi} + q_2 \frac{\partial \omega}{\partial \eta} + q_3 \omega + q_4, \tag{39}$$

where

$$q_3 = \frac{R}{2} f h_\eta \frac{u_\xi}{\sigma} \frac{\partial \sigma}{\partial \xi} + \frac{R}{2} h_\eta \frac{u_\eta}{\sigma} \frac{\partial \sigma}{\partial \eta} - \left(\frac{f}{\sigma} \frac{\partial \sigma}{\partial \xi}\right)^2 - \left(\frac{1}{\sigma} \frac{\partial \sigma}{\partial \eta}\right)^2. \tag{40}$$

The other coefficients in (39) are not given explicitly because only q_3 is required in the following discussion.

Now, let us consider the simplest problem of a biaxial straining flow around a spherical bubble. For a spherical bubble, if we take the distortion factor $f = \pi\xi/2$, then the coordinate transformation of Eq. (30) is given by

$$x = \xi^{-1} \cos\left(\frac{\pi}{2}\eta\right),$$

$$\sigma = \xi^{-1} \sin\left(\frac{\pi}{2}\eta\right), \tag{41}$$

with

$$h_\eta = \frac{\pi}{2}\xi^{-1},$$

$$h_\xi = \xi^{-2}.$$

Furthermore, let us assume that the velocity field is given by the potential flow solution around a spherical bubble,

$$u_\xi = \mp\frac{1}{2h_\eta}(1-\xi^5)\Big[2x\frac{\partial\sigma}{\partial\eta} + \sigma\frac{\partial x}{\partial\eta}\Big], \tag{42a}$$

$$u_\eta = \mp\frac{1}{2h_\xi}\Big[-2x(1-\xi^5)\frac{\partial\sigma}{\partial\xi} - \sigma(1-\xi^5)\frac{\partial x}{\partial\xi} + 5\sigma x\xi^4\Big], \tag{42b}$$

where "-" and "+" of "$\mp$" refer to the uniaxial and biaxial straining flows, respectively. By substituting (41) and (42) into (40), we get

$$\begin{aligned} q_3 &= \mp\Big(\frac{Rf}{2}\Big)\Big[\frac{\pi}{4}\Big(\frac{1-\xi^5}{\xi^3}\Big) + \frac{5\pi}{4}x\xi^3\cos\Big(\frac{\pi}{2}\eta\Big)\Big] - \Big(\frac{\pi}{2}\Big)^2\Big[\frac{1}{\sin^2\big(\frac{\pi}{2}\eta\big)}\Big] \\ &\simeq \mp R\Big(\frac{\pi}{4}\Big)^2\Big[\Big(\frac{1-\xi^5}{\xi^2}\Big) + 5\xi^3\cos^2\Big(\frac{\pi}{2}\eta\Big)\Big] \qquad \text{for} \quad R >> 1. \end{aligned} \tag{43}$$

Now, let us consider the numerical solution of (39) on an $N \times N$ grid system for the domain $0 \le \xi,\ \eta \le 1$, with the boundary conditions

$$\omega = 0 \quad \text{at} \quad \eta = 0, \quad \eta = 1, \quad \text{and} \quad \xi = 0,$$

$$\omega = \omega_o(\eta) \quad \text{at} \quad \xi = 1.$$

Spatial discretization of (39) with the second-order central difference scheme gives us a system of linear algebraic equations of the form

$$\mathbf{A}\mathbf{w} = \mathbf{b}, \tag{44}$$

where

$$\mathbf{w} = (\omega_{11}, \cdots, \omega_{1N}, \cdots, \omega_{N1}, \cdots, \omega_{NN}),$$

and $\mathbf{A}$ is a $N^2 \times N^2$ matrix. The solution method used in I for (44) is the ADI method, which is based on the transformation of (44) into a fictitious initial value problem

$$\frac{d\mathbf{w}}{d\tau} = \mathbf{A}\mathbf{w} - \mathbf{b}. \tag{45}$$

Then, the stability of the numerical scheme is completely determined by the eigenvalues of matrix **A**. The *necessary* condition for stability is that the trace of **A** should be negative; i.e.,

$$\sum_{k=1}^{N^2} \lambda_k = \sum_{k=1}^{N^2} a_{kk} < 0; \tag{46}$$

otherwise, at least one eigenvalue must be positive, implying instability. The diagonal elements of **A** can be expressed as

$$\begin{aligned} a_{kk} &= -\frac{2}{h^2}(f_{ij}^2 + 1) + q_{3,ij} \\ &\simeq -\frac{2}{h^2}\left(\left(\frac{\pi}{2}\right)^2 \xi_{ij}^2 + 1\right) \mp R\left(\frac{\pi}{4}\right)^2 \left[\left(\frac{1-\xi_{ij}^5}{\xi_{ij}^2}\right) + 5\xi_{ij}^3 \cos^2\left(\frac{\pi}{2}\eta_{ij}\right)\right], \end{aligned} \tag{47}$$

where $h = \frac{1}{N}$, $k = (i-1) \times N + j$, and the indices i and j stand for the grid point $(\xi_{ij}, \eta_{ij}) = (ih, jh)$. The necessary condition for stability is satisfied for all R in the case of uniaxial straining flow, because $a_{kk} < 0$ for all k as we can see in (47) ("-" of $\mp$ is for the uniaxial straining flow). However, the necessary condition for stability is violated as $R \to \infty$ in the case of biaxial straining flow, because

$$\begin{aligned} \sum_{k=1}^{N^2} a_{kk} &\simeq \sum_{k=1}^{N^2} \left[-\frac{2}{h^2}\left(\left(\frac{\pi}{2}\right)^2 \xi_{ij}^2 + 1\right) + R\left(\frac{\pi}{4}\right)^2 \left\{\left(\frac{1-\xi_{ij}^5}{\xi_{ij}^2}\right)\right\} + 5\xi_{ij}^3 \cos^2\left(\frac{\pi}{2}\eta_{ij}\right)\right], \\ &> -2\left(\frac{1}{3}\left(\frac{\pi}{2}\right)^2 + 1\right)\frac{1}{h^4} + R\left(\frac{\pi}{4}\right)^2 \frac{1}{h^3} \\ &> \frac{-8 + Rh}{2h^4}. \end{aligned} \tag{48}$$

Therefore, if $R > \frac{8}{h}$, the numerical scheme must be unstable. In fact, when a 40×40 grid system was used in our numerical computation, the ADI scheme with the non-conservative difference scheme failed to converge for $R > 5$ in the case of biaxial straining flow, while convergent solutions were obtained for all R up to the maximum value considered (100) in the uniaxial straining flow problem.

Now, the question is how we can get around this difficulty while maintaining second-order accuracy in the spatial discretization. The answer is given in the following subsection.

B. Modified difference scheme for the vorticity transport equation

Let us begin with the vorticity transport equation for an axisymmetric problem in the (ξ, η, ϕ)-coordinate system

$$\frac{R}{2}\Big[\mathbf{u}\cdot\nabla\omega - \Big(\frac{\omega}{\sigma}\frac{u_\xi}{h_\xi}\frac{\partial\sigma}{\partial\xi} + \frac{\omega}{\sigma}\frac{u_\eta}{h_\eta}\frac{\partial\sigma}{\partial\eta}\Big)\Big] = L^2(\omega\sigma). \tag{49}$$

In (49), it may be noted that $\mathbf{u}\cdot\nabla\omega = \nabla\cdot(\omega\mathbf{u})$ because of the continuity equation $(\nabla\cdot\mathbf{u} = 0)$. The main idea of the modification is to adopt the conservative form $\nabla\cdot(\omega\mathbf{u})$ instead of $\mathbf{u}\cdot\nabla\omega$. Therefore,

$$\begin{aligned}\mathbf{u}\cdot\nabla\omega &= \nabla\cdot(\omega\mathbf{u}) \\ &= \frac{1}{h_\xi h_\eta\sigma}\Big[\frac{\partial}{\partial\xi}(h_\eta\sigma\omega u_\xi) + \frac{\partial}{\partial\eta}(h_\xi\sigma\omega u_\eta)\Big].\end{aligned} \tag{50}$$

Substituting (50) into (49), we get

$$\frac{R}{2}\frac{1}{h_\xi h_\eta}\Big[\frac{\partial}{\partial\xi}(h_\eta\omega u_\xi) + \frac{\partial}{\partial\eta}(h_\xi\omega u_\eta)\Big] = L^2(\omega\sigma), \tag{51}$$

and we can express (51) in the form

$$0 = f^2\frac{\partial^2\omega}{\partial\xi^2} + \frac{\partial^2\omega}{\partial\eta^2} + \tilde{q}_1\frac{\partial\omega}{\partial\xi} + \tilde{q}_2\frac{\partial\omega}{\partial\eta} + \tilde{q}_3\omega + \tilde{q}_5\Big[\frac{\partial}{\partial\xi}(h_\eta\omega u_\xi) + \frac{\partial}{\partial\eta}(h_\xi\omega u_\eta)\Big], \tag{52}$$

where

$$\tilde{q}_3 = -\Big[\Big(\frac{f}{\sigma}\frac{\partial\sigma}{\partial\xi}\Big)^2 + \Big(\frac{1}{\sigma}\frac{\partial\sigma}{\partial\eta}\Big)^2\Big],$$

$$\tilde{q}_5 = -\frac{R}{2}f.$$

In discretizing (52), we apply the conservative difference form to the last two terms. For example,

$$\frac{\partial}{\partial\xi}(h_\eta\omega u_\xi) = \frac{(h_\eta\omega u_\xi)_{i+1,j} - (h_\eta\omega u_\xi)_{i-1,j}}{2h} + O(h^2). \tag{53}$$

If we write the discretized equation in the form

$$\frac{d\mathbf{w}}{d\tau} = \tilde{\mathbf{A}}\mathbf{w} - \tilde{\mathbf{b}}, \tag{54}$$

the diagonal element of $\tilde{\mathbf{A}}$ is given as

$$\tilde{a}_{kk} = -\frac{2}{h^2}(f_{ij}^2 + 1) + \tilde{q}_{3,ij} < 0 \qquad \text{for all } k,$$

where $h = \frac{1}{N}$, $k = (i-1) \times N + j$. Therefore, the *necessary* condition for stability is automatically satisfied for all types of axisymmetric flow and for all Reynolds numbers, while second-order accuracy is preserved as we can see in (53).

Now, we are going to show that the difference scheme in (53) has the conservative property, to show that we consider the term

$$\nabla \cdot (\frac{\omega}{\sigma}\mathbf{u}) = \frac{1}{h_\xi h_\eta \sigma}\Big[\frac{\partial}{\partial \xi}(h_\eta \omega u_\xi) + \frac{\partial}{\partial \eta}(h_\xi \omega u_\eta)\Big].$$

Then what we need to show is that the discretized equation also satisfies

$$\int_V \nabla \cdot (\frac{\omega}{\sigma}\mathbf{u}) dV = \int_S (\frac{\omega}{\sigma}\mathbf{u}) \cdot \mathbf{n} dS,$$

where V is an arbitrary, axisymmetric closed volume in the flow region and S is the closed surface of V. Consider any domain such as the shaded region in Fig. 3 for which the grid system is given as

$$n(j) - \frac{1}{2} \le i \le N(j) + \frac{1}{2}, \quad \text{where } n \le n(j) \le N(j) \le N,$$

$$m(i) - \frac{1}{2} \le j \le M(i) + \frac{1}{2}, \quad \text{where } m \le m(i) \le M(i) \le M.$$

Then,

$$\begin{aligned}
&\int_V \nabla \cdot (\frac{\omega}{\sigma}\mathbf{u}) dV \\
&\quad = \int_R \Big[\frac{\partial}{\partial \xi}(h_\eta \omega u_\xi) + \frac{\partial}{\partial \eta}(h_\xi \omega u_\eta)\Big] d\xi d\eta \\
&\quad = \sum_{j=m}^{M} \sum_{i=n(j)}^{N(j)} \Big[\frac{(h_\eta \omega u_\xi)_{i+1,j} - (h_\eta \omega u_\xi)_{i-1,j}}{2h}\Big] \cdot h^2
\end{aligned}$$

$$
\begin{aligned}
&+\sum_{i=n}^{N}\sum_{j=m(i)}^{M(i)}\left[\frac{(h_\xi\omega u_\eta)_{i,j+1}-(h_\xi\omega u_\eta)_{i,j-1}}{2h}\right]\cdot h^2\\
&=\sum_{j=m}^{M}\Bigg[\frac{(h_\eta\omega u_\xi)_{N(j)+1,j}+(h_\eta\omega u_\xi)_{N(j),j}}{2}\\
&\quad-\frac{(h_\eta\omega u_\xi)_{n(j)-1,j}+(h_\eta\omega u_\xi)_{n(j),j}}{2}\Bigg]\cdot h\\
&\quad+\sum_{i=n}^{N}\Bigg[\frac{(h_\xi\omega u_\eta)_{i,M(i)+1}+(h_\xi\omega u_\eta)_{i,M(i)}}{2}\\
&\quad-\frac{(h_\xi\omega u_\eta)_{i,m(i)-1}+(h_\xi\omega u_\eta)_{i,m(i)}}{2}\Bigg]\cdot h\\
&=\sum_{j=m}^{M}\left[(h_\eta\omega u_\xi)_{N(j)+\frac{1}{2},j}-(h_\eta\omega u_\xi)_{n(j)-\frac{1}{2},j}\right]\cdot h\\
&\quad+\sum_{i=n}^{N}\left[(h_\xi\omega u_\eta)_{i,M(i)+\frac{1}{2}}-(h_\xi\omega u_\eta)_{i,m(i)-\frac{1}{2}}\right]\cdot h\\
&=\int_S\left(\frac{\omega}{\sigma}\mathbf{u}\right)\cdot\mathbf{n}dS.
\end{aligned}
\tag{55}
$$

Therefore, the difference scheme of (53) satisfies the conservative property. As an example, let us consider the vorticity distribution in an axisymmetric, steady inviscid flow. Since $\nabla\cdot\left(\frac{\omega}{\sigma}\mathbf{u}\right)=0$, we have

$$\int_S\left(\frac{\omega}{\sigma}\mathbf{u}\right)\cdot\mathbf{n}dS=0. \tag{56}$$

Also, we know that

$$\int_S\mathbf{u}\cdot\mathbf{n}dS=0 \tag{57}$$

is true if we use the stream function and vorticity formulation in the numerical analysis. The only way to satisfy both conditions simultaneously is if $\omega/\sigma =$ *constant* along a stream line, which is, in fact, a steady-state version of Kelvin's circulation theorem. Therefore, the conservative difference scheme in the present study is guaranteed to satisfy Kelvin's circulation theorem.

In the following sections the numerical results obtained via the modified scheme will be presented.

VI. RESULTS OF STEADY STATE ANALYSIS

We have done computations for $R = 0$, 1, 10, 50, 100, 200, and for potential flow, gradually increasing W in each case until a highly deformed shape was obtained (i.e., until a very large aspect ratio l/b was obtained, where l is the length of the longer axis and b is the length of the shorter axis). In contrast to the case of uniaxial straining flow, which exhibited a critical Weber number beyond which no steady-state solution was possible, the biaxial flow problem does not appear to have any limit point with finite deformation (i.e., $l/b = O(1)$) even at large but finite Reynolds numbers. The computed bubble shapes for various Reynolds numbers and Weber numbers are shown in Fig. 4, and the stream lines and vorticity contours for various Reynolds numbers and Weber numbers are also shown in Fig. 5. A detailed discussion of the results will be given in the remainder of this section.

At very low Reynolds numbers, represented in Fig. 4 by $R = 0$ and $R = 1$, there is a general trend for a bubble to be flattened monotonically to an oblate shape with an increase in the capillary number, $Ca = \mu Ea/\gamma = W/R$ (if $R \neq 0$). As a consequence of this deformation of shape, the curvature of the interface becomes very large at the edge of the bubble, but positive curvature is maintained at the stagnation points on the symmetry axis for all values of Ca that we have considered. Since no theoretical work is available for this extremely deformed (flattened) bubble, no explicit comparison can be given. For the problem of a bubble in a biaxial straining flow, we are aware of only one previous analysis by Frankel and Acrivos.[12] They computed bubble shapes in the creeping flow limit ($R = 0$) up to an intermediate capillary number ($Ca = 0.2$) via a semi-analytical approach. The results of Frankel and Acrivos for $R = 0$ are compared with those of the present work in Fig. 6. Also given are the numerical results for a uniaxial creeping flow by Youngren and Acrivos[2] and Ryskin and Leal.[4] In Fig. 6, the measure of deformation is defined as $D = (l - b)/(l + b)$, where l is the radius of the longer axis and b is the radius of the shorter axis.

As the Reynolds number increases, the edge of the bubble at the equatorial plane first becomes more rounded and then flattened at higher Reynolds numbers, and the surface near the stagnation point on the symmetry axis also becomes increasingly flattened until eventually it shows a negative curvature, for large W and $R \geq 50$. Negative curvatures may also occur at very high W values for lower Reynolds numbers, but this is not evident in the present solutions. The negative curvatures at the axial stagnation points are not surprising because it is only through negative curvature that a balance can be maintained with the high stagnation pressure. However, in the case of uniaxial straining flow, no stable steady shape with negative curvature has been observed (see Ryskin and Leal and I), in spite of the fact (or perhaps "because" of it) that the negative curvature that occurs in that case at the stagnation point on the equatorial plane, involves only one component of the curvature $\kappa_{(\eta)}$; i.e.,

$$\kappa_{(\eta)} = -\frac{1}{h_\eta^2}\frac{\partial^2 \sigma}{\partial \eta^2} < 0 \qquad \text{at} \quad \eta = 1,$$

but

$$\kappa_{(\phi)} = \frac{1}{\sigma} > 0 \qquad \text{at} \quad \eta = 1.$$

The present results at the highest Reynolds numbers exhibit especially interesting behavior. For small Weber numbers, there is a marginal Reynolds number as predicted in Sec. III at which the elongational direction is changed. The estimated marginal Reynolds number in Sec. III was $R_m = 115$, and it can be seen from Fig. 4 that the numerical solution does change form between $R = 100$ and $R = 200$. The bubble at $R = 100$ (for either $W = 2$ or 4) is elongated in the direction of the equatorial plane, but the bubble at $R = 200$ ($W = 2$ or 4) is elongated in the axial direction. Although the latter result seems quite surprising, it is possible because the stress (mainly pressure at a high Reynolds number) distribution is dominated by the pressure at a high Reynolds number and the latter is governed by Bernoulli's theorem. This trend toward shapes that are elongated in the axial direction for those slightly deformed bubbles is

smoothly continued to the potential flow limit. However, for finite Reynolds number above the marginal value (e.g. $R = 200$), the elongation in the direction of the symmetry axis is not maintained as the Weber number increases. Instead, the bubble again becomes elongated in the equatorial direction for higher Weber numbers. By comparison with the potential flow result, it is obvious the behavior with an increase in W is fundamentally different for $R = \infty$ and R large, but finite ($R = 200$)! Although this, in itself, might seem quite unexceptional since $R = 200$ is hardly $R = \infty$, the fact is that the corresponding solution at $R = 200$ for a bubble in a uniaxial straining flow (solution for $R = 100$ is obtained in Ryskin and Leal[4]) agrees very closely with the potential flow solution over the whole range of W where steady-state solutions existed.

The implication of the preceding paragraph is that the potential flow solution for the biaxial flow problem appears to correspond to the limit for $R \to \infty$ only when W is small (and bubble deformation is small), and this represents a fundamental difference from the uniaxial flow problem. Another striking difference is that stable, steady-state shapes are obtained for very high Weber numbers ($W > 10$), while the maximum Weber number for existence of a stable steady shape in the uniaxial flow at $R = 200$ was only about 2.4. It may also be noted that steady solutions exist in the potential flow problem up to a maximum Weber number of 2.7. Although we could not obtain solutions with adequate resolution for $R > 200$ with the 40×40 grid system that has been employed in the present work, the trend of solutions for the higher Reynolds numbers seems to suggest that we might expect steady solutions to exist for very large W, with an edge of infinite curvature formed as $R \to \infty$. Since increasing vorticity would be generated with increase of R as the curvature increases, it is likely that flow separation may occur in the limit $R \to \infty$. Once there is flow separation (or any alternative flow figuration with large vorticity generation), the potential flow will not provide a valid approximation to the real flow for the limit $R \to \infty$. As we can see in Fig. 5, no flow separation has been observed up to $R = 200$, but

the vorticity in the downstream zone increases drastically as $R \to \infty$.

So far we have discussed the limiting behavior of the solution for the biaxial straining flow problem in the limit $R \to \infty$. We have found that the potential solution is not the uniformly valid limiting solution (for all Weber numbers) for the real flow problem in that limit. In general, if the effect of vorticity due to viscosity vanishes as $R \to \infty$, then the potential flow solution corresponds to the real flow in the limit. In the biaxial flow case, the effect of vorticity may not vanish as $R \to \infty$ because the generation of vorticity increases via the increase of the curvature at the edges as the Reynolds number increases. In contrast to the biaxial flow case, the potential flow solution is the limiting solution as $R \to \infty$ in the uniaxial flow case. In the uniaxial flow case, the limit point of the existence of the steady-state solution changes smoothly to the limit point of the potential flow solution, and the shapes at subcritical Weber numbers also change smoothly to those of the potential flow solution (see Ryskin and Leal and I).

Now, the question is what kind of fundamental difference exists between the uniaxial and biaxial flow cases for $R \neq \infty$, which may explain the differences in the limiting behavior in two cases. The basis of the answer to this question, in our view, must lie in the interaction between the bubble shape, the production of vorticity due to the curvature of the bubble surface, and the enhancement of vorticity in the near "wake" region downstream of the bubble by vortex stretching. Indeed, for finite R where vorticity can be produced, the fundamental difference between uniaxial and biaxial flow is that the principal axis of elongation in the near-wake "downstream" of the bubble is orthogonal to the vorticity axis for the uniaxial case (so that vorticity only convects and diffuses but is not enhanced through vortex stretching), while for the biaxial case the elongation direction and the vorticity are parallel so that the vorticity can be increased in magnitude by vortex-line stretching. Thus, all else being equal, the vorticity levels downstream (near the equatorial plane) for the biaxial case

should be larger than downstream (along the axis of symmetry) in the uniaxial case. As a result, a larger pressure decrease is also expected in the downstream zone because the level of vorticity is a measure of deviation of real flow from the potential flow, and this is the reason why the bubble becomes elongated in the equatorial direction with an increase of W. The pressure distributions along the bubble surface are shown in Fig. 7, where η is the η-coordinate value in the numerical analysis (see Fig. 3). As we can see in Fig. 7, the pressure near the equatorial stagnation point decreases as the Weber number increases.

The other factor, which contributes to the difference in behavior between the uniaxial and biaxial case, is that the pressure induced indentation along the symmetry axis, combined with stretching in the equatorial plane, produces shapes with increasing curvature in the transition between these two regions, and this, in turn, leads to increasing vorticity production with increase of W (or for fixed $W > 4$, with increase of R). To discuss this deformation behavior and the difference between this and the uniaxial flow case, it is convenient to decompose the normal stress into two parts as following:

$$-N = (-N)_p + (-N)_v,$$

where $(-N)_p$ is corresponding to the potential flow solution and $(-N)_v$ is the difference between the total value and the potential flow part. Here we must note that $(-N)_p = p_p$, where p_p is the pressure distribution due to the potential flow solution. The deformation behavior of a bubble in the two types of flow is schematically illustrated in Fig. 8. The effect of p_p is the same for both cases and induces an elongation in the direction of the symmetry axis because the pressure due to potential flow is invariant to the change of the flow direction (see the discussion in Sec. III.A). However, the viscous effect is obviously dependent on the flow direction of the flow, i.e., elongation in the equatorial direction in the biaxial straining flow and elongation in the direction of symmetry axis in the uniaxial straining flow. Therefore, the elongation direction due to viscous and pressure effects coincides in the case of uniaxial straining flow while the

elongation directions are perpendicular in the case of the biaxial straining flow. In the case of uniaxial straining flow, the viscous effect smooths out the high curvature regions by pulling out the axial stagnation point. Therefore, the maximum curvature of $\kappa(\eta)$ at the points between the stagnation point occurs for the potential flow solution (see Fig. 1 of Ryskin and Leal). Consequently, there is a smooth change of curvature as $R \to \infty$, and this implies that the potential flow solution corresponds to the limiting solution of the real flow in the limit $R \to \infty$. In the biaxial straining flow, on the other hand, a smooth transition to the potential flow solution is possible only when the Weber number is small enough to maintain finite curvature everywhere. If the Weber number is large, as discussed earlier, the bubble seems to evolve, with an increase of W or R, toward shapes with increasing curvature at the edges. These regions of high curvature with the increase of R may explain why the potential flow solution is not a uniformly valid limiting solution of the real flow for all W in the biaxial straining flow case.

Finally, a comment should be made about the related problem of a rising bubble in a quiescent fluid. The potential flow solution is the appropriate approximation for the limit $R \to \infty$ if the curvature remains finite everywhere. If, however, we develop an infinite curvature edge (e.g., spherical cap bubble), the potential flow solution cannot provide a valid approximation for $R \to \infty$. Similarly, it appears that the bubble deformation in a biaxial straining flow is another example of a free surface problem for which the potential flow solution is not a uniformly valid (for all Weber numbers) approximation for the limit $R \to \infty$.

VII. RESULTS OF THE UNSTEADY DEFORMATION ANALYSIS

For the unsteady state analysis, the algorithm in I has been used with the modification in the difference scheme for the vorticity transport equation, which is dicussed in Sec. IV. Since the steady numerical analysis exhibited no critical Weber number for the existence of steady-state shapes for $R \leq 200$ in the range

of the Weber numbers considered in the present study, the present unsteady analysis is limited to very few cases.

A. Unsteady deformation in potential flow

It was shown in Sec. III that the steady-state shapes in potential flow are exactly the same for both uniaxial and biaxial straining flows. It was also shown that the oscillation frequencies of the primary mode are the same in both types of flow up to $O(W)$. However, since no general relationship between the bubble deformations in transient flows is available, we have done two different numerical experiments for unsteady deformation in potential flow. One is for unsteady deformation at a supercritical Weber number, and the other is for unsteady deformation at a subcritical Weber number.

First, the unsteady deformation at a supercritical Weber number was computed to see if there exists a stable steady state for $W > W_c$. Starting from the steady-state solution for $W = 2.7$, the Weber number was increased to 2.9 at $t = 0$. In Fig. 9, the unsteady deformation is shown for $1.7 \leq t \leq 4.5$. Surprisingly enough, the bubble initially elongates against the flow direction, but later elongation in that direction is stopped. In order for a bubble to be elongated against the flow direction, the bubble must do enough work on the fluid to overcome the inertia of the flow. Therefore, indefinite elongation against the flow is impossible for this biaxial straining flow. Indeed, as this elongation against the flow slows down, the region near the equatorial stagnation plane shows negative curvature ($\kappa_{(\eta)} < 0$), which increases rapidly as t increases. Therefore, in spite of the fact that the steady bubble shape is identical in the potential flow limit for uniaxial and biaxial straining flows, the transient deformations for supercritical Weber numbers are fundamentally different. A bubble is extended indefinitely in a uniaxial straining flow, while in a biaxial extensional flow the deformation corresponds to an increase of negative curvature ($\kappa_{(\eta)}$) along the equatorial plane without much extension in the axial direction.

The oscillation of a bubble in a biaxial straining flow was also computed for the case of $W = 1$ in the potential flow limit. Starting with the steady-state solution for $W = 2.7$, the Weber number was decreased to 1.0 at $\tilde{t} = 0$. In Fig. 10, the radius of a bubble in the axial direction is plotted as a function of surface-tension based time scale $\tilde{t}$, and it is compared with that of a bubble in a uniaxial straining flow. For the uniaxial flow problem, the initial condition is also the steady-state solution for $W = 2.7$. As we can see in Fig. 10, the phases are different, but the frequencies are almost same for both cases. This result is consistent with the fact that the formula $\omega_2^2 = \omega_{2,0}^2(1 - 0.31W) + o(W)$ is true for both cases, but extends the result to finite W.

B. Unsteady deformation in high Reynolds number flow

As shown in Sec. V, a bubble in biaxial straining flow at a high Reynolds number has a shape with negative curvature at the axial stagnation points if the Weber number is sufficiently large (see Fig. 4). In this section, we are going to show that the steady-state shapes obtained in Sec. VI are stable by showing that an initially deformed bubble, with a small disturbance or even with a large disturbance, is eventually attracted to the steady-state shape obtained via the steady-state analysis.

First, we studied the unsteady deformation of a bubble at $R = 100$ and $W = 12$ whose initial state is the $R = 100$ and $W = 10$ steady-state solution. The consecutive bubble shapes are overlapped in Fig. 11. As we can see in Fig. 11, the bubble is attracted directly to the steady-state shape for $R = 100$ and $W = 12$. In addition, we studied the unsteady deformation of a bubble started from rest; i.e., at $t = 0$, the flow is turned on with the bubble shape initially being spherical for two cases ($R = 50/W = 12$ and $R = 100/W = 10$). The consecutive bubble shapes are shown in Fig. 12. As we can see, the bubble shapes are smoothly attracted once again to the steady-state shapes. The poles (the intersections of the bubble surface and the symmetry axis) move inward monotonically except for a nearly negligible overshoot near the steady state.

However, the behavior of the surface near the equator is different. Initially, the equatorial lines are moving inward because of the high stagnation pressure at the equator, but the negative curvatures eventually disappear as the deformation proceeds. By comparing the $R = 50/W = 12$ and $R = 100/W = 10$ cases, we can see that the initial effect of higher stagnation pressures is more prominent for the higher Reynolds number. However, in both cases, the bubble shape eventually recovers positive curvature ($\kappa_{(\eta)} > 0$) on the equatorial plane. Of course, one mechanism for this change is the decrease in pressure at the equatorial plane because of the increasing vorticity levels as described before. One question, however, is the role of surface tension in the transient evolution of the bubble shape. In order to assess the effects of surface tension, we did the same computation for $R = 100$ and $W = 1000$, where the surface tension effect may be safely neglected. The consecutive deformations are shown in Fig. 13. As we can see in Fig. 13, the negative curvature grows monotonically and very high curvature edges are formed as time increases. Clearly, surface tension effects are playing a critical role in the previous observations. The flow field around the deformed bubble at $t = 0.575$ is also shown in Fig. 13. It is quite interesting to note that the stagnation points are inside the fluid rather than on the bubble surface.

VIII. CONCLUSION

From the analytical and numerical studies of steady and unsteady bubble deformation in a biaxial straining flow we have reached the following conclusions.

(1) Numerical Analysis: We found that the ADI method with a non-conservative difference scheme for the vorticity equation is unconditionally unstable for $R >> 1$ in the present biaxial straining flow problem. However, the ADI method with a conservative difference scheme for the vorticity equation turned out to be stable for the whole range of Reynolds numbers considered in the present work.

(2) Fluid Mechanics:

(a) The shape of a bubble in an inviscid, biaxial straining flow is identical to that in a uniaxial straining flow, and no stable steady state has been found for the supercritical Weber numbers, $W > W_c$, where W_c is between 2.7 and 2.8.

(b) A slightly deformed oscillating bubble in an inviscid, biaxial straining flow has the same frequency of the lowest mode as that of a bubble in an inviscid, uniaxial straining flow up to $O(W)$. The frequency is a decreasing function of W, and it is given by $\omega_2^2 = \omega_{2,0}^2(1 - 0.31W) + o(W)$.

(c) No critical Weber number, for non-existence of steady-state solutions in biaxial flow, is found numerically, for the ranges of Weber number and Reynolds number considered in this work.

(d) From the steady-state analysis for small Weber numbers, we have found that there exists a *marginal* Reynolds number at which the elongational direction is changed from equatorial to axial. Both the analytical and the numerical studies show that the marginal Reynolds number is between 100 and 200. Also, we have found that for a fixed Reynolds number above the marginal value there exists a Weber number at which the radii in the axial and the equatorial directions are the same.

(e) At high Reynolds numbers ($R > 50$), negative curvature shows up at the axial stagnation point as the Weber number increases, and the curvature at the edge of the cylindrical bubble increases with an increase of either R or W.

(f) The potential flow solution is not a uniformly valid (for all W) limiting solution for the real flow in the limit $R \to \infty$. In that limit, it appears that a bubble at a high Weber number may have edges with infinite curvature that will induce flow separation via infinite vorticity generation.

ACKNOWLEDGMENT

This work was supported by a grant from the Fluid Mechanics Program at the National Science Foundation.

REFERENCES

[1] I.S. Kang and L.G. Leal, Phys. Fluids, **30**, 1929 (1987).

[2] G.K. Youngren and A. Acrivos, J. Fluid Mech. **76**, 433 (1976).

[3] M.J. Miksis, Phys. Fluids **24**, 1229 (1981).

[4] G. Ryskin and L.G. Leal, J. Fluid Mech. **148**, 37 (1984).

[5] G.I. Taylor, Proc. R. Soc. Lond. **A 146**, 501 (1934).

[6] G.I. Taylor, in *Proc. 11th Intl Congr. Appl. Mech., (Munich, 1964)*, ed. by H. Görtler (Springer-Verlag, Berlin, 1966), p. 790.

[7] J.D. Buckmaster, J. Fluid Mech. **55**, 385 (1972).

[8] D. Barthes-Biesel and A. Acrivos, J. Fluid Mech. **61**, 1 (1973).

[9] A. Acrivos and T.S. Lo, J. Fluid Mech. **86**, 641 (1978).

[10] E.J. Hinch, J. Fluid Mech. **101**, 545 (1980).

[11] I.S. Kang and L.G. Leal, J. Fluid Mech., in press (1987).

[12] N.A. Frankel and A. Acrivos, J. Fluid Mech., **44**, 65 (1970).

[13] J.O. Hinze, AIChE J., **1**, 289 (1955).

[14] D.A. Lewis and J.F. Davidson, Trans. I. Chem E., **60**, 283 (1982).

[15] G.K. Batchelor, *An Introduction to Fluid Dynamics* (Cambridge U. Press, Cambridge, 1967).

[16] G. Ryskin and L.G. Leal, J. Fluid Mech. **148**, 1 (1984).

[17] P.J. Roache, *Computational Fluid Dynamics* (Hermosa, Albuquerque, 1972).

FIGURE CAPTIONS

Fig. 1. A bubble in a biaxial straining flow.

Fig. 2. $\Delta g = g(0) - g(\frac{\pi}{2})$ in terms of Reynolds number, where the shape of the bubble is given by $r_s(\theta) = 1 + \frac{W}{4} g(\theta)$. (– – – – –: biaxial straining flow, ——————: uniaxial straining flow).

Fig. 3. A boundary-fitted coordinate system and an arbitrary axisymmetric closed volume V in the flow.

Fig. 4. Steady-state shapes of a bubble in a biaxial straining flow for various Reynolds numbers and Weber numbers.

Fig. 5. Stream lines and vorticity contours for various Reynolds numbers and Weber numbers.

Fig. 6. Comparison of the present results for a bubble in a biaxial straining flow at $R = 0$ with the result of Frankel and Acrivos[12], and the results for the problem of uniaxial straining flow. (——: present result for biaxial flow, •: Frankel and Acrivos[12] for biaxial flow, – – – –: Youngren and Acrivos for uniaxial flow, ■: Ryskin and Leal[4] ($R = 0.1$) for uniaxial flow).

Fig. 7. Pressure distributions along the bubble surface when $R = 200$.

Fig. 8. Schematic diagram to explain the fundamental difference of deformation behaviors in two types of straining flow.

Fig. 9. Consecutive deformations of a bubble in an inviscid, biaxial straining flow at $W = 2.9$ starting from the steady state for $W = 2.7$ ($1.7 \leq t \leq 4.5$).

Fig. 10. Oscillation of a bubble in an inviscid, straining flow at $W = 1$ (——: biaxial straining flow, – – – –→: uniaxial straining flow, and $\tilde{t}$ is the surface-tension based dimensionless time, $\tilde{t} = \sqrt{\frac{2}{W}}t$).

Fig. 11. Unsteady deformation of a bubble in a biaxial straining flow at $R = 100$ and $W = 12$ (starting from the steady state at $R = 100$ and $W = 10$).

Fig. 12. Unsteady deformation of a bubble in a biaxial straining flow starting from the spherical shape. (a) $R = 50$ and $W = 12$, (b) $R = 100$ and

$W = 10$.

Fig. 13. (a) Unsteady deformation of a bubble in a biaxial straining flow at $R = 100$ and $W = 1000$ starting from sphere. (b) Velocity field at $t = 0.575$.

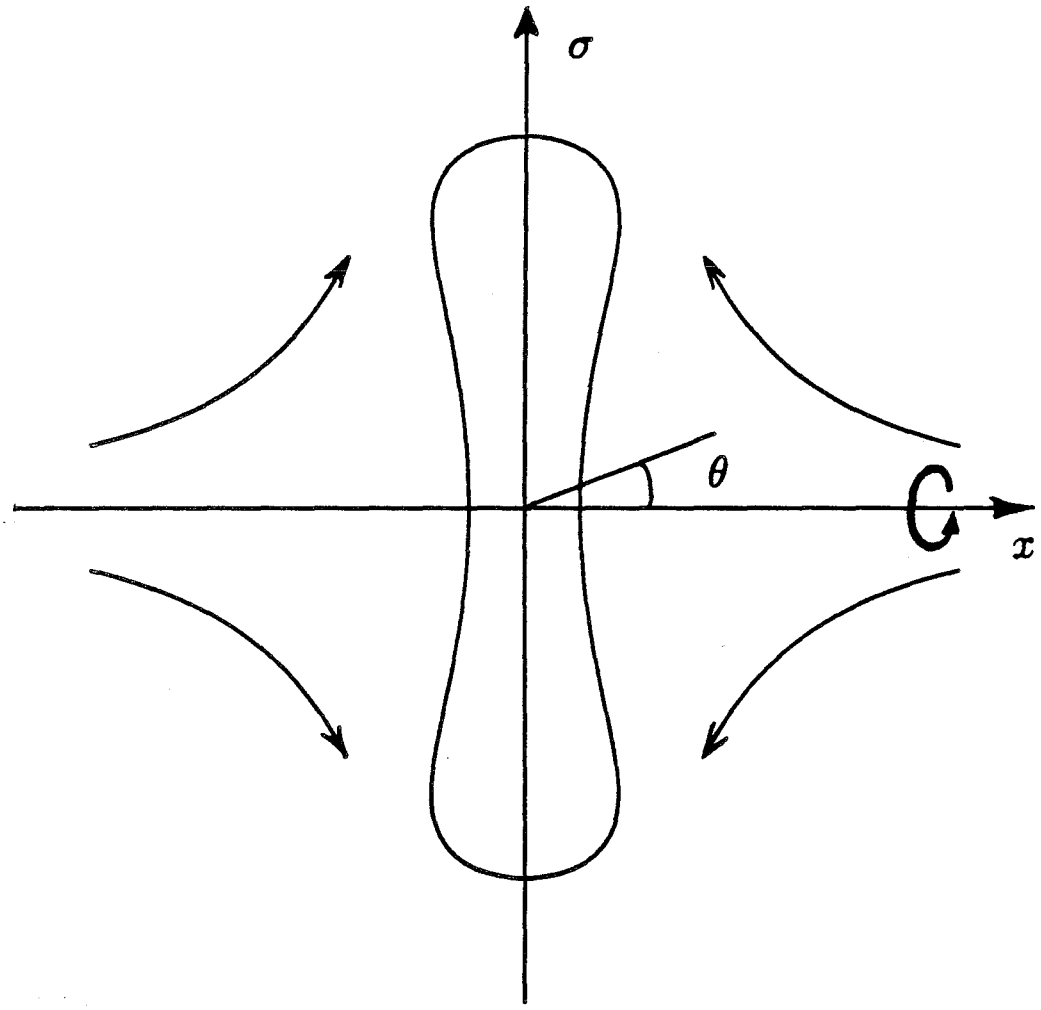

Figure 1

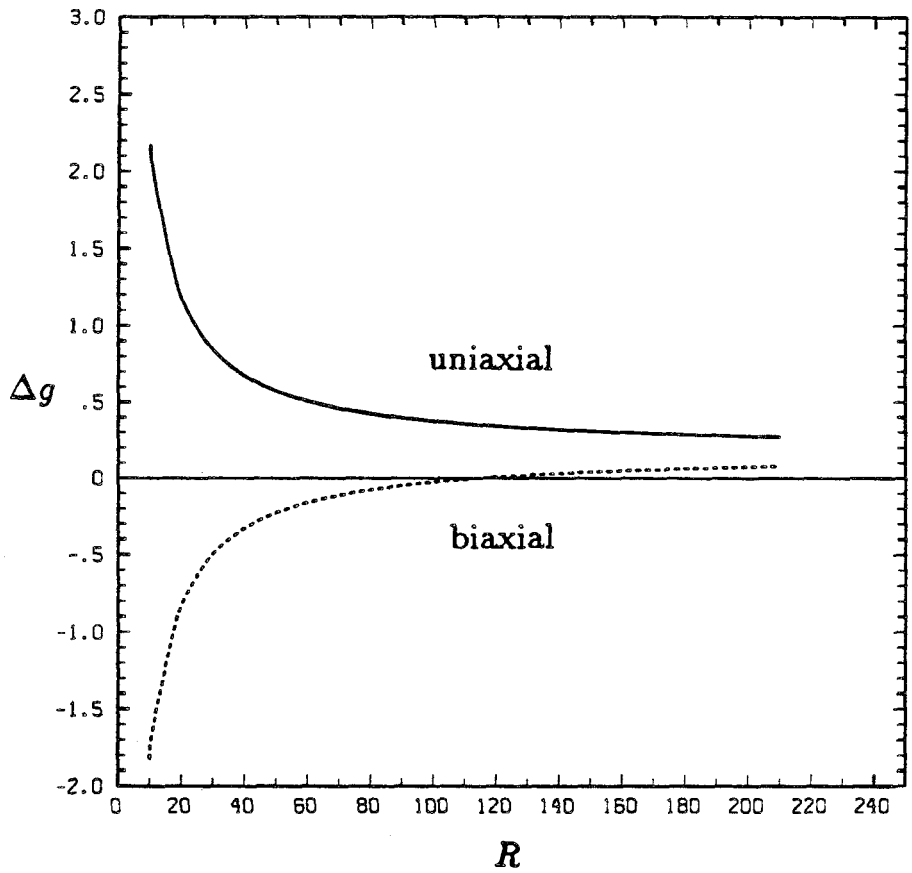
3.0
2.5
2.0
1.5
1.0
.5
0
-.5
-1.0
-1.5
-2.0
Δg
uniaxial
biaxial
0
20
40
60
80
100
120
140
160
180
200
220
240
R

Figure 2

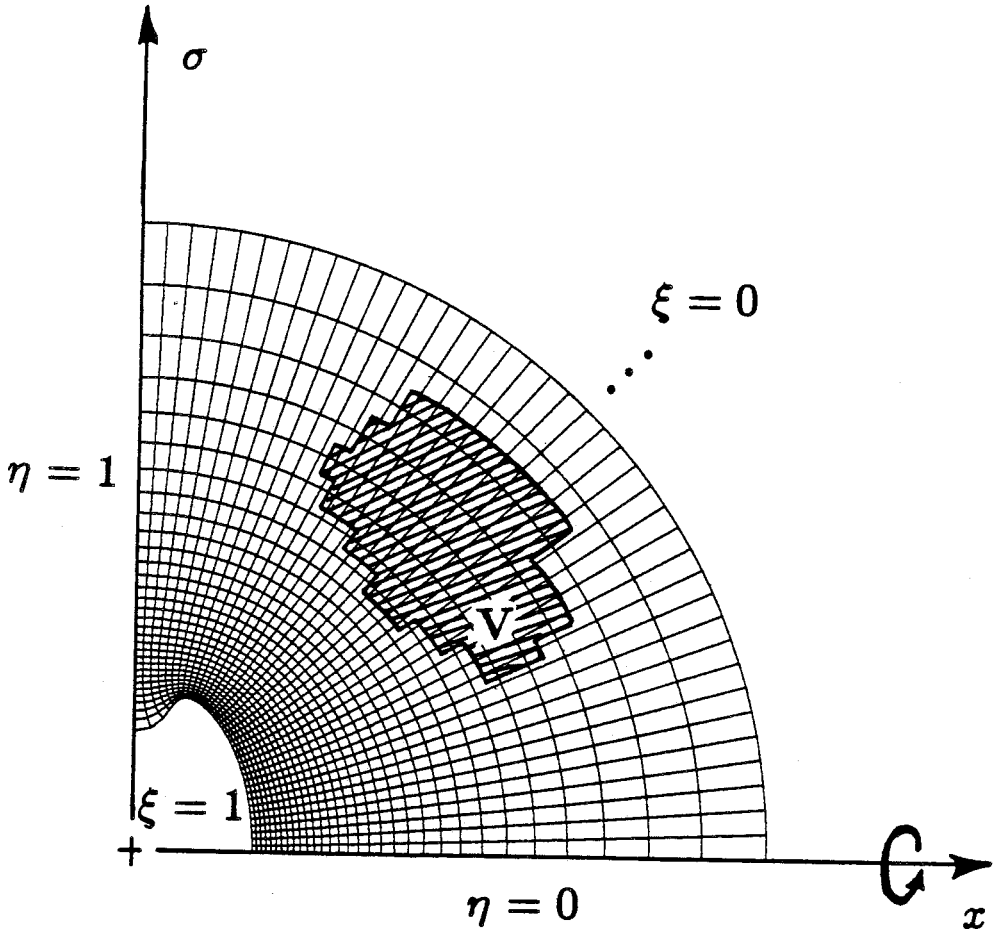

Figure 3

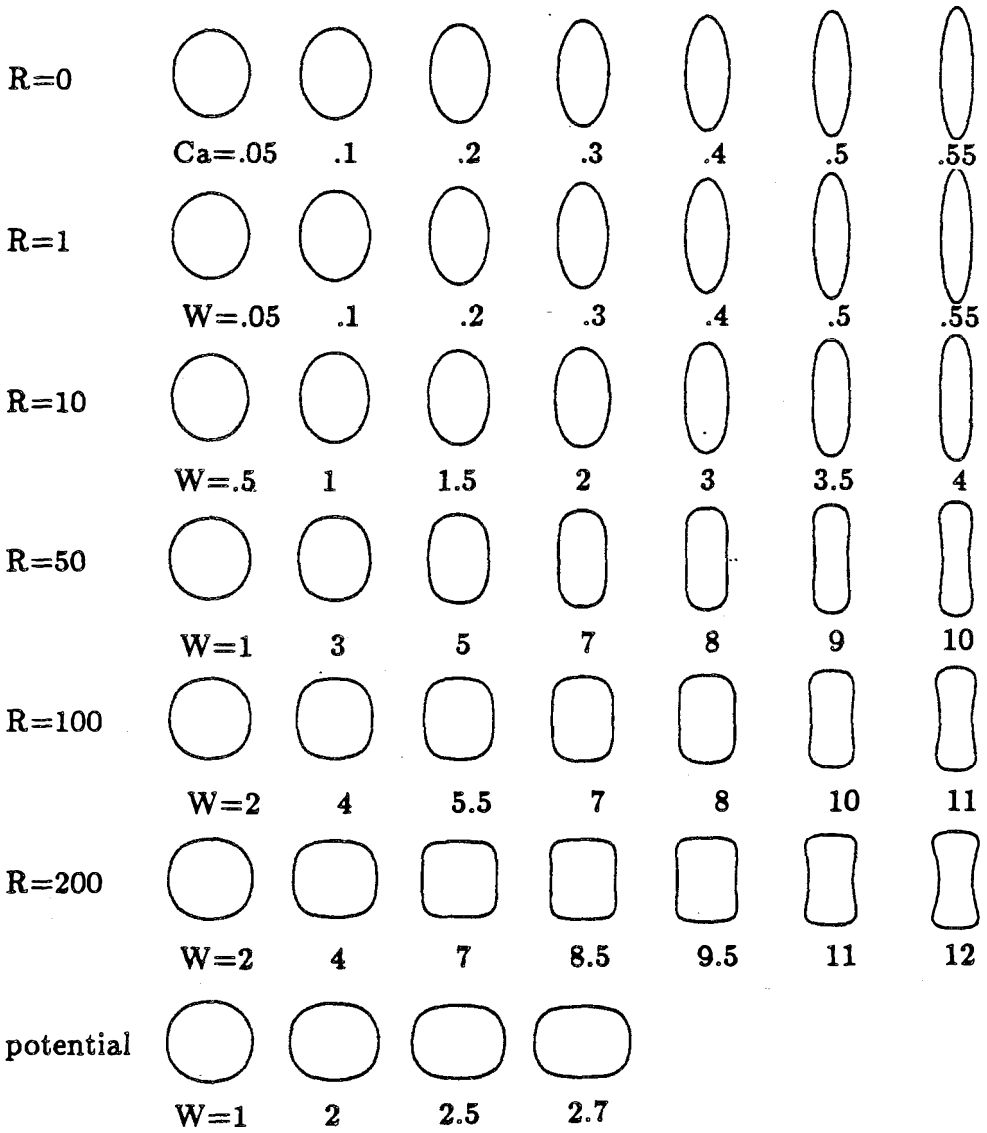
R=0
Ca=.05
.1
.2
.3
.4
.5
.55
R=1
W=.05
.1
.2
.3
.4
.5
.55
R=10
W=.5
1
1.5
2
3
3.5
4
R=50
W=1
3
5
7
8
9
10
R=100
W=2
4
5.5
7
8
10
11
R=200
W=2
4
7
8.5
9.5
11
12
potential
W=1
2
2.5
2.7

Figure 4

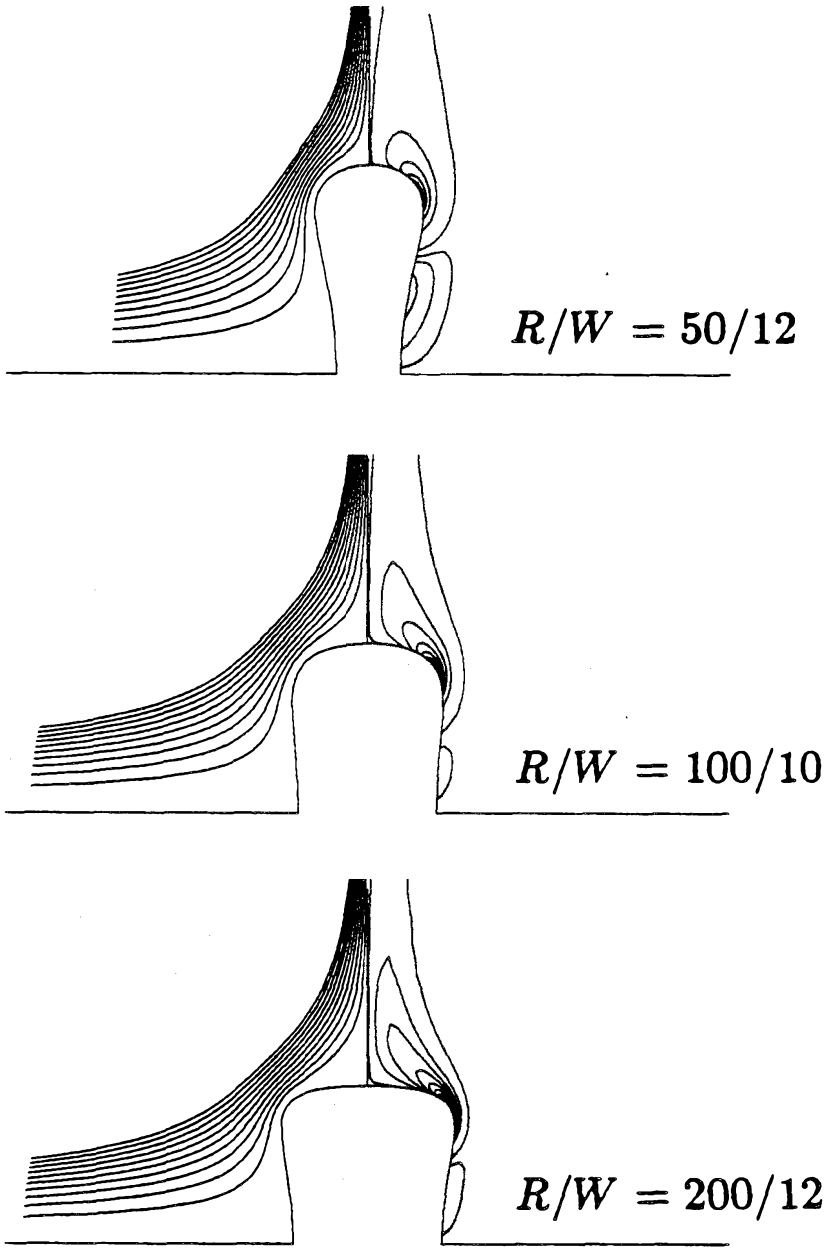

(a)

Figure 5a

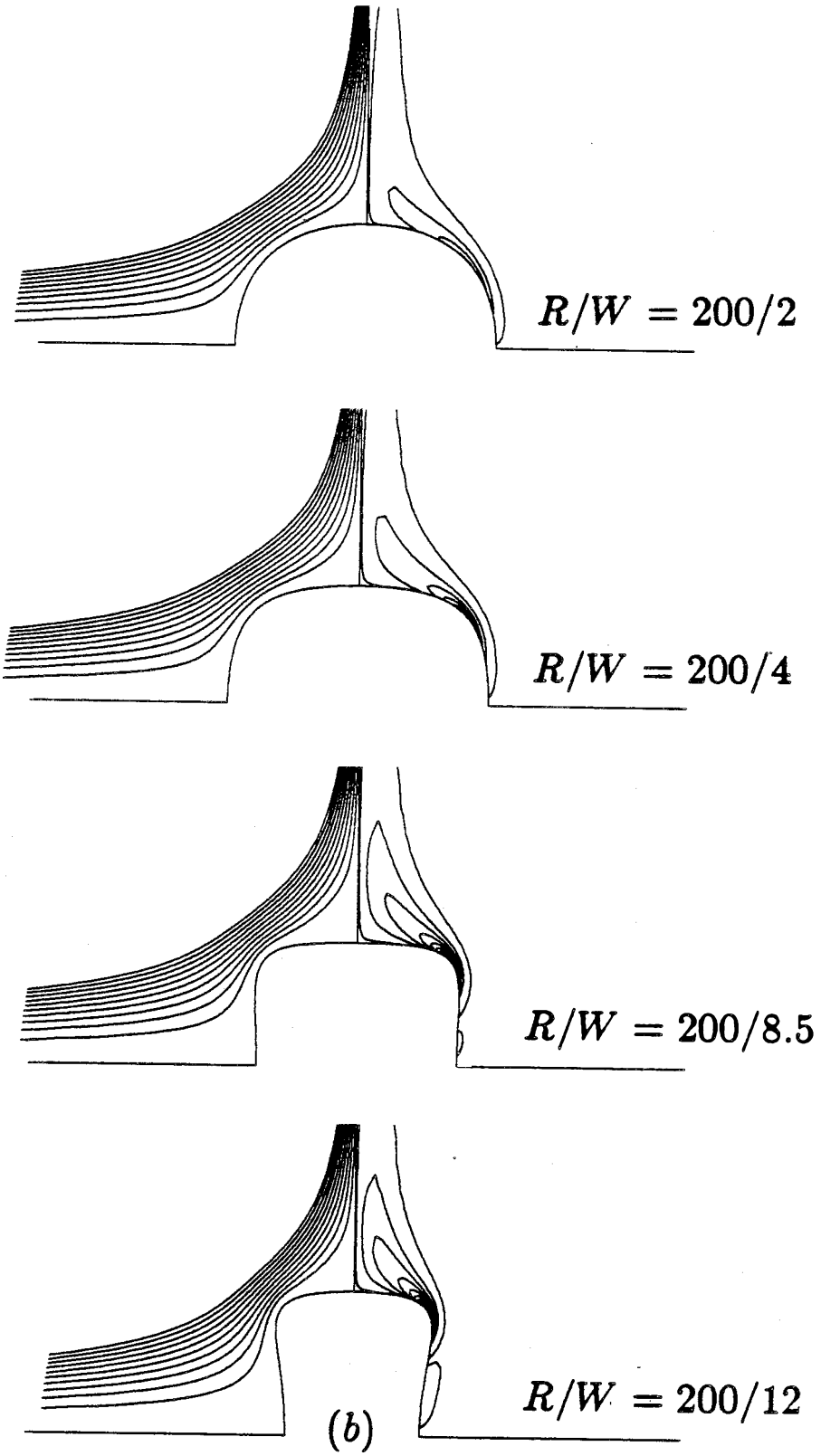

Figure 5b

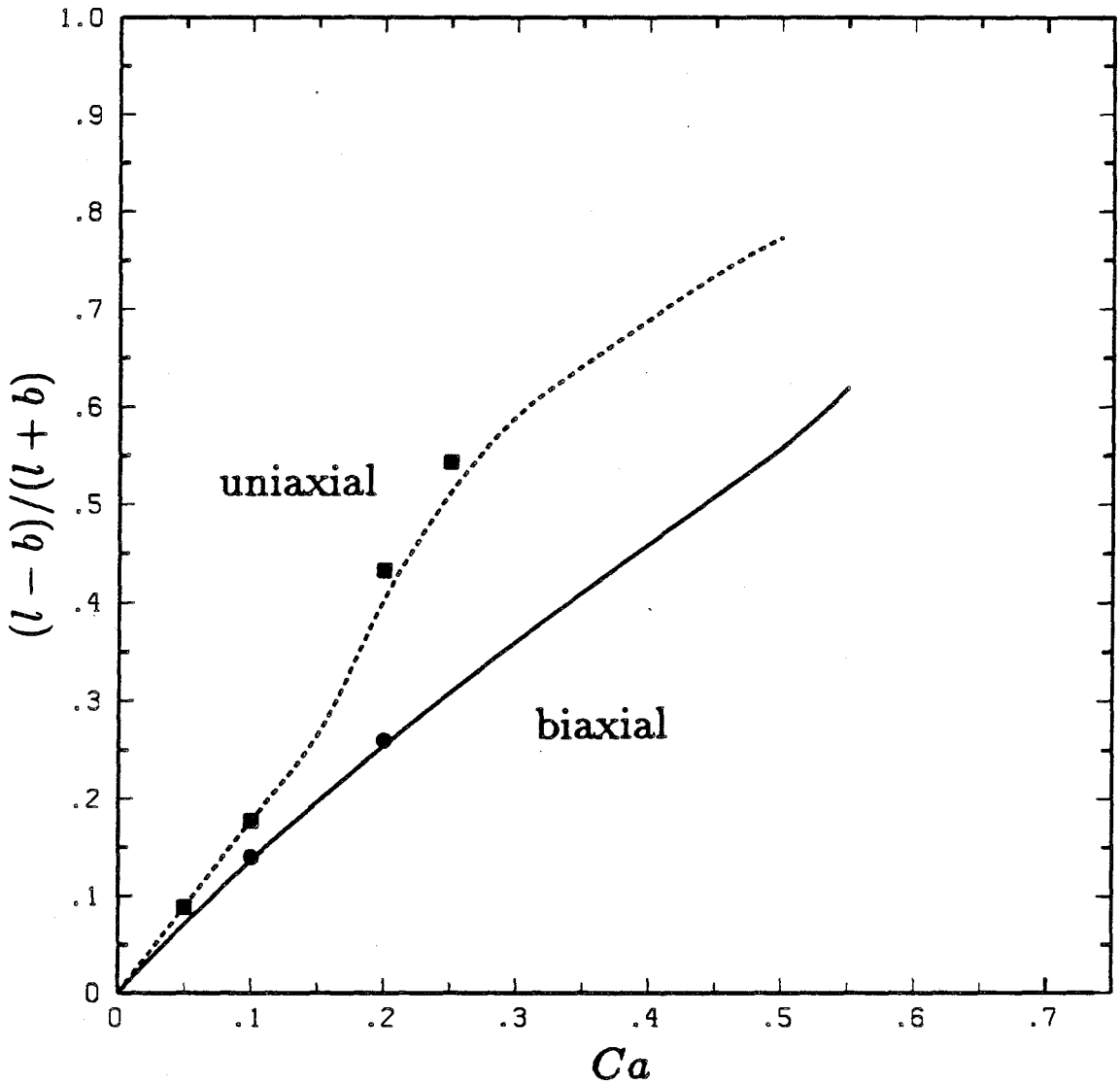

Figure 6

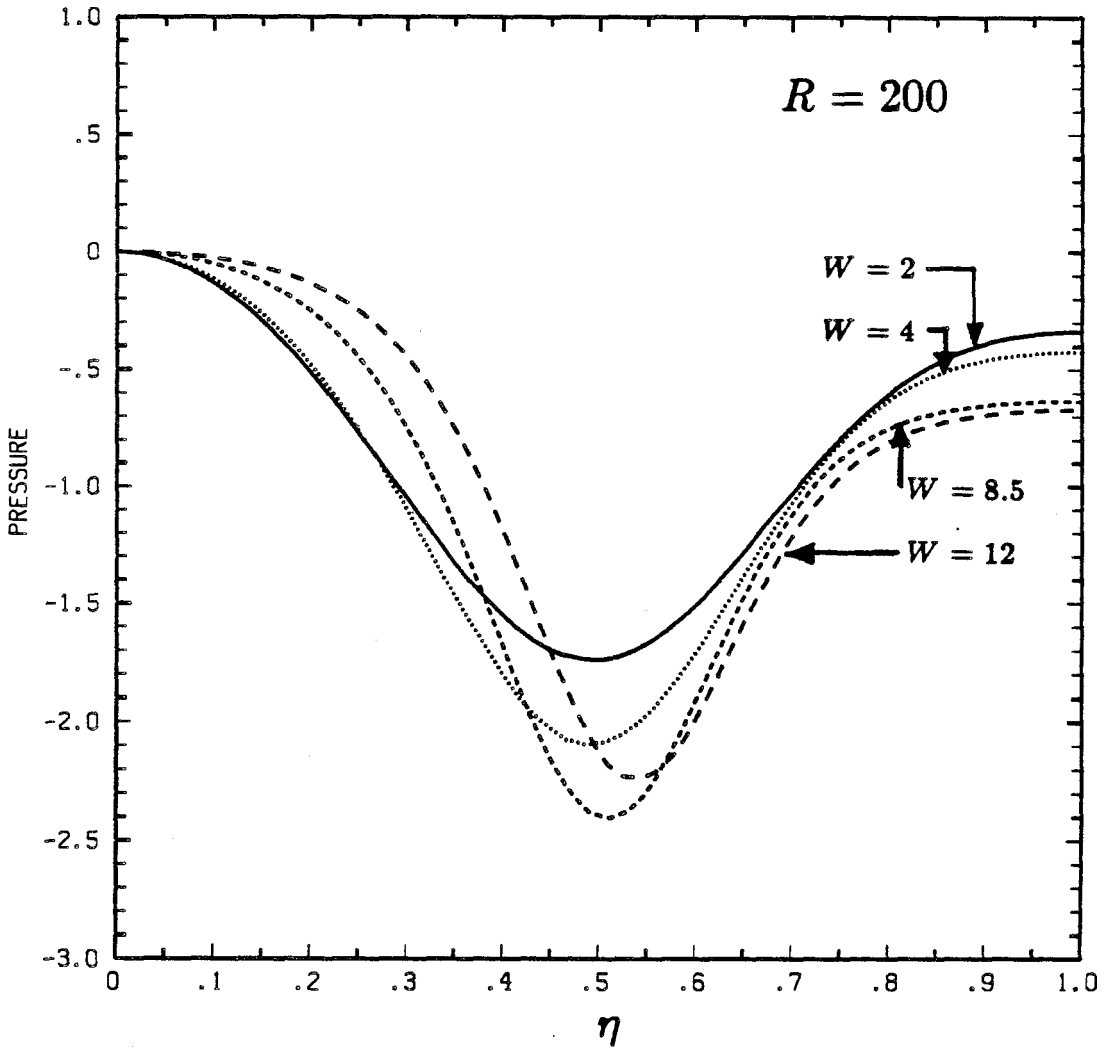
R = 200
W = 2
W = 4
W = 8.5
W = 12
PRESSURE
η
1.0
.5
0
-.5
-1.0
-1.5
-2.0
-2.5
-3.0
0
.1
.2
.3
.4
.5
.6
.7
.8
.9
1.0

Figure 7

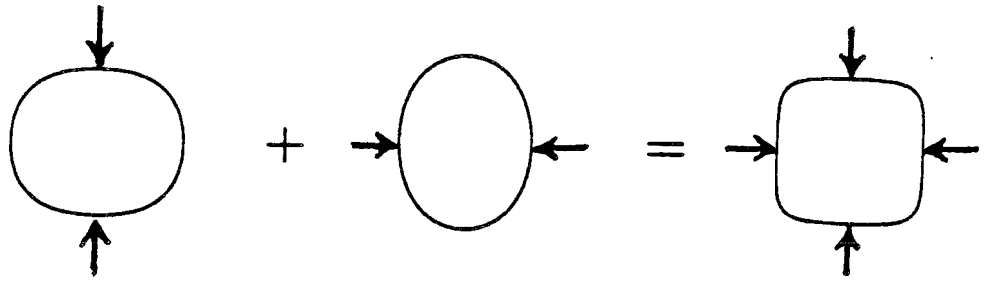

biaxial

$$(-N)_p \quad + \quad (-N)_v \quad = \quad (-N)$$

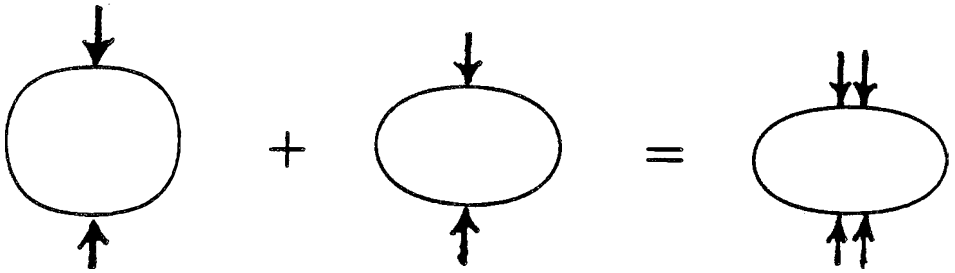

uniaxial

Figure 8

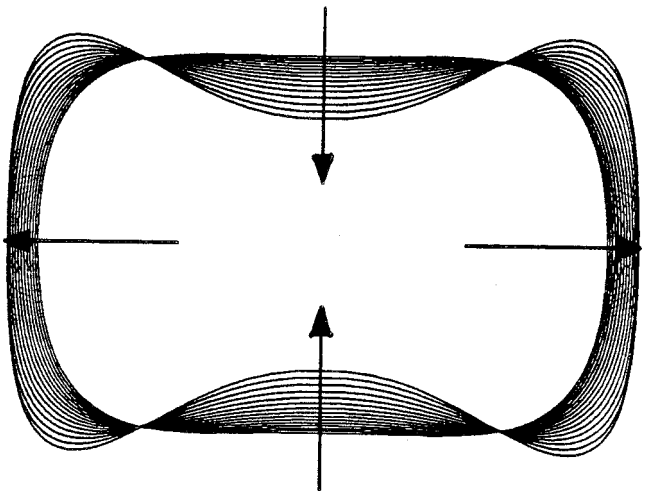

Figure 9

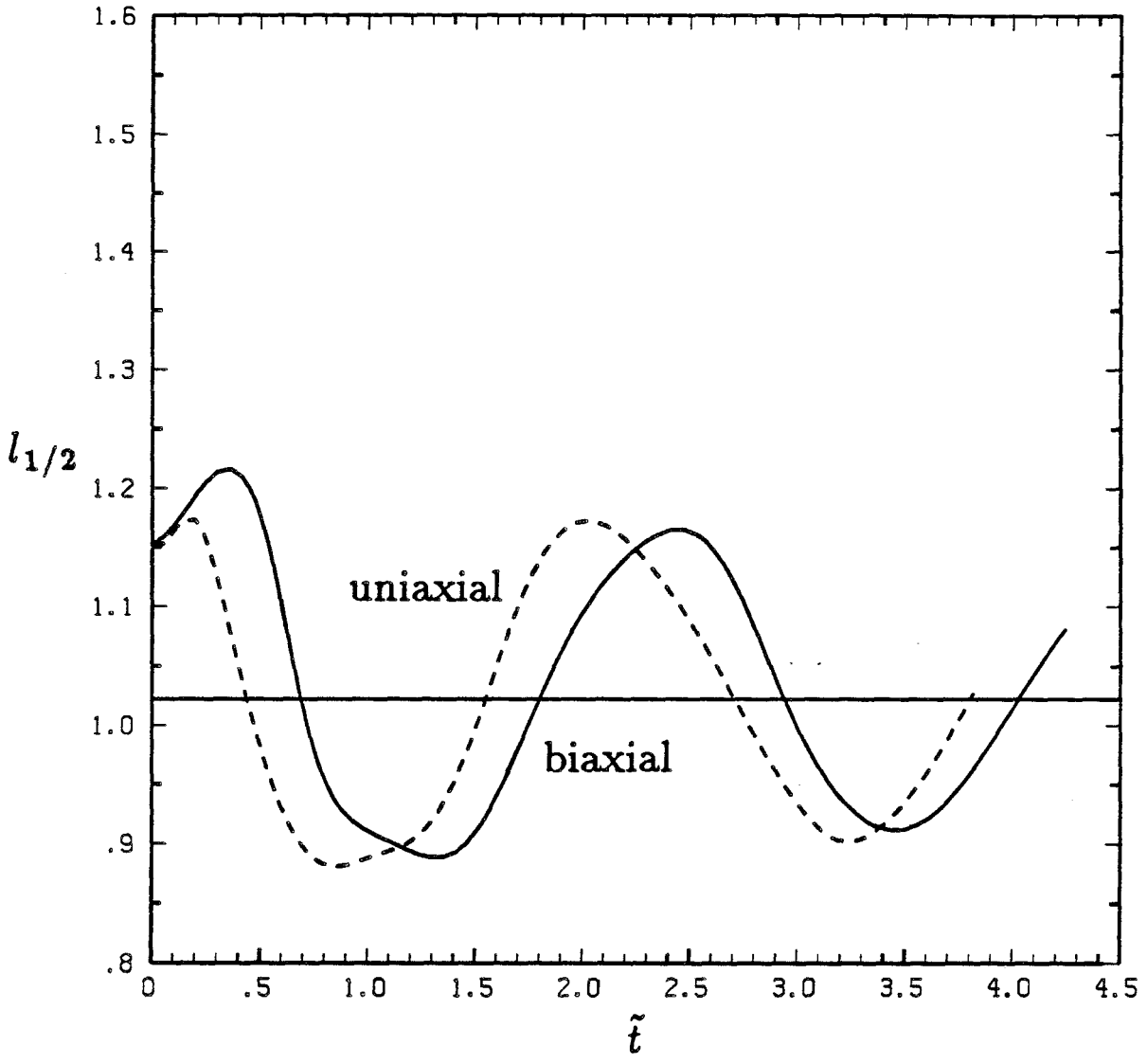
1.6
1.5
1.4
1.3
1.2
1.1
1.0
.9
.8
$l_{1/2}$
uniaxial
biaxial
0
.5
1.0
1.5
2.0
2.5
3.0
3.5
4.0
4.5
$\tilde{t}$

Figure 10

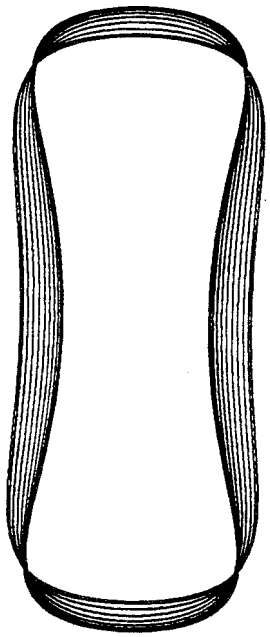

Figure 11

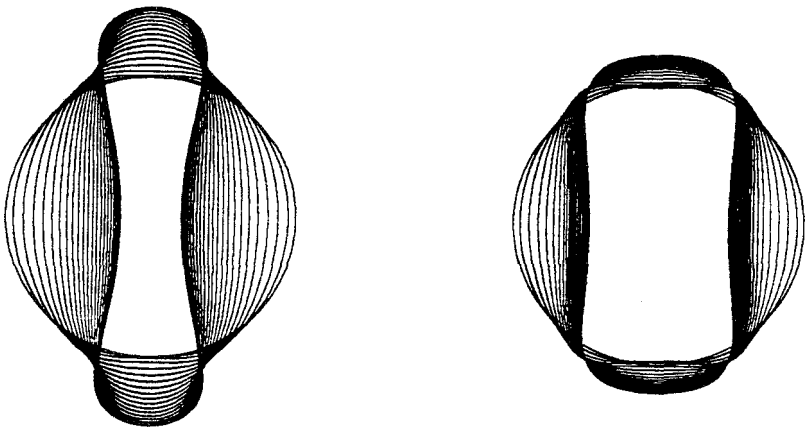

(a) (b)

Figure 12

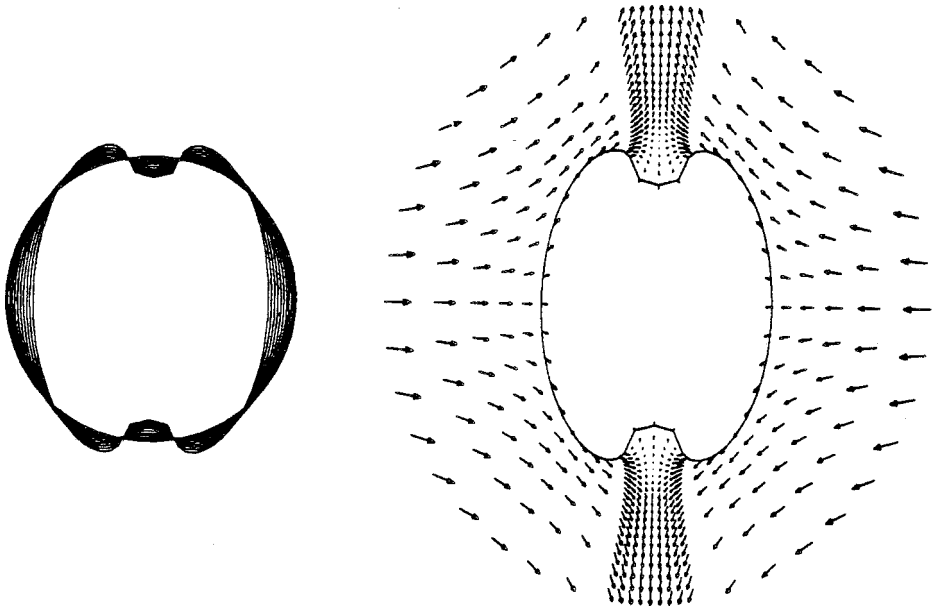

(a) (b)

Figure 13

Chapter III

Small amplitude perturbations of shape for a nearly spherical bubble in an inviscid straining flow (steady shapes and oscillatory motion)

The text of Chapter III consists of an article that has been accepted for publication in the *Journal of Fluid Mechanics*.

Small amplitude perturbations of shape for a nearly spherical bubble in an inviscid straining flow (steady shapes and oscillatory motion)

I.S. Kang and L.G. Leal

Department of Chemical Engineering
California Institute of Technology
Pasadena, California 91125

Abstract

The method of domain perturbations is used to study the problem of a nearly spherical bubble in an inviscid, axisymmetric straining flow. Steady-state shapes and axisymmetric oscillatory motions are considered. The steady-state solutions suggest the existence of a limit point at a critical Weber number, beyond which no solution exists on the steady-state solution branch, which includes the spherical equilibrium state in the absence of flow (e.g., the critical value of 1.73 is estimated from the third-order solution). In addition, the first-order steady-state shape exhibits a maximum radius at $\theta = \frac{\pi}{6}$, which clearly indicates the barrellike shape that was found earlier via numerical finite-deformation theories for higher Weber numbers. The oscillatory motion of a nearly spherical bubble is considered in two different ways. First, a small perturbation to a spherical base state is studied with the *ad hoc* assumption that the steady-state shape is spherical for the complete Weber number range of interest. This analysis shows that the frequency of oscillation decreases as the Weber number increases, and that a spherical bubble shape is unstable if the Weber number is larger than 4.62. Second, the correct steady-state shape up to $O(W)$ is included to obtain a rigorous asymptotic formula for the frequency change at a small Weber number. This asymptotic analysis also shows that the frequency decreases as the Weber number increases; for example, in the case of the principal mode $(n = 2)$, $\omega^2 = {\omega_0}^2(1-0.31W)$, where ω_0 is the oscillation frequency of a bubble in a quiescent fluid.

1. Introduction

We consider the motion of a gas bubble in a uniaxial inviscid straining flow. Specifically, we use the method of domain perturbations to study small steady deformations of shape from spherical, and small amplitude oscillatory motions of a bubble that is initially deformed slightly to a non-equilibrium shape.

Steady-state numerical solutions for the finite-amplitude deformation of a bubble in a uniaxial inviscid straining flow were obtained recently by Miksis (1981) and Ryskin & Leal (1984). Ryskin and Leal used a steady-state, iterative method to solve the full Navier-Stokes equations for a series of finite values of the Reynolds number, with $R = \infty$ included as a limiting case. They found, for each $R \geq 10$, that steady, converged solutions could not be obtained beyond a certain maximum Weber number, which we term below the critical Weber number. Miksis considered only the inviscid limit, but was then able to employ the powerful boundary-integral method in conjunction with Newton's method to demonstrate that the point of non-convergence was actually a limit point in the branch of steady solutions which contains the sphere in the absence of flow (i.e. $W \equiv 0$).

In a companion to the present paper, Kang & Leal (1987) used a full time-dependent numerical code, to study again the problem of bubble deformation in a uniaxial extensional flow at several Reynolds numbers (including $R = \infty$), and a range of Weber numbers near the steady-state critical values obtained by Ryskin & Leal (1984). They found that a bubble is elongated continuously if the Weber number is larger than the steady-state critical value. They also found that a bubble with a sufficiently large initial deformation will elongate in a similar manner even for smaller, subcritical Weber numbers. Thus, a steady state solution is possible only if the Weber number is smaller than the critical value found by Ryskin & Leal (1984), and then only if the initial shape is not too far from the steady-state solution. Finally, in the inviscid flow limit, Kang & Leal (1987) found that an initially deformed bubble exhibited oscillatory changes

of shape at Weber numbers below critical. They also found that the frequency of oscillation decreases as the Weber number increases, approaching zero at Ryskin and Leal's critical Weber number for steady solutions. However, these numerical solutions of the initial value problem are not sufficient to understand the oscillatory motion of a bubble in a straining flow, because we can get only the lumped global behavior of the oscillatory motion. To understand the details of oscillatory motion such as the frequency change of each mode, the mode-mode interactions, or the evolution of a low frequency mode to a higher frequency mode, etc., we need a complementary analytical study.

The free oscillation of drops and bubbles in a quiescent fluid has been studied extensively since Rayleigh (1879, see also Lamb 1932) first analyzed the small-amplitude oscillations of an inviscid globe. These linear results have been extended to include viscous effects (Reid 1960; Miller & Scriven 1968; Prosperetti 1977; Marston 1980), and nonlinear oscillations of a liquid drop in a quiescent fluid have also been analyzed (Tsamopoulos & Brown 1983, 1984; Natarajan & Brown 1986). In addition, some work has been done recently on more complicated problems such as oscillatory motion of a rotating drop (Busse 1984; Annamalai et al. 1985). In spite of the extensive literature on oscillating bubbles and drops, however, relatively little has been done yet to determine how the phenomena are modified in the presence of a mean motion relative to the bubble or drop. We are aware of only one paper in this direction by Subramanyam (1969), who studied the oscillations of a drop moving in another fluid at low values of Reynolds number and Weber number. In view of the importance of the oscillatory motion problem in understanding phenomena such as acoustic noise generation in bubbly liquids, where the bubble is almost always subjected to some non-trivial mean motion of the suspending fluid, this is rather surprising, and provides one primary motivation for the present study of the oscillatory motion of a bubble in an inviscid straining flow.

In addition, however, the analysis of small amplitude oscillations of shape

can also provide an alternative to numerical computation in determining the significance of the *critical* Weber number for non-convergence of steady solutions that was found by Miksis (1981) and Ryskin & Leal (1984). In particular, since the linearized equations governing small amplitude oscillations are the same as those derived via a linear stability analysis, the Jacobian matrix for a small disturbance to the steady state becomes singular at the zero frequency (or zero eigenvalue) point of the lowest frequency oscillating mode. Thus, if we were to use the exact steady solution as the base state, the zero frequency point of the lowest frequency oscillating mode should be the same as the limit point of the steady solution branch, which includes the spherical shape as the zero Weber number solution, provided only that the limit point corresponds to a physical limit, not a numerical artifact. Unfortunately, the exact steady shape is not known analytically for finite Weber numbers where the deformation becomes finite. Thus, we cannot use the exact steady solution for an analysis of oscillatory disturbance modes. The best we can do is to study the asymptotic limit for small Weber numbers where the steady shape is only slightly deformed. We may anticipate, however, that the results of such a study will be at least qualitatively reasonable for W up to $O(1)$, because even the steady shapes at the critical Weber number are not drastically deformed.

In this paper, we therefore consider both steady-state shapes and small amplitude oscillatory motions of a bubble in an inviscid straining flow for small W. For the steady-state analysis, it is advantageous to choose *the magnitude of the* $P_2(\cos\theta)$ *mode of deformation* $< R, P_2 >$ as the small parameter instead of W. In this way, the limit point that appears on the stable solution branch at the critical $W = W_c$ is transformed to a regular point on the solution curve, and we can determine the Weber number as a function of $< R, P_2 >$ for both the unstable and stable branches for $W \leq W_c$. The perturbation solution based on W is then nothing but a special form of the expansion in $< R, P_2 >$ for the limit $W \ll 1$ on the stable branch. For the analysis of oscillatory motion, we consider

two levels of approximation. In the first, we study small perturbations to a spherical base state. In the second, we analyze the first asymptotic correction for a small Weber number by including the $O(W)$ contribution to the steady-state shape. From this analysis we get an asymptotic formula for the dependence of the frequency of an oscillating bubble on W in a straining flow. Finally, we briefly consider weak viscous effects on the oscillation about the spherical shape. To do this, we approximate the velocity field via the potential flow solution right up to the boundary. Thus, viscous effects are included only via the viscous stress term and the pressure correction term in the normal stress condition: this is equivalent to the classical approach of Lamb (1932), who estimated the effect of viscosity for bubble oscillation in a quiescent fluid by calculating the viscous contribution to dissipation using the inviscid flow velocity field as a first approximation for large but finite Reynolds numbers.

2. Problem Formulation

We consider an incompressible gas bubble of volume $\frac{4}{3}\pi a^3$ that is undergoing small oscillations of shape in the presence of an axisymmetric, uniaxial extensional flow of a fluid with density ρ and zero viscosity as sketched in figure 1. The surface of the bubble is assumed to be characterized completely by a uniform surface tension γ. Furthermore, we neglect all effects of gravity including the hydrostatic pressure variation in the fluid. Then the governing equation of motion is

$$\nabla^2\phi' = 0. \tag{2.1}$$

On the bubble surface the kinematic condition and the normal stress condition must be satisfied.

$$-\frac{1}{|\nabla F'|}\frac{\partial F'}{\partial t'} = \nabla\phi' \cdot \mathbf{n}, \tag{2.2}$$

$$G'(t') + \rho\frac{\partial \phi'}{\partial t'} + \frac{\rho}{2}\nabla\phi' \cdot \nabla\phi' = \gamma\left(\nabla \cdot \mathbf{n}\right), \tag{2.3}$$

where F' is a function that describes the bubble shape as $F'(\mathbf{x}', t') = 0$, and $G'(t')$ is an unknown time-dependent constant that must be determined to satisfy the constraint of volume conservation. The undisturbed, uniaxial extensional flow far from the bubble is given by

$$\mathbf{u}' = \mathbf{E} \cdot \mathbf{r}', \quad \mathbf{E} = E \begin{pmatrix} 1 & 0 & 0 \\ 0 & -\frac{1}{2} & 0 \\ 0 & 0 & -\frac{1}{2} \end{pmatrix}, \quad E > 0, \tag{2.4}$$

where E is the principal strain rate. In order to non-dimensionalize the equations, we introduce characteristic velocity, length and time scales. Since all terms in the normal stress condition are equally important for oscillatory motion, the most appropriate choice is

$$\begin{aligned} \phi_c &= \left(\frac{\gamma a}{\rho}\right)^{\frac{1}{2}}, \\ t_c &= \left(\frac{\rho a^3}{\gamma}\right)^{\frac{1}{2}}, \\ l_c &= a, \end{aligned} \tag{2.5}$$

where a is the radius of the undeformed spherical bubble. Then the governing equation in dimensionless form is

$$\nabla^2 \phi = 0, \tag{2.6}$$

while the kinematic condition takes the form

$$-\frac{1}{|\nabla F|}\frac{\partial F}{\partial t} = \nabla \phi \cdot \mathbf{n}, \tag{2.7}$$

and the normal stress condition becomes

$$G(t) + \frac{\partial \phi}{\partial t} + \frac{1}{2}\nabla \phi \cdot \nabla \phi = (\nabla \cdot \mathbf{n}). \tag{2.8}$$

The far-field condition (2.4), expressed in terms of the potential function ϕ becomes

$$\phi_\infty = \sqrt{\frac{W}{2}}\frac{1}{2}(3\cos^2\theta - 1)\left(\frac{1}{2}r^2\right), \tag{2.9}$$

where W is the Weber number defined as $W = 2\rho(Ea)^2 a/\gamma$, and θ is the angle measured from the axis of symmetry.

In addition to the differential equations and boundary conditions (2.6)-(2.9), the solution for a bubble shape must satisfy two overall constraints. First, the volume of the bubble must be constant, equal to $(4/3)\pi a^3$, i.e.,

$$\int_0^\pi R^3(\theta,t)\sin\theta\ d\theta = 2, \tag{2.10}$$

where $R(\theta)$ is the unknown shape function, defined in terms of $F(\mathbf{x},t)$, as $F \equiv r - R(\theta,t)$. Here, we have assumed that the bubble shape is axisymmetric and thus is a function of the polar angle θ only. In addition to (2.10), the shape function must be defined in such a way that the center-of-mass of the bubble remains at the origin. This condition can be expressed in the form

$$\int_0^\pi R^4(\theta,t)\cos\theta\sin\theta\ d\theta = 0. \tag{2.11}$$

3. Perturbation Solution for Steady-State Shapes

We consider first the steady-state problem in the limit of a small deformation where the shape is nearly spherical. In this limit, it is usual to expand the solution in the form of a perturbation expansion for small $W << 1$, i.e.,

$$\phi = \sqrt{\frac{W}{2}}(\phi_0 + W\phi_1 + W^2\phi_2 + \cdots) \tag{3.1a}$$

and

$$R = 1 + W\varsigma_1 + W^2\varsigma_2 + \cdots. \tag{3.1b}$$

However, if we know, or anticipate, the existence of a limit point in the branch of stable steady solutions at some finite $W = W_c$, it will be more convenient to pick a measure of the magnitude of deformation as an alternative small parameter ϵ, and to expand the solution in terms of ϵ rather than W. In particular, if we try to obtain an asymptotic expansion in W, the limit point appears as a pole

in the solution, which requires an infinite number of terms to resolve. However, if we expand directly in terms of an appropriate measure of the amplitude of deformation, ϵ, and treat W as a dependent function of ϵ, the point corresponding to $W = W_c$ becomes a regular point on the solution curve, and there is no difficulty with the approach to W_c.

For the present problem, a convenient measure of the degree of deformation, which can be used as the small parameter for an asymptotic solution, is the magnitude of the $P_2(\cos\theta)$ mode of deformation; i.e.,

$$\begin{aligned} \epsilon &= < R(\theta;\epsilon), P_2(\cos\theta) > \\ &= \int_0^\pi R(\theta;\epsilon) P_2(\cos\theta) \sin\theta d\theta. \end{aligned} \tag{3.2}$$

We denote the expansion in terms of ϵ as the P_2-perturbation and the expansion in terms of W as the W-perturbation. The P_2-perturbation takes the form

$$\begin{pmatrix} \phi \\ R \\ W \end{pmatrix} = \sum_{n=0}^{\infty} \epsilon^n \begin{pmatrix} \sqrt{\frac{W}{2}}\tilde{\phi}_n \\ R_n \\ W_n \end{pmatrix}, \tag{3.3}$$

in which W is treated as a function of ϵ, as noted above. The expansion in terms of ϵ is equivalent to interchanging the dependent and independent variables from $< R, P_2 >$ and W, respectively, to W and $< R, P_2 >$. As shown in figure 2, the solution curve for the magnitude of the P_2 mode as a function of W, which is singular at $W = W_c$, is effectively turned on its side. In the representation (3.3), the solution is regular for all ϵ. Substituting (3.3) into the governing equations and boundary-conditions, we obtain

$$\nabla^2 \tilde{\phi}_n = 0, \qquad \text{n} = 0, 1, 2, \cdots. \tag{3.4}$$

This equation is to be solved subject to the kinematic condition $\mathbf{u} \cdot \mathbf{n} = 0$, together with the asymptotic form (2.9) for $r \to \infty$. The bubble shape at each order in ϵ is then obtained from the normal stress balance (2.8).

To simplify the analysis, it is convenient to use the method of domain perturbations to transform the kinematic and the normal stress conditions at

the bubble surface to equivalent conditions applied at $r = 1$. The method is well known and we simply quote the results for the kinematic condition, which becomes

$$\begin{aligned}
&\Phi_{r0} + \epsilon\Big[\Phi_{r1} - \frac{\partial R_1}{\partial\theta}\Phi_{\theta 0}\Big] \\
&\quad + \epsilon^2\left[\Phi_{r2} - \Phi_{r1}\frac{\partial R_1}{\partial\theta} - \Phi_{\theta 0}\Big(\frac{\partial R_2}{\partial\theta} - R_1\frac{\partial R_1}{\partial\theta}\Big) - \frac{1}{2}\Big(\frac{\partial R_1}{\partial\theta}\Big)^2\Phi_{r0}\right] \\
&\quad + O(\epsilon^3) = 0 \qquad \text{at} \quad r = 1,
\end{aligned} \tag{3.5}$$

and the normal stress condition, which takes the form

$$\begin{aligned}
&W_0({\Phi_{r0}}^2 + {\Phi_{\theta 0}}^2) \\
&+ \epsilon\Big[W_1({\Phi_{r0}}^2 + {\Phi_{\theta 0}}^2) + W_0(2\Phi_{r0}\Phi_{r1} + 2\Phi_{\theta 0}\Phi_{\theta 1})\Big] \\
&+ \epsilon^2\Big[W_2({\Phi_{r0}}^2 + {\Phi_{\theta 0}}^2) + W_1(2\Phi_{r0}\Phi_{r1} + 2\Phi_{\theta 0}\Phi_{\theta 1}) \\
&+ W_0({\Phi_{r1}}^2 + 2\Phi_{r0}\Phi_{r2} + {\Phi_{\theta 1}}^2 + 2\Phi_{\theta 0}\Phi_{\theta 2})\Big] \\
&+ \epsilon^3\Big[W_3({\Phi_{r0}}^2 + {\Phi_{\theta 0}}^2) + W_2(2\Phi_{r0}\Phi_{r1} + 2\Phi_{\theta 0}\Phi_{\theta 1}) \\
&+ W_1({\Phi_{r1}}^2 + 2\Phi_{r0}\Phi_{r2} + {\Phi_{\theta 1}}^2 + 2\Phi_{\theta 0}\Phi_{\theta 2}) + W_0(\cdots)\Big] \\
&= 4(\nabla\cdot\mathbf{n}).
\end{aligned} \tag{3.6}$$

In (3.5) and (3.6) the Φ_i's are defined by

$$\begin{aligned}
\Phi_{r0} &= \frac{\partial\tilde{\phi}_0}{\partial r}, \\
\Phi_{r1} &= \frac{\partial\tilde{\phi}_1}{\partial r} + R_1\Big(\frac{\partial^2\tilde{\phi}_0}{\partial r^2}\Big), \\
\Phi_{r2} &= \frac{\partial\tilde{\phi}_2}{\partial r} + R_1\frac{\partial^2\tilde{\phi}_1}{\partial r^2} + \frac{1}{2}{R_1}^2\frac{\partial^3\tilde{\phi}_0}{\partial r^3} + R_2\frac{\partial^2\tilde{\phi}_0}{\partial r^2}, \\
\Phi_{\theta 0} &= \frac{\partial\tilde{\phi}_0}{\partial\theta}, \\
\Phi_{\theta 1} &= \frac{\partial\tilde{\phi}_1}{\partial\theta} + R_1\Big(\frac{\partial^2\tilde{\phi}_0}{\partial r\partial\theta} - \frac{\partial\tilde{\phi}_0}{\partial\theta}\Big), \\
\Phi_{\theta 2} &= \frac{\partial\tilde{\phi}_2}{\partial\theta} + R_1\Big(\frac{\partial^2\tilde{\phi}_1}{\partial r\partial\theta} - \frac{\partial\tilde{\phi}_1}{\partial\theta}\Big) + \frac{1}{2}{R_1}^2\Big(2\frac{\partial\tilde{\phi}_0}{\partial\theta} - 2\frac{\partial^2\tilde{\phi}_0}{\partial r\partial\theta} + \frac{\partial^3\tilde{\phi}_0}{\partial r^2\partial\theta}\Big) \\
&\quad + R_2\Big(\frac{\partial^2\tilde{\phi}_0}{\partial r\partial\theta} - \frac{\partial\tilde{\phi}_0}{\partial\theta}\Big).
\end{aligned}$$

We expand the bubble shape functions R_i at each order in ϵ as a series of Legendre polynomials,

$$R_i = \sum_{n=0}^{\infty} \beta_n^{(i)} P_n(\eta), \qquad i = 0, 1, 2, \cdots, \tag{3.7}$$

where η is defined by $\eta = \cos\theta$. Then the mean curvature that appears in the normal stress condition (3.6) can be expanded as

$$\begin{aligned}
\nabla \cdot \mathbf{n} = 2 &+ \epsilon \sum_{i=2}^{\infty} (i-1)(i+2)\beta_i^{(1)} P_i(\eta) \\
&+ \epsilon^2 \left[\sum_{j=0}^{\infty} (j-1)(j+2)\beta_j^{(2)} P_j - 2\sum_{i=2}^{\infty} \beta_i^{(1)} P_i \sum_{i=2}^{\infty} (i^2+i-1)\beta_i^{(1)} P_i \right] \\
&+ \epsilon^3 \left[\sum_{k=0}^{\infty} (k-1)(k+2)\beta_k^{(3)} P_k + 3\sum_{i=2}^{\infty} \beta_i^{(1)} P_i \sum_{i=2}^{\infty} (i^2+i-1)\beta_i^{(1)} P_i \right. \\
&- 2\left(\sum_{i=2}^{\infty} \beta_i^{(1)} P_i \sum_{j=0}^{\infty} (j^2+j-1)\beta_j^{(2)} P_j + \sum_{j=0}^{\infty} \beta_j^{(2)} P_j \sum_{i=2}^{\infty} (i^2+i-1)\beta_i^{(1)} P_i \right) \\
&\left. + \frac{1}{2} \sum_{i=2}^{\infty} \beta_i^{(1)} P_i' \sum_{i=2}^{\infty} \beta_i^{(1)} (1-\eta^2) P_i' \left(-3\sum_{i=2}^{\infty} i(i+1)\beta_i^{(1)} P_i + 2\sum_{i=2}^{\infty} \beta_i^{(1)} \eta P_i' \right) \right],
\end{aligned} \tag{3.8}$$

where $i = 0$ and $i = 1$ are not included to satisfy the volume conservation and the center of mass condition in $O(\epsilon)$ solution.

Finally, in addition to the boundary conditions listed above, the solution at each order in ϵ must satisfy the condition of volume conservation, which is given by

$$\int_{-1}^{1} (R_0 + \epsilon R_1 + \epsilon^2 R_2 + \cdots)^3 d\eta = 2, \tag{3.9}$$

and the consistency condition, from the definition of ϵ, which takes the form

$$\epsilon \equiv \int_{-1}^{1} (R_0 + \epsilon R_1 + \epsilon^2 R_2 + \cdots) P_2(\eta) d\eta. \tag{3.10}$$

In this steady-state problem, the center of mass condition is automatically satisfied because of the symmetry property. Now, it is straightforward to obtain solutions up to $O(\epsilon^3)$, and the solution method will be briefly presented in the following section.

3.1. *Perturbation Solution up to* $O(\epsilon^3)$

3.1.a) $O(1)$ Problem

The equations and boundary conditions for $O(1)$ problem are

$$\nabla^2\tilde{\phi}_0 = 0 \qquad (1 \le r < \infty, -1 \le \eta \le 1), \tag{3.11a}$$

$$\tilde{\phi}_0 \to \frac{1}{2}P_2(\eta)r^2 \qquad \text{as} \quad r \to \infty, \tag{3.11b}$$

$$\frac{\partial\tilde{\phi}_0}{\partial r} = 0 \qquad \text{at} \quad r = 1, \tag{3.11c}$$

$$W_0({\Phi_{r0}}^2 + {\Phi_{\theta 0}}^2) + \text{constant} = 8 \qquad \text{at} \quad r = 1, \tag{3.11d}$$

$$\int_{-1}^{1} {R_0}^3 d\eta = 2, \tag{3.11e}$$

$$\int_{-1}^{1} R_0 P_2 d\eta = 0. \tag{3.11f}$$

The solution of (3.11a), which satisfies (3.11b) and (3.11c), is

$$\tilde{\phi}_0 = P_2(\eta)\left(\frac{1}{2}r^2 + \frac{1}{3}r^{-3}\right), \tag{3.12}$$

which is the well-known potential flow solution around the undisturbed sphere. In order to satisfy (3.11d), we have $W_0 = 0$, and from (3.11e), we get $R_0 = 1$. Then (3.11f), arising from the definition of ϵ, is automatically satisfied at this level of approximation.

3.1.b) $O(\epsilon)$ Problem

Let us now turn to the $O(\epsilon)$ problem. The governing equations and boundary conditions in this case are

$$\nabla^2\tilde{\phi}_1 = 0 \qquad (1 \le r < \infty, -1 \le \eta \le 1), \tag{3.13a}$$

$$\tilde{\phi}_1 \to o(r^2) \qquad \text{as} \quad r \to \infty, \tag{3.13b}$$

$$\Phi_{r1} - \frac{\partial R_1}{\partial\theta}\Phi_{\theta 0} = 0 \qquad \text{at} \quad r = 1, \tag{3.13c}$$

$$W_1({\Phi_{r0}}^2 + {\Phi_{\theta 0}}^2) = 4\sum_{i=2}^{\infty}(i-1)(i+2)\beta_i^{(1)}P_i(\eta) \qquad \text{at} \quad r=1, \tag{3.13d}$$

$$\int_{-1}^{1} R_1 d\eta = 0, \tag{3.13e}$$

$$\int_{-1}^{1} R_1 P_2 d\eta = 1. \tag{3.13f}$$

In the normal stress condition (3.13d), we imposed the constraint of volume conservation (3.13e) and the center of mass condition, i.e., $\beta_0^{(1)} = \beta_1^{(2)} = 0$.

Now, the shape function at $O(\epsilon)$ can be obtained using the normal stress condition (3.13d) and the known potential function $\tilde{\phi}_0$ from the $O(1)$ solution. In particular, by plugging the known solution $\tilde{\phi}_0$ into the normal stress condition (3.13d), we can solve for the coefficients $\beta_n^{(1)}$'s in $R_1 = \sum_{n=0}^{\infty}\beta_n^{(1)}P_n(\eta)$,

$$\begin{aligned} &\beta_2^{(1)} = \frac{25}{672}W_1, \qquad \beta_4^{(1)} = -\frac{5}{252}W_1, \\ &\beta_n^{(1)} = 0 \quad \text{for} \quad n \neq 2,\ 4. \end{aligned} \tag{3.14}$$

Then from the constraint (3.13f), because of the definition of ϵ, we get

$$W_1 = 67.2. \tag{3.15}$$

Finally, we can determine the flow field at $O(\epsilon)$ by solving (3.13a) with (3.13b) and (3.13c). The solution of (3.13a), which satisfies the condition (3.13b) at infinity, is given by

$$\tilde{\phi}_1 = \sum_{n=0}^{\infty}\alpha_n^{(1)}r^{-(n+1)}P_n(\eta). \tag{3.16}$$

From the kinematic condition with known R_1 and $\tilde{\phi}_0$, we can easily determine the coefficients in this expression,

$$\begin{aligned} \alpha_2^{(1)} &= \frac{275}{18144}W_1, \\ \alpha_4^{(1)} &= \frac{325}{11088}W_1, \\ \alpha_6^{(1)} &= -\frac{125}{8316}W_1, \\ \alpha_n^{(1)} &= 0, \quad n \neq 2,\ 4,\ 6. \end{aligned} \tag{3.17}$$

The constant volume constraint is automatically satisfied by R_1.

3.1.c) $O(\epsilon^2)$ Problem

The equations governing the $O(\epsilon^2)$ problem are

$$\nabla^2\tilde{\phi}_2 = 0 \qquad (1 \le r < \infty, -1 \le \eta \le 1), \tag{3.18a}$$

$$\tilde{\phi}_2 \to o(r^2) \qquad \text{as} \quad r \to \infty, \tag{3.18b}$$

$$\Phi_{r2} - \Phi_{\theta 1}\frac{\partial R_1}{\partial \theta} - \Phi_{\theta 0}\left(\frac{\partial R_2}{\partial \theta} - R_1\frac{\partial R_1}{\partial \theta}\right) = 0, \quad \text{at} \quad r = 1, \tag{3.18c}$$

$$\begin{aligned} &W_2({\Phi_{r0}}^2 + {\Phi_{\theta 0}}^2) + W_1(2\Phi_{r0}\Phi_{r1} + 2\Phi_{\theta 0}\Phi_{\theta 1}) \\ &= 4\left[\sum_{j=0}^{\infty}(j-1)(j+2)\beta_j^{(2)}P_j(\eta) - 2\sum_{i=2}^{\infty}\beta_i^{(1)}P_i\sum_{i=2}^{\infty}(i^2+i-1)\beta_i^{(1)}P_i\right] \end{aligned} \tag{3.18d}$$

$$\int_{-1}^{1}({R_1}^2 + R_2)d\eta = 0, \tag{3.18e}$$

$$\int_{-1}^{1} R_2 P_2 d\eta = 0. \tag{3.18f}$$

Again, the shape function, R_2, at $O(\epsilon^2)$ can be obtained from (3.18d) using the known functions $\tilde{\phi}_0$, $\tilde{\phi}_1$ and the shape coefficients $\beta_i^{(1)}$ at $O(\epsilon)$. We find

$$\begin{aligned} \beta_0^{(2)} &= -0.321 \times 10^{-3}W_1^2, \\ \beta_2^{(2)} &= 0, \\ \beta_4^{(2)} &= 2.092 \times 10^{-3}W_1^2, \\ \beta_6^{(2)} &= -1.260 \times 10^{-3}W_1^2, \\ \beta_8^{(2)} &= 0.467 \times 10^{-3}W_1^2, \\ \text{others} &= 0. \end{aligned} \tag{3.19}$$

Then, from (3.18f), we obtain

$$W_2 = -0.1671W_1^2 = -754.7. \tag{3.20}$$

Finally, the solution of (3.18a), satisfying (3.18b), is $\tilde{\phi}_2 = \sum_{n=0}^{\infty} \alpha_n^{(2)} r^{-(n+1)} P_n(\eta)$ and the coefficients $\alpha_n^{(2)}$ are obtained from (3.18c)

$$\begin{aligned}
\alpha_0^{(2)} &= -5.110 \times 10^{-5} W_1^2, \\
\alpha_2^{(2)} &= -1.025 \times 10^{-4} W_1^2, \\
\alpha_4^{(2)} &= 1.298 \times 10^{-3} W_1^2, \\
\alpha_6^{(2)} &= 2.019 \times 10^{-3} W_1^2, \\
\alpha_8^{(2)} &= -2.914 \times 10^{-3} W_1^2, \\
\alpha_{10}^{(2)} &= 9.517 \times 10^{-4} W_1^2, \\
\text{others} &= 0.
\end{aligned} \tag{3.21}$$

3.1.d) $O(\epsilon^3)$ problem

Since the $O(\epsilon^3)$ problem is extremely complicated, we calculate only W_3 from the normal stress condition and the consistency requirement from the definition of ϵ. The normal stress condition is

$$\begin{aligned}
&W_3({\Phi_{r0}}^2 + {\Phi_{\theta 0}}^2) + W_2(2\Phi_{r0}\Phi_{r1} + 2\Phi_{\theta 0}\Phi_{\theta 1}) \\
&+ W_1({\Phi_{r1}}^2 + 2\Phi_{r0}\Phi_{r2} + {\Phi_{\theta 1}}^2 + 2\Phi_{\theta 0}\Phi_{\theta 2}) \\
&= 4\Bigg[\sum_{k=0}^{\infty}(k-1)(k+2)\beta_k^{(3)}P_k + 3\sum_{i=2}^{\infty}\beta_i^{(1)}P_i\sum_{i=2}^{\infty}(i^2+i-1)\beta_i^{(1)}P_i \\
&- 2\Bigg(\sum_{i=2}^{\infty}\beta_i^{(1)}P_i\sum_{j=0}^{\infty}(j^2+j-1)\beta_j^{(2)}P_j + \sum_{j=0}^{\infty}\beta_j^{(2)}P_j\sum_{i=2}^{\infty}(i^2+i-1)\beta_i^{(1)}P_i\Bigg) \\
&+ \frac{1}{2}\sum_{i=2}^{\infty}\beta_i^{(1)}P_i'\sum_{i=2}^{\infty}\beta_i^{(1)}(1-\eta^2)P_i'\Bigg(-3\sum_{i=2}^{\infty}i(i+1)\beta_i^{(1)}P_i + 2\sum_{i=2}^{\infty}\beta_i^{(1)}\eta P_i'\Bigg)\Bigg],
\end{aligned} \tag{3.22}$$

and the definition of ϵ requires $\beta_2^{(3)} = 0$. Substituting the known solutions of $\tilde{\phi}_0$, $\tilde{\phi}_1$, $\tilde{\phi}_2$, R_1, and R_2 into (3.22), we get

$$\beta_2^{(3)} = 0.1488 W_3 - 0.937 \times 10^{-3} W_1^3,$$

and the condition $\beta_2^{(3)} = 0$ then yields

$$W_3 = 6.2970 \times 10^{-3} W_1^3 = 1910.9. \tag{3.23}$$

3.2. *Estimation of the Critical Weber Number*

The most important feature of the solution obtained in this subsection is that it exhibits multiple (double) steady-state solutions for Weber numbers below the critical value, but no steady-state solution beyond the critical value. Let us start with the second-order solution because we have the full solution to this accuracy. The Weber number as a function of ϵ is given by

$$\begin{aligned} W &= \epsilon W_1 + \epsilon^2 W_2 \\ &= (\epsilon W_1) - 0.1671(\epsilon W_1)^2 \\ &= 67.2\epsilon - 754.7\epsilon^2. \end{aligned} \tag{3.24}$$

The critical Weber number occurs where $\partial W/\partial \epsilon = 0$ - see figure 2B. This point can thus be estimated from (3.24), and equation (3.24) gives

$$W_c = 1.50 \qquad \text{at} \quad \epsilon_c = 0.0445. \tag{3.25}$$

This estimate of the critical Weber number 1.50 is considerably below the value 2.76 obtained numerically by Miksis (1981), but the general features of the solutions are more or less the same (see figure 3 in next subsection).

The third order solution for W as a function of ϵ is

$$\begin{aligned} W &= \epsilon W_1 + \epsilon^2 W_2 + \epsilon^3 W_3 \\ &= (\epsilon W_1) - 0.1671(\epsilon W_1)^2 + 0.0063(\epsilon W_1)^3 \\ &= 67.2\epsilon - 754.7\epsilon^2 + 1910.9\epsilon^3. \end{aligned} \tag{3.26}$$

Equation (3.26) predicts

$$W_c = 1.73 \qquad \text{at} \quad \epsilon_c = 0.0568. \tag{3.27}$$

The critical Weber number 1.73 is still below the numerical value 2.76, but comparison of the $O(\epsilon^2)$ and $O(\epsilon^3)$ solutions indicates that the estimate of the critical Weber number may approach 2.76 as the accuracy of the perturbation

solution is increased. In the later part of this section, the second- and the third-order perturbation solutions will be compared with the W-perturbation solution and the numerical solutions by Miksis (1981) and Ryskin & Leal (1984).

It is interesting to note that the stability of the solution branch is exchanged at the point $\epsilon = \epsilon_c$ (see Iooss & Joseph (1980) for the exchange of stability at a regular turning point). To show this, we consider the following simple *model* equation for bubble dynamics in terms of the amplitude of the P_2-mode, ϵ, which has the same steady state as the second-order solution (3.24)

$$\frac{d^2\epsilon}{dt^2} = K(\epsilon;W)\Big[W - (67.2\epsilon - 754.7\epsilon^2)\Big]. \tag{3.28}$$

Here, $K(\epsilon;W)$ is a nonlinear function of ϵ, which must be nonzero to insure that (3.24) is the unique steady-state solution of (3.28). In fact, it is clear that $K(\epsilon;W)$ must be a positive function since the driving force for the P_2-mode deformation is just $K(\epsilon;W)\cdot W$. In (3.28), we must also note that the first order time derivative term is not included because viscous damping is not expected. Linearization of (3.28) about the steady-state solution gives

$$\frac{d^2x}{dt^2} + (67.2 - 1509.4\epsilon_s)K(\epsilon_s;W)x = 0, \tag{3.29}$$

where $x = \epsilon - \epsilon_s$. In (3.29) the coefficient of the second term changes sign at $\epsilon = \epsilon_c$ from positive to negative, which clearly means that the branch for $0 \le \epsilon < \epsilon_c$ is stable (oscillatory motion), whereas the other branch is unstable.

3.3. *The W-Perturbation as a Limiting Form of the P_2-Perturbation*

One advantage of the P_2-perturbation scheme is that the W-perturbation solution, as shown in (3.1), is nothing but a special form of the P_2-perturbation solution for the limit $W \ll 1$ on the stable branch. Thus, we can obtain the W-perturbation solution very easily from the P_2-perturbation by simply taking the appropriate limiting form. The W-perturbation solution obtained here will be used as the base state for analysis of the oscillatory motion of a bubble.

In the small Weber number limit, the solution can be expanded as

$$\phi = \sqrt{\frac{W}{2}}(\phi_0 + W\phi_1 + W^2\phi_2 + \cdots), \tag{3.1a}$$

$$R = 1 + W\zeta_1 + W^2\zeta_2 + \cdots, \tag{3.1b}$$

where

$$\phi_i = \sum_{n=0}^{\infty} \gamma_n^{(i)} r^{-(n+1)} P_n \qquad i \geq 1,$$

$$\zeta_i = \sum_{n=0}^{\infty} \delta_n^{(i)} P_n \qquad i \geq 1,$$

while in the P_2-perturbation the solution is expanded as

$$\phi = \sqrt{\frac{W}{2}}(\tilde{\phi}_0 + \epsilon\tilde{\phi}_1 + \epsilon^2\tilde{\phi}_2 + \cdots), \tag{3.30a}$$

$$R = 1 + \epsilon R_1 + \epsilon^2 R_2 + \cdots, \tag{3.30b}$$

where

$$\tilde{\phi}_i = \sum_{n=0}^{\infty} \alpha_n^{(i)} r^{-(n+1)} P_n \qquad i \geq 1,$$

$$R_i = \sum_{n=0}^{\infty} \beta_n^{(i)} P_n \qquad i \geq 1.$$

From the section 3.1, we see that $\alpha_n^{(i)} = \tilde{\alpha}_n^{(i)} W_1^i$, and $\beta_n^{(i)} = \tilde{\beta}_n^{(i)} W_1^i$, where $\tilde{\alpha}_n^{(i)}$, $\tilde{\beta}_n^{(i)}$ are parameter-free constants. Thus, we can write (3.30) as

$$\phi = \sqrt{\frac{W}{2}}\left(\phi_0 + (\epsilon W_1)\sum_{n=0}^{\infty} \tilde{\alpha}_n^{(1)} r^{-(n+1)} P_n + (\epsilon W_1)^2 \sum_{n=0}^{\infty} \tilde{\alpha}_n^{(2)} r^{-(n+1)} P_n + \cdots\right), \tag{3.31a}$$

$$R = \phi_0 + (\epsilon W_1)\sum_{n=0}^{\infty} \tilde{\beta}_n^{(1)} P_n + (\epsilon W_1)^2 \sum_{n=0}^{\infty} \tilde{\beta}_n^{(2)} P_n + \cdots. \tag{3.31b}$$

Also, from the relationship between W and (ϵW_1) in (3.24) (i.e., for the second-order solution), we can express (ϵW_1) for the stable branch in terms of W

$$(\epsilon W_1) = W + 0.1671W^2 + O(W^3). \tag{3.32}$$

Then, the W-perturbation solution is simply obtained by plugging (3.32) into (3.31) and collecting the same order terms in W.

The shape function up to $O(W^2)$ is given by

$$R = 1 + (\frac{25}{672}P_2 - \frac{5}{252}P_4)W \tag{3.33}$$
$$+ (-0.321P_0 + 6.217P_2 - 1.223P_4 - 1.260P_6 + 0.467P_8) \times 10^{-3}W^2$$
$$+ O(W^3).$$

Thus, we see that the first-order, $O(W)$, shape function is

$$\begin{aligned} \varsigma_1 &= \frac{25}{672}P_2(\eta) - \frac{5}{252}P_4(\eta) \\ &= -\frac{5}{192}(1 - 5\eta^2 + \frac{10}{3}\eta^4). \end{aligned} \tag{3.34}$$

This solution (3.34) is exactly the same $O(W)$ solution as obtained by Miksis for comparison with his numerical results. Even at this leading order of approximation, the bubble shape exhibits quite interesting results. In particular, the bubble shape is not ellipsoidal at the leading order of approximation (unlike the solution of the same problem at zero Reynolds number, where $\varsigma_1 = C_1P_2(\eta)$ and the shape is ellipsoidal). In the present case, the maximum radius does not occur at $\theta = 0$ (stagnation point), but rather at

$$\theta_{max} = \frac{\pi}{6}. \tag{3.35}$$

This is a very clear first indication of the initially surprising barrellike steady-state shape that Miksis (1981) and Ryskin & Leal (1984) obtained numerically. This interesting shape is obtained because the only source of deformation in this inviscid flow is the dynamic pressure variation on the bubble surface, and the dynamic pressure is clearly a maximum at the stagnation points of the flow (i.e., at the ends of the bubble and at its equator). It is also amusing to note that the maximum radius occurs at $\theta = (\frac{\pi}{2})/2$ for the corresponding 2-D problem (Vanden-Broeck & Keller 1980), while the maximum radius occurs at $\theta = (\frac{\pi}{2})/3$ for the present axisymmetric problem. The second-order solution for W can be

used to calculate the degree of deformation at the stagnation points, since it is these values that are usually given in experiments or numerical analysis.

$$f(\theta = 0) = 0.01736W + 0.00388W^2$$

$$f(\theta = \frac{\pi}{2}) = -0.02604W - 0.00336W^2 \tag{3.36}$$

Finally, we compared the two perturbation solutions (P_2-perturbation and W-perturbation) with the numerical solutions by Miksis (1981) and Ryskin & Leal (1984) in figure 3. Although the critical Weber number predicted by the P_2-perturbation solution is substantially below the value obtained numerically, we can see that the solution behavior predicted by the P_2-perturbation scheme is more or less the same as the exact numerical solutions. Furthermore, the perturbation solution appears to approach the numerical results as the accuracy of approximation is increased. The W-perturbation gives a reasonable estimate of the stable portion of the solution branch but cannot expose the limit point, which appears as a singular point, and thus would require an infinite number of terms to resolve.

4. Small Amplitude Oscillation about the Steady-State Shapes

In this section, we study small amplitude oscillations of a bubble in an inviscid, uniaxial straining flow. We are especially interested in the frequency of oscillation which our recent numerical studies indicate as changing because of the straining flow. However, in spite of the fact that steady solutions can be obtained to any desired order in W, such a rigorous study would be too complicated to be tractable. Here, we approach the problem at two different levels of approximation. First, we study the unsteady dynamics of small disturbances from a *spherical* shape. Strictly speaking, the spherical shape represents only the limit of the steady-state solution for zero Weber number. However, Ryskin and Leal's numerical calculations indicate that the deviation from sphericity is, in fact, relatively small ($f_{s,max} < 0.2$) even at the critical point ($2.7 < W_c < 2.8$).

Hence, we may anticipate that results for a sphere will be at least qualitatively correct even for Weber numbers of $O(1)$. As a partial check on this assumption, we obtain a second solution based upon the correct steady-state shape up to $O(W)$. The latter analysis yields a first order asymptotic formula for the frequency change as a function of the Weber number.

4.1. *Oscillatory Motion of a Bubble about the Spherical Shape*

We begin with the complete equations and boundary conditions governing an axisymmetric time-dependent variation of bubble shape in an inviscid fluid. These are the equation of motion

$$\nabla^2\phi = 0, \tag{4.1}$$

the kinematic condition

$$-\frac{\partial F}{\partial t} = \nabla\phi \cdot \nabla F \qquad \text{at} \qquad r = 1 + f(\theta, t), \tag{4.2}$$

where the bubble surface is specified by the shape function $F = r-(1+f(\theta,t)) = 0$, and the normal stress condition

$$G(t) + \frac{\partial \phi}{\partial t} + \frac{1}{2}\nabla\phi \cdot \nabla\phi = (\nabla \cdot \mathbf{n}) \qquad \text{at} \qquad r = 1 + f(\theta, t). \tag{4.3}$$

In this first subsection, we consider small disturbances of shape for a spherical bubble in a uniaxial straining flow. The motivation for this approximate analysis was given above. The inherent assumption is that the oscillations of a sphere in a flow should reflect at least the qualitative behavior of a *real* deformed bubble in the same flow. A partial check on this assumption is provided by comparing the results obtained here with the asymptotic results of section 4.2, in which we include the small $O(W)$ deformation in the steady-state bubble shape. Physically, the analysis of a spherical bubble will provide qualitatively correct results if the primary influence of the external flow is a direct consequence of hydrodynamic interaction between that flow and the fluctuating modes, rather

than an indirect consequence of the modifications of bubble shape that are induced by the mean flow.

Let us then express the limiting forms of (4.1) - (4.3) that apply for a small disturbance from a spherical bubble shape. To do this, we introduce a small disturbance into the expression for the velocity potential for a spherical bubble, i.e.,

$$\phi = \sqrt{\frac{W}{2}}\phi_s + \epsilon\phi_u, \tag{4.4}$$

where

$$\phi_s = \frac{1}{2}(3\cos^2\theta - 1)(\frac{1}{2}r^2 + \frac{1}{3}r^{-3}) = P_2(\eta)\left(\frac{1}{2}r^2 + \frac{1}{3}r^{-3}\right), \tag{4.5}$$

and $\eta = \cos\theta$. Similarly, the shape of the bubble surface is assumed to take the form

$$R = 1 + f = 1 + \epsilon\,\zeta_u = 1 + \epsilon\sum_{n=2}^{\infty}\delta_n(t)P_n(\eta). \tag{4.6}$$

Then, to obtain equations governing ϕ_u and ζ_u, we substitute (4.4) and (4.6) into (4.1) - (4.3), and retain terms of $O(\epsilon)$. To obtain self-consistent results at any nonzero Weber number, W, with the sphere as a base case, it is necessary to neglect *steady-state* terms in (4.2) and (4.3), which would otherwise superpose a deterministic evolution of the base shape toward the correct equilibrium shape at any W. On this basis, the governing equations for small, time-dependent oscillations of bubble shape for a spherical bubble are:

$$\nabla^2\phi_u = 0, \tag{4.7}$$

with the kinematic condition

$$\frac{\partial\zeta_u}{\partial t} = \frac{\partial\phi_u}{\partial r} + \sqrt{\frac{W}{2}}\zeta_u\frac{\partial^2\phi_s}{\partial r^2} - \sqrt{\frac{W}{2}}\frac{\partial\zeta_u}{\partial\theta}\frac{\partial\phi_s}{\partial\theta} \quad \text{at} \quad r = 1, \tag{4.8}$$

and the normal stress condition

$$\frac{\partial\phi_u}{\partial t} + \sqrt{\frac{W}{2}}(\nabla\phi_s\cdot\nabla\phi_u) + \frac{1}{2}\left(\frac{W}{2}\right)\zeta_u\frac{\partial}{\partial r}(\nabla\phi_s\cdot\nabla\phi_s)$$
$$= \sum_{n=2}^{\infty}(n-1)(n+2)\delta_n P_n(\eta) \qquad \text{at} \quad r = 1, \tag{4.9}$$

where $\eta = \cos\theta$. In deriving equations (4.8) and (4.9), the domain perturbation technique was used to transform the boundary conditions at $r = 1 + \epsilon\varsigma_u$ to the equivalent boundary conditions at $r = 1$.

Since the solution of (4.7), which satisfies the far field velocity condition, $\nabla\phi_u \to 0$ as $r \to \infty$, is given by

$$\phi_u = \sum_{n=0}^{\infty} \gamma_n(t)\, r^{-(n+1)} P_n(\eta), \tag{4.10}$$

and we assume ς_u to be expressed in the form given in (4.6), the conditions (4.8) and (4.9) lead directly to dynamical equations for $\delta_n(t)$ and $\gamma_n(t)$,

$$\begin{aligned} \dot{\delta_n} = & -(n+1)\gamma_n \\ & -\xi\left(\frac{n(n+1)(n+2)}{(2n+3)(2n+5)}\delta_{n+2} - \frac{n(n+1)}{(2n-1)(2n+3)}\delta_n - \frac{(n-1)n(n+1)}{(2n-3)(2n-1)}\delta_{n-2}\right) \end{aligned} \tag{4.11}$$

and

$$\begin{aligned} \dot{\gamma_n} = & (n-1)(n+2)\delta_n \\ & -\xi\left(\frac{(n+1)(n+2)(n+3)}{(2n+3)(2n+5)}\gamma_{n+2} + \frac{n(n+1)}{(2n-1)(2n+3)}\gamma_n - \frac{(n-2)(n-1)n}{(2n-3)(2n-1)}\gamma_{n-2}\right) \\ & -\xi^2\left(I_{+4}(n)\delta_{n+4} + I_{n+2}(n)\delta_{n+2} + I_{+0}(n)\delta_n + I_{-2}(n)\delta_{n-2} + I_{-4}(n)\delta_{n-4}\right), \end{aligned} \tag{4.12}$$

where $\xi = \frac{5}{2}\sqrt{\frac{W}{2}}$ and the $I_i(n)$'s are given by

$$\begin{aligned} I_{+4}(n) &= A(n+4)A(n+2), \\ I_{+2}(n) &= A(n+2)B(n) + A(n+2)B(n+2) - A(n+2), \\ I_{+0}(n) &= A(n)C(n-2) + B(n)B(n) + C(n)A(n+2) - B(n), \\ I_{-2}(n) &= C(n-2)B(n-2) + C(n-2)B(n) - C(n-2), \\ I_{-4}(n) &= C(n-4)C(n-2), \end{aligned}$$

with

$$\begin{aligned} A(n) &= n(n-1)/(2n-1)(2n+1), \\ B(n) &= (2n^2+2n-1)/(2n-1)(2n+3), \\ C(n) &= (n+1)(n+2)/(2n+1)(2n+3). \end{aligned}$$

In the derivation of (4.11) and (4.12), we have used the well-known recurrence formulae for Legendre polynomials

$$(1-\eta^2)P_n'(\eta) = \frac{n(n+1)}{2n+1}\big(P_{n-1}(\eta) - P_{n+1}(\eta)\big),$$

$$\eta P_n(\eta) = \frac{n}{2n+1}P_{n-1} + \frac{n+1}{2n+1}P_{n+1}, \tag{4.13}$$

$$\eta^2 P_n(\eta) = \frac{n(n-1)}{(2n-1)(2n+1)}P_{n-2} + \frac{(2n^2+2n-1)}{(2n-1)(2n+3)}P_n + \frac{(n+1)(n+2)}{(2n+1)(2n+3)}P_{n+2}.$$

By eliminating γ_n from (4.11) and (4.12), we obtain an equation for the amplitude of the shape coefficients, $\delta_n(t)$,

$$\begin{aligned}
&\ddot{\delta}_n + \Big((n^2-1)(n+2) - \xi^2 G_0(n)\Big)\delta_n \\
&\quad = -\xi\Big(J_{+2}(n)\dot{\delta}_{n+2} - J_{-2}(n)\dot{\delta}_{n-2}\Big) \\
&\qquad -\xi^2\Big(G_{+4}(n)\delta_{n+4} - G_{+2}(n)\delta_{n+2} - G_{-2}(n)\delta_{n-2} + G_{-4}(n)\delta_{n-4}\Big),
\end{aligned} \tag{4.14}$$

where

$$\begin{aligned}
J_{+2}(n) &= \frac{(n+1)(n+2)(2n+1)}{(2n+3)(2n+5)}, \\
J_{-2}(n) &= \frac{n(n+1)}{2n-1}, \\
G_{+4}(n) &= (n+1)\big(H_{+4}(n) - I_{+4}(n)\big), \\
G_{+2}(n) &= (n+1)\big(H_{+2}(n) + I_{+2}(n)\big), \\
G_{+0}(n) &= (n+1)\big(H_{+0}(n) + I_{+0}(n)\big), \\
G_{-2}(n) &= (n+1)\big(H_{-2}(n) + I_{-2}(n)\big), \\
G_{-4}(n) &= (n+1)\big(H_{-4}(n) - I_{-4}(n)\big),
\end{aligned}$$

and

$$H_{+4}(n) = \frac{(n+1)(n+2)^2(n+3)(n+4)}{(2n+3)(2n+5)(2n+7)(2n+9)},$$

$$H_{+2}(n) = \frac{(n+1)(n+2)^2(n+3)}{(2n+3)^2(2n+5)(2n+7)} - \frac{n^2(n+1)(n+2)}{(2n-1)(2n+3)^2(2n+5)},$$

$$H_{+0}(n) = \frac{(n+1)^2(n+2)^2(n+3)}{(2n+1)(2n+3)^2(2n+5)} + \frac{n^2(n+1)}{(2n-1)^2(2n+3)^2} + \frac{(n-2)^2(n-1)n^2}{(2n-1)^2(2n-3)(2n+1)},$$

$$H_{-2}(n) = \frac{(n-1)n^2(n+1)}{(2n-3)(2n-1)^2(2n+3)} - \frac{(n-2)^2(n-1)n}{(2n-5)(2n-3)(2n-1)^2},$$

$$H_{-4}(n) = \frac{n(n-1)(n-2)^2(n-3)}{(2n-1)(2n-3)(2n-5)(2n-7)}.$$

From equation (4.14), we note that there is no $\dot{\delta}_n$ term (i.e., no *damping*, as expected in an analysis that neglects all viscous effects), but there is a form of mode-mode interaction in which even modes interact only with other even mode oscillations (or odd modes interact only with odd modes). In the absence of the mean flow (i.e., for $\xi = 0$), interactions between modes occur only at higher order in the amplitude parameter, ϵ.

Since (4.14) is a system of highly coupled equations, it is advantageous to begin by studying the asymptotic behavior for several limiting cases. First, we study the asymptotic form for the limit $n \to \infty$, and then, the asymptotic form for very small values of the Weber number. Following this, we study the behavior of equation (4.14) for a wide range of Weber numbers by evaluating the eigenvalues numerically.

4.1.a) Asymptotic form for the limit $n \to \infty$

Equation (4.14) reduces to a very simple asymptotic form in the limit $n \to \infty$. If we rescale time as $\tilde{t} = \omega t$, then

$$\omega^2 \frac{d^2\delta_n}{d\tilde{t}^2} + \left((n^2-1)(n+2)\right)\delta_n$$

$$= -\xi \left(J_{+2}(n)\omega \frac{d\delta_{n+2}}{d\tilde{t}} - J_{-2}(n)\omega \frac{d\delta_{n-2}}{d\tilde{t}} \right) - \xi^2 \left(O(n^2) \right).$$

Thus, if we take $\omega^2 = (n^2 - 1)(n + 2)$, it is clear that the right hand side will be $O(n^{\frac{5}{2}})$ because J_i's are $O(n)$, and equation (4.14) is reduced to

$$\frac{d^2\delta_n}{d\tilde{t}^2} + \delta_n = 0, \quad \text{as} \quad n \to \infty.$$

The physical significance of this result is that the high frequency modes undergo pure oscillation with no mode-mode interactions. Therefore, if there is no high frequency oscillation initially, then there will be no induced high frequency oscillation. It may also be noted that the oscillation frequency, in this limit, is identical to the oscillation frequency of a bubble in the absence of any bulk flow.

4.1.b) Asymptotic form for very small Weber number ($O(\sqrt{W})$)

As shown in the analysis of section 3, the steady state bubble shape is spherical up to $O(\sqrt{W})$. Therefore, the unsteady motion represented by (4.14) is asymptotically rigorous for only very small values of Weber number. In this subsection, we analyze this limit by retaining terms up to $O(\xi)$ from (4.14) ($\xi = \frac{5}{2}\sqrt{\frac{W}{2}}$). The result is

$$\ddot{\delta}_n + ((n^2 - 1)(n + 2))\delta_n = -\xi J_{+2}(n)\dot{\delta}_{n+2} + \xi J_{-2}(n)\dot{\delta}_{n-2} \qquad (4.15)$$

$$\text{for} \qquad n \geq 2.$$

In fact, (4.15) is a system of infinitely many coupled equations. However, because we know that there is uncoupling of the modes in the limit $n \to \infty$, it is sufficient to study a truncated system containing an arbitrary, but finite, number of coupled equations, say N equations.

We can easily demonstrate, for arbitrarily large (but finite) N, that the real parts of the eigenvalues are always zero, which means that the bubble motion is purely oscillatory in this small W limit. In order to do this, it is convenient to rewrite (4.15) in the form

$$\ddot{\delta}_n + K_n\delta_n = -L_n\dot{\delta}_{n+2} + M_n\dot{\delta}_{n-2}, \qquad (4.16)$$

where $n \leq 2N$ (an arbitrary, but finite number), and K_n, L_n, and M_n are positive functions of n. Then, changing variables as

$$x_{n-1} = \delta_n,$$

$$x_n = \dot{\delta}_n,$$

the equation (4.16) can be expressed (e.g., for the even mode oscillations) in terms of the coupled set

$$\dot{x}_{n-1} = x_n,$$

$$\dot{x}_n = -K_n x_{n-1} - L_n x_{n+2} + M_n x_{n-2} \qquad \text{for} \quad n = 2, 4, \cdots, 2N.$$

In vector form, this can be written as

$$\dot{\mathbf{x}} = \mathbf{A} \cdot \mathbf{x}, \tag{4.17}$$

where $\mathbf{A}$ is

$$\mathbf{A} = \begin{pmatrix} 0 & 1 & & & & & & & \\ -K_2 & 0 & 0 & -L_2 & & & & & \\ & 0 & 0 & 1 & & & & & \\ & M_4 & -K_4 & 0 & 0 & -L_4 & & & \\ & & & 0 & 0 & 1 & & & \\ & & & M_6 & -K_6 & 0 & 0 & -L_6 & \\ & & & & & & \ddots & & \\ & & & & & & 0 & 0 & 1 \\ & & & & & & M_{2N} & -K_{2N} & 0 \end{pmatrix}.$$

This coefficient matrix has the generalized antisymmetric property

$$a_{ij} = -c(i,j) a_{ji},$$

where $c(i,j)$ is a constant whose value depends on i and j (it is important to note that there is no summation intended in this equation). It is easy to show that a diagonal matrix $\mathbf{S}$ exists, which transforms a matrix of the form $\mathbf{A}$ in (4.17) into a true antisymmetric matrix $\mathbf{B}$; i.e.,

$$\mathbf{B} = \mathbf{S}^{-1}\mathbf{A}\mathbf{S}, \tag{4.18}$$

where

$$b_{ij} = -b_{ji}. \tag{4.19}$$

Moreover, the matrices **A** and **B** have the same eigenvalues. But a general property of antisymmetric matrices is that all its eigenvalues are purely imaginary. Thus, it follows that the system of equations (4.15), for arbitrarily large but finite N, has only purely imaginary eigenvalues, and the motion of a bubble for $W \ll 1$ will be strictly oscillatory.

Although a general solution of (4.15) does not appear at first to be possible because of mode coupling, it is instructive to examine the truncated system for $2N = 4$ in which we consider the interaction between only the $n = 2$ and $n = 4$ modes. Solving (4.15) for $2N = 4$, we find

$$-\lambda_2^2 = \omega_2^2 = 12 + O(\xi^2), \tag{4.20a}$$

$$-\lambda_4^2 = \omega_4^2 = 90 + O(\xi^2). \tag{4.20b}$$

Thus, mode interaction is negligible up to $O(\xi)$ (or $O(\sqrt{W})$). Although we have considered explicitly only the interaction between $n = 2$ and $n = 4$, this result can be generalized for arbitrary n and N. The general treatment will be given in the next subsection following equation (4.34). From this argument, we can see that the frequency of oscillation does not change due to the straining flow up to this order, i.e. there is no $O(\sqrt{W})$ term in the axisymmetric expression for the frequency change as a function of Weber number.

4.1.c) Numerical evaluation of eigenvalues for larger Weber number

In deriving (4.14), no restriction was imposed on the Weber number except indirectly via the assumption that the steady shape is spherical. In the present subsection, we adopt the *ad hoc* point of view discussed at the beginning of this section, and we numerically evaluate the eigenvalues of (4.14) for the whole range of Weber numbers up to values of $O(1)$, in order to study the influence of

the bulk flow on shape oscillations for a spherical bubble. As discussed earlier, we presume that this will reflect at least qualitatively the behavior of a *real* (deformed) bubble in the same situation.

We begin by rewriting equation (4.14) in the form

$$\ddot{\delta}_n + \tilde{K}_n \delta_n = -L_n \dot{\delta}_{n+2} + M_n \dot{\delta}_{n-2} - S_n \delta_{n+4} + T_n \delta_{n+2} + U_n \delta_{n-2} - V_n \delta_{n-4}. \quad (4.21)$$

Thus, defining $x_{n-1} = \delta_n$, $x_n = \dot{\delta}_n$ (e.g., for even modes) again, we find

$$\dot{x}_{n-1} = x_n,$$

$$\dot{x}_n = -\tilde{K}_n x_{n-1} - L_n x_{n+2} + M_n x_{n-2} - S_n x_{n+3} + T_n x_{n+1} + U_n x_{n-3} - V_n x_{n-5}$$

$$\text{for } n = 2, 4, \cdots, 2N. \quad (4.22)$$

In vector form

$$\dot{\mathbf{x}} = \mathbf{A} \cdot \mathbf{x}, \quad (4.23)$$

where $\mathbf{A}$ is

$$\mathbf{A} = \begin{pmatrix}
0 & 1 & & & & & & & \\
-\tilde{K}_2 & 0 & T_2 & -L_2 & -S_2 & & & & \\
0 & 0 & 0 & 1 & 0 & & & & \\
U_4 & M_4 & -\tilde{K}_4 & 0 & T_4 & -L_4 & -S_4 & & \\
0 & 0 & 0 & 0 & 0 & 1 & 0 & & \\
-V_6 & 0 & U_6 & M_6 & -\tilde{K}_6 & 0 & T_6 & -L_6 & \\
 & & & & & & \ddots & & \\
 & & & 0 & 0 & 0 & 0 & 0 & 1 \\
 & & & -V_{2N} & 0 & U_{2N} & M_{2N} & -\tilde{K}_{2N} & 0
\end{pmatrix}.$$

The eigenvalues of $\mathbf{A}$ were calculated numerically for several Weber numbers by varying N until converged values were obtained for the particular mode, n, of interest. From this numerical calculation, we found that the eigenvalues can be either purely real or purely imaginary. For example, the eigenvalues of the $n = 2$ mode for several Weber numbers and different levels of truncation (i.e., values

of N) are shown in table 1. As we can see, the calculated eigenvalues for the $n = 2$ mode show very good convergence as N increases. With a large number N included, the critical Weber number, at which the square of the $n = 2$ mode eigenvalue changes sign from negative to positive, was found to be 4.62. If we neglect any intermode interaction (i.e., consider only $2N = n = 2$ corresponding to the first column in table 1), we get the crudest estimation of the critical Weber number as 4.95. Since this crudest estimation overestimates the final critical value of 4.62 by only 7 % , it is obvious that intermode interaction does not have a strong effect on the results.

In figure 4, the eigenvalues for both the $n = 2$ and $n = 3$ modes (estimated for $2N = 20$) are shown as a function of the Weber number. The upper graph shows that both eigenvalues change from pure imaginary to pure real at critical Weber numbers (4.62 for $n = 2$ mode and 8.58 for $n = 3$ mode). The lower graph shows the real parts of these eigenvalues as a function of the Weber number. Since the magnitude of the imaginary eigenvalue decreases with an increase of W, for small W, we can see that the frequency of oscillation of these two modes decreases as the Weber number increases, and becomes zero at the critical values. At a higher Weber number the bubble motion is unstable because the real part of one eigenvalue becomes positive.

The fact that the frequency of oscillation decreases in a straining flow has an important physical significance, because it provides one example of frequency modification of a bubble in a certain type flow. Although we do not include any steady-state shape correction in this analysis, it does provide the simplest approximation to the actual oscillatory motion of a bubble in a straining flow. In particular, though the frequency of oscillation and the critical Weber number value will clearly deviate from the true values for a deformed bubble, the qualitative result that the frequency decreases and becomes zero at a certain critical value of W will be the same. This fact is confirmed by the asymptotic analysis, with the $O(W)$ steady state shape correction included, in the next subsection,

and is also confirmed by the numerical solution of Kang & Leal (1987). The significance of a critical Weber number, where the true frequency of oscillation becomes zero, is that this critical value will correspond exactly to a limit point of the corresponding steady state solution. Therefore, the existence of a limit point of the steady solution, which was predicted by the numerical analyses of Miksis (1981) and Ryskin & Leal (1984), is again confirmed by a totally different approach, subject only to the assumption that the oscillatory behavior of a spherical bubble is at least qualitatively representative of that for a real deformed bubble. The fact that the zero frequency point is predicted here to occur at $W = 4.62$, whereas the steady-state limit of convergence was found to be $W = 2.76$, is presumably a consequence of the restriction to a spherical base case in the present analysis.

4.2. *Oscillation of a Slightly Deformed Bubble for* $W << 1$

In the previous subsection, we studied the effect of straining flow on the stability and oscillatory motion of a spherical bubble. Insofar as it can be applied to a spherical bubble, our analysis is applicable for an arbitrary Weber number. However we showed numerically (Ryskin & Leal) and via the perturbation analysis of section 3 that the steady-state shape at finite Weber number is not spherical in an axisymmetric straining flow, and an immediate question arises about the effect of the non-spherical shape on the oscillatory motion. In this subsection we therefore consider the oscillatory motion of a bubble with the steady-state shape corrected to leading order (i.e., $O(W)$) based upon the small W expansion of section 3. To be consistent with the previous subsection, we should not introduce any assumption except that the steady-state shape is given by $R = 1 + W\zeta_s$ (ζ_s is given in (3.34)) over the whole range of interesting W values. However, then, the problem becomes extremely complicated because the change of steady-state shape ($W\zeta_s$) requires an $O(W^{3/2})$ correction of the steady-state velocity potential, whose solution is itself moderately complicated.

Instead, we confine ourselves to a strict asymptotic analysis for the limit of very small Weber numbers, including all $O(W)$ terms (only) in the solution.

The analysis follows that of the preceding subsection (4.1) but with the steady shape function corrected to include the $O(W)$ term from section 3. Thus, the velocity potential and the shape function can be written as

$$\phi = \tilde{\phi}_s + \tilde{\phi}_u = \sqrt{\frac{W}{2}}\phi_s + O(W^{\frac{3}{2}}) + \epsilon\phi_u, \tag{4.24}$$

$$f = f_s + f_u = W\zeta_s + O(W^2) + \epsilon\zeta_u, \tag{4.25}$$

where

$$\begin{aligned}
\phi_s &= P_2(\eta)(\frac{1}{2}r^2 + \frac{1}{3}r^{-3}),\\
\zeta_s &= \delta_2^{(s,1)}P_2(\eta) + \delta_4^{(s,1)}P_(\eta)\\
&= \frac{25}{672}P_2(\eta) - \frac{5}{252}P_4(\eta),\\
\phi_u &= \sum_{n=0}^{\infty}\gamma_n(t)r^{-(n+1)}P_n(\eta),\\
\zeta_u &= \sum_{n=0}^{\infty}\delta_n(t)P_n(\eta).
\end{aligned}$$

In (4.24) $\tilde{\phi}_s$ and $\tilde{\phi}_u$ denote the steady velocity potential and the disturbance velocity potential, respectively, while f_s and f_u denote the shape function and the disturbance shape function, respectively. The governing equation for the disturbance velocity potential is simply Laplace's equation. The asymptotically correct boundary conditions for an infinitesimal disturbance of $O(\epsilon)$ at a small Weber number are derived as follows. First, formally perturb the kinematic condition and the normal stress condition about the steady state, $\phi = \tilde{\phi}_s$ and $f = f_s$ for an arbitrary fixed W, and retain only the $O(\epsilon)$ terms. The resulting $O(\epsilon)$ boundary conditions are partial differential equations with a single parameter W. To achieve the correct, leading-order asymptotic form for the boundary conditions for $W \ll 1$, we substitute the steady-state velocity potential and the steady-state shape function ($\tilde{\phi}_s = \sqrt{\frac{W}{2}}\phi_s + O(W^{\frac{3}{2}}), \quad f_s = W\zeta_s + O(W^2)$) into the boundary conditions, and retain terms up to $O(W)$.

The boundary conditions at $O(\epsilon)$ and $O(W)$, obtained by the domain perturbation technique, are a bit more complicated than those of the previous analysis. In particular, the kinematic condition is

$$\frac{\partial \zeta_u}{\partial t} = \frac{\partial \phi_u}{\partial r} + \sqrt{\frac{W}{2}}\left(\zeta_u \frac{\partial^2 \phi_s}{\partial r^2} - \frac{\partial \zeta_u}{\partial \theta}\frac{\partial \phi_s}{\partial \theta}\right) + W\left(\zeta_s \frac{\partial^2 \phi_u}{\partial r^2} - \frac{\partial \zeta_s}{\partial \theta}\frac{\partial \phi_u}{\partial \theta}\right) \quad \text{at} \quad r = 1, \tag{4.26}$$

and the normal stress condition becomes

$$\begin{aligned} &\frac{\partial \phi_u}{\partial t} + W\zeta_s \frac{\partial^2 \phi_u}{\partial r \partial t} + \sqrt{\frac{W}{2}}(\nabla\phi_s \cdot \nabla\phi_u) + \frac{1}{2}\left(\frac{W}{2}\right)\zeta_u \frac{\partial}{\partial r}(\nabla\phi_s \cdot \nabla\phi_s) \\ &\quad = \sum_{n=0}^{\infty}(n-1)(n+2)\delta_n P_n(\eta) \\ &\quad - 2W\delta_2^{(s,1)} \sum_{k=0}^{\infty} \delta_k (k^2+k+4) P_2(\eta) P_k(\eta) \\ &\quad - 2W\delta_4^{(s,1)} \sum_{l=0}^{\infty} \delta_l (l^2+l+18) P_4(\eta) P_k(\eta) \qquad \text{at} \quad r = 1. \end{aligned} \tag{4.27}$$

Also, we must use the fact that the volume of the bubble is conserved and that the bubble center remains at the origin. These conditions can be easily derived from equations (2.10) and (2.11):

$$\int_{-1}^{1} (\zeta_u + 2W\zeta_s\zeta_u)\, d\eta = 0, \tag{4.28}$$

$$\int_{-1}^{1} \eta(\zeta_u + 3W\zeta_s\zeta_u)\, d\eta = 0. \tag{4.29}$$

Here, we note that these latter conditions were satisfied in the analysis of the previous subsection by letting $\delta_0 = \delta_1 = 0$ in equation (4.9).

By a similar procedure to that shown in the previous section, we can derive the following asymptotic equations for the amplitude functions $\delta_n(t)$, valid up to O(W) (or O(ξ^2)),

$$\delta_0(t) = -\frac{16}{25}\xi^2\left(\frac{1}{5}\delta_2^{(s,1)}\delta_2(t) + \frac{1}{9}\delta_4^{(s,1)}\delta_4(t)\right),$$

$$\delta_1(t) = -\frac{48}{25}\xi^2\left[\frac{9}{35}\delta_3(t)\delta_2^{(s,1)} + \left(\frac{4}{21}\delta_3(t) + \frac{5}{33}\delta_5(t)\right)\delta_4^{(s,1)}\right],$$

and

$$\begin{aligned}\dot{\delta}_n + \Big((n^2-1)(n+2) - \xi^2\big(G_{+0}(n) + \Delta(n)\big)\Big)\delta_n \\ = -\xi\Big(J_{+2}(n)\dot{\delta}_{n+2} - J_{-2}(n)\dot{\delta}_{n-2}\Big) \\ -\xi^2\Big(\sum_{k=-2,k\neq 0}^{+2} D_{2k}\delta_{n+2k}\Big) \qquad \text{for} \quad n \geq 2,\end{aligned} \tag{4.30}$$

where

$$\begin{aligned}\Delta(n) = \frac{8}{25}\Big((n^2-1)(n+2)\big(\delta_2^{(s,1)}Q_0(n) + \delta_4^{(s,1)}R_0(n)\big) \\ -(n-1)(n+2)\big(\delta_2^{(s,1)}S_0(n) + \delta_4^{(s,1)}T_0(n)\big) \\ +2\delta_2^{(s,1)}(n+1)(n^2+n+4)Q_0(n) \\ +2\delta_4^{(s,1)}(n+1)(n^2+n+18)R_0(n)\Big),\end{aligned}$$

with

$$\begin{aligned}Q_0(n) &= \frac{2n+1}{2}\int_{-1}^{1} P_2P_nP_n dx, \\ R_0(n) &= \frac{2n+1}{2}\int_{-1}^{1} P_4P_nP_n dx, \\ S_0(n) &= \frac{2n+1}{2}\int_{-1}^{1} (1-x^2)P_2'P_n'P_n dx, \\ T_0(n) &= \frac{2n+1}{2}\int_{-1}^{1} (1-x^2)P_4'P_n'P_n dx.\end{aligned}$$

In (4.30) the D_{2k}'s are very complicated functions of n of $O(n^3)$, which are not given here explicitly because the effect of the terms involving these coefficients will be shown below to be at most $O(\xi^3)$ (or $O(W^{3/2})$).

To evaluate the eigenvalues of the system of equations (4.30), we assume that the solution can be expressed as

$$\delta_n = \delta_{n0}e^{\lambda t}. \tag{4.31}$$

Then, by substituting (4.31) into (4.30), we get the following equation for the truncated system of equations (arbitrarily large)

$$\mathbf{A} \cdot \mathbf{x} = 0, \tag{4.32}$$

where the elements of $\mathbf{A}$ and $\mathbf{x}$ are given by

$$\begin{aligned}
a_{i,i} &= \lambda^2 + \Big((4i^2-1)(2i+2) - \xi^2(G_0(2i) + \Delta(2i))\Big), \\
a_{i,i+1} &= \lambda\xi J_{+2}(2i) + D_2(2i)\xi^2, \\
a_{i,i+2} &= D_4(2i)\xi^2, \\
a_{i,i-1} &= -\lambda\xi J_{-2}(2i) + D_{-2}(2i)\xi^2, \\
a_{i,i-2} &= D_{-4}(2i)\xi^2, \\
a_{i,j} &= 0 \qquad \text{if } \mid i-j \mid > 2,
\end{aligned}$$

and

$$x_i = \delta_{(2i)0}.$$

Then the characteristic equation for the eigenvalues is given by

$$\det(\mathbf{A}) = 0. \tag{4.33}$$

By definition, we can calculate the determinant as

$$\det(\mathbf{A}) = \sum_{(k_1,\cdots,k_N)} \epsilon(k_1,\cdots,k_N) a_{1k_1}\cdots a_{Nk_N}, \tag{4.34}$$

where the summation extends over all $N!$ arrangements $(k_1,\cdots,k_N)$ of $(1,\cdots,N)$ and $\epsilon(k_1,\cdots,k_N) \equiv \mathrm{sgn}\Pi_{1\le r\le s\le N}(k_s\cdots k_r)$. Now, we can show, for any $N\times N$ matrix, that the number of off-diagonal elements in the term $a_{1k_1}\cdots a_{Nk_N}$ of (4.34) cannot be one. To show that, let us consider any off-diagonal element in the term $a_{1k_1}\cdots a_{Nk_N}$ (say a_{ik_i} for i-th row and k_i-th column, $i \neq k_i$). Then, for the k_i-th row we cannot take $a_{k_ik_i}$ (diagonal element), because any two elements in the term $a_{1k_1}\cdots a_{Nk_N}$ cannot come from the same column. Therefore, we

must pick one of the off-diagonal elements for the k_i-th row. This proves that the number of off-diagonal element in $a_{1k_1}\cdots a_{Nk_N}$ of (4.34) cannot be one.

Two important consequences can be drawn from this fact. First, the effect of off-diagonal elements is at most $O(\xi^2)$ (or $O(W)$), which applies to the discussion following equation (4.20) in the previous subsection. Therefore, there is no $O(\sqrt{W})$ term in the asymptotic expression for the oscillation frequency as a function of the Weber number. Second, the effect of the D_{2k}'s in equation (4.30) is at most $O(\xi^3)$ because $D_{2k}\xi^2$ must be multiplied by at least one of the other off-diagonal elements, which are at most $O(\xi)$. Therefore, for our asymptotic analysis, which is rigorous up to $O(\xi^2)$, we can neglect the terms in (4.30) which involve the D_{2k}'s.

Let us return to the asymptotic solution of (4.30) for small W. For this purpose, we retain only terms in (4.30) up to $O(W)$. The resulting equation is

$$\ddot{\delta}_n+\Big((n^2-1)(n+1)-\xi^2\big(G_{+0}(n)+\Delta(n)\big)\Big)\delta_n$$
$$=-\xi\Big(J_{+2}(n)\dot{\delta}_{n+2}-J_{-2}(n)\dot{\delta}_{n-2}\Big)\qquad \text{for}\quad n\geq 2. \tag{4.35}$$

Since the coefficient of δ_n in (4.35) is positive for $W \ll 1$, where the present analysis is intended to apply, equation (4.35) is of the same type as equation (4.15) in the previous subsection, and the same procedure can be used to prove that the eigenvalues are again purely imaginary. Indeed, in this case, if we consider the truncated system involving only the $n = 2$ and $n = 4$ modes, we obtain the same result as before, equation (4.20), but with the $O(W)$ correction to the oscillation frequency now evaluated

$$-\lambda_2^2=\omega_2^2\simeq 12\Big(1-\big(\frac{G_0(2)+\Delta(2)}{12}\big)\xi^2-\frac{\xi^2}{28.665}\Big)=12(1-0.31W), \tag{4.36}$$

$$-\lambda_4^2=\omega_4^2\simeq 90\Big(1-\big(\frac{G_0(4)+\Delta(4)}{90}\big)\xi^2+\frac{\xi^2}{28.665}\Big)=90(1+0.016W), \tag{4.37}$$

where

$$G_0(2)=0.776,\quad \Delta(2)=-0.00635,$$
$$G_0(4)=2.12,\quad \Delta(4)=0.555.$$

Although these results were obtained by considering the interaction between only the first two even modes, it can be rigorously shown that the inclusion of higher-order modes does not affect the asymptotic formula (4.36) for the $n = 2$ mode up to $O(\xi^2)$.

To show that this is true, let us consider again the characteristic equation for the eigenvalues of the truncated system of (4.35). Then by a procedure similar to that used earlier, we can show that the characteristic equation is given by a determinant of a tridiagonal matrix. If we denote the determinant of the $m \times m$ tridiagonal matrix as $|\mathbf{A}|_m$, then all we must show is that $|\mathbf{A}|_N = o(\xi^2)$ for any $N \geq 2$, provided that $|\mathbf{A}|_1 = O(\xi^2)$ and $|\mathbf{A}|_2 = o(\xi^2)$ (these last two conditions are satified by (4.36)). To do so, assume $|\mathbf{A}|_{k-1} \leq O(\xi^2)$ and $|\mathbf{A}|_k = o(\xi^2)$. Then

$$\begin{aligned} |\mathbf{A}|_{k+1} &= -a_{k,k+1}a_{k+1,k}|\mathbf{A}|_{k-1} + a_{k+1,k+1}|\mathbf{A}|_k \\ &= O(\xi)\ O(\xi)\ O(\xi^2) + O(1)\ o(\xi^2) \\ &= o(\xi^2) \end{aligned}$$

and for $k = 2$, the assumption is true. This proves that the formula (4.36) is asymptotically rigorous up to $O(\xi^2)$.

One interesting result from the analysis of this subsection, which is asymptotically rigorous to $O(W)$, is that the frequency of the principal mode (i.e., $n = 2$ or $n = 3$) decreases as Weber number increases, thus corroborating the *ad hoc* numerical result for a spherical bubble obtained in the preceding section 4.1.c. We shall present a comparison of all of results obtained in sections 4.1 and 4.2 later in section 5. For now, let us simply note that the asymptotic formula, extrapolated to $W \sim O(1)$, suggests that the frequency ω_2 will go to zero at $W \sim 3.2$. It is interesting that this value is closer to the numerical limit point of 2.76, obtained by Miksis(1981) and Ryskin & Leal (1984), than the value 4.62 obtained in the preceding section via numerical analysis for a spherical bubble.

4.3. *The Influence of Weak Viscous Effects on Bubble Oscillation*

From the analysis of the preceding section we found that the frequency of oscillation decreases with an increasing Weber number in an inviscid straining flow. In this section, we explore the effect of a small viscous contribution to bubble oscillation in a uniaxial straining flow. Here, we again introduce the *ad hoc* approximation that the steady-state shape is spherical for the whole Weber number range of interest, as in subsection 4.1.c.

If viscous forces are very small relative to non-viscous forces, then viscous effects will be confined to a very thin boundary layer near the bubble surface. If the interface separates two liquids, or a gas and a liquid with appreciable kinematic viscosity in the gas, explicit account must be given of the boundary layer. When the bubble has a negligible kinematic viscosity or is a *void*, however, viscous effects are extremely weak and a first approximation to their effect on bubble motion can be obtained from the inviscid solution. One approach, first used by Lamb (1932), is to use the inviscid solution in the whole fluid to estimate the viscous dissipation associated with bubble oscillation (Lamb 1932; Miller & Scriven 1968). However, there is a difficulty in application of this dissipation method to the present problem, because the total kinetic energy of the external flow is not defined. In the present analysis, we therefore use an alternative method, which is equivalent to Lamb's dissipation method, in which we ignore the boundary layer and use the potential flow solution right up to the boundary, with the effect of viscosity included by adding a viscous pressure correction and the viscous stress term to the normal stress balance, using the inviscid flow solution to estimate their values.

The normal stress condition, with the pressure correction and the viscous stress terms included, is given by

$$-p_v' + \left(G'(t') + \rho\frac{\partial\phi'}{\partial t'} + \frac{\rho}{2}\nabla\phi'\cdot\nabla\phi'\right) + 2\mu\frac{\partial^2\phi'}{\partial n'^2} = \gamma\,(\nabla\cdot\mathbf{n})$$
$$\text{at} \qquad r' = a + f'(\theta,t'),$$

where p_v' is the pressure correction due to viscosity, and $\frac{\partial}{\partial n'}$ denotes differentiation in the direction of the outward normal vector (cf. equation 2.3 for

comparison). Non-dimensionalization with the characteristic scales (2.5) gives

$$-p_v + \left(G(t) + \frac{\partial \phi}{\partial t} + \frac{1}{2}\nabla\phi \cdot \nabla\phi\right) + 2S\frac{\partial^2 \phi}{\partial n^2} = (\nabla \cdot \mathbf{n}) \qquad (4.38)$$

$$\text{at} \quad r = 1 + f(\theta, t),$$

where the dimensionless parameter S is defined as

$$S = \frac{\mu\phi_c/a^2}{\rho\phi_c/t_c} = \frac{t_c}{a^2/\nu} = \frac{t_{c,sur}}{t_{c,vis}} .$$

It is evident that S can be interpreted as the ratio of a surface tension based time scale and the viscosity diffusion time, a^2/ν. S can also be expressed in terms of the Weber and Reynolds numbers as

$$S = \frac{\sqrt{2W}}{Re},$$

where Reynolds number Re is defined as $Re = 2\rho E a^2/\mu$. In the present analysis we assume that $S << 1$.

As stated earlier, we consider the influence of weak viscous effects ($S << 1$) on the oscillation of a bubble that is assumed to be spherical at steady state for the whole range of Weber numbers, $W = O(1)$. Hence, a small disturbance to the spherical shape is introduced as before,

$$\phi = \sqrt{\frac{W}{2}}\phi_s + \epsilon\phi_u \qquad (4.39a)$$

$$= \sqrt{\frac{W}{2}}P_2(\eta)(\frac{1}{2}r^2 + \frac{1}{3}r^{-3}) + \epsilon\sum_{n=0}^{\infty}\gamma_n(t)r^{-(n+1)}P_n(\eta),$$

$$R = 1 + \epsilon\,\zeta_u = 1 + \epsilon\sum_{n=2}^{\infty}\delta_n(t)P_n(\eta), \qquad (4.39b)$$

but this time it includes the viscous terms in equation (4.38). The governing equation and the boundary conditions are the same as those in section 4.1 except for the normal stress condition. Following the approach of section 4.1, it would seem that a convenient form of the normal stress condition for the unsteady,

disturbance variables could be obtained by application of the domain perturbation technique to transform (4.38) applied at the actual, time-dependent bubble surface to an equivalent condition applied at $r = 1$. This procedure can, in fact, be applied to all terms in (4.38) except for the viscous pressure correction, where it does not work. The problem with $p_v(r,\theta)$ is that it is confined to a very thin boundary layer so that the usual approximation

$$p_v(1+\epsilon\zeta_u,\theta) = p_v(1,\theta) + \epsilon\zeta_u \frac{\partial p_v}{\partial r}(1,\theta) + \cdots$$

breaks down ($\partial p_v/\partial r$ is large). In spite of this difficulty with p_v, however, it is still useful to apply the domain perturbation to all other terms in (4.38). If we do this, subtract the steady normal stress condition for the steady-state bubble shape† and then retain only terms of $O(\epsilon)$, we obtain

$$\begin{aligned} -\tilde{p}_v + \Big[& \frac{\partial \phi_u}{\partial t} + \sqrt{\frac{W}{2}}(\nabla\phi_s \cdot \nabla\phi_u) + \frac{1}{2}\left(\frac{W}{2}\right)\zeta_u \frac{\partial}{\partial r}(\nabla\phi_s \cdot \nabla\phi_s) \\ & + 2S\Big(\frac{\partial^2\phi_u}{\partial r^2} + \zeta_u\sqrt{\frac{W}{2}}\frac{\partial}{\partial r}\Big(\frac{\partial^2\phi_s}{\partial r^2}\Big) + 2\sqrt{\frac{W}{2}}\Big(\frac{\partial\zeta_u}{\partial\theta}\Big)\Big(\frac{\partial\phi_s}{\partial\theta}\Big)\Big)\Big]_{r=1} \\ & = \sum_{n=2}^{\infty}(n-1)(n+2)\delta_n P_n(\eta). \end{aligned} \tag{4.40}$$

Here, $\tilde{p}_v$ is the disturbance of the pressure correction due to unsteady deformation, which can be expressed in the form

$$\tilde{p}_v = \frac{1}{\epsilon}\big(p_v(1+\epsilon\zeta_u,\theta) - p_v^s(1,\theta)\big), \tag{4.41}$$

where $p_v(1+\epsilon\zeta_u,\theta)$ denotes the pressure correction due to viscosity at the perturbed, unsteady bubble surface, and $p_v^s(1,\theta)$ denotes the steady-state, viscous pressure correction at the spherical bubble surface.

---

† In spite of the fact that the steady-state normal stress balance is not exactly satisfied for the assumed spherical steady-state base shape, we subtract the full steady-state condition to remove terms that would otherwise act to superpose a time-dependent evolution toward the correct steady shape onto the time-dependent oscillations of shape that concern us here.

The viscous pressure correction $p_v(1+\epsilon\zeta_u,\theta)$ in (4.41) should be obtained, in principle, by solving the Navier-Stokes equation with boundary conditions applied at the actual deformed bubble surface ($R = 1+\epsilon\zeta_u$). In practice, however, this is extremely difficult for the high Reynolds number problem, because the usual domain perturbation technique is not again applicable to the tangential stress condition (the tangential stress has a singular-like behavior near the boundary at high Reynolds numbers that is very similar to p_v). As a consequence, in the present work, we adopt the *ad hoc* approximation of applying the tangential stress condition at the undeformed spherical surface ($R = 1$) rather than at the actual deformed bubble surface ($R = 1+\epsilon\zeta_u$). This approximation results in an error in the viscous pressure correction of $O(\epsilon p_v^*(1,\theta))$ (where $p_v^*(1,\theta)$ denotes the pressure correction obtained with the approximation), i.e.

$$p_v(1+\epsilon\zeta_u,\theta) = p_v^*(1,\theta) + \epsilon\zeta_u O(p_v^*(1,\theta)). \tag{4.42}$$

The effect of the error terms will be discussed later.

A general formula relating the viscous pressure correction to the vorticity distribution is derived in the appendix for a spherical bubble in an arbitrary axisymmetric flow. This formula can be applied in the present problem to evaluate $p_v^*(1,\theta)$ and $p_v^s(1,\theta)$, and thus, via the approximation (4.42), we can approximate $\tilde{p}_v$ in equation (4.40). Since we ignore the boundary layer, the pressure corrections at $r = 1$, obtained from the formula (A10) derived in the appendix, can be expressed in the forms

$$p_v^*(1,\theta) \simeq \sum_{n=0}^{\infty} nST_n(1)P_n(\cos\theta), \tag{4.43a}$$

$$p_v^s(1,\theta) \simeq \sum_{n=0}^{\infty} nST_n^s(1)P_n(\cos\theta). \tag{4.43b}$$

The coefficients $T_n(1)$ in (4.43) are obtained from the vorticity value at $r = 1$,

$$\omega = -\sum_{n=0}^{\infty} \frac{T_n}{r}\frac{dP_n}{d\theta} = \frac{\partial u_\theta}{\partial r} + \frac{u_\theta}{r} - \frac{1}{r}\frac{\partial u_r}{\partial\theta}, \tag{4.44}$$

and the tangential stress condition that must be satisfied at $r = 1$

$$\frac{\partial u_\theta}{\partial r} - \frac{u_\theta}{r} + \frac{1}{r}\frac{\partial u_r}{\partial \theta} = 0. \tag{4.45}$$

By eliminating $\partial u_\theta / \partial r$, we get

$$-\sum_{n=0}^{\infty} \frac{T_n}{r}\frac{dP_n}{d\theta} = 2\Big(\frac{u_\theta}{r} - \frac{1}{r}\frac{\partial u_r}{\partial \theta}\Big) \simeq 2\Big(\frac{u_{p\theta}}{r} - \frac{1}{r}\frac{\partial u_{pr}}{\partial \theta}\Big). \tag{4.46}$$

By substituting the potential flow field in (4.39a) into (4.46), and by comparing the coefficients of $dP_n/d\theta$, we obtain

$$T_2(1) = -\frac{5}{3}\sqrt{\frac{W}{2}} - 2\epsilon(n+2)\gamma_n, \qquad \text{for} \quad n = 2, \tag{4.47a}$$

$$T_n(1) = -2\epsilon(n+2)\gamma_n, \qquad \text{for} \quad n \neq 2. \tag{4.47b}$$

For the steady-state problem, we have

$$T_2^s(1) = -\frac{5}{3}\sqrt{\frac{W}{2}}, \qquad \text{for} \quad n = 2, \tag{4.47c}$$

$$T_n^s(1) = 0, \qquad \text{for} \quad n \neq 2. \tag{4.47d}$$

Thus, using (4.42), (4.43), and (4.47), we can estimate the disturbance of the viscous pressure $\tilde{p}_v$ in (4.41) as

$$\tilde{p}_v = -(2S)\sum_{n=2}^{\infty} n(n+2)\gamma_n P_n + \varsigma_u \cdot O(S\sqrt{W}). \tag{4.48}$$

Then, the normal stress condition (4.40) can be written as

$$\sum_{n=2}^{\infty}\Big[\gamma_n + (2S)(2n+1)(n+2)\gamma_n\Big]P_n(\eta) + \sqrt{\frac{W}{2}}(\nabla\phi_s \cdot \nabla\phi_u)$$
$$= \sum_{n=2}^{\infty}\Big[(n-1)(n+2) - O(S\sqrt{W}) - \frac{1}{2}\Big(\frac{W}{2}\Big)\frac{\partial}{\partial r}(\nabla\phi_s \cdot \nabla\phi_s)\Big]\delta_n P_n(\eta)$$
$$\text{at} \quad r = 1. \tag{4.49}$$

Although we do not know the details of the $O(S\sqrt{W})$ term, it can be safely neglected if $S \ll 1$ and $\sqrt{W} \ll 1$ because $S\sqrt{W} \ll S$. If $\sqrt{W} = O(1)$ and

$S \ll 1$, on the other hand, the $O(S\sqrt{W})$ term is apparently comparable to the $O(S)$ term. However, the roles of the two terms are totally different. In particular, the $O(S\sqrt{W})$ term yields a negligible correction to the oscillation frequency, while the $O(S)$ term contributes to viscous damping at the leading order. Therefore, in deriving an equation for the amplitude of shape coefficients, $\delta_n(t)$, it is not unreasonable to neglect the $O(S\sqrt{W})$ term up to $W \sim O(1)$, as long as $S \ll 1$.

Now, we obtain a modified version of (4.14) by a similar procedure to that shown in the previous subsection 4.1, but this time we includes a viscous damping term,

$$\begin{aligned}
&\ddot{\delta}_n + (2S)(2n+1)(n+2)\dot{\delta}_n + \Big((n^2-1)(n+2) - \xi^2 G_0(n)\Big)\delta_n \\
&\quad = -\xi\Big(J_{+2}(n)\dot{\delta}_{n+2} - J_{-2}(n)\dot{\delta}_{n-2}\Big) \\
&\qquad -\xi^2\Big(G_{+4}(n)\delta_{n+4} - G_{+2}(n)\delta_{n+2} - G_{-2}(n)\delta_{n-2} + G_{-4}(n)\delta_{n-4}\Big),
\end{aligned} \tag{4.50}$$

where $\xi = \frac{5}{2}\sqrt{\frac{W}{2}}$, and the other coefficients are given in equation (4.14).

As in the subsection 4.1, it is advantageous to begin by studying the asymptotic behavior of (4.50) for several limiting cases. First, we study the asymptotic form for the limit $n \to \infty$, and then, the asymptotic form for asymptotically very small Weber numbers. Following this, we study the behavior of equation (4.50) for a wide range of Weber numbers but small S, by evaluating the eigenvalues numerically.

4.3.a) Asymptotic form for the limit $n \to \infty$

For the limit $n \to \infty$, if we rescale time as $\tilde{t} = \omega t = n^{3/2}t$, equation (4.50) is reduced to the form

$$\frac{d^2\delta_n}{d\tilde{t}^2} + (4S)n^{1/2}\frac{d\delta_n}{d\tilde{t}} + \delta_n = 0 \qquad \text{as} \quad n \to \infty.$$

The physical significance of this result is that the high-frequency modes are damped out faster than the low-frequency modes. It may also be noted that only aperiodic damping is possible for all high-frequency modes with $n > n_c = 1/4S^2$.

4.3.b) $\xi \ll S \ll 1$ case

In this limit, the effect of the straining flow can be neglected ($\xi = 0$). The result (4.50) for $\xi = 0$ is identical to that obtained many years ago by Lamb (1932) using the dissipation argument cited earlier. For this zero mean flow limit, it is well known that only aperiodic damping is possible for $S \geq \{(n^2-1)/(n+2)/(2n+1)^2\}^{1/2}$ (e.g., $S \geq 0.173$ for $n = 2$).

4.3.c) Numerical evaluation of eigenvalues for larger Weber numbers but small S

Finally, the eigenvalue for the $n = 2$ mode is numerically evaluated for a wide range of Weber numbers. The real and the imaginary parts are shown in figure 5 for several values of S. For a very small S ($S < 0.05$), the solution behavior is more or less the same as in the zero viscosity case except that the oscillation is weakly damped. In particular, the frequencies of oscillation are almost the same as in the inviscid case. The numerical results also show that the eigenvalues can be either complex numbers with negative real parts, or pure real numbers. For a given S below 0.173, two eigenvalues for the principal mode ($n = 2$) are complex numbers with negative real parts in the range of $0 \leq W \leq W_{c1}$, two are pure negative real numbers for $W_{c1} \leq W \leq W_{c2}$, and one is a negative real number but the other is a positive real number for $W > W_{c2}$. Therefore, for $S < 0.173$, a bubble can undergo oscillatory damping, or aperiodic damping, or an unstable deformation, depending on the value of the Weber number.

The two critical values of W_{c1} and W_{c2} for the principal mode are shown as a function of S in figure 6. From this figure we can see that the critical value for W_{c1} decreases as S increases as expected, and that an oscillatory damping does not exist for $S > 0.173$. The critical value W_{c2} for instability, on the other

hand, is almost constant, independent of S. Here we must note that we have used the *ad hoc* assumption of a spherical base state and neglected $O(S\sqrt{W})$ terms in the analysis. If we included the steady-state shape effect and/or the $O(S\sqrt{W})$ terms, then possibly different results for W_{c2} would be obtained. Kang and Leal's (1987) full time-dependent numerical analysis showed that W_{c2} is a decreasing function of S ($W_{c2} \sim 2.8$ for $S = 0$, $W_{c2} \sim 2.2$ for $S = 0.021$, and $W_{c2} \sim 1.0$ for $S = 0.14$).

5. Discussion of Results

5.1. *Accuracy of the Steady State Solution*

In figure 7, we compare the shape function $f(\equiv R - 1)$ at the stagnation points (at $\theta = 0$ and $\theta = \frac{\pi}{2}$), as estimated from the first-order and the second-order W-perturbation solution with the numerical solutions of Ryskin & Leal (1984). The upper limit on W corresponds to the point beyond which a numerical solution of the steady-state problem could not be achieved. The second order W-perturbation solution shows very good agreement with the numerical solution for $W \leq 1.5$, but the discrepancy for higher Weber numbers clearly shows the need for higher-order terms to get the accurate results for higher Weber numbers (though it is possible that no finite number of terms would give good results for $W \simeq W_c$; see section 3). The first-order solution agrees very well with the numerical solution up to $W = 0.5$, and shows reasonable agreement up to $W = 1$. Since we used the first-order, steady-state solution to derive the asymptotic formula for frequency change at small Weber number, the accuracy of the first-order, steady-state solution provides valuable insight into the range of Weber numbers where the asymptotic formula can be expected to give reasonable quantitative results. On this basis, the asymptotic formula for the oscillation frequency should be accurate at least up to $W = 0.5$, and reasonably good for even higher Weber numbers.

5.2. *Small Amplitude Oscillation about the Steady-State Shape*

In figure 8, we plot the square of the frequency for the $n = 2$ mode ($\omega_2{}^2$) as predicted by the perturbation analysis, together with the numerical results of Kang and Leal (1987). As shown in the previous section, the small amplitude analysis is performed in two ways. In the first approach, we assume that the steady state shape is spherical for the complete Weber number range of interest. The curved broken line in figure 8 represents the numerically evaluated frequencies in this analysis. Since the true steady-state shape deviates from spherical as the Weber number increases, a quantitative discrepancy between this *spherical* solution and the numerical result is not surprising for the higher Weber number region, as is indeed shown in figure 8. The critical Weber number at which the frequency becomes zero is found to be 4.62 for this perturbation about a sphere. In contrast, the numerical solution shows that the critical value should be between 2.7 and 2.8, if bubble deformation were taken into account. The relatively large discrepancy between these values is clearly due to the neglect of deformation in the steady state shape. Note, however, that the qualitative effect of the flow on the oscillation frequency is more or less the same as that found numerically.

The second result shown in figure 8 is the rigorous asymptotic analysis, where the steady-state shape deformation is included up to $O(W)$. The simple asymptotic formula obtained for the frequency change of the $n = 2$ mode is $\omega_2{}^2 = 12(1-0.31W)$, which is shown as the dotted straight line in figure 8. This asymptotic formula shows excellent agreement with the numerical solution up to $W \simeq 2$, and the predicted critical value 3.2 is much closer to the numerically obtained result.

It is worthwhile to note that the existence of a zero-frequency Weber number is equivalent to the existence of a limit point for the steady-state solution. In fact, the critical value for zero frequency predicted numerically by Kang & Leal (1987) is precisely the same as the limit point of the steady-state solution found numerically by Miksis (1981) and Ryskin & Leal (1984). The reason why

the zero-frequency point is equivalent to the limit point of the steady state solution is very clear. Since the small amplitude oscillation corresponds to the unsteady behavior of a small disturbance to the steady-state solution, the Jacobian matrix for the small perturbation clearly must become singular at the zero frequency point (or zero-eigenvalue point). In addition, we can show that the limit point is a turning point. Therefore, the steady state solution of the branch emanating from the spherical shape for $W = 0$ does not exist for $W > W_c$ in the neighborhood of the critical point (see Miksis (1981)). From this point of view, the zero-frequency point (or the transition point from a purely imaginary eigenvalue to a purely real eigenvalue) obtained by the perturbation anaysis is clearly an asymptotically predicted limit point for the existence of the steady state solution, rather than a simple onset point for instability of the steady state.

5.3. *The Influence of Weak Viscosity Effects*

The analysis of weak viscous effects shows that viscosity has a stabilizing effect in damping the amplitude of oscillation. However, for a given fixed viscosity (or S), the unsteady bubble motion can be categorized as one of damped oscillation, aperiodic damping, and unstable indefinite deformation depending on the value of the Weber number. Thus, there are two kinds of critical Weber number when viscous effects are included in the analysis. They are the zero-frequency point where the bubble motion changes from oscillatory damping to aperiodic damping, and the zero eigenvalue point where the steady-state bubble shape reaches a limit point.

6. Conclusions

The analyses reported in this paper have led to the following general conclusions:

1. The steady-state analysis based on the small parameter $\epsilon =< R, P_2 >$ enables us to obtain an estimate of the critical Weber number beyond which no

steady state solution is found (e.g., the critical value 1.73 is estimated from the third order solution).

2. The first-order steady solution in W shows that the maximum radius occurs at $\theta = \pi/6$, which clearly indicates the barrellike steady state shape for higher a Weber number, which was first obtained by the numerical analysis of Miksis (1981) and Ryskin & Leal (1984).

3. The small amplitude oscillation analysis about the spherical steady-state shape shows that a bubble still oscillates in an inviscid straining flow, but that the frequency decreases as the Weber number increases. For the spherical bubble, the frequency goes to zero at $W = W_c = 4.62$. Thus, a spherical bubble in an inviscid straining flow would be unstable for Weber numbers larger than 4.62.

4. The result of the asymptotic analysis for small amplitude oscillation, including the correct steady-state shape up to $O(W)$, also shows that a bubble undergoes oscillatory motion with a reduced frequency because of the straining flow, for example, for the $n = 2$ mode, $\omega^2 = \omega_0{}^2(1 - 0.31W)$, where ω_0 is the oscillation frequency of the bubble in a quiescent fluid (for the same mode).

5. When we consider weak viscous effects, we find that small amplitude bubble motions in a uniaxial straining flow can be categorized into three types depending on the value of the Weber number: a damped oscillation for Weber numbers below the zero-frequency point (the eigenvalue becomes pure real at this point); an aperodic damping between the zero-frequency point and the zero eigenvalue point (at least one eigenvalue becomes zero at this point); and an unstable indefinite deformation above the zero-eigenvalue point.

This work was supported by a grant from the Fluid Mechanics Program of the National Science Foundation. The authors wish to thank Prof. R.A. Brown for his insightful comments on an earlier version of this paper.

Appendix: Derivation of a general formula for the viscous pressure correction for a spherical bubble in an arbitrary axisymmetric flow.

Let us begin by considering a weak viscous flow superposed on a given potential flow field.

$$\mathbf{u} = \mathbf{u}_p + \mathbf{u}_v$$

Then, the Navier-Stokes equation for the viscous correction for small S in dimensionless form is given by

$$\frac{\partial \mathbf{u}_v}{\partial t} + (\mathbf{u}_p \cdot \nabla)\mathbf{u}_v + (\mathbf{u}_v \cdot \nabla)\mathbf{u}_p = -\nabla p_v + S\nabla^2 \mathbf{u}_v + o(\sqrt{S}) \qquad (A1)$$

with the boundary conditions $\mathbf{u}_v \to 0$ as $r \to \infty$, and $u_{vr} = 0$ at $r = 1$. By taking the curl of equation (A1), we get the vorticity equation ($\underline{\omega} = \nabla \times \mathbf{u}_v$)

$$\frac{\partial \underline{\omega}}{\partial t} + \nabla \times (\underline{\omega} \times \mathbf{u}_p) = -S\nabla \times (\nabla \times \underline{\omega}). \qquad (A2)$$

Since the vorticity field is solenoidal ($\nabla \cdot \underline{\omega} = 0$), we can express the vorticity for this axisymmetric problem in terms of toroidal (**T**) fields (Chandrasekhar 1961; Prosperetti 1977).

$$\underline{\omega} = \mathbf{T} = \nabla \times (\sum_{n=0}^{\infty} T_n(r,t) P_n(\cos\theta)\mathbf{e}_r) \qquad (A3)$$

Also, the viscous correction to the velocity field of the axisymmetric problem can be expressed, in general, as

$$\mathbf{u}_v = (\sum_{n=0}^{\infty} T_n P_n)\mathbf{e}_r - \nabla\Phi = (\sum_{n=0}^{\infty} T_n P_n)\mathbf{e}_r - \nabla(\sum_{n=0}^{\infty} \Phi_n) \qquad (A4)$$

where Φ is an unknown potential function that must be determined to satisfy the incompressibility condition and the boundary conditions. From the incompressibility condition, we have

$$\nabla^2 \Phi_n = \nabla \cdot (T_n P_n \mathbf{e}_r). \qquad (A5)$$

The solution of (A5) satisfying the kinematic condition ($u_{vr}(1,\theta) = 0$) was obtained by Prosperetti (1977).

$$\Phi_n = P_n\Bigg[\Big(\alpha_n(t) + \frac{n+1}{2n+1}\int_1^r s^{-n}T_n(s,t)ds\Big)r^n + \Big(\frac{n}{n+1}\alpha_n(t) + \frac{n}{2n+1}\int_1^r s^{n+1}T_n(s,t)ds\Big)r^{-(n+1)}\Bigg] \qquad (A6)$$

The unknown coefficient $\alpha_n(t)$ in (A6) is determined by the regularity condition at infinity.

$$\alpha_n(t) = -\frac{n+1}{2n+1}\int_1^\infty s^{-n}T_n(s,t)ds \qquad (A7)$$

A differential equation for $T_n(r,t)$ is obtained by substituting (A3) into (A2)

$$\sum_{n=0}^{\infty}\Bigg[\frac{\partial T_n}{\partial t}P_n + \frac{\partial}{\partial r}(u_{pr}T_n)P_n - \frac{\partial}{\partial r}\Big(T_n\int_0^\theta P_n\frac{\partial u_{pr}}{\partial\theta}d\theta\Big) + \frac{T_n u_{p\theta}}{r}\frac{dP_n}{d\theta} + S\Big(\frac{n(n+1)}{r^2}T_n - \frac{\partial^2 T_n}{\partial r^2}\Big)P_n\Bigg] = G(r,t), \qquad (A8)$$

where $G(r,t)$ denotes the terms that are independent of θ. Finally, an equation for the viscous pressure correction p_v is obtained from (A1), (A4), and (A6),

$$\sum_{n=0}^{\infty}\Bigg[\frac{\partial T_n}{\partial t}P_n + \frac{T_n u_{p\theta}}{r}\frac{dP_n}{d\theta} + S\frac{n(n+1)}{r^2}T_nP_n\Bigg] + \frac{\partial}{\partial r}(-\dot{\Phi} + \mathbf{u}_v\cdot\mathbf{u}_p + p_v) = 0. \qquad (A9)$$

Upon integrating (A9) with $p_v(\infty) = 0$ and eliminating the time-derivative terms, we get

$$p_v(1,\theta) = \sum_{n=0}^{\infty}\Bigg[n\int_1^\infty r^{-n-1}\sum_{k=-\infty}^{\infty}f_{n,k}(r)T_{n+k}dr + \int_1^\infty\sum_{l=-\infty}^{\infty}\Big((r^{-n}g_{n,l}(r) - r^{-n-l}g_{n,l}(1))T_{n+l}\Big)dr + nST_n(1)\Bigg]P_n(\cos\theta), \qquad (A10)$$

where

$$\sum_{n=0}^{\infty}\Big(\sum_{k=-\infty}^{\infty}f_{n,k}T_{n+k}\Big)P_n = \sum_{n=0}^{\infty}\Big((u_{pr}P_n - \int_0^\theta P_n\frac{\partial u_{pr}}{\partial\theta}d\theta)T_n\Big),$$

$$\sum_{n=0}^{\infty}\Big(\sum_{l=-\infty}^{\infty} g_{n,l}T_{n+l}\Big)P_n = \sum_{n=0}^{\infty}\Big(\frac{T_n}{r}u_{p\theta}\frac{dP_n}{d\theta}\Big).$$

The general formula (A10) can be used to estimate the viscous pressure correction for a spherical bubble in an arbitrary axisymmetric flow field.

References

Annamalai, P., Trinh, E., & Wang, T.G. 1985 Experimental study of the oscillations of the rotating drop. *J. Fluid Mech.*, **158**, 317-327.

Busse, F.H. 1984 Oscillations of a rotating liquid drop. *J. Fluid Mech.*, **142**, 1-8.

Chandrasekhar, S. 1961 *Hydrodynamic and hydromagnetic stability.* Dover publications.

Iooss, G. & Joseph, D.D. 1980 *Elementary stability and bifurcation theory.* Springer-Verlag.

Kang, I.S. & Leal, L.G. 1987 Numerical solution of unsteady free-boundary problems at finite Reynolds number - I. Finite-difference scheme and its application to the deformation of a bubble in a uniaxial straining flow. *Phys. Fluids*, **30**, 1929-1940.

Lamb, H. 1932 *Hydrodynamics.* 6th ed. Dover Publications.

Marston, P.L. 1980 Shape oscillation and static deformation of drops and bubbles driven by modulated radiation stress: theory. *J. Acoust. Soc. Am.*, **67**, 15-26.

Miksis, M. 1981 A bubble in an axially symmetric shear flow. *Phys. Fluids*, **24**, 1229 - 1231.

Miller, C.A. & Scriven, L.E. 1968 The oscillations of a fluid droplet immersed in another fluid. *J. Fluid Mech.*, **32**, 417-435.

Natarajan, R. & Brown, R.A. 1986 The role of three-dimensional shapes in the breakup of charged drops. *Proc. R. Soc. Lond.*, submitted.

Prosperetti, A. 1977 Viscous effects on perturbed spherical flows. *Quart. Appl. Math.*, **34**, 339-352.

Rayleigh, J.W.S. 1879 On the capillary phenomena of jets. *Proc. R. Soc. Lond.*, **29**, 71-97.

Reid, W.H. 1960 The oscillations of a viscous liquid drop. *Q. Appl. Math.*, **18**, 86-89.

Ryskin, G. & Leal, L.G. 1984 Numerical solutions of free-boundary problems in fluid mechanics. Part 3. Bubble deformation in an axisymmetric straining flow. *J. Fluid Mech.*, **148**, 37-43.

Subramanyam, S.V. 1969 A note on the damping and oscillations of a fluid drop moving in another fluid. *J. Fluid Mech.*, **37**, 715-725.

Tsamopoulos, J.A. & Brown, R.A. 1983 Nonlinear oscillations of inviscid drops and bubbles. *J. Fluid Mech.*, **127**, 519-537.

Tsamopoulos, J.A. & Brown, R.A. 1984 Resonant oscillations of inviscid charged drops. *J. Fluid Mech.*, **147**, 373-395.

Vanden-Broeck, J.-M. & Keller, J.B. 1980 Bubble or drop distortion in a straining flow in two dimensions. *Phys. Fluids*, **23**, 1491-1495.

Table 1. Eigenvalue of $n = 2$ mode as a function of the Weber number and the number of coupled equations.

W \ $2N$	2	4	6	10	20
0	3.464i	3.464i	3.464i	3.464i	3.464i
0.1	3.429i	3.410i	3.410i	3.410i	3.410i
1.0	3.095i	2.932i	2.921i	2.921i	2.921i
2.0	2.675i	2.401i	2.360i	2.358i	2.358i
3.0	2.175i	1.847i	1.757i	1.752i	1.752i
4.0	1.519i	1.214i	1.027i	1.017i	1.017i
4.618	...	...	...	...	0.
5.0	0.343	0.302	0.750	0.745	0.745
6.0	1.594	1.144	1.338	1.307	1.306

Figure Captions

Figure 1. An oscillating bubble in an inviscid straining flow.

Figure 2. Representation of steady-state solutions in two different ways ($A :< R, P_2 >$ in terms of W; W in terms of $< R, P_2 >$).

Figure 3. Comparison of the perturbation solutions for steady shape with the numerical analysis results of Miksis (1981) and Ryskin & Leal (1984) (— — — 1,2,3 : the first-, second-, and third-order solutions obtained by W-perturbation; - - - - - I, II, III: the first-, second-, and third-order solutions obtained by the P_2-perturbation; the first order solutions are identical in both perturbation methods; ————: numerical results).

Figure 4. Eigenvalues as functions of Weber number for the $n = 2$ and $n = 3$ mode oscillations.

Figure 5. The effect of small viscosity on the eigenvalues for the $n = 2$ mode oscillation.

Figure 6. Three different types of bubble motion in a slightly viscous straining flow.

Figure 7. Comparison of the present results for steady shapes with the numerical results of Ryskin & Leal (1984) (- - - - - : the first-order perturbation solution; — — — : the second-order perturbation solution; —◇—: numerical solution).

Figure 8. Comparison of the perturbation solution with the numerical analysis results of Kang & Leal for the square of the eigenvalues of the $n = 2$ mode oscillation (—◇— : numerical solution; - - - -: perturbation solution for the oscillation about the spherical base shape; — — — : asymptotic solution for the oscillation about the steady-state shape, $\omega^2 = \omega_0^2(1 - 0.31W)$).

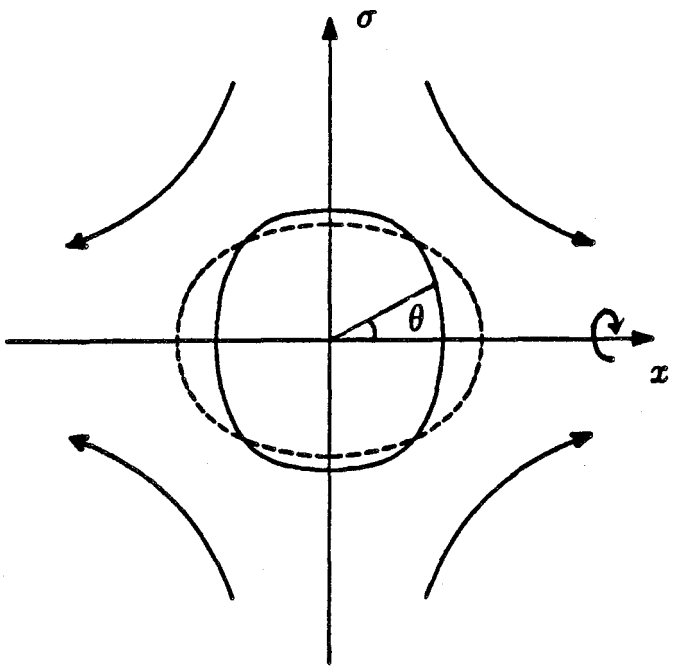

Figure 1

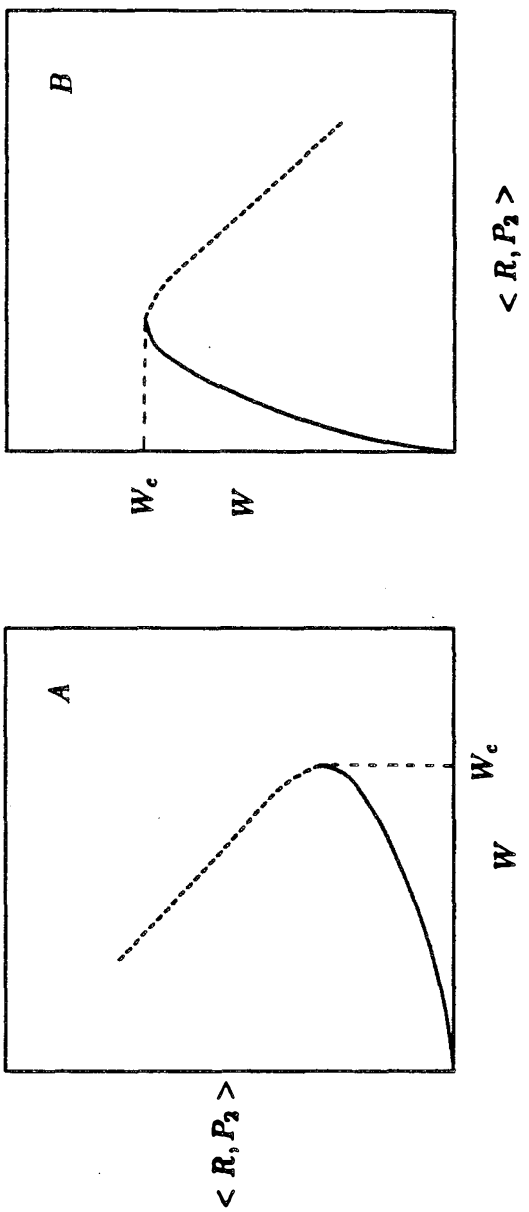

Figure 2

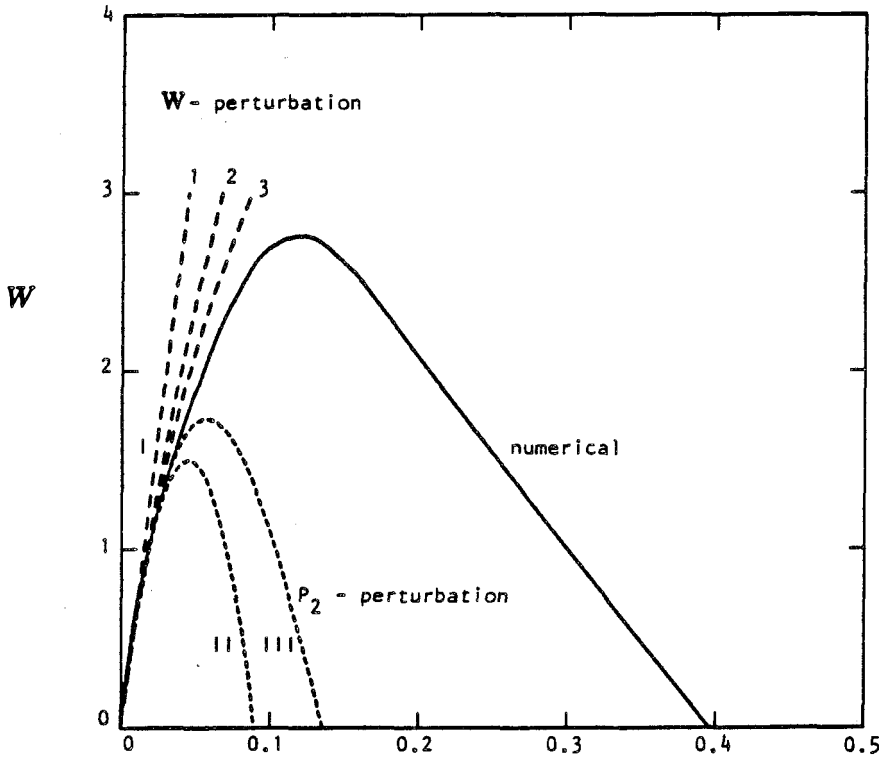
W
4
3
2
1
0
W - perturbation
1
2
3
numerical
I
P_2 - perturbation
II
III
0
0.1
0.2
0.3
0.4
0.5
$\epsilon \equiv < R, P_2 >$

Figure 3

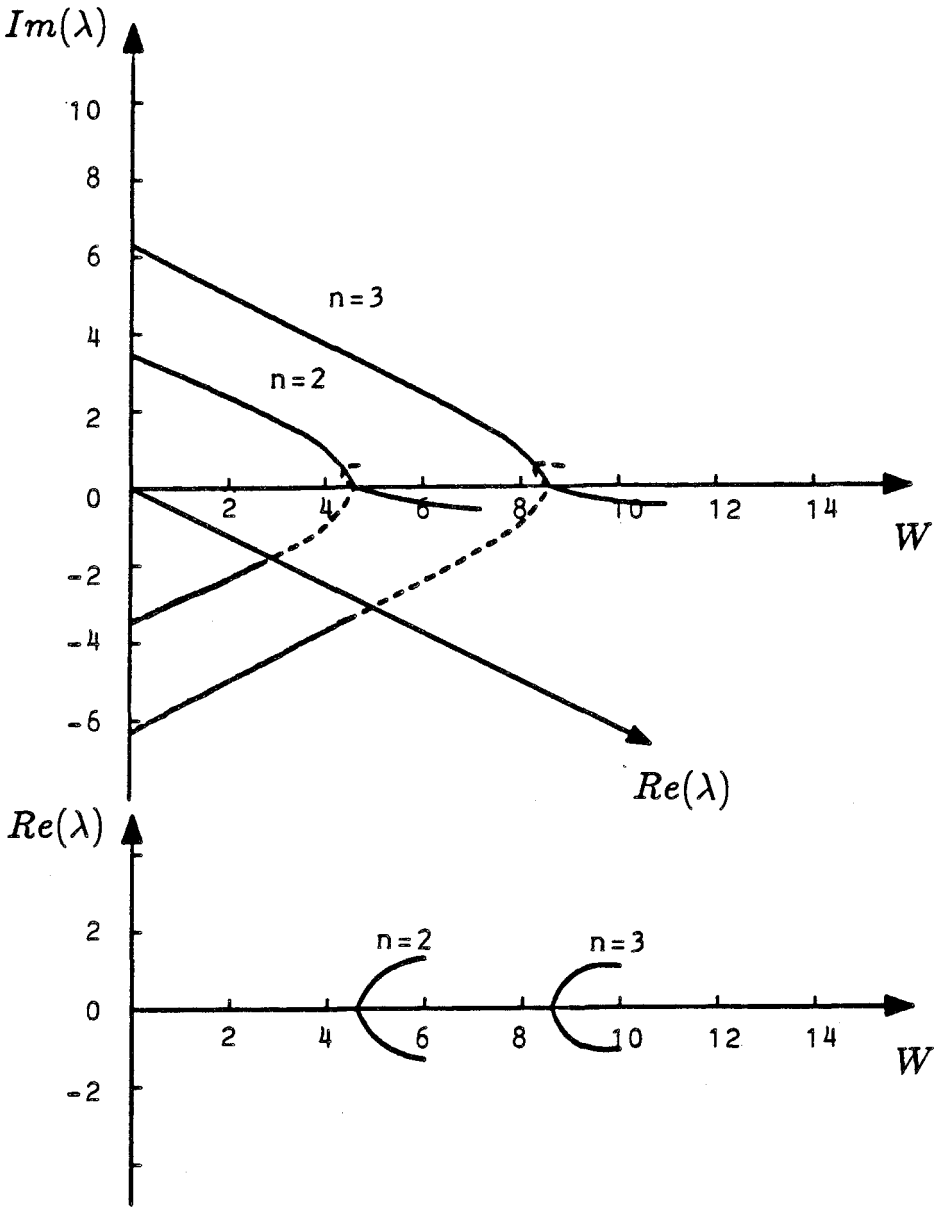
Im(λ)
10
8
6
4
2
0
-2
-4
-6
n=3
n=2
2
4
6
8
10
12
14
W
Re(λ)
Re(λ)
2
0
-2
n=2
n=3
2
4
6
8
10
12
14
W

Figure 4

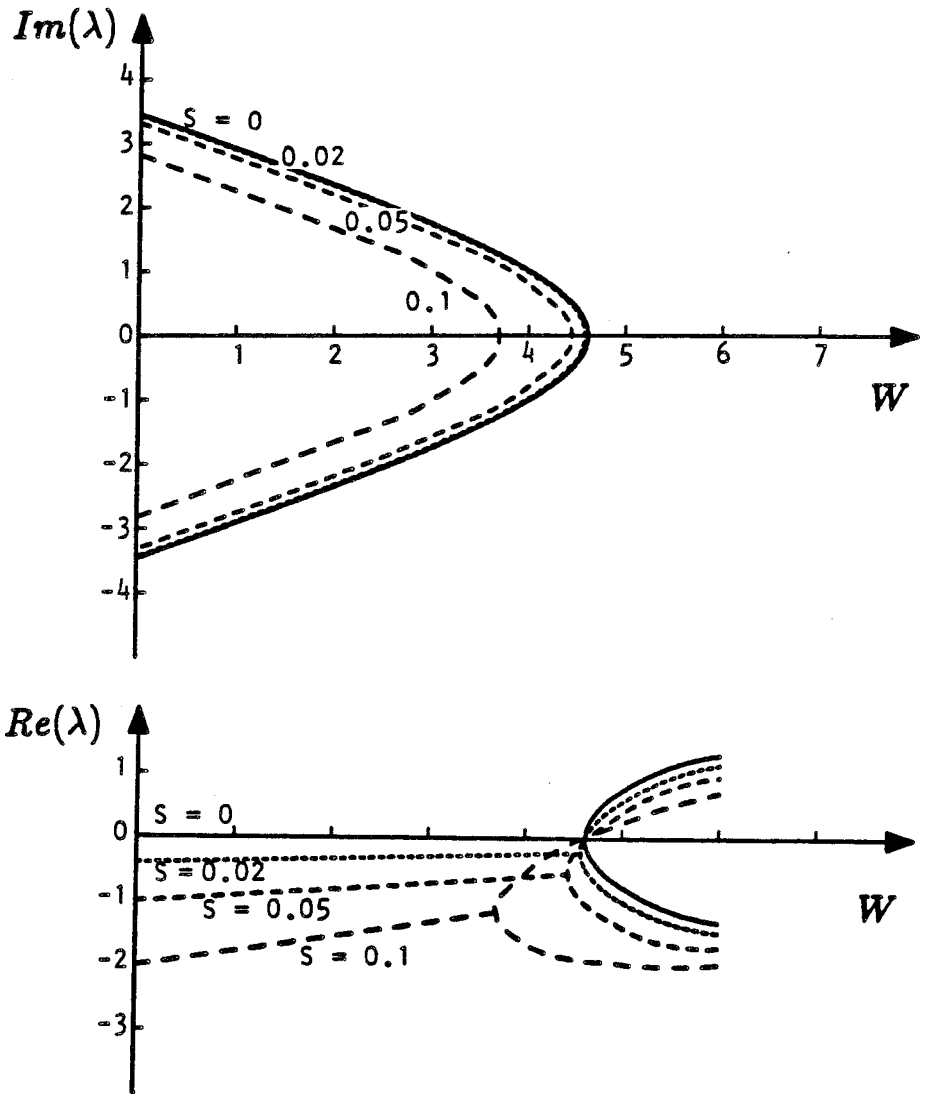
Im(λ)
4
3
2
1
0
-1
-2
-3
-4
S = 0
0.02
0.05
0.1
1
2
3
4
5
6
7
W
Re(λ)
1
0
-1
-2
-3
S = 0
S = 0.02
S = 0.05
S = 0.1
W

Figure 5

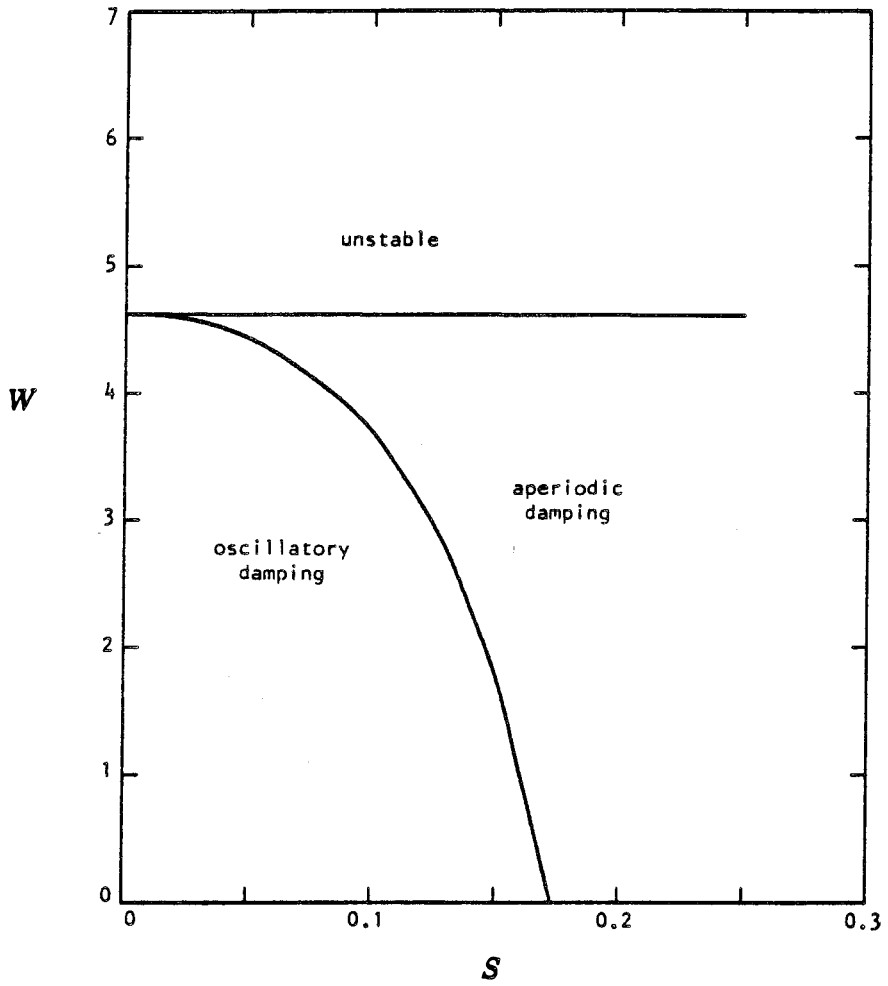
7
6
5
4
3
2
1
0
W
unstable
aperiodic
damping
oscillatory
damping
0
0.1
0.2
0.3
S

Figure 6

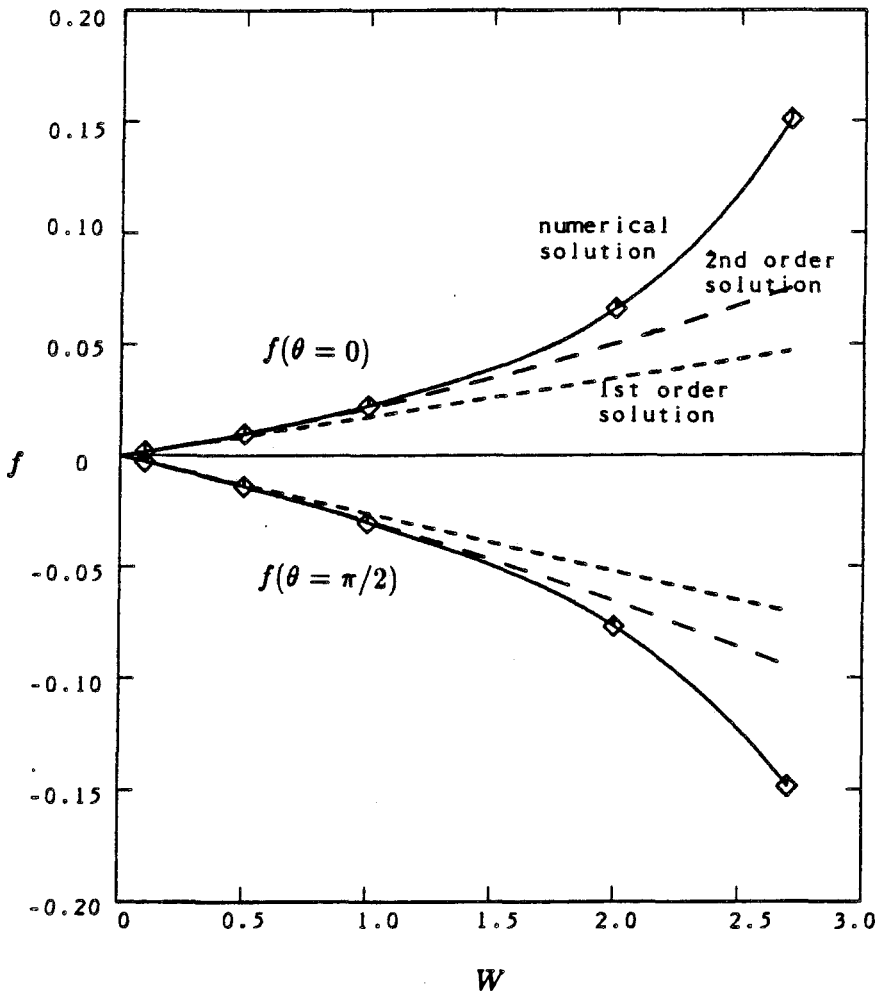
0.20
0.15
0.10
0.05
0
-0.05
-0.10
-0.15
-0.20
f
0
0.5
1.0
1.5
2.0
2.5
3.0
W
numerical solution
2nd order solution
1st order solution
$f(\theta = 0)$
$f(\theta = \pi/2)$

Figure 7

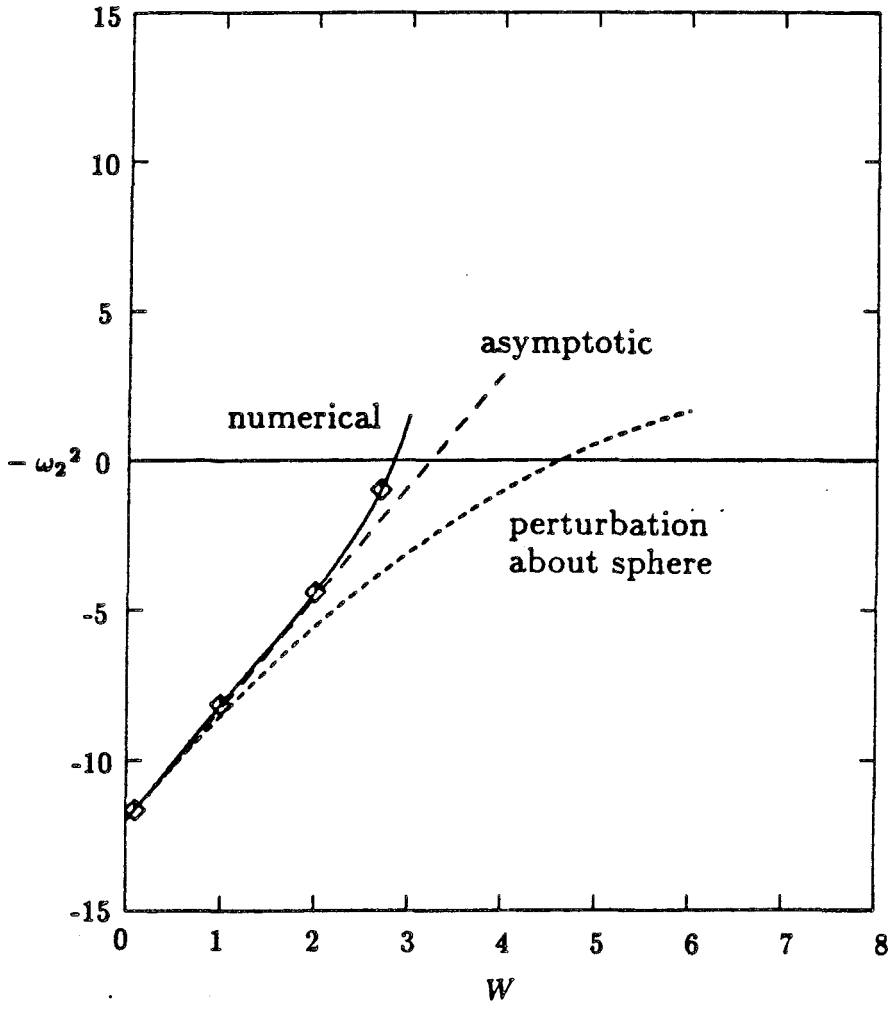
15
10
5
-5
-10
-15
$-\omega_2^2$ 0
0
1
2
3
4
5
6
7
8
W
asymptotic
numerical
perturbation
about sphere

Figure 8

Chapter IV

The drag coefficient for a spherical bubble in a uniform streaming flow

The text of Chapter IV consists of an article which has been accepted for publication in the *Physics of Fluids*.

The drag coefficient for a spherical bubble in a uniform streaming flow

I.S. Kang and L.G. Leal

Department of Chemical Engineering
California Institute of Technology
Pasadena, California 91125

Abstract

The drag coefficient $C_D = 48/R$ for a spherical bubble in a uniform streaming flow at a high Reynolds number, which was first obtained via a dissipation method by Levich [Zh. Eksp. Theoret. Fiz. **19**, 18 (1949)], is rederived here by direct integration of the normal stress over the bubble surface. The present study also shows that the drag coefficient up to $O(R^{-1})$ depends only on the $O(1)$ vorticity distribution right on the bubble surface, and is independent of the vorticity distribution in the fluid. Therefore, the drag coefficient up to $O(R^{-1})$ is completely determined by the irrotational flow solution, which is perfectly consistent with the dissipation method.

I. INTRODUCTION

In the present paper, we are concerned with the classical problem of the drag coefficient on a spherical bubble in a uniform streaming flow at large Reynolds numbers.

The famous result $C_D = 48/R$, which is accurate to $O(R^{-1})$, was first obtained via a dissipation method by Levich[1] and Ackeret.[2] The dissipation method is extremely powerful and simple. Since it derives from an overall macroscopic mechanical energy balance, it requires neither the stress nor pressure distributions on the bubble surface, nor yields any information about their form. Although this is a great advantage from a computational point of view, we must recognize that no insight is possible to understand how the simple result $C_D = 48/R$ can be obtained from the presumably complicated pressure and stress distributions at the bubble surface. Thus, in principle, a direct integration of the normal stress contributions over the bubble surface would provide at least a desirable complement to the macroscopic approach. However, attempts to carry out this calculation have so far been unsuccessful. In particular, Moore[3] obtained $C_D = 32/R$ by integrating an approximation to the normal stress over the bubble surface. However, Moore included only the normal viscous stress, which was approximated using the irrotational flow solution, plus the inviscid pressure field obtained via Bernoulli's theorem. The discrepancy between Moore's result and the result of the dissipation method, as pointed out by Batchelor (in Moore[4]), was due to the neglect of viscous corrections to the pressure in the boundary layer; i.e., the pressure correction in the boundary layer is the same order as the normal viscous stress term ($O(R^{-1})$).

Later, Moore[4] reported a complete boundary layer analysis, including the viscous pressure correction. Unfortunately, however, he was not able to get a uniformly valid solution in the vicinity of the rear stagnation point, and thus a uniformly valid pressure correction was also not obtained. Therefore, instead of calculating the drag coefficient by a direct integration of normal stress forces

over the bubble surface, Moore utilized a macroscopic momentum balance (*momentum defect*), as suggested by Landau and Lifshitz,[5] to obtain the correct drag coefficient $C_D = 48/R$. He also improved upon Levich's result by calculating the dissipation from the boundary layer, stagnation region and wake, to obtain

$$C_D = \frac{48}{R}\left(1 - \frac{2.2}{R^{1/2}}\right) + o(R^{-3/2}).$$

Although Moore's[4] result is complete up to $O(R^{-3/2})$, his boundary layer solution does not give any help in terms of the viscous stress and pressure distributions, in understanding the contributions that yield the result $C_D = 48/R$ obtained by the macroscopic methods. In particular, Moore's expression for the viscous pressure correction (denoted by p_v), obtained from the boundary layer solution, does not give a contribution of $16/R$ to the drag coefficient, which is the difference between the viscous stress contribution (Moore[3]) of $32/R$ and the accepted result $48/R$ from dissipation arguments. Moore's[4] prediction of $p_v(1,\tilde{\theta})$ for a spherical bubble is readily obtained by setting $y = 0$ in his Eq. (2.37)

$$p_v(1,\tilde{\theta}) = \frac{4}{R}(1-\cos\tilde{\theta})^2(2+\cos\tilde{\theta})/\sin^2\tilde{\theta},$$

where $\tilde{\theta}$ is the angle measured from the front stagnation point. This viscous pressure prediction $p_v(1,\tilde{\theta})$ is a monotonically increasing function of $\tilde{\theta}$ and becomes unbounded as $\tilde{\theta} \to \pi$. In fact, Moore's expression for $p_v(1,\tilde{\theta})$ is incomplete because it neglects the contribution to pressure due to displacement thickness effects, which are expected to be important at the rear of the bubble. Unfortunately, however, the displacement thickness correction has not yet been successfully evaluated.

Thus, to date, the drag coefficient for motion of a spherical bubble has still not been obtained by direct integration of the normal viscous stress and pressure over the bubble surface. In this paper, we derive a uniformly valid viscous pressure correction in a way that is different from the conventional boundary layer analysis, and we avoid the problem of non-uniform validity for $\tilde{\theta} \to \pi$. To

do this, we obtain a uniformly valid pressure correction by means of a general relationship between the viscous pressure correction and the vorticity distribution for a spherical bubble in an arbitrary axisymmetric flow that was derived by Kang and Leal.[6] Although it is extremely difficult to determine the vorticity distribution in detail, we show that the information needed to calculate the drag coefficient can be readily obtained from the irrotational flow solution. Thus, as a final step, we calculate the drag coefficient, to $O(R^{-1})$, by integrating the normal viscous stress and pressure over the bubble surface, and we show that Levich's original result is reproduced.

II. PROBLEM FORMULATION

We aim to calculate the drag coefficient for a spherical bubble of volume $4\pi a^3/3$ in a steady uniform streaming flow at a high Reynolds number. The fluid is characterized by a constant density ρ and viscosity μ, and the equation of motion in dimensionless form is given as

$$\mathbf{u} \cdot \nabla \mathbf{u} = -\nabla p + (\frac{2}{R}) \nabla^2 \mathbf{u}. \tag{1}$$

In Eq. (1), we have used the following characteristic scales

$$U_c = U_\infty,$$

$$l_c = a,$$

$$p_c = \rho U_\infty^2,$$

where U_∞ denotes the magnitude of the velocity of the undisturbed streaming flow. The Reynolds number in (1) is defined as

$$R = \frac{2\rho a U_\infty}{\mu}.$$

The boundary conditions at the bubble surface are

$$\mathbf{u} \cdot \mathbf{n} = 0 \quad \text{at} \quad r = 1, \tag{2a}$$

$$\tau_{r\theta} = 0 \qquad \text{at} \qquad r = 1, \tag{2b}$$

and the condition at infinity is given as

$$\mathbf{u} \to U_\infty \mathbf{e}_x \qquad \text{as} \qquad r \to \infty, \tag{2c}$$

where $\mathbf{e}_x$ denotes a unit vector in the direction of streaming flow.

III. DRAG COEFFICIENT BY DIRECT INTEGRATION OF NORMAL STRESS

Our aim is to calculate the dimensionless drag force for a spherical bubble by direct integration of the normal stress at the bubble surface. Hence,

$$\begin{aligned} F_x = \frac{F_x'}{\rho U^2 a^2} &= \int_S \tau_{rr} \mathbf{e}_x \cdot \mathbf{e}_r dS \\ &= 2\pi \int_0^\pi \tau_{rr} P_1(\cos\theta) \sin\theta d\theta, \end{aligned} \tag{3}$$

where F_x' is the dimensional drag force, and θ is the angle measured from the rear stagnation point; i.e., $\theta = \pi - \tilde{\theta}$. The dimensionless total normal stress τ_{rr} is given by $\tau_{rr} = -p + (4/R)(\partial u_r/\partial r)$. The drag coefficient is thus given as

$$C_D = \frac{F_x'}{\frac{1}{2}\rho U^2 \pi a^2} = 4 \int_0^\pi \tau_{rr} P_1(\cos\theta) \sin\theta d\theta. \tag{4}$$

Clearly, to carry out this calculation, we must determine all viscous stress and pressure contributions to τ_{rr} up to an accuracy of $O(R^{-1})$. The viscous stress contribution can be obtained directly from the solution for irrotational flow around a sphere

$$u_{p\theta} = -\sin\theta\left(1 + \frac{1}{2r^3}\right), \tag{5a}$$

$$u_{pr} = \cos\theta\left(1 - \frac{1}{r^3}\right), \tag{5b}$$

where the subscript p stands for the irrotational flow. As shown by Moore,[3] the irrotational flow solution (5) provides a uniformly valid, leading order approximation for the velocity field, satisfying (1) and (2) in the limit $R \to \infty$. The normal stress can thus be obtained as

$$\begin{aligned} \tau_{rr} &= -p + (\frac{4}{R})(\frac{\partial u_r}{\partial r}) \\ &= -p_v - p_p + (\frac{4}{R})(\frac{\partial u_{pr}}{\partial r}) + o(\frac{1}{R}). \end{aligned} \tag{6}$$

Here, p_p is the pressure distribution correponding to the solution (5), while p_v denotes the viscous pressure correction at $O(R^{-1})$ due to viscous effects. The normal viscous stress term in (6) is easily obtained to $O(R^{-1})$ from the irrotational flow solution; i.e.,

$$(\frac{4}{R})(\frac{\partial u_{pr}}{\partial r}) = (\frac{12}{R})\cos\theta = (\frac{12}{R})P_1(\cos\theta) \qquad \text{at} \quad r = 1. \tag{7}$$

The irrotational flow pressure distribution, which is $O(1)$, does not contribute to the drag. However, to obtain a complete result for the drag at $O(R^{-1})$, it is necessary to calculate the viscous pressure contribution at $O(R^{-1})$. We have seen that this has so far proven impossible because of the lack of a uniformly valid expression for the viscous pressure correction, p_v.

IV. VISCOUS PRESSURE CORRECTION AND DRAG COEFFICIENT

In this section, the drag coefficient is calculated up to $O(R^{-1})$ using Eqs. (4), (6), and (7). We do this by making use of a general relationship between the viscous pressure correction and the vorticity distribution for a spherical bubble in an arbitrary axisymmetric flow that was derived by Kang and Leal.[6]

Kang and Leal[6] derived the general formula under the assumption that the velocity perturbation around a bubble due to viscosity approaches zero everywhere in the domain as $R \to \infty$; i.e.,

$$\| \mathbf{u}_v \| << \| \mathbf{u}_p \| \qquad \text{for} \quad R >> 1, \tag{8}$$

which is known from the earlier work of Moore.[4] Indeed, Moore showed that $\| \mathbf{u}_p \| = O(1)$, $\| \mathbf{u}_v \| = O(R^{-1/2})$ in the boundary layer, and that $\| \mathbf{u}_p \| = O(R^{-1/6})$, $\| \mathbf{u}_v \| = O(R^{-1/3})$ in the region near the rear stagnation point of linear size $O(R^{-1/6})$. He also showed that $\| \mathbf{u}_p \| = O(1)$ and $\| \mathbf{u}_v \| = O(R^{-1/2})$ in the wake region. Therefore, the assumption made in (8) is valid everywhere in the solution domain. Since the vorticity is solenoidal ($\nabla \cdot \underline{\omega} = 0$), Kang and Leal expressed the vorticity in terms of toroidal ($\mathbf{T}$) fields for an arbitrary axisymmetric problem, following Chandrasekhar[7] and Prosperetti.[8]

$$\underline{\omega} = \mathbf{T} = \nabla \times \left(\sum_{n=0}^{\infty} T_n(r,t) P_n(\cos\theta) \mathbf{e}_r \right) \tag{9}$$

By substituting (9) into the vorticity transport equation and expressing the perturbed Navier-Stokes equation for $\mathbf{u}_v$ in terms of the T_n's, Kang and Leal derived the following formula for the viscous pressure correction at the surface of a spherical bubble in an arbitrary axisymmetric flow (steady or unsteady) at a high Reynolds number (see Kang and Leal[6] for a detailed derivation).

$$\begin{aligned} p_v(1,\theta,t) = \sum_{n=0}^{\infty} \Bigg[& n \int_1^{\infty} r^{-n-1} \sum_{k=-\infty}^{\infty} f_{n,k}(r) T_{n+k} \, dr \\ & + \int_1^{\infty} \sum_{l=-\infty}^{\infty} \left(\left(r^{-n} g_{n,l}(r) - r^{-n-l} g_{n,l}(1) \right) T_{n+l} \right) dr \\ & + n \left(\frac{2}{R} \right) T_n(1,t) \Bigg] P_n(\cos\theta), \end{aligned} \tag{10}$$

where

$$\sum_{n=0}^{\infty} \Big(\sum_{k=-\infty}^{\infty} f_{n,k} T_{n+k} \Big) P_n = \sum_{n=0}^{\infty} \left(\left(u_{pr} P_n - \int_0^{\theta} P_n \frac{\partial u_{pr}}{\partial \theta} d\theta \right) T_n \right),$$

$$\sum_{n=0}^{\infty} \Big(\sum_{l=-\infty}^{\infty} g_{n,l} T_{n+l} \Big) P_n = \sum_{n=0}^{\infty} \left(\frac{T_n}{r} u_{p\theta} \frac{dP_n}{d\theta} \right).$$

Before going on to the specific problem of utilizing this result in Eqs. (4) and (6) to obtain an expression for the drag coefficient for a spherical bubble

rising through a quiescent fluid, let us consider the viscous pressure correction from a qualitative, order-of-magnitude view point. The most important result of (10) is that the viscous pressure correction within the boundary layer is $O(R^{-1})$ for an arbitrary axisymmetric flow at a high Reynolds number. If we denote the boundary layer thickness by δ, then in the boundary layer $f_{n,k}(r) = O(\delta)$ (because $u_{pr}(1) = 0$), and $\{r^{-n}g_{n,l}(r) - r^{-n-l}g_{n,l}(1)\} = O(\delta)$ (because the L.H.S.=0 at $r = 1$). Since we also have $T_n(r,t) = O(1)$ in the boundary layer (because $T_n(1,t) = O(1)$) and $T_n(r,t) \simeq 0$ outside the boundary layer, the integral contributions in (10) are $O(\delta^2)$. Also we know that $\delta = O(R^{-1/2})$ at a high Reynolds number from the boundary layer theory. Therefore, $p_v(1,\theta,t) = O(R^{-1})$; i.e., p_v contributes to the drag on the bubble to the same order as the viscous stresses. This is consistent with the result of the boundary layer analysis of Moore.[4]

Returning to the problem of a bubble in a streaming flow, we have the base irrotational flow solution as

$$u_{pr} = \cos\theta(1 - \frac{1}{r^3}) \equiv F(r)\cos\theta, \tag{11a}$$

$$u_{p\theta} = -\sin\theta(1 + \frac{1}{2r^3}) \equiv -G(r)\sin\theta. \tag{11b}$$

Thus,

$$\sum_{n=0}^{\infty}\Big((u_{pr}P_n - \int_0^{\theta} P_n\frac{\partial u_{pr}}{\partial\theta}d\theta)T_n\Big)$$
$$= \sum_{n=0}^{\infty}\Big[\Big\{\frac{n+2}{2n+3}F(r)\Big\}T_{n+1} + \Big\{\frac{n-1}{2n-1}F(r)\Big\}T_{n-1}\Big]P_n, \tag{12}$$

and

$$\sum_{n=0}^{\infty}\Big(\frac{T_n}{r}u_{p\theta}\frac{dP_n}{d\theta}\Big)$$
$$= \sum_{n=0}^{\infty}\Big[\Big\{\frac{(n+1)(n+2)}{2n+3}\frac{G(r)}{r}\Big\}T_{n+1} - \Big\{\frac{n(n-1)}{2n-1}\frac{G(r)}{r}\Big\}T_{n-1}\Big]P_n. \tag{13}$$

Hence, substituting (12) and (13) into the general formula (10), we obtain

$$p_v(1,\theta) = \sum_{n=0}^{\infty}\Big[\int_1^{\infty} r^{-n-1}\{\frac{n(n+2)}{2n+3}F(r) + \frac{(n+1)(n+2)}{2n+3}(G(r)-G(1))\}T_{n+1}(r)dr$$
$$+ \int_1^{\infty} r^{-n-1}\frac{n(n-1)}{2n-1}\{F(r)-G(r)+r^2G(1)\}T_{n-1}(r)dr$$
$$+ n(\frac{2}{R})T_n(1)\Big]P_n(\cos\theta). \tag{14}$$

Rewriting (14) in order to take advantage of the fact that only the $P_1(\cos\theta)$ mode makes a contribution to the drag, we have

$$p_v(1,\theta) = \Big[\frac{3}{5}\int_1^{\infty} r^{-2}\{F(r)+2(G(r)-G(1))\}T_2(r)dr$$
$$+ \frac{2}{R}T_1(1)\Big]P_1(\cos\theta) + \sum_{n\neq 1} C_nP_n(\cos\theta), \tag{15}$$

where, C_n's are constants that can be evaluated if we know $T_n(r)$'s for $r > 1$. Furthermore, referring to the definitions of $F(r)$ and $G(r)$ in (11), we see

$$F(r) + 2\big(G(r) - G(1)\big) \equiv 0. \tag{16}$$

The fact that the integrand in (15) vanishes for all r means that the viscous drag is completely independent of the vorticity distribution in the region outside the bubble up to $O(R^{-1})$, although the vorticity distribution and viscous pressure corrections are both complicated functions of r and θ. This fact is perfectly consistent with the fact that the irrotational flow provides a correct leading order estimate of the dissipation; i.e., in the dissipation method, the vorticity in the region outside the bubble is totally neglected.

The vorticity value at the bubble surface is obtained as

$$\omega(1,\theta) = -\sum_{n=0}^{\infty}\frac{T_n(r)}{r}\frac{dP_n}{d\theta}|_{r=1} = 2\big(\frac{u_{p\theta}}{r} - \frac{1}{r}\frac{\partial u_{pr}}{\partial\theta}\big)|_{r=1} + o(1)$$
$$= -3\sin\theta + o(1). \tag{17}$$

In deriving (17), we applied the vanishing tangential stress condition at the bubble surface (Eq. (2b)) and used the fact that the velocity perturbation is

negligible up to $O(1)$. From (17), we obtain

$$T_1(1) = -3. \tag{18}$$

Therefore, we have

$$p_v(1,\theta) = -\frac{6}{R}P_1(\cos\theta) + \sum_{n\neq 1} C_n P_n(\cos\theta) + o(\frac{1}{R}). \tag{19}$$

By substituting (7) and (19) into (6), we obtain the total normal stress distribution on the bubble surface.

$$\tau_{rr}(1,\theta) = \frac{18}{R}P_1(\cos\theta) + \sum_{n\neq 1} \tilde{C}_n P_n(\cos\theta) + o(\frac{1}{R}) \tag{20}$$

Hence, substituting (20) into (4), we obtain Levich's well-known result for the drag coefficient on a spherical bubble in a uniform streaming flow

$$C_D = \frac{48}{R} + o(\frac{1}{R}), \tag{21}$$

which was previously obtained only via macroscopic mechanical energy (dissipation) and momentum balances.

V. COMPARISON WITH NUMERICAL ANALYSIS RESULTS

The analytic results obtained in previous sections are compared with results obtained by numerical analysis in Figs. 1 and 2. For the numerical analysis, a simplified version of Ryskin and Leal's[9] algorithm was used to solve the full steady Navier-Stokes equation for a spherical bubble. The profiles of $\frac{\partial u_r}{\partial r}\,|_{r=1}$ for various Reynolds numbers are given in Fig. 1, where $\tilde{\theta}$ is the angle measured from the front stagnation point; i.e., $\tilde{\theta} = \pi - \theta$. Since $\frac{\partial u_r}{\partial r}\,|_{r=1} \to \frac{\partial u_{pr}}{\partial r}\,|_{r=1}$ uniformly as $R \to \infty$, the validity of the approximation in (6), $\frac{\partial u_r}{\partial r}\,|_{r=1} = \frac{\partial u_{pr}}{\partial r}\,|_{r=1} + o(1)$, is verified numerically.

In Fig. 2, the viscous pressure corrections, $p_v = p - p_p$, are plotted against $\tilde{\theta}$. When $\tilde{\theta} \leq 0.6\pi$, the viscous pressure correction is an increasing function

of $\tilde{\theta}$ as Moore's[4] solution predicts. However, at the backside of the bubble ($0.6\pi \leq \tilde{\theta} \leq \pi$), the viscous pressure correction decreases very rapidly. Moore's solution, which was obtained from the boundary layer analysis, does not predict this pressure decrease at the backside of the bubble. As discussed earlier, however, Moore's result is incomplete because it does not include displacement thickness effects; it assumes that $p_v(r, \tilde{\theta})$ tends to zero at the outer edge of the boundary layer. This may account for the poor agreement between Moore's result and the numerical results. Since the viscous drag is due only to the $P_1(\cos\tilde{\theta})$ components of the normal stress, the $P_1(\cos\tilde{\theta})$ components obtained numerically are also compared with the theoretical prediction of the present work. In Fig. 2, we must note that the $P_1(\cos\tilde{\theta})$ component obtained numerically approaches the theoretical prediction as the Reynolds number increases, even though the distribution of p_v changes considerably. This fact can be explained as follows. Since the convective contribution increases with respect to the diffusive contribution as the Reynolds number increases, the vorticity distribution in the region outside the bubble also should change. However, the vorticity distribution right on the bubble surface remains unchanged up to $O(1)$ (see Eq. (17)). As we can see in (15) and (16) (note that $\tilde{\theta} = \pi - \theta$), $p_v(1, \tilde{\theta})$ itself is a function of the vorticity distribution in the region outside the bubble, but the $P_1(\cos\tilde{\theta})$ contribution up to $O(R^{-1})$ depends only on the vorticity distribution right on the bubble surface. Therefore, the $P_1(\cos\tilde{\theta})$ component of $R \cdot p_v$ should remain unchanged up to $O(1)$.

VI. CONCLUSION

1. The drag coefficient $C_D = 48/R$, which was obtained by the dissipation method by Levich,[1] was rederived via direct integration of the total normal stress over the bubble surface.

2. Examination of the normal stress distribution on the bubble surface shows that the drag coefficient to $O(R^{-1})$ is independent of the vorticity distri-

bution in the region outside the bubble. In particular, the vorticity distribution in the region outside the bubble does not contribute at all to the $P_1(\cos\theta)$ mode pressure distribution up to $O(R^{-1})$. This fact is perfectly consistent with the result obtained earlier by the dissipation method, in which the vorticity in the region outside the bubble is neglected for calculation of the drag coefficient to $O(R^{-1})$.

3. The reason why the simple result $C_D = 48/R$ is obtained even with the complicated functional dependence of the normal stress on θ, which has not been understood by the dissipation method, is clearly explained by showing that $P_1(\cos\theta)$ contribution to the pressure distribution at $O(R^{-1})$ depends only on the $O(1)$ vorticity distribution right on the bubble surface. The $O(1)$ vorticity distribution on the bubble surface is readily obtained from the irrotational flow solution and it has a simple functional dependence on θ.

ACKNOWLEDGMENTS

The authors wish to thank Professors A. Acrivos and D.W. Moore for their interest and valuable comments on the earlier version of this paper.

This work was supported by a grant from the Fluid Mechanics Program of the National Science Foundation.

REFERENCES

[1] V. Levich, Zh. Eksp. Theoret. Fiz. **19**, 18 (1949).

[2] J. Ackeret, Z. angew. Math. Phys. **3**, 259 (1952).

[3] D.W. Moore, J. Fluid Mech. **6**, 113 (1959).

[4] D.W. Moore, J. Fluid Mech. **16**, 161 (1963).

[5] L.D. Landau and E.M. Lifshitz, *Fluid Mechanics* (Pergamon, London, 1961).

[6] I.S. Kang and L.G. Leal, submitted to J. Fluid Mech.

[7] S. Chandasekhar, *Hydrodynamic and Hydromagnetic Stability* (Dover, New York, 1961).

[8] A. Prosperetti, Quart. Appl. Math. **34**, 339 (1977).

[9] G. Ryskin and L.G. Leal, J. Fluid Mech. **148**, 1 (1984).

FIGURE CAPTIONS

FIG. 1. The distribution of $\frac{\partial u_r}{\partial r}$ at the bubble surface (- - - - - - numerical results; ———— potential flow solution).

FIG. 2. The distribution of viscous pressure corrections and their $P_1(\cos\tilde{\theta})$ components (- - - - - numerical results for the viscous pressure correction; ———— Moore's viscous pressure correction; - - - - - - numerical results for the $P_1(\cos\tilde{\theta})$ component; ———— $P_1(\cos\tilde{\theta})$ component of the present work).

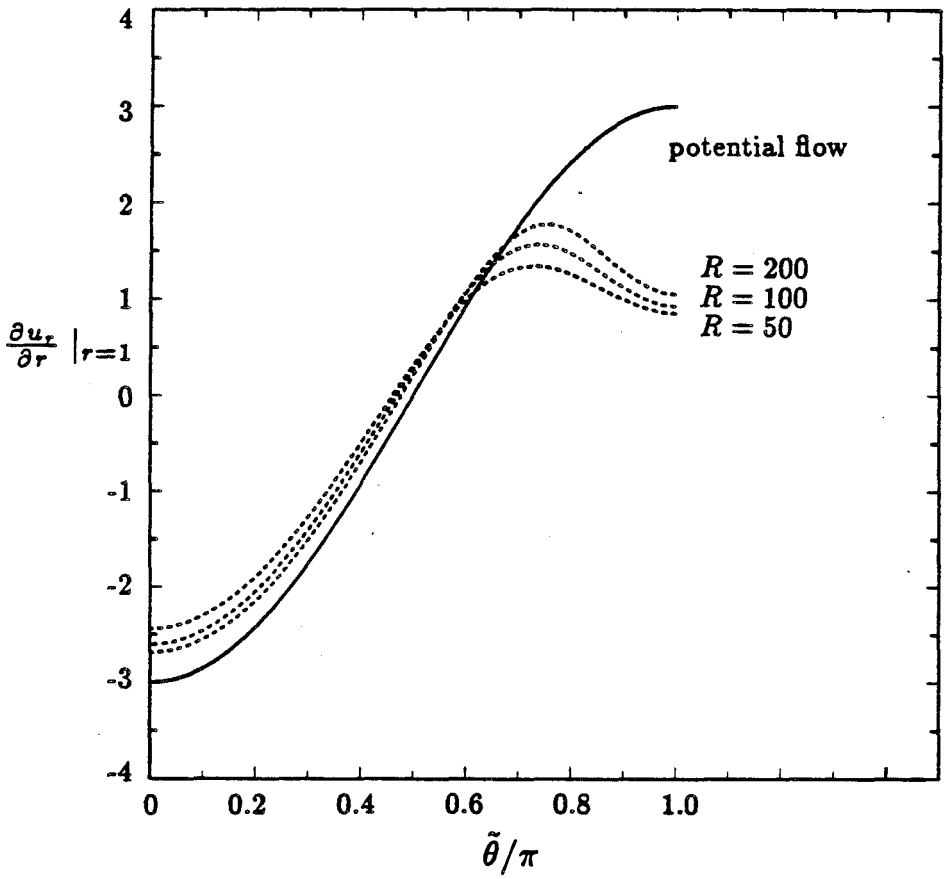
4
3
2
1
0
-1
-2
-3
-4
0
0.2
0.4
0.6
0.8
1.0
$\frac{\partial u_r}{\partial r}\,|_{r=1}$
$\tilde{\theta}/\pi$
potential flow
$R = 200$
$R = 100$
$R = 50$

Figure 1

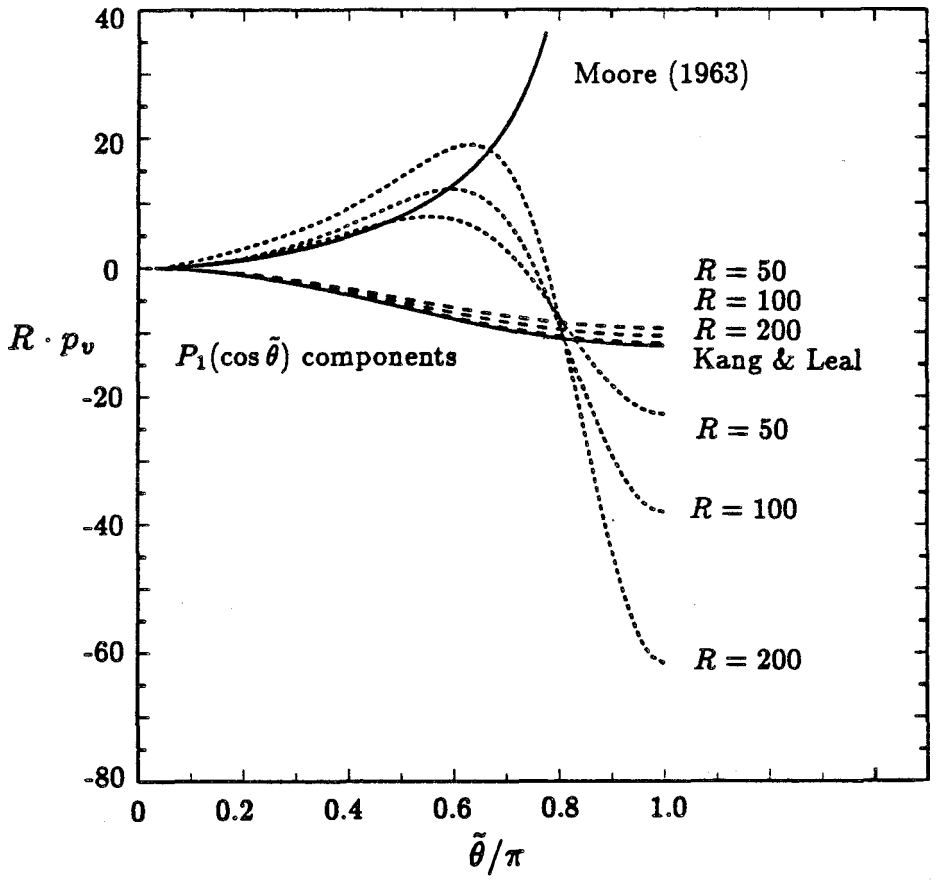
40
20
0
-20
-40
-60
-80
0
0.2
0.4
0.6
0.8
1.0
$\tilde{\theta}/\pi$
$R \cdot p_v$
Moore (1963)
$R = 50$
$R = 100$
$R = 200$
Kang & Leal
$P_1(\cos\tilde{\theta})$ components
$R = 50$
$R = 100$
$R = 200$

Figure 2

Appendix

Low Reynolds number Voidage Bubble in a Fluidized Bed

Abstract

A voidage bubble in a fluidized bed is considered for the low Reynolds number limit. The problem has been formulated as a generalized drop problem with an additional parameter $W = u_s/U_b$, where u_s and U_b are the magnitudes of the slip and the bubble rise velocities. In the creeping flow limit, the steady and unsteady deformations are invariant to the change of W. A cloud formation is predicted also for the creeping flow limit, and the thickness of the cloud is larger than that for the potential flow limit at the same value of $\beta = W/(1-\alpha)$, where α is the volume fraction of solid in the mixture phase. When the inertial effect is considered, the effect of W on the deformation first appears. The deformation is either faster or slower than the case of $W = 0$, depending on the values of κ and γ, where they are the ratios of viscosity and density of the pure fluid inside the bubble to those of the mixture phase outside the bubble.

I. Introduction

One of the most important but least understood problems in chemical engineering is the problem of a voidage bubble in a fluidized bed. Voidage bubble formation is common in gas-fluidized beds and may also occur in a liquid-fluidized bed when the ratio of the particle to the liquid density is large. Rising voidage bubbles in a fluidized bed have significant effects on the fluid mixing patterns and the heat and mass transfer; consequently, a clear understanding of this problem is essential to the practical applications such as development or improvement of the fluidized beds. Furthermore, a voidage bubble problem can provide an excellent model problem in studying the multiphase flows; for example, we can verify the validity of a proposed constitutive equation by comparing the theoretical predictions of the bubble behaviors and those observed in the experiments.

Above all, the remarkable similarity between the shapes of the voidage bubble in a fluidized bed and the gas bubble in a pure liquid has attracted attention of many researchers. The endeavor on development of theories on a fluidized bed bubble was initially focused on solving model equations with the assumption of the fixed shapes to predict a correct qualitative description of fundamental bubble properties.

The first model of a bubble in an extended uniform fluidized bed was suggested by Davidson (1963), who considered simultaneously the irrotational flow of a continuum representing the particulate phase around the bubble, and the filtration of the interstitial fluid within a porous body of moving particles (so-called *two-interpenetrating-phase model*). Jackson (1963) included a mass acceleration term in the equation for the particle motion and he further allowed for local variation of voidage in the viscinity of the bubble. Another model of the steady motion of a single bubble was given by Murray (1965), who used a modified Oseen technique. He pointed out that only three of his four equations (two continuity equations and two equations of motion) were independent. Later,

Buyevich (1975) noted that this result came from the assumption of uniform voidage in the suspension.

Models of same general type were developed in such a way as to include non-stationary effects accompanying initial motion of bubbles (Murray 1967; Collins 1971), the interaction with other bubbles and interaction with the walls of a container (Collins 1971; Clift et al. 1972). An interesting model that allows bubble growth or shrinkage during the rise of bubbles was also considered by Buyevich (1975), with spherical and spherical-cap bubbles considered as limiting cases. Finally, Collins (1982) analyzed the cloud patterns around an expanding bubble.

In spite of the appreciable numbers of existing, theoretical studies of voidage bubble motion, it should be noted that there is still considerable uncertainty in the form of basic equations for two-phase flows. This is particularly true of the constitutive equations and boundary conditions where present studies normally resort to the simplest possible *ad hoc* assumptions. Nevertheless, comparison of the theoretical model predictions with experimental data in the case of voidage bubble motion shows that theories yield a correct qualitative description of many fundamental bubble properties. There are, nonetheless, systematic differences between the theoretical conclusions and the observed phenomena. Moreover, there exists an inherent defect characteristic of all of the above theories, which lies in presuming the bubble shape to be given *a priori*, whereas it ought to be found as a part of a solution.

The first paper in this direction was published by Batchelor (1974), who assumed that the part of the fluidized bed containing particles is statistically homogeneous in composition and behaves like a Newtonian fluid whose density and viscosity are different from those of the pure fluid inside the bubble (so-called *one-mixture-phase model* ; in this model the motion of particle phase with respect to the average velocity of the mixture phase is described in terms of slip velocity). He then analyzed the bubble deformation in the creeping flow regime

by solving Stokes equation with the *ad hoc* boundary conditions of velocity continuity, stress continuity and a kinematic condition at the bubble surface. Although his solution is not of direct practical value because of the creeping flow approximation, Batchelor clearly showed the way to treat this intriguing kind of two-phase flow system (he showed that the spherical shape is the steady-state solution in the creeping flow regime).

As we can see above, previous investigations have been mostly confined to either irrotational flow or creeping flow of Newtonian fluid around a given shape *a priori* (although Batchelor considered the problem as a free-boundary problem, the trivial spherical shape is the solution for his problem). Therefore, in the present paper, we attempt to extend Batchelor's analysis via formulating the problem as a full, free-boundary problem and analyzing it for steady and unsteady deformation at a low Reynolds number. Although the current analysis is limited to the low Reynolds number problem due to the analytical solution method adopted here, the same kind of formulation can be easily extended to the finite Reynolds number problem and it can be analyzed via numerical analysis.

II. Problem Formulation

1. Governing Equations and Boundary Conditions

The first step in studying the suspension flow is to determine the equations that govern the flow. These equations are written in terms of the average density $\rho = \alpha\rho_p + (1-\alpha)\rho_f$, the volume-averaged velocity $\mathbf{u} = \alpha\mathbf{u}_p + (1-\alpha)\mathbf{u}_f$, and the slip velocity $\mathbf{u}_s = \mathbf{u}_p - \mathbf{u}$, where ρ_p and ρ_f are the particle and fluid densities, $\mathbf{u}_p$ and $\mathbf{u}_f$ are the local average particle and fluid velocities, and α is the volume fraction of solids. If we assume that the suspension can be modeled as a Newtonian fluid with an effective viscosity depending on the local concentration, the governing equations are:

continuity:

$$\nabla \cdot \mathbf{u} = 0, \tag{1}$$

particle continuity:

$$\frac{D_p \alpha}{Dt} = -\alpha \nabla \cdot \mathbf{u}_s, \tag{2}$$

where $\frac{D_p}{Dt}$ is the convective time derivative moving with the particle velocity.

momentum:

$$\begin{aligned}
&\rho_p \alpha \frac{D_p \mathbf{u}_p}{Dt} + \rho_f (1-\alpha) \frac{D_f \mathbf{u}_f}{Dt} \\
&= \rho \frac{D\mathbf{u}}{Dt} + (\rho_p - \rho_f)\left[\frac{D\mathbf{u}_s}{Dt} + \mathbf{u}_s \cdot \nabla \mathbf{u}\right] + \frac{\rho_p \alpha(\alpha-1) - \rho_f \alpha^2}{\alpha - 1} \mathbf{u}_s \cdot \nabla \mathbf{u}_s \\
&\quad + \frac{\alpha}{1-\alpha} \rho_f \mathbf{u}_s (\nabla \cdot \mathbf{u}_s) + \frac{\rho_f \mathbf{u}_s}{(1-\alpha)^2} \mathbf{u}_s \cdot \nabla \alpha \\
&= -\nabla p + \nabla \cdot \mu(\alpha)(\mathbf{u} + \mathbf{u}^T) + \rho \mathbf{g},
\end{aligned} \tag{3}$$

where p is the local mean value of -1/3-times the trace of the stress tensor. The slip velocity is determined from the particle equation of motion

$$\rho_p V_p \frac{D_p \mathbf{u}_p}{Dt} = \sum \mathbf{F} = \mathbf{F}_D + (\rho_p - \rho_f) V_p \mathbf{g}, \tag{4}$$

where $\mathbf{F}_D$ is the drag force on the particle and V_p is the volume of the particle of interest. For low particle Reynolds numbers, we assume that the drag on a single particle is only concentration-dependent, which is equivalent to the drift flux formation:

$$\mathbf{F}_D = 6\pi\mu a(\mathbf{u}_p - \mathbf{u}_f) F(\alpha).$$

If the system Reynolds number is small ($Re << 1$), we can assume that the particle time scale is small with respect to fluid motion, so that the particles are essentially in equilibrium. Then Eq.(4) simplifies to

$$\mathbf{u}_s = \frac{(1-\alpha)}{F(\alpha)} u_o \mathbf{e}_g = \mathbf{u}_o f(\alpha) \mathbf{e}_g, \tag{5}$$

where u_o is the terminal velocity of a single particle in fluid, and $\mathbf{e}_g$ is the unit vector in the direction of gravity, and $f(\alpha) \to 1$ as $\alpha \to 0$.

Since uniform α can be a solution of (2), let us assume α is uniform and constant in the mixture phase. Then (3) can be simplified to the following simple form with (5) and uniformity of α,

$$\rho\Big(\frac{D\mathbf{u}}{Dt} + k\mathbf{u}_s \cdot \nabla\mathbf{u}\Big) = -\nabla p + \mu\nabla^2\mathbf{u} + \rho\mathbf{g}, \tag{6}$$

where

$$k = \frac{\alpha(\rho_p - \rho_f)}{\rho}.$$

Now, we have the complete governing equations for the mixture phase outside the voidage bubble (see Fig. 1)

$$\nabla \cdot \mathbf{u} = 0, \tag{1}$$

$$\rho\Big(\frac{D\mathbf{u}}{Dt} + k\mathbf{u}_s \cdot \nabla\mathbf{u}\Big) = -\nabla p + \mu\nabla^2\mathbf{u} + \rho\mathbf{g}, \tag{6}$$

$$\mathbf{u}_s = u_o f(\alpha)\mathbf{e}_g. \tag{5}$$

Inside the bubble, the Navier-Stokes equation for the pure fluid is used

$$\nabla \cdot \hat{\mathbf{u}} = 0, \tag{7}$$

$$\hat{\rho}\frac{D\hat{\mathbf{u}}}{Dt} = -\nabla\hat{p} + \hat{\mu}\nabla^2\hat{\mathbf{u}} + \hat{\rho}\mathbf{g}. \tag{8}$$

The matching conditions at the discontinuous surface are

1) velocity continuity

$$\mathbf{u} = \hat{\mathbf{u}}, \tag{9}$$

2) stress jump condition

$$\Big[\mathbf{n} \cdot \mathbf{T}\Big] = \Big[\mathbf{n} \cdot (1-\alpha)\rho_f(\mathbf{u}_f - \mathbf{u}_p^o)(\mathbf{u}_f - \mathbf{u}_p^o)\Big], \tag{10}$$

where $\mathbf{n}$ is the outward unit normal on the bubble surface and $\mathbf{u}_p^o$ denotes the velocity of solid phase at the boundary;

3) kinematic condition

$$\mathbf{n} \cdot (\mathbf{u}_p^o - \mathbf{U}_b) = -\frac{1}{|\nabla F|}\frac{\partial F}{\partial t}, \tag{11}$$

where $\mathbf{U}_b$ denotes the velocity of the center of the bubble with respect to the fixed frame. In (11) F is the function that describes the bubble shape by $F(\mathbf{x}-\mathbf{x}_o,t)=0$, where $\mathbf{x}_o(t)$ denotes the position vector of the center of mass.

2. Dimensionless equations with respect to the moving frame of reference

The dimensional equations shown above are non-dimensionalized with the following characteristic scales,

$$U_c = \| \mathbf{U}_b \|,$$

$$l_c = a,$$

$$p_c = \frac{\mu U_c}{a}.$$

Since the bubble rise velocity is often measured in experiments, $\| \mathbf{U}_b \|$ is chosen as the characteristic velocity scale. The governing equations for the domain outside the bubble become (for convenience, the same notations are used for the dimensionless variables and hereafter the dimensional variables will be denoted by the superscript $'$)

$$\nabla \cdot \mathbf{u} = 0, \tag{12a}$$

$$Re\Big(\frac{a}{U^2}\frac{\partial \mathbf{u}'}{\partial t} + \mathbf{u}\cdot\nabla\mathbf{u} + k\mathbf{u}_s\cdot\nabla\mathbf{u}\Big) = -\nabla p + \nabla^2\mathbf{u} - Re\frac{a}{U^2}\frac{d\mathbf{U}_b'}{dt'}, \tag{12b}$$

$$\mathbf{u}_s = We_g, \tag{12c}$$

where p is the dimensionless dynamic pressure. For the domain inside the bubble, we have

$$\nabla \cdot \hat{\mathbf{u}} = 0, \tag{13a}$$

$$\gamma Re\Big(\frac{a}{U^2}\frac{\partial \hat{\mathbf{u}}'}{\partial t} + \hat{\mathbf{u}}\cdot\nabla\hat{\mathbf{u}}\Big) = -\nabla\hat{p} + \kappa\nabla^2\hat{\mathbf{u}} - \gamma Re\frac{a}{U^2}\frac{d\mathbf{U}_b'}{dt'}. \tag{13b}$$

The dimensionless numbers in (12) and (13) are defined as

$$Re = \frac{\rho a U_c}{\mu}, \tag{14a}$$

$$k = \frac{\alpha(\rho_p - \rho_f)}{\rho}, \tag{14b}$$

$$\kappa = \hat{\mu}/\mu = \mu_f/\mu, \tag{14c}$$

$$\gamma = \hat{\rho}/\rho = \rho_f/\rho, \tag{14d}$$

$$W = \frac{u_s}{U_c} = \frac{u_o f(\alpha)}{U_c}. \tag{14e}$$

In (14), k and γ are not independent of each other, and we can easily show that they have the relationship such that

$$k + \gamma = 1. \tag{15}$$

The boundary conditions in dimensionless variables at the discontinuous interface are given as

$$u_n = \hat{u}_n, \tag{16a}$$

$$u_t = \hat{u}_t, \tag{16b}$$

$$N = \hat{N} + O(ReW^2), \tag{16c}$$

$$T = \hat{T} + O(ReW^2), \tag{16d}$$

$$\mathbf{u}_p^o \cdot \mathbf{n} = \frac{\frac{a}{U}\frac{\partial R'}{\partial t'}}{\sqrt{1 + \left(\frac{1}{R'}\frac{\partial R'}{\partial \theta}\right)^2}}, \tag{16e}$$

where N and T denote the normal and tangential stresses, respectively. In (16e) R' is the shape function of the bubble surface, which is given by the equation

$$F'(\mathbf{x}' - \mathbf{x}'_o, t') = r' - R'(\theta, t') = 0,$$

where $\mathbf{x}'_o$ is the position vector of the center of mass of the bubble. The kinematic condition (16e) can be rewritten as the following form by means of the relationship $\mathbf{u}_p = \mathbf{u} + \mathbf{u}_s = \mathbf{u} + W\mathbf{e}_g$

$$u_n = \hat{u}_n = -W\mathbf{e}_g \cdot \mathbf{n} + \frac{\frac{a}{U}\frac{\partial R'}{\partial t'}}{\sqrt{1 + \left(\frac{1}{R'}\frac{\partial R'}{\partial \theta}\right)^2}}. \tag{16e'}$$

Finally, the far field condition is given as

$$\mathbf{u} \to (1-W)\mathbf{e}_g \qquad \text{as} \qquad r \to \infty. \tag{17}$$

Now, let us introduce the following assumptions in order to get an asymptotic result by perturbation analysis.

i) The Reynolds number is small; i.e., $Re << 1$.

ii) The degree of deformation from the sphere is small; i.e. $\| \frac{R'}{a} - 1 \| \equiv \epsilon << 1$.

iii) $W << 1$.

Under these assumptions we can neglect the terms of $O(Re \cdot \epsilon)$ terms in governing equations, $O(W^2)$ terms in the stress balance, and the terms of $O(\epsilon^2)$ terms in the kinematic condition. Then, the simplified equations are

$$Re\Big(\mathbf{u} \cdot \nabla \mathbf{u} + k\mathbf{u}_s \cdot \nabla \mathbf{u}\Big) = -\nabla p + \nabla^2 \mathbf{u}, \tag{12b'}$$

$$\gamma Re\Big(\hat{\mathbf{u}} \cdot \nabla \hat{\mathbf{u}}\Big) = -\nabla \hat{p} + \kappa \nabla^2 \hat{\mathbf{u}}, \tag{13b'}$$

$$N = \hat{N}, \tag{16c'}$$

$$T = \hat{T}, \tag{16d'}$$

$$u_n = \hat{u}_n = -W\mathbf{e}_g \cdot \mathbf{n} + \frac{\partial R}{\partial t}. \tag{16e'}$$

We can simplify the equations further by introducing the following changes of variables

$$\mathbf{u}^* = \mathbf{u} + W\mathbf{e}_g, \tag{18a}$$

$$\hat{\mathbf{u}}^* = \hat{\mathbf{u}} + W\mathbf{e}_g. \tag{18b}$$

Then the governing equations for the small Reynolds number in terms of $\mathbf{u}^*$ and $\hat{\mathbf{u}}^*$ are given by

$$\nabla \cdot \mathbf{u}^* = 0, \tag{19a}$$

$$Re\Big[\{\mathbf{u}^* + (k-1)W\mathbf{e}_g\} \cdot \nabla \mathbf{u}^*\Big] = -\nabla p^* + \nabla^2 \mathbf{u}^*, \tag{19b}$$

$$\nabla \cdot \hat{\mathbf{u}}^* = 0, \tag{19c}$$

$$\gamma Re\Big[\{\hat{\mathbf{u}}^* - W\mathbf{e}_g\}\cdot\nabla\hat{\mathbf{u}}^*\Big] = -\nabla\hat{p}^* + \kappa\nabla^2\hat{\mathbf{u}}^*. \tag{19d}$$

Also, the boundary conditions are given by

$$u_n^* = \hat{u}_n^*, \tag{20a}$$

$$u_t^* = \hat{u}_t^*, \tag{20b}$$

$$N^* = \hat{N}^*, \tag{20c}$$

$$T^* = \hat{T}^*, \tag{20d}$$

$$u_n^* = \hat{u}_n^* = \frac{\partial R}{\partial t}, \tag{20e}$$

and the far-field condition is given as

$$\mathbf{u}^* \to \mathbf{e}_g \qquad \text{as} \qquad r \to \infty. \tag{20f}$$

From (19)-(20), we can draw several conclusions without solving the problem explicitly. First, we can see the equations and boundary conditions of (19)-(20) degenerate to the conventional drop problem for $Re = 0$; thus, the steady-state shape and the unsteady deformation of shape for creeping flow ($Re = 0$) are exactly the same as those for the conventional drop problem. Therefore, for the creeping flow limit, we do not need any separate analysis. Second, if $Re \neq 0$, the steady or unsteady deformation will be different from those of the conventional drop problem unless $W = 0$ or $k = 1$ (i.e., $\gamma = 0$).

To solve the problem, we introduce the stream functions ψ^* and $\hat{\psi}^*$, which satisfy the relationships

$$u_r^* = -\frac{1}{r^2}\frac{\partial\psi^*}{\partial\eta}, \qquad u_\theta^*\sqrt{1-\eta^2} = -\frac{1}{r}\frac{\partial\psi^*}{\partial r}, \tag{21}$$

where $\eta = \cos\theta$, and θ is the angle measured from the rear stagnation point. Then the governing equations in terms of ψ^* and $\hat{\psi}^*$ are given as

$$\begin{aligned} E^4\psi^* = Re\Big[&\frac{1}{r^2}\frac{\partial(\psi^*, E^2\psi^*)}{\partial(r,\eta)} + \frac{2}{r^2}(E^2\psi^*)\Big\{\frac{\eta}{1-\eta}\frac{\partial\psi^*}{\partial r} + \frac{1}{r}\frac{\partial\psi^*}{\partial\eta}\Big\} \\ &+ \frac{1}{r^2}\frac{\partial(\psi', E^2\psi^*)}{\partial(r,\eta)} + \frac{2}{r^2}(E^2\psi^*)\Big\{\frac{\eta}{1-\eta}\frac{\partial\psi'}{\partial r} + \frac{1}{r}\frac{\partial\psi'}{\partial\eta}\Big\}\Big], \end{aligned} \tag{22a}$$

$$\kappa E^4\hat{\psi}^* = \gamma Re\Big[\frac{1}{r^2}\frac{\partial(\hat{\psi}^*, E^2\hat{\psi}^*)}{\partial(r,\eta)} + \frac{2}{r^2}(E^2\hat{\psi}^*)\Big\{\frac{\eta}{1-\eta}\frac{\partial\hat{\psi}^*}{\partial r} + \frac{1}{r}\frac{\partial\hat{\psi}^*}{\partial\eta}\Big\}$$
$$+ \frac{1}{r^2}\frac{\partial(\hat{\psi}', E^2\hat{\psi}^*)}{\partial(r,\eta)} + \frac{2}{r^2}(E^2\hat{\psi}^*)\Big\{\frac{\eta}{1-\eta}\frac{\partial\hat{\psi}'}{\partial r} + \frac{1}{r}\frac{\partial\hat{\psi}'}{\partial\eta}\Big\}\Big], \qquad (22b)$$

where

$$E^2 = \frac{\partial^2}{\partial r^2} + \frac{1-\eta^2}{r^2}\frac{\partial^2}{\partial\eta^2}$$

with

$$\psi' = (1-k)WQ_1(\eta)r^2$$

and

$$\hat{\psi}' = WQ_1(\eta)r^2.$$

In (22), $Q_n(\eta)$ is the Gegenbauer polynomial, which is defined as

$$Q_n(\eta) = \int_{-1}^{\eta} P_n(\xi)d\xi. \qquad (23)$$

In the following sections, we discuss the creeping flow solution and the small inertial effect on the deformation.

III. Creeping Flow Solution ($Re = 0$)

The steady-state solution for the conventional drop problem in the creeping flow limit is the well-known *Hadamard–Rybczynski* solution. For the unsteady problem, the small deformation from the spherical shape was analyzed by Kojima et al. (1984). Since we have shown the governing equations and the boundary conditions in terms of the changed variables $\mathbf{u}^*$ and $\hat{\mathbf{u}}^*$ are exactly the same as the conventional drop problem in this limit, we can utilize the results obtained by previous workers.

1. Steady-state solution

The well-known Hadamard-Rybczynski solution in terms of the modified variables is given by

$$R_0 = 1, \qquad (24a)$$

$$\psi_0^* = -Q_1(\eta)\Big[r^2 - \frac{3\kappa+2}{2(\kappa+1)}r + \frac{\kappa}{2(\kappa+1)}\frac{1}{r}\Big], \tag{24b}$$

and

$$\hat{\psi}^* = Q_1(\eta)\frac{(r^2-r^4)}{2(\kappa+1)}. \tag{24c}$$

Then the solution in terms of original variables is easily recovered by the relationship (18), which is expressed in terms of stream functions as following:

$$\psi = \psi^* + WQ_1(\eta)r^2, \tag{25a}$$

$$\hat{\psi} = \hat{\psi}^* + WQ_1(\eta)r^2. \tag{25b}$$

Therefore,

$$R_0 = 1, \tag{26a}$$

$$\psi_0 = -Q_1(\eta)\Big[(1-W)r^2 - \frac{3\kappa+2}{2(\kappa+1)}r + \frac{\kappa}{2(\kappa+1)}\frac{1}{r}\Big], \tag{26b}$$

and

$$\hat{\psi} = Q_1(\eta)\Big[\Big(\frac{1}{2(\kappa+1)} + W\Big)r^2 - \frac{r^4}{2(\kappa+1)}\Big]. \tag{26c}$$

This zero-th order solution was first obtained by Batchelor (1974) by means of the general solution for the creeping flow.

Now, it is instructive to examine the special cases of (26).

(i) $W = 0$: The solution (26) reduces to the well-known Hadamard-Rybczynski solution.

(ii) $\kappa \to 0$:

This case cooresponds to the gas-fluidized bed. In this case (26b) reduces to the simple form

$$\psi_0 = -Q_1(\eta)\Big[(1-W)r^2 - r\Big]. \tag{27}$$

The particle-phase and gas-phase stream functions corresponding to (27) are

$$\psi_0^p = -Q_1(\eta)\Big[r^2 - r\Big], \tag{28a}$$

$$\psi_0^g = -Q_1(\eta)\Big[(1-\beta)r^2 - r\Big], \tag{28b}$$

where $\beta = \frac{W}{1-\alpha}$.

The important feature of the solution (28b) is that it predicts the cloud formation for $U_b' > u_{g\infty}'$, which has been observed experimentally and predicted by Davidson's potential flow solution, but predicts no cloud formation for $U_b' < u_{g\infty}'$. The ratio β in (28) has a special physical interpretation. Since the solid phase has zero velocity at the points far from the bubble, the slip velocity is given as

$$u_s' = (1-\alpha)u_{g\infty}', \tag{29}$$

where u_s' and $u_{g\infty}'$ are the magnitude of the dimensional slip velocity and the gas phase velocity. By dividing both sides by the bubble rise velocity, and from the definition of W, (14e), we have

$$\beta = \frac{W}{1-\alpha} = \frac{u_{g\infty}'}{U_b'}.$$

Therefore, β is the ration of average gas phase velocity to the bubble rise velocity. The radius of the cloud for $\beta < 1$ is obtained from (28b) as

$$r_c = \frac{1}{1-\beta} = 1 + \beta + \beta^2 + O(\beta^3). \tag{30}$$

Davidson's potential flow solution (1963) predicts the radius of cloud as

$$r_c = \left(\frac{1+2\beta}{1-\beta}\right)^{1/3} = 1 + \beta + O(\beta^3). \tag{31}$$

In Fig. 2, the cloud thicknesses in both limits are compared as functions of the parameter β. As we can see in Fig. 2, a thicker cloud is predicted in the creeping flow than in the potential flow limit for the same value of β.

2. Time-dependent kinematics (unsteady deformation)

As discussed above, the unsteady deformation of a voidage bubble in a fluidized bed is exactly the same as the result of the corresponding conventional drop problem. The unsteady-deformation of a drop in a creeping streaming flow

was solved by Kojima et al. (1984) via perturbation analysis for the cases of small deformation from spherical shape. Here, therefore, we simply mention the key results of Kojima et al. The shape of a slightly deformed drop can be described in terms of the Legendre polynomial

$$R(\theta,t) = 1 + \epsilon \sum_{n=2}^{\infty} (2n+1) f_n P_n(\cos\theta) + O(\epsilon^2), \tag{32}$$

where ϵ is the measure of deformation and P_n is the Legendre polynomial of order n. The absence of terms P_0 and P_1 in Eq. (32) ensures that volume is conserved and that the origin remains at the center of mass of the drop.

For the small deformation, Kojima et al. derived the following dynamic equation for f_n of (32):

$$G_n \frac{df_n}{dt} = -H_n f_{n+1} + L_n f_{n-1}, \qquad n \geq 2, \tag{33}$$

where

$$\begin{aligned}
G_n =& \frac{2(\kappa+1)(2n+1)}{n(n+1)} \Big[(4n^4 + 8n^3 + 2n^2 - 8n - 6)\kappa^2 \\
&+ (8n^4 + 16n^3 + 4n^2 - 4n + 3)\kappa \\
&+ (4n^4 + 8n^3 + 2n^2 + 4n) \Big], \\
H_n =& (4n^4 + 8n^3 + 14n^2 + 10n + 9)\kappa^2 \\
&+ (8n^4 + 16n^3 + 34n^2 - 40n - 27)\kappa \\
&+ (4n^4 + 8n^3 + 20n^2 + 22n + 18), \\
L_n =& 2(\kappa+1)(n+2)(n-2)[(2n^2 + 4n + 3)\kappa \\
&+ (2n^2 + 4n)],
\end{aligned}$$

with $\kappa \equiv \hat{\mu}/\mu$.

The characteristics of the system of Eq. (33) are fully discussed by Kojima et al., so here we briefly follow their asymptotic result for $n \to \infty$. As $n \to \infty$, (32) becomes

$$\frac{df_n}{dt} = \frac{1}{2(\kappa+1)} \frac{n(n+1)}{(2n+1)} [f_{n-1} - f_{n+1} + O(n^{-2})]. \tag{34}$$

Let $f \sim \sum_{n=1}^{\infty}(2n+1)f_n P_n(\cos\theta)$ which, according to Eq. (34), satisfies

$$\frac{\partial f}{\partial t} - \frac{1}{2(\kappa+1)}\sin\theta\frac{\partial f}{\partial \theta} = \frac{\cos\theta}{\kappa+1}f, \tag{35}$$

if the $O(n^{-2})$ terms are omitted. From (35), f is given by

$$f(t) = f(0)\Big(\frac{1+\cot^2\theta(t)/2}{1+\cot^2\theta(0)/2}\Big)^2 \exp(\frac{-t}{\kappa+1}) \tag{36a}$$

along the characteristics

$$[\cot\theta(0)/2]\exp(t/2(\kappa+1)) = \cot\theta(t)/2. \tag{36b}$$

Asymptotic form of (35) as $t \to \infty$ is given by the following simple results. If we let $\theta(0) \to 0$, we obtain

$$f(t) \to f(0)\exp(t/(\kappa+1)),$$

whereas in the opposite limiting case, $\theta(0) \to \pi$,

$$f(t) \to f(0)\exp(-t/(\kappa+1)).$$

From the asymptoic result, we can see that the front stagnation point is stable, whereas the rear stagnation point is unstable (see the details in Kojima et al.).

IV. Inertial Effects

We turn our attention to the deformation of a spherical voidage bubble in the presence of small inertia. As we have seen in previous sections, the presence of inertia can produce different solution features from those for the conventional drop problem. Here we confine ourselves to the unsteady deformation of a voidage bubble due to the inertia starting from the spherical shape. As Kojima et al. showed for the conventional drop problem, the time-dependent kinematics of a nearly spherical voidage bubble in the presence of small inertia can be analyzed with very few modifications to the creeping flow solution. In this case

we have the small parameter $\epsilon = Re$ and assume that the measure of deformation is also $O(\epsilon)$; then the boundary conditions for normal velocity can be expanded as

$$u_n = u_{r0} + \epsilon(u_{r1} + u_{\theta 0} f' \sin\theta + f\frac{\partial u_{r0}}{\partial r}) + O(\epsilon^2)$$
$$= \hat{u}_{r0} + \epsilon(\hat{u}_{r1} + \hat{u}_{\theta 0} f' \sin\theta + f\frac{\partial \hat{u}_{r0}}{\partial r}) + O(\epsilon^2) = \hat{u}_n,$$

where the subscripts 0, 1, $\cdots$ denote the degree of deformation, and u_{r0} can be again expanded as

$$u_{r0} = u_{r0}^0 + \epsilon u_{r0}^1 + \cdots,$$

where supersripts 0, 1, $\cdots$ denote the order of Reynolds number. Also, u_{r1} can be expanded as

$$u_{r1} = u_{r1}^0 + \epsilon u_{r1}^1 + \cdots$$

Therefore, continuity of the normal component of the velocity can be expressed as

$$u_{r0}^0 = \hat{u}_{r0}^0 \qquad \text{for} \quad O(1),$$

$$u_{r0}^1 + u_{r1}^0 + u_{\theta 0}^0 f' \sin\theta + f\frac{\partial u_{r0}^0}{\partial r} = \hat{u}_{r0}^1 + \hat{u}_{r1}^0 + \hat{u}_{\theta 0}^0 f' \sin\theta + f\frac{\partial \hat{u}_{r0}^0}{\partial r}$$

$$\text{for} \quad O(\epsilon).$$

Now, since we have $u_{r0}^1 = \hat{u}_{r0}^1$ for the spherical bubble, the normal velocity condition is exactly the same as the condition for the creeping flow problem up to $O(\epsilon)$. In the same manner, we can also show that the same argument is true for the tangential velocity condition and the tangential stress condition. However, this is not the case for the normal stress condition because $\tau_{rr0}^1 \neq \hat{\tau}_{rr0}^1$; i.e., a spherical shape does not satisfy the normal stress condition for a non-zero Reynolds number. Let us discuss the normal stress condition in detail. The nomal stress condition can be expanded as follows:

$$N = N_0^0 + \epsilon(N_0^1 + N_1^0) + O(\epsilon^2) = \hat{N}_0^0 + \epsilon(\hat{N}_0^1 + \hat{N}_1^0) + O(\epsilon^2) = \hat{N}.$$

Since $N_0^0 = \hat{N}_0^0$ (the spherical shape satisfies the normal stress condition in the creeping flow limit), we have

$$N_1^0 - \hat{N}_1^0 = -(N_0^1 - \hat{N}_0^1) = -(\tau_{rr0}^1 - \hat{\tau}_{rr0}^1). \tag{37}$$

Therefore, inclusion of the inertia effect up to $O(Re)$ (or $O(\epsilon)$) simply results in the modification of the normal stress balance, otherwise exactly the same as the creeping flow problem. Now, let us calculate the normal stress imbalance for a spherical voidage bubble at a non-zero Reynolds number to supply the inhomogeneous term in the normal stress condition (Eq. (37)).

1. Normal stress imbalance for a spherical voidage bubble at small Reynolds number

As we can see in (22), the governing equations for the voidage bubble have extra forcing terms compared with those for the conventional drop problem. The extra terms do not cause any significant difficulties in analysis, and the normal stress imbalance for a spherical voidage at a non-zero Reynolds number can be easily derived by following the analysis for the conventional drop problem by Taylor and Acrivos (1964). Here we give only the final result

$$N_0^1 - \hat{N}_0^1 = \Big[-U(\kappa;\gamma) + \gamma V(\kappa) W + O(W^2)\Big] P_2(\cos\theta), \tag{37}$$

where

$$U(\kappa;\gamma) = -(N_0^1 - \hat{N}_0^1)\,|_{W=0}\,/P_2(\cos\theta) = \frac{(3\kappa+2)(27\kappa^2+58\kappa+30)}{80(\kappa+1)^3} + \frac{1-\gamma}{12(\kappa+1)^2},$$

and

$$V(\kappa) = \frac{19\kappa^3 + 36\kappa^2 + 16\kappa - 1}{10(\kappa+1)^3}.$$

In (37), it should be noted that the characteristic scale for pressure in this analysis is chosen as

$$p_c = \frac{\mu U_c}{a}.$$

The function $V(\kappa)$ is shown in Fig. 3. Since the imbalance at $\theta = 0$ (rear stagnation point) of the conventional drop is $-U(\kappa;\gamma)$ and the function $-U$ is negative for $\gamma < 1$ (rising drop), we can see that if $\kappa < 0.0554$, then the imbalance gets bigger and if $\kappa > 0.0554$, the imbalance is reduced.

2. Inertial effect on the unsteady deformation

Following Kojima et al. (1984), we can show that the normal stress imbalance for the spherical bubble results in an inhomogeneous term $n = 2$ in Eq. (33), which now becomes

$$G_n \frac{df_n}{dt} = -H_n f_{n+1} + L_n f_{n-1} - \delta_{n2}\alpha_w, \qquad n \geq 2, \tag{38}$$

where

$$\alpha_w = \alpha_0 \Big[1 - \frac{\gamma V(\kappa) W}{U(\kappa;\gamma)}\Big]$$

with

$$\alpha_0 = \frac{5}{(\kappa+1)}\Big[\Big(\frac{81}{80}\kappa^3 + \frac{57}{20}\kappa^2 + \frac{103}{40}\kappa + \frac{3}{4}\Big) - \frac{\gamma-1}{12}(\kappa+1)\Big].$$

The ratios of α_w/α_0 are shown in Fig. 4 for various γ and κ. Since the effect of the inhogeneous term was discussed in detail by Kojima et al., here we simply quote the result of their asymptotic analysis for $n \to \infty$. The asymptotic form of (38) in the limit $n \to \infty$ satisfies the following partial differential equation

$$\frac{\partial f}{\partial t} - \frac{1}{2(\kappa+1)} \sin\theta \frac{\partial f}{\partial \theta} = \frac{\cos\theta}{\kappa+1} f - \alpha_{W1} P_2(\cos\theta), \tag{39}$$

where

$$\alpha_{W1} = \frac{5\alpha_w}{G_2},$$

and G_2 is given below Eq. (33). Eq. (39) has the solution

$$\begin{aligned} f(t) =& (\kappa+1)\alpha_{W1}\cos\theta \\ &+ \big(f(0) - (\kappa+1)\alpha_{W1}\cos\theta(0)\big)\Big(\frac{1+\cot^2\theta(t)/2}{1+\cot^2\theta(0)/2}\Big)^2 \exp\Big(\frac{-t}{\kappa+1}\Big) \end{aligned} \tag{40}$$

along the characteristics given by Eq. (36b). In (40), $f(0)$ is the shape function at $t = 0$. Expanding Eq. (40) at small time yields

$$f = f(0) - t\left[\alpha_{W1} P_2 - \{f(0)/(\kappa+1)\}\cos\theta\right] + o(t), \tag{41}$$

while, as $t \to \infty$,

$$f(t) \to [f(0) - (\kappa+1)\alpha_{W1}]\exp(t/(\kappa+1)) \tag{42a}$$

at $\theta = 0$, and

$$f(t) \to [f(0) + (\kappa+1)\alpha_{W1}]\exp(-t/(\kappa+1)) \tag{42b}$$

at $\theta = \pi$. As we can see (42a) and (42b), the spherical shape is stable near the front stagnation point, whereas it is unstable near the rear stagnation point. In the usual cases $\alpha_w > 0$, as we can see in (38) for $W << 1$, the voidage bubble will deform as shown in Fig. 5(a). However, if $\kappa > \kappa_c = 0.0554$, then $\alpha_w < \alpha_0$, so we have slower deformation than the conventional drop problem provided all parameters are the same for both cases except W. Although our analysis is based on the assumption $W << 1$, if we assume the result is valid even for $W = O(1)$, quite interesting solution behaviors are obtained. For example, $\alpha_w = 0$ at $W = W_c$, which is given by

$$W_c = \frac{U(\kappa;\gamma)}{\gamma V(\kappa)}.$$

If $\alpha_w = 0$, the spherical shape is the steady solution for the non-zero Reynolds number (Fig. 5(b)). If $\alpha_w < 0$, the voidage bubble will be deformed as shown in Fig. 5(c).

V. Conclusion

In the present paper, we formulated the voidage bubble problem as a generalized drop problem incorporating the assumptions described in Sec. II. The

generalized drop problem includes an additional parameter $W = u_s/U_b$, and it degenerates to the conventional drop problem for $W = 0$. In the analysis given in preceding sections, therefore, a particular interest has been given to the effect of the parameter W on the solution behavior. From the analysis of the steady and unsteady deformation of the voidage bubble we have reached the following conclusions:

(1) In the creeping flow limit, the steady and unsteady deformations are invariant to the change of W; i.e., the deformation of a voidage bubble is exactly the same as a conventional drop, provided two problems have the same dimensionless parameters except for W.

(2) Cloud formation is predicted also in the creeping flow limit and the thickness of the cloud for the voidage bubble in a gas fluidized is given as $r_c - 1 = \beta/(1-\beta)$, where $\beta = W/(1-\alpha)$. According to Davison & Harrison (1963), the prediction of $r_c - 1$ for the potential flow limit is $r_c - 1 = (1 + 2\beta/1 - \beta)^{1/3} - 1$. Therefore, the predictions for both cases can be described as $r_c - 1 = \beta + O(\beta^2)$ for $\beta << 1$.

(3) When $Re = 0$, the front stagnation point of the steady state shape is stable; in contrast, the rear stagnation point is unsteable with respect to the small disturbance.

(4) When the inertia effect is considered, the effect of W on the deformation first appears. If $\kappa < 0.0554$, the normal stress imbalance gets bigger, but if $\kappa > 0.0554$, the normal stress imbalance is reduced (here κ is the viscosity ratio of inner fluid to the outer mixture phase). Consequently, for a positive W, the unsteady deformation of a voidage bubble starting from a spherical shape is faster if $\kappa < 0.0554$, but slower than the $W = 0$ case if $\kappa > 0.0554$.

Appendix

The continuum models employed in the multiphase flow study can be largely categorized into the following two major models.

1. one-mixture-phase model
2. two-interpenetrating-continuum model

In the first model, the mixture phase of solid and fluid is considered as a statistically homogeneous Newtonian (or non-Newtonian) fluid that has the effective properties such as viscosity, density etc. This model has been used for the low Reynolds number problems such as the settling problem and the low Reynolds number voidage bubble problem (Batchelor 1974; Acrivos & Herbolzheimer 1979). In the second model, the solid phase and fluid phase are assumed to take the whole space with certain probabilities (which are usually the volume fractions). This model has been used mainly for the modeling of a voidage bubble and the stability analysis of a fluidized bed (Anderson & Jackson 1967; Buyevich 1972a, 1975; Davidson & Harrison 1963; Homsy et al. 1980; Drew 1983) Although each model has its own merit with respect to the other, there are still many questions to be answered in both models. For example, in the first model, the governing equation for the solid phase has not been formulated except for the problem of a very small Reynolds number. The question in the interpenetrating-continuum-model is due to the unmeasurable physical quantities such as solid phase stress. Even worse is that the relationship between two models has not been clearly understood yet. Therefore, here, we attempt to show that the two models are equivalent at least in the limit $Re \to 0$ via deriving the one-phase model from the other.

Let us begin by writing the accepted governing equations in the interpenetrating continuum model

$$\rho_f(1-\alpha)\Big(\frac{\partial \mathbf{u}_f}{\partial t} + \mathbf{u}_f \cdot \nabla \mathbf{u}_f\Big) = (1-\alpha)\nabla \cdot \mathbf{T}_f - (1-\alpha)\mathbf{F}_I + (1-\alpha)\rho_f \mathbf{g}, \quad (A1)$$

$$\rho_p \alpha\Big(\frac{\partial \mathbf{u}_p}{\partial t} + \mathbf{u}_p \cdot \nabla \mathbf{u}_p\Big) = \alpha\nabla \cdot \mathbf{T}_f + \nabla \cdot \mathbf{T}_p + (1-\alpha)\mathbf{F}_I + \alpha\rho_p \mathbf{g}, \quad (A2)$$

where $(1-\alpha)\mathbf{F}_I$ is the interaction force between two phases due to drag etc., and $\mathbf{F}_I$ is assumed to have the form for a low Reynolds number $\mathbf{F}_I = C(\alpha)(\mathbf{u}_f - \mathbf{u}_p)$. In (A2), $\mathbf{T}_p$ is the so-called solid phase stress tensor, which is believed to come

from the particle interactions such as collision or random behavior of particles. As discussed above, this quantity has so far been known to be unmeasurable. Only one available information for this quantity is due to Buyevich. Buyevich (1972a,b) derived this stress tensor in the following form via statistical mechanical analysis for the special case of uniform fluidization

$$\mathbf{T}_p = \rho_p \mathbf{L}^p \parallel \mathbf{u}_f - \mathbf{u}_p \parallel^2, \tag{A3}$$

where $\mathbf{L}^p$ is tensor function of voidage as shown in Fig. 7 of Buyevich (1972b). From his Fig. 7, we must note that $\parallel \mathbf{L}^p \parallel < 0.6$ and $\parallel \mathbf{L}^p \parallel \rightarrow 0$ as $\alpha \rightarrow 0$. An immediate conclusion from the formula for $\mathbf{T}_p$ is that

$$\parallel \mathbf{T}_p \parallel = O(\frac{\mu U_c}{a}) O(Re). \tag{A4}$$

Now we can derive the governing equation for the mixture as shown in Eq. (3) of Sec. II. By adding (A1) and (A2), we get

$$\rho_p \alpha \frac{D_p \mathbf{u}_p}{Dt} + \rho_f (1-\alpha) \frac{D_f \mathbf{u}_f}{Dt} = \nabla \cdot (\mathbf{T}_f + \mathbf{T}_p) + \rho \mathbf{g}. \tag{A5}$$

Then, from (A5) with (A4) we have

$$\nabla \cdot \mathbf{T}_f + \rho \mathbf{g} = O(\frac{\mu U_c}{a}) O(Re). \tag{A6}$$

By substituting (A4) and (A6) into (A2) we get

$$\mathbf{F}_I + \alpha(\rho_p - \rho_f)\mathbf{g} = O(\frac{\mu U_c}{a}) O(Re). \tag{A7}$$

Eq. (A7) becomes equivalent to Eq. (5) in Sec. II as $Re \rightarrow 0$. Therefore, the interpenetrating continuum model reduces to our one-phase model adopted in the present study at least for $Re << 1$.

REFERENCES

1. Acrivos,A. and Herbolzheimer,E., *J. Fluid Mech.*, **92**, 435 (1979).

2. Anderson,T.B. and Jackson,R., *I&EC Fund.*, **6**, 527 (1967).
3. Batchelor,G.K., *Arch. of Mech.*, **26**, 339 (1974).
4. Buyevich,Y.A., *J. Fluid Mech*, **49**, 489 (1971).
5. Buyevich,Y.A., *J. Fluid Mech*, **52**, 345 (1972a).
6. Buyevich,Y.A., *J. Fluid Mech*, **56**, 313 (1972b).
7. Buyevich,Y.A., *Int. J. Multiphase Flow*, **2**, 337 (1975).
8. Clift,R., Grace,J.R., Cheung,L., and Do,T.H. *J. Fluid Mech.*, **51**, 187 (1972).
9. Collins,R., *Chem. Eng. Sci.*, **26**, 995 (1971).
10. Collins,R., *J. Fluid Mech.*, **122**, 155 (1982).
11. Davidson,J.F. and Harrison,D., *Fluidized Particles*, Cambridge U. Press, London, 1963.
12. Drew,D.A., *Ann. Rev. Fluid Mech.*, **15**, 261 (1983).
13. Homsy,G.M., El-Kaissy,M.M., and Didwania,A. *Int. J. Multiphase Flow*, **6**, 305 (1980).
14. Jackson,R., *Trans. Instn Chem. Engrs (London)*, **41**, 22 (1963).
15. Kojima.M., Hinch,E.J., and Acrivos,A., *Phys. Fluids*, **27**, 19 (1984).
16. Murray,J.D., *J. Fluid Mech.*, **22**, 57 (1965).
17. Murray,J.D., *J. Fluid Mech.*, **28**, 417 (1967).
18. Taylor,T.D. and Acrivos,A., *J. Fluid Mech.*, **18**, 466 (1964).

Figure Captions

Figure 1. A voidage bubble in a fluidized bed.

Figure 2. Comparison of Batchelor's prediction for the cloud thickness in the creeping flow limit and the Davidson's prediction for the potential flow limit.

Figure 3. The function $V(\kappa)$ defined in Eq. 37, where $\kappa = \tilde{\mu}/\mu$.

Figure 4. The ratio α_w/α_0 as a function of W for various κ and γ.

Figure 5. Unsteady deformation of a voidage bubble starting from spherical shape at a non-zero Reynolds number.

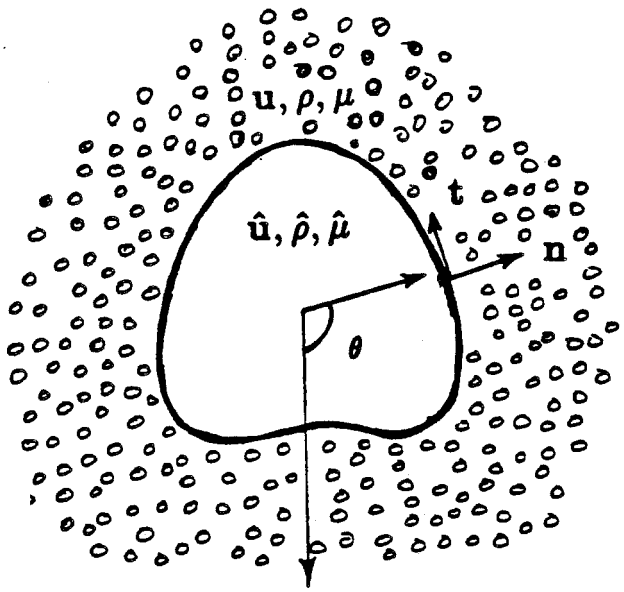

Figure 1

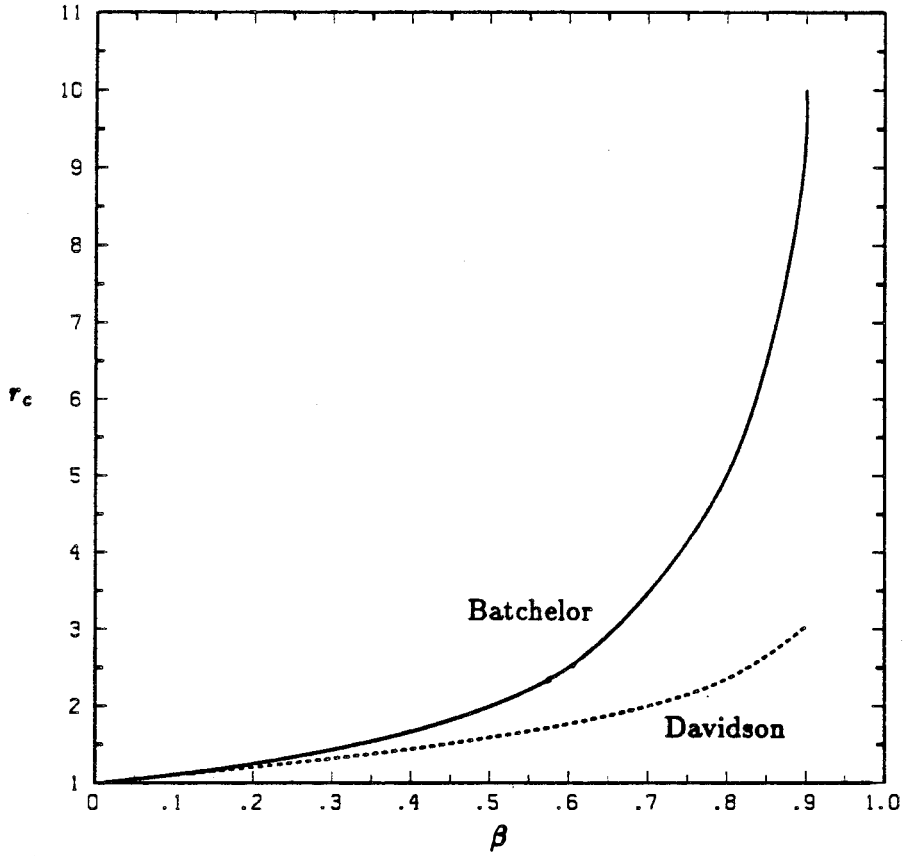

Figure 2

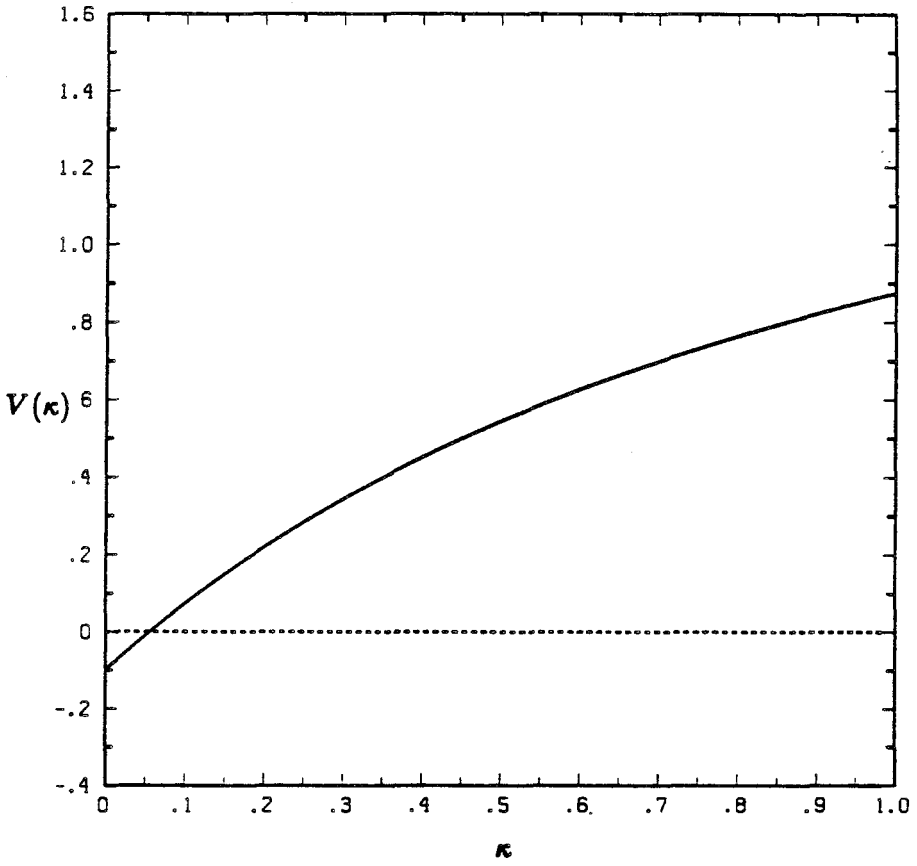

Figure 3

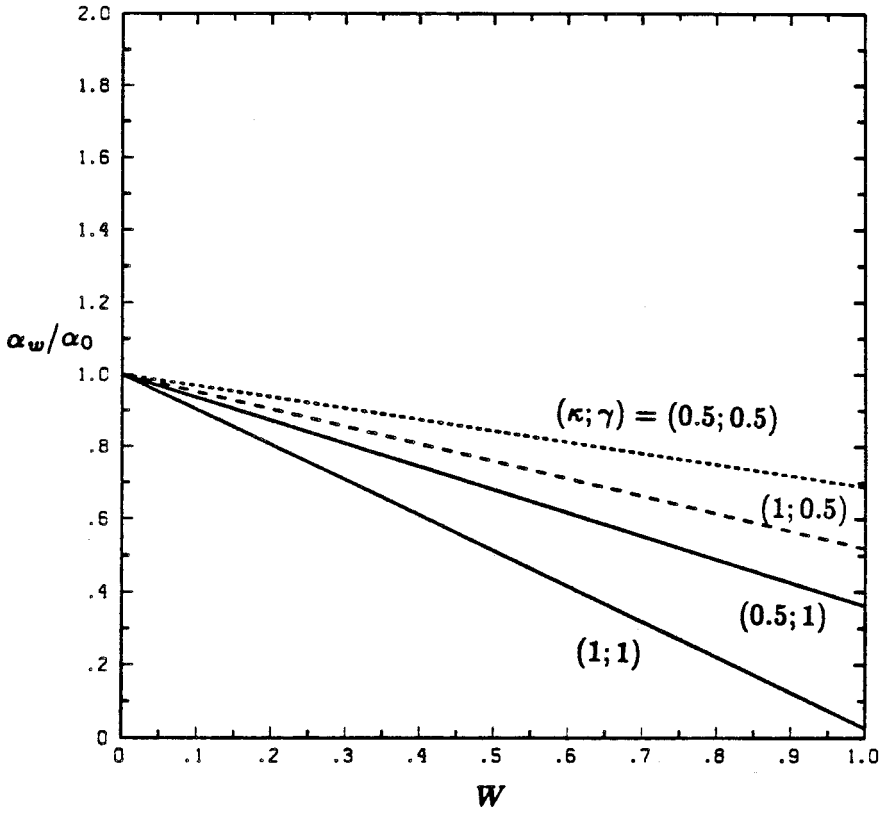
2.0
1.8
1.6
1.4
1.2
α_w/α_0
1.0
.8
.6
.4
.2
0
0
.1
.2
.3
.4
.5
.6
.7
.8
.9
1.0
W
$(\kappa;\gamma) = (0.5;0.5)$
$(1;0.5)$
$(0.5;1)$
$(1;1)$

Figure 4

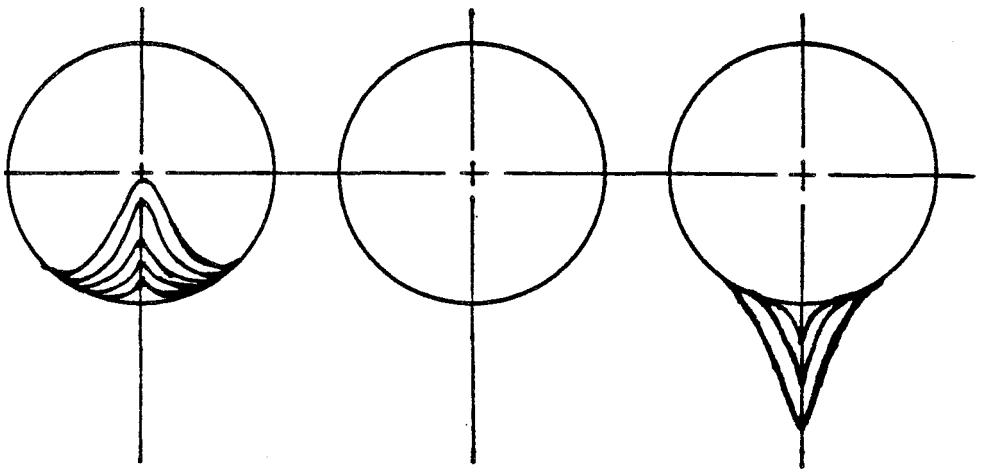

(a) (b) (c)

$\alpha_w > 0$ $\alpha_w = 0$ $\alpha_w < 0$

Figure 5